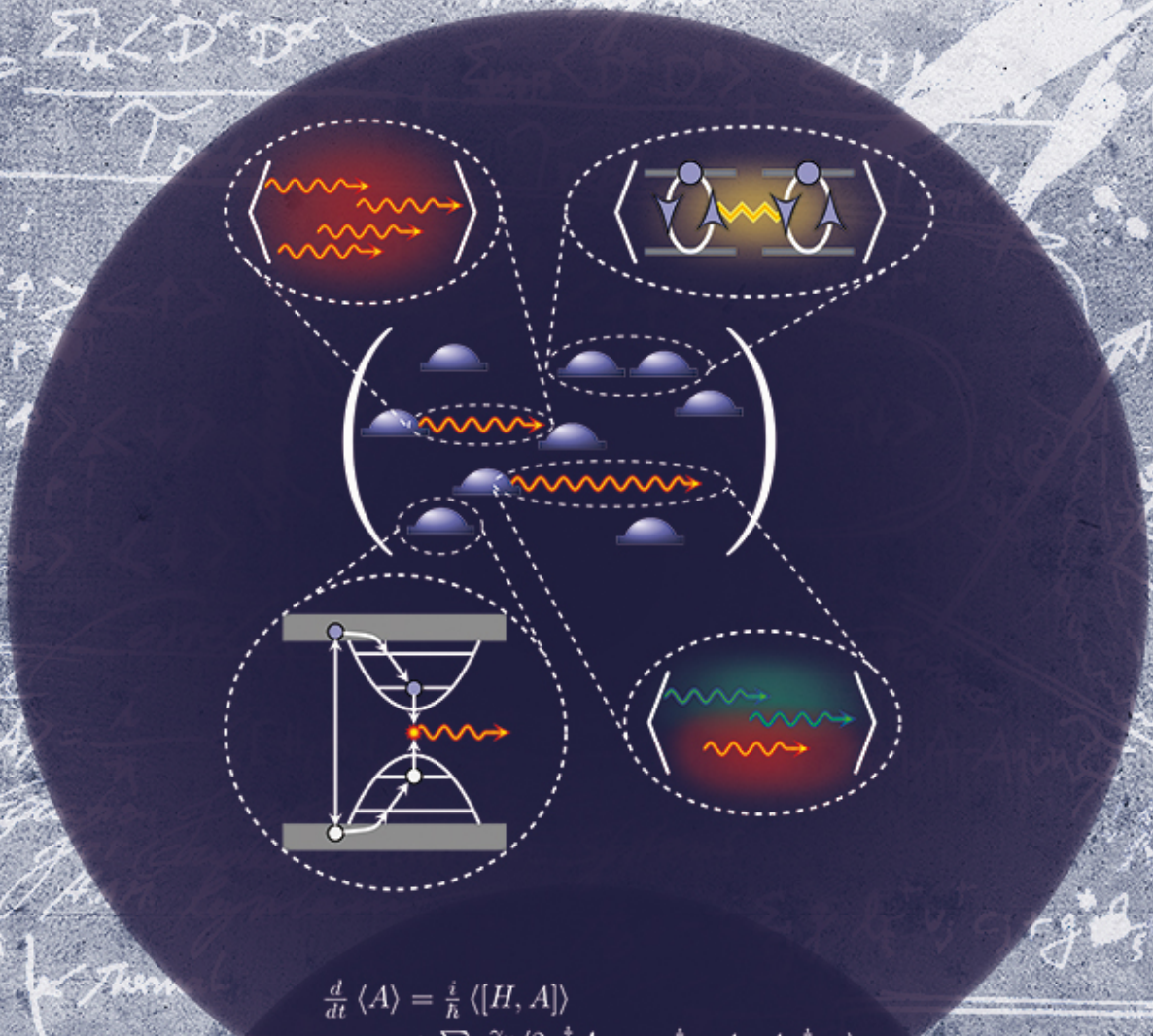


Heinrich Alexander Magnus  
Leymann

# theory of many-particle correlations and optical properties of semiconductor quantum dots

## photons & quantum dots



$$\frac{d}{dt} \langle A \rangle = \frac{i}{\hbar} \langle [H, A] \rangle + \sum_{\nu} \frac{\gamma_{\nu}}{2} \langle 2\eta_{\nu}^{\dagger} A \eta_{\nu} - \eta_{\nu}^{\dagger} \eta_{\nu} A - A \eta_{\nu}^{\dagger} \eta_{\nu} \rangle$$



$$\mathcal{F}^{-1} \Delta_{\delta \neq I-1} \mathcal{F} \langle b^I \rangle = - \sum_{P \in P_I \setminus I} c_P \prod_{J \in P} \langle b^J \rangle$$



# Theory of many-particle correlations and optical properties of semiconductor quantum dots

photons and quantum dots

## **Dissertation**

zur Erlangung des akademischen Grades

**doktor rerum naturalium**

**(Dr.rer.nat.)**

genehmigt durch die Fakultät für Naturwissenschaften der  
Otto-von-Guericke-Universität Magdeburg

von Dipl.-Phys. Heinrich Alexander Magnus Leymann  
geb. am 16.03.1985 in Preetz/Plön

Gutachter: Prof. Dr. rer. nat. habil. Jan Wiersig  
Prof. Dr. rer. nat. habil. Andreas Knorr

eingereicht am: 17.12.2015

verteidigt am: 19.04.2016



# Abstract

In this work, the optical properties of semiconductor quantum dots (QDs) are studied and a particular emphasis is placed on many-particle correlations of the confined carriers and the emitted photons. In each part of this thesis a different aspect of the light-matter interaction in semiconductor QDs is examined. According to the requirements of the physical situation the theoretical methods are modified and further developed.

As a first step a microscopic theory for the luminescence into free space of a single semiconductor QD is developed. To formulate this theory the well established cluster expansion is used with the twist that here, all possible many-particle correlations of the carriers confined to the QD are included exactly. Furthermore the developed theory allows for a consistent description of scattering and dephasing, that goes beyond phenomenological relaxation rates.

Based on the presented modifications of the cluster expansion a general formalism to derive equations of motion for open many-particle systems is introduced. This formalism, although more flexible than the cluster expansion, is equivalent to the former and it allows to go to considerably higher orders of approximation. With this approach the photon autocorrelation functions of light emitted by a QD based microcavity laser are calculated and the convergence of the cluster expansion is demonstrated.

To understand results of recent experiments performed in the group of Prof. Reitzenstein (TU Berlin) on bimodal microcavity lasers, a two-mode laser theory is presented. It is shown how the interaction of the two cavity modes mediated by the QDs triggers super-thermal intensity fluctuations. The results of the microscopic theory are in excellent agreement with the experimental results. In order to understand the observed intensity fluctuations in terms of the photon statistics an intuitive and exactly solvable master-equation model is developed, which is able to reproduce the results qualitatively. A comprehensive physical picture of the observed effects is given by the dynamics of the first order autocorrelation function.

In the models presented so far the correlations of either the cavity photons or the carriers confined to a QD have played an important role. However, correlations between different emitters (QDs) have been neglected so far as this is typically done in standard laser models as well. To further understand the threshold behavior of current state of the art micro/nano cavity lasers the influence of quantum mechanical correlations between different QDs is investigated. It turns out that additionally to the laser transition, a system that is dominated by inter emitter correlations, undergoes a second transition from the sub- to superradiant regime. It is further demonstrated that the inter emitter correlations can be the decisive reason for the system to enter the lasing regime.

# Contents

<b>1</b>	<b>Introduction</b>	<b>1</b>
<b>2</b>	<b>Basic aspects of the Theory of Light-Matter Interaction in semi-conductors</b>	<b>11</b>
2.1	Electronic and photonic single-particle states . . . . .	11
2.2	Many-particle Hamiltonian . . . . .	14
2.3	Equation of motion for the reduced density operator . . . . .	16
<b>3</b>	<b>Single Quantum Dot Photoluminescence into free-space</b>	<b>19</b>
3.1	Cluster expansion for semiconductor systems . . . . .	19
3.2	Many-body treatment of the embedded QD system . . . . .	22
3.2.1	Equation-of-motion formulation for the electronic degrees of freedom . . . . .	23
3.2.2	Many-body description for mixed expectation values . . . . .	24
3.3	Environment coupling: Treatment of scattering and dephasing processes	27
3.3.1	System-reservoir interaction . . . . .	27
3.3.2	Lindblad terms in the equation-of-motion technique . . . . .	28
3.4	Equations of Motion for single QD PL . . . . .	29
3.4.1	Hamiltonian dynamics . . . . .	30
3.4.2	System-bath interaction . . . . .	34
3.4.3	Luminescence dynamics and spectrum . . . . .	38
3.5	Photoluminescence into free-space . . . . .	38
3.6	Numerical results for a single QD in a microcavity . . . . .	44
3.7	Chapter Conclusion . . . . .	46
<b>4</b>	<b>Expectation Value Based Cluster Expansion</b>	<b>49</b>
4.1	Numerical approaches for interacting many-particle systems . . . . .	49
4.2	The concept of correlation functions . . . . .	50
4.2.1	Definition of correlation functions . . . . .	51
4.2.2	Approximations by lower-order quantities . . . . .	52
4.3	Equations of motion . . . . .	54
4.3.1	Infinite Hierarchy . . . . .	55
4.3.2	Expectation value based cluster expansion . . . . .	58
4.3.3	Equation of motion for mixed Hilbert spaces . . . . .	60
4.4	Applications . . . . .	61

4.4.1	Hierarchy induced by the dipole Hamiltonian . . . . .	61
4.4.2	Classification of former approaches by the proposed truncation scheme . . . . .	68
4.5	Chapter Conclusion . . . . .	70
<b>5</b>	<b>Coherence properties of Microcavity QD Lasers</b>	<b>73</b>
5.1	Characterization of micro laser emission in the single-mode case . . .	74
5.1.1	Photon autocorrelation function . . . . .	75
5.1.2	Laser transition in higher-order photon autocorrelation functions	78
5.2	Intensity fluctuations in bimodal micropillar lasers . . . . .	83
5.2.1	Experiment . . . . .	84
5.2.2	Theory . . . . .	88
5.2.3	Microscopic Semiconductor Theory . . . . .	88
5.2.4	Extended Birth-Death Approach . . . . .	94
5.2.5	Conclusion and comparison of the experimental and theoreti- cal results . . . . .	100
5.3	Unconventional Collective Normal-Mode Coupling in Quantum-Dot- based Bimodal Microlasers . . . . .	102
5.3.1	The strong coupling regime . . . . .	102
5.3.2	Theoretical Model . . . . .	104
5.3.3	Mode coupling . . . . .	105
5.3.4	Cavity Mode Spectra . . . . .	106
5.3.5	Experimental Realization . . . . .	107
5.3.6	Conclusion . . . . .	109
5.4	Chapter Conclusion . . . . .	110
<b>6</b>	<b>Sub- and Superradiance in QD Nanolasers</b>	<b>111</b>
6.1	Introduction . . . . .	111
6.2	Laser theory formulated in configuration operators . . . . .	113
6.3	Signatures of Radiative Coupling in the Input-Output Characteristics of Nanolasers . . . . .	115
6.4	Statistical Properties of the Emission and Effective Spontaneous Emis- sion Rate . . . . .	117
6.5	Influence of the Emitter Number and Coherence Per Photon . . . . .	120
6.6	Dicke States of Pairs of Emitters . . . . .	122
6.7	Chapter Conclusion . . . . .	124
<b>7</b>	<b>Final Conclusions</b>	<b>127</b>
<b>A</b>	<b>Equations of motion for single QD PL into free Space</b>	<b>131</b>
A.1	Hamiltonian . . . . .	131
A.2	Equations of motion . . . . .	132
A.2.1	Light-matter interaction . . . . .	132
A.2.2	Coulomb interaction . . . . .	133

A.2.3	System-bath interaction . . . . .	135
<b>B</b>	<b>Equations of motion for the microscopic bimodal laser model</b>	<b>139</b>
<b>C</b>	<b>Details of the laser theory formulated in configuration operators</b>	<b>141</b>
C.1	Configuration Operators . . . . .	141
C.2	Equation-of-motion hierarchy . . . . .	142
C.3	Coupling to the continuum states . . . . .	145
C.4	Total emission rate into the laser mode . . . . .	146
<b>D</b>	<b>The computer algebra system FORM</b>	<b>149</b>
D.1	Establishing standard order . . . . .	149
D.2	Factorization . . . . .	151
D.3	The truncation Operator . . . . .	152
	<b>Acknowledgments</b>	<b>173</b>



# Chapter 1

## Introduction

**Lasers** are an essential tool for fundamental and applied research and even play an important role in our everyday life [Perkowitz, 2010, Max et al., 2010]. In the last two decades the development of optical cavities [Reitzenstein and Forchel, 2010, Cao and Wiersig, 2015] and lasers has shown a remarkable miniaturization [He et al., 2013, Vahala, 2003, Kryzhanovskaya et al., 2014] that has led to highly efficient (laser-)devices with a very low laser threshold [Reitzenstein et al., 2008b]. Reference [Gourley, 1998] gives a good popular introduction to micro/nano-lasers, and Ref. [Samuel et al., 2009] reviews the traditional criteria a light source has to fulfill to be called a laser.

One of the main effects that makes micro/nano-lasers more efficient than conventional lasers is the Purcell-Effect [Purcell, 1946]. The Purcell effect is the modification (enhancement) of the spontaneous emission from the light source by its electromagnetic environment into certain modes. The factor that quantifies the enhancement of the spontaneous emission into a cavity mode compared to the spontaneous emission into free space is called the Purcell factor [Kleppner, 1981, Lodahl et al., 2004, Haroche and Kleppner, 2008]. The enhancement is largest for high-quality modes (i.e. modes with a very long photon dwelling times) with a low mode volume.

The important quantity to characterize a laser device is the  $\beta$ -factor which is closely related to the Purcell factor. The  $\beta$ -factor is the fraction of spontaneous emission into the laser mode compared to the overall spontaneous emission of the laser-gain medium. Conventional gas lasers have  $\beta$ -factors of roughly  $10^{-6}$  meaning that only one of a million spontaneously emitted photons actually goes into the laser mode. Nowadays many micro lasers with  $\beta$ -factors around 0.1 are used in experiments e.g. [Lermer et al., 2013, Musiał et al., 2015] and there are experiments that claim to have lasers with a  $\beta$ -factor close to one [Strauf et al., 2006, Thyrestrup et al., 2010]. The  $\beta$ -factor of a laser determines the threshold behavior. The following rule of thumb, that is only exact for a simple rate equation analysis, still gives a good impression of the (in conventional lasers dramatic) changes a laser undergoes at the threshold and demonstrates the significance of the  $\beta$ -factor: 'In a log-log scale input-output plot, the intensity jump at the laser-threshold is proportional to  $\beta^{-1}$ ' [Rice and Carmichael, 1994].

The threshold behavior of a laser is of course influenced by various effects [Chow

---

and Jahnke, 2013, Chow et al., 2014, Gies et al., 2007] and some of them will be addressed in this thesis. For conventional lasers the threshold and the  $\beta$ -factor can simply be determined by the intensity jump over several orders of magnitude at the threshold. In a micro/nano-laser where almost the entire spontaneous emission goes into the lasing mode, there is no sharp intensity jump and the onset of lasing cannot be determined by the input/output curve alone. To characterize such 'threshold-less' micro/nano-lasers, new theories [Rice and Carmichael, 1994] and experiments [Ulrich et al., 2007] have been developed that monitor the transition into lasing by the changes in the photon statistics of the emitted light [Wiersig et al., 2009]. The theories have to take photon correlations into account that arise from the quantum nature of light, in order to describe the light-matter interaction in the laser accurately. These more advanced theories and experiments show that the emitted light changes qualitatively even if no threshold is visible in the input-output curve. Independent from the height of the intensity jump the process dominating the system, changes from spontaneous to stimulated emission at the laser threshold. This transition from the spontaneous to the stimulated emission regime changes the statistical properties of the emitted light from thermal to coherent. In the lasing regime the photons no longer obey thermal statistics but have a Poisson-distribution, typical for a coherent state. The change of the photon statistics is measurable in the photon correlation function [Ulrich et al., 2007, Wiersig et al., 2009] and is used to determine the laser threshold and characterize the coherence properties of the emitted light.

**Optical microresonators** facilitate the confinement of light to a very small spatial region, which is required to achieve low threshold laser devices and to couple a single mode to the gain medium [Vahala, 2003]. There are many different types of microresonators, and their design, optimization, characterization, and experimental realization are research fields of their own. The type of microresonators that are used for the experiments described in this thesis are micropillars like the one shown in Fig. 1.1. In axial direction the light is confined by Bragg-reflection accomplished by several  $\frac{\lambda}{4}$ -layers of different refractive index material below and above the region where the light is confined to and where the gain material is located [Sebald et al., 2009]. In lateral direction the light is confined by air-dielectric guiding [Vahala, 2003].

**Semiconductor Quantum Dots** Next to the laser-mode resonator that stores the photons and modifies their emission, the gain medium, that actually emits the photons into the laser mode is the second crucial component of a laser. While atoms in the gas phase are the traditional gain medium, semiconductor lasers offer a variety of advantages [Alferov, 2001], with respect e.g. in miniaturization and mass production. The progress made in growth technologies has led to nano structured low dimensional gain materials. These new materials allow to tailor their optical and electronic properties [Bimberg et al., 1999, Bimberg et al., 2009, Reitzenstein, 2012], and offer a variety of possible applications in quantum cryptography, quantum computing, and optoelectronics [Petroff et al., 2001].

In this thesis the gain material under consideration are zero dimensional struc-

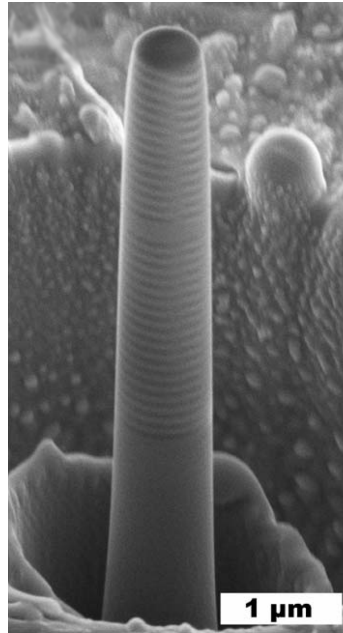


Figure 1.1: Scanning electron-microscopy picture of a micropillar based on ZnSe and MgS with a diameter 700 nm. The pillar has been fabricated by the groups of D. Hommel and J. Gutowski in Bremen [Lohmeyer et al., 2006].

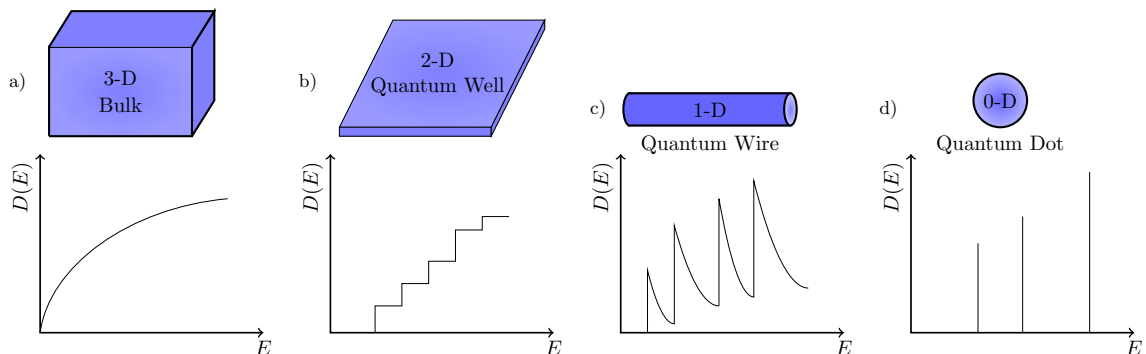


Figure 1.2: Free density of states for systems with three-, two-, one-, and zero-dimensional extension [Singleton, 2001, Haug and Koch, 2004].

tures. In these structures the carriers are confined in all three spatial directions, that is why early works have called them 'quantum boxes' [Asada et al., 1986] or 'artificial atoms' [Fafard et al., 1999]. These names arise from the discrete atom-like density of states that can be understood by a simple box potential model for the carrier confinement. Whenever the wave function of the schrödinger equation is confined to a finite region in all spatial directions the energy level structure of the single-particle states becomes discrete in contrast to the (quasi) continuous states of systems where carrier propagation is allowed in at least one direction. The influence of the dimension of a system on the free density of states is illustrated in Fig. 1.2. Today 'quantum dot' (QD) is the most common term for these zero dimensional structures. The QDs studied in this thesis are ensembles of several thousand

atoms of a certain semiconductor material located in a different semiconductor material with a larger band gap. These 'islands' of atoms with an extension of several nanometers create the 'potential box' that confines the quasi-free carriers in all spacial directions.

For more than a decade QDs are of high interest [Michler, 2003] for fundamental research and their potential applications. In contrast to atoms the confining potential and with this the level spacing of the confined carriers can be tailored by the size, geometry and material of the QDs. For example InGaAs QDs on a GaAs substrate exhibit a direct band-gap in the infrared spectrum. Among many different applications it was demonstrated early on that due to their high gain [Asada et al., 1986] and low temperature dependence [Arakawa and Sakaki, 1982] QDs are a very promising material for low threshold lasers. One way of fabricating QDs is the self organized growth in the Stranski-Krastanow-mode [Jacobi, 2003, Anders et al., 2002]: By molecular beam epitaxy or metal organic gas epitaxy a semiconductor material is grown on top of a substrate material with a larger band gap. At the beginning the new material layer grows homogeneously with the same lattice constant as the substrate, this introduces tension between the two materials. At a critical thickness this tension is reduced by the rise of small material island, the actual QDs. This process results in a thin homogeneous wetting layer with randomly distributed QDs as shown in Fig. 1.3. Subsequently the substrate is grown on top of the wetting layer with the QDs.

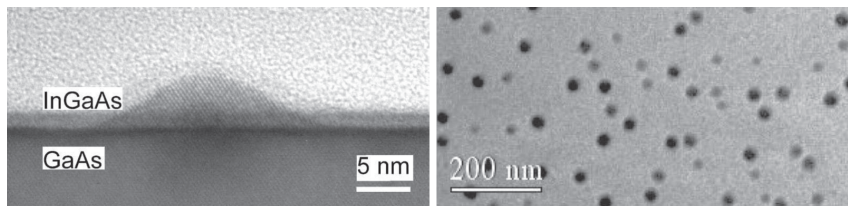


Figure 1.3: Transmission electron microscope of self organized InGaAs QDs. Left: Single QD with the wetting layer on a GaAs substrate. Right: Top view of a sample with randomly distributed QDs. Both pictures are taken from Ref. [Anders et al., 2002].

One main task for theorists describing the light-matter interaction of semiconductor QDs is to identify differences in behavior between QDs and atoms. Since the level spacing of the lowest confined states is much smaller for QDs than for atoms, the energetically higher states have to be taken into account. This gives rise to many-particle effects. As a result, a simple two-level description of the QDs which is often used for atomic systems is generally no longer valid. Semiconductor QDs cannot be regarded as isolated systems; they are located in a dense semiconductor environment. The confined carrier states couple to phonons, the electronic (quasi)continuum states of the wetting layer, and the bulk material. The interaction with the environment triggers various processes that have to be taken into account for a realistic QD model. A generic QD model is portrayed in Fig. 1.4.

**Superradiance** Successful realizations of single QD lasers have been reported [Reitzenstein et al., 2008a, Nomura et al., 2009, Nomura et al., 2010, Xie et al., 2007]

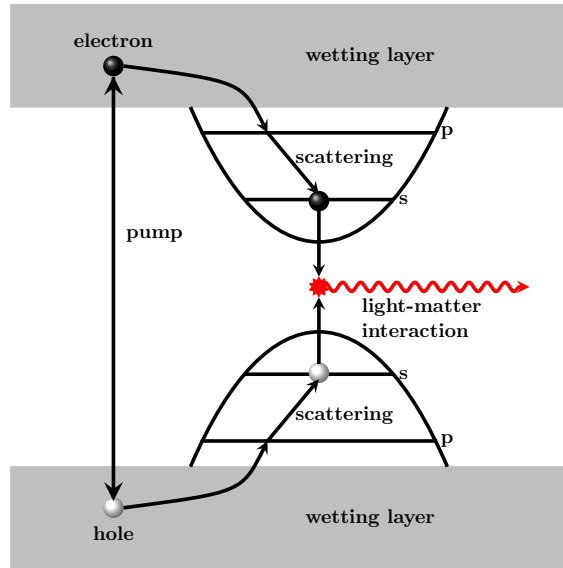


Figure 1.4: Illustration of the various processes that take place in a QD. For electrically pumped QDs, electrons and holes are created in the quasicontinuum states and relax into the upper confined QD states. In the QD model used throughout this thesis, this process is mapped onto the direct creation of electrons and holes in the p-shell. The carriers within the QD can relax further into the QD via scattering with the continuum- and the phonon-states. When multiple carriers are confined to the QD their Coulomb interaction has to be taken into account, as well. The recombination of electron-hole pairs creates photons and the reverse process absorbs them.

and these devices present a very interesting field for theoretical research [Ritter et al., 2010, Gies et al., 2011, Gies et al., 2012]. However, state-of-the-art micropillar-lasers have between twenty and several hundred QDs as their active material [Reitzenstein et al., 2008b]. These are the systems that are studied in this thesis. When several emitters are coupled to the same radiation field, they can exhibit a phenomenon that is called superradiance (SR). Superradiance was originally discussed by Dicke for the coherent spontaneous emission of light by an ensemble of initially excited atoms in the gas phase [Dicke, 1954]. Dicke showed that the spontaneous emission from an ensemble of atoms can be enhanced simply by the fact that the atoms "share" the excitation. The concept of shared excitation can be understood with the introduction of superpositions of energetically degenerate states [Mandel and Wolf, 1995]. When this superposition is symmetric with respect to the commutation of two emitters, the initially excited ensemble emits a SR burst of light. This emitted pulse is significantly larger than and of a shorter duration compared to the emission profile of a single emitter multiplied by the number of emitters in the former case.

The concept of SR and collective emission has led to many studies in various fields of research, reaching from single-photon emission enhancement [Scully and Svidzinsky, 2009, Chen et al., 2012] over photosynthetic bio-complexes [Ferrari et al., 2014] to Dicke phase transitions [Liu et al., 2014] and directional SR emission from statistically independent incoherent sources [Oppel et al., 2014]. Light

---

sources based on alkaline-earth atoms can emit collectively photons with an extremely narrow linewidth [Meiser et al., 2009], which has triggered the development of a recently reported new kind of “nearly photon-less” SR laser [Bohnet et al., 2012]. For semiconductor systems, SR effects resulting in radiative lifetime changes have been shown for an ensemble of semiconductor QDs [Scheibner et al., 2007]. For a few (up to three) quantum emitters it is shown that the coupling to a common reservoir can increase the coherence of the emitted light by inducing additional quantum correlations between the emitters [Su et al., 2013]. Also in quantum well systems spontaneous-emission enhancement has been demonstrated [Timothy Noe Li et al., 2012] that originates from superfluorescence, a collective effect closely related to SR (see [Mandel and Wolf, 1995] for details).

**Outline of this Thesis** This general introduction to the main physical topics of this thesis is followed by an outline of the chapters. Figure 1.5 gives a graphical overview on the subjects of this thesis. An extended introduction to the corresponding topics is given at the beginning of each chapter. The chapters are roughly in the order in which they have been worked out, and start with the initial task that motivated this thesis: ‘The technical and conceptional improvement of the cluster expansion method for semiconductor QD systems’.

**Chapter 2** gives a short introduction to general aspects of the theoretical description of light-matter interaction in semiconductor nano structures. The calculation of the single-particle states for the confined carriers and the cavity modes is sketched. In a second step the construction of the many-particle Hamiltonian, in the framework of the second quantization is shown. For this thesis the single-particle states enter only indirectly into the theory via the matrix elements of the many-particle Hamiltonian describing the Coulomb-interaction of the carriers and the light-matter interaction of photons and electron-hole pairs in the dipole approximation. To describe the influence of the environment on the localized carrier and photon states a reduced density matrix formalism is applied which results in the von Neumann Lindblad (vNL) equation for the density operator of the coupled system.

**Chapter 3** introduces one formulation of the cluster expansion (CE) [Fricke, 1996b, Fricke, 1996a, Fricke et al., 1997, Schoeller, 1994], an approximation method to solve the vNL equation indirectly, that is used and further developed in this thesis. Direct numerical exact solutions of the vNL equation have been successfully applied for the description of small systems containing one or very few QDs [Ritter et al., 2010, Gies et al., 2011, Florian et al., 2013a]. Greens function methods have also been used to investigate the light-matter interaction of semiconductor QD systems [Bányai et al., 1998, Binder et al., 1992, Lorke et al., 2006, Schneider et al., 2004, Seebeck et al., 2005], but they have the shortcoming that second-order photon correlations are very hard to obtain [Florian, 2014]. For large systems the derivation and solution of EoM hierarchies like the CE is an established method in the field of semiconductor quantum optics [Hoyer et al., 2004, Kira and Koch, 2011, Jahnke, 2012]. An important result of this thesis is the extension and reformulation of the CE. The CE is based on the neglect of many-particle correlation functions and allows one to systematically include higher-order many-particle correlations and truncate the well known Bogolyubov-Born-Green-Kirkwood-Yvon (BBGKY)

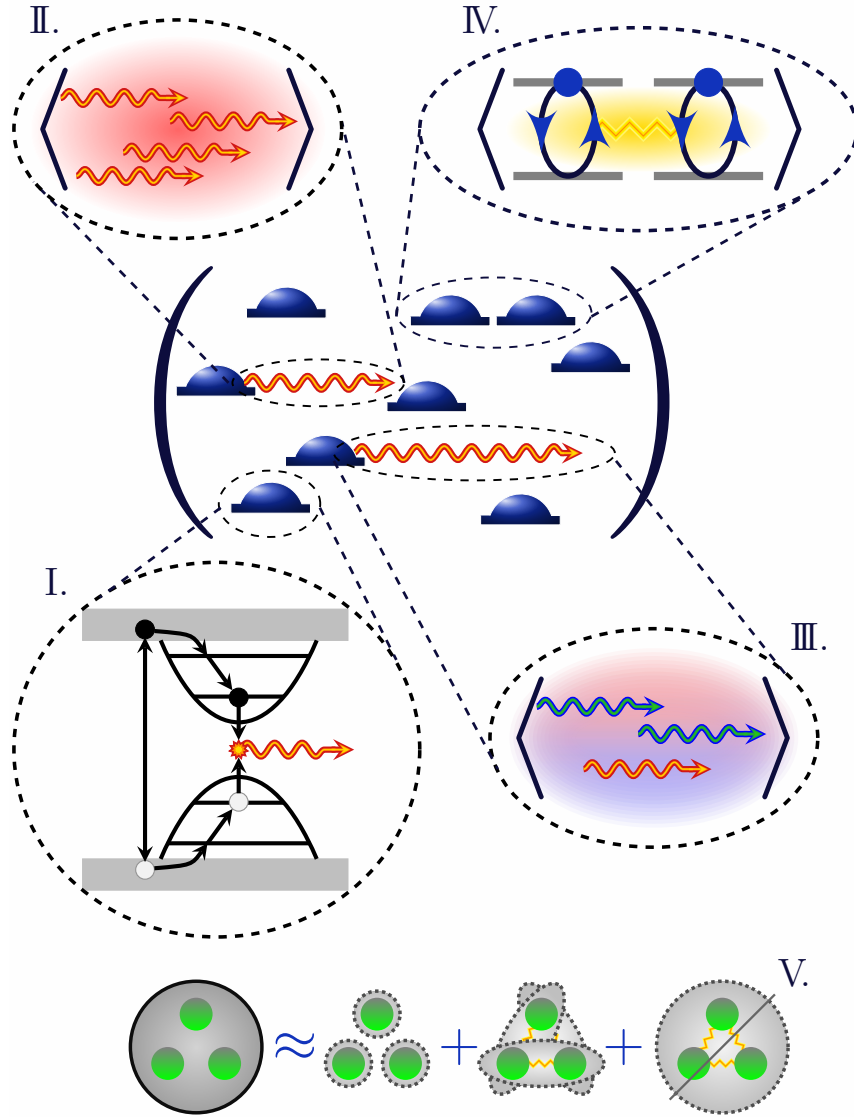


Figure 1.5: Graphical table of contents of this thesis: I. the quantum mechanical description of the processes that take place in a single QD (chapter 3), II. the photon correlations and coherence properties of a single-mode microcavity laser (section 5.1), III. the photon correlations and coherence properties of a bimodal microcavity laser (section 5.2 and 5.3), IV. the influence of inter-QD correlations on the laser threshold (chapter 6), and V. the cluster expansion (chapter 4).

hierarchy in many-particle physics. Originally the CE was designed for large systems i.e. systems with a (quasi-)continuous Hilbert space with a large number of single-particle states, since the neglect of many-particle correlations relies partly on the large size of the Hilbert space. The application of the CE to QD systems introduces subtle difficulties, since a QD accommodates only a limited number of carriers confined to very few states.

In chapter 3 it is shown how the discrete and finite level structure of a QD can be incorporated into the traditional formulation of the CE. It is also demonstrated in

---

Chapter 3, how the influence of the environment can be incorporated in the CE via the Lindblad formalism. In this context the relation between scattering, dephasing and the build up of correlations due to the environment is discussed as well. As an application of the modified CE the photo luminescence of a single QD into free space is investigated. The obtained spectra exhibit the expected biexcitonic signatures, and the peak heights, widths and positions can be interpreted by connecting them to the underlying physical process. In these new results the nonphysical behavior produced by the conventional CE used in previous approaches [Baer et al., 2006] are no longer present.

**Chapter 4** takes the ideas developed in chapter 3 and uses them to radically reformulate the CE. Instead of modifying the traditional CE by adding corrective terms to account for the finite number of carriers confined to a QD as done in chapter 3, the expectation value based cluster expansion (EVCE) is introduced. The EVCE is entirely formulated in terms of expectation values instead of correlation functions. It is shown in this chapter that the EVCE can produce exactly the same results as the CE. However, the EVCE is conceptually much simpler, allows for a straight forward application of the Lindblad formalism to all orders, a flexible implementation of finite size effects e.g. in QDs and reduces the algebraic effort considerably.

**Chapter 5** focuses on the coherence properties of QD-based micro/nano cavity lasers. In the first section the EVCE is applied to a single-mode QD-based microcavity laser. As shown in chapter 4 the EVCE enables one to go to higher orders in the BBGKY-hierarchy than the CE. This particular advantage of the EVCE is used in this chapter to show (for the first time) that the CE actually converges when applied to a QD laser system. As discussed in the above paragraph, for increasing  $\beta$ -factors the typical intensity jump at the lasers-threshold vanishes [Rice and Carmichael, 1994]. To monitor the transition to lasing for these nearly threshold less devices one has to investigate the statistical properties of the emitted light [Chow et al., 2014]. The second-order photon correlation function at zero delay time  $g^{(2)}(0)$  is commonly accepted as a good indicator for the onset of lasing [Jin et al., 1994, Gies et al., 2007, Chow et al., 2014]. However, at the lasing threshold the entire statistics of the emitted light changes, not just its second moment  $g^{(2)}(0)$ . Having access to higher orders of the BBGKY-hierarchy one can also monitor the laser transition according to higher-order photon correlation function at zero delay time  $g^{(n)}(0)$ , with  $n = 3, 4, 5$ . The theoretical study of these higher-order functions becomes more relevant. On the one hand since improvements of experimental techniques [Zhou et al., 2013, Dynes et al., 2011, Stevens et al., 2010] have made it possible to measure them in various systems e.g. in Bose-Einstein Condensates [Hodgman et al., 2011], in micro- and nano-lasers [Aßmann et al., 2009, Elvira et al., 2011], and in strongly coupled QD-cavity systems [Rundquist et al., 2014]. On the other hand there are many situations e.g. [Leymann et al., 2013c] where the study of only the second moments is not sufficient to gain enough information about the character of the full photon statistics.

In the second section of chapter 5 the microscopic theory for semiconductor QD-based single-mode microcavity lasers, presented in Ref. [Gies et al., 2007], is extended to a two-mode theory. This theory is used to explain the experimentally observed super thermal intensity fluctuations in a bimodal microcavity laser [Leymann et al.,



2013c, Leymann et al., 2013a]. In electrically contacted micropillars a small asymmetry of the cross section leads to a splitting of the two degenerate fundamental modes. Thus two cavity modes with slightly different frequencies are supported, that emit linear (orthogonal) polarized light. The gain competition of these two high-quality modes leads to the observed intensity fluctuations in the weaker mode. A very good agreement between the experimental results and the microscopic theory is achieved, within the framework of the CE.

However, for a more intuitive understanding of the underlying physics, a master equation based on a simple birth-and-death model is derived [Rice and Carmichael, 1994]. In this model all specific semiconductor aspects are ignored and it solely features two modes competing for laser gain. The simplicity of this model allows one to solve its master equation numerically exact, and obtain to the full photon statistics. The examination of the full photon statistics reveals that the peculiar intensity fluctuations of the weak mode are related to a double peak structure in the photon statistics. The photon statistics of each mode is composed of a thermal- and a Poisson-like part producing one maximum at the zero photon state and one Poisson-like peak around the average photon number.

The third section of chapter 5 deals with the spectral properties of the modes, that are directly related to their gain-mediated interaction. Equations of motion for the first order autocorrelation-function  $g^{(1)}(\tau)$  are derived [Wiersig, 2010]. Starting from the microscopic CE, the key aspects describing the interaction of the two modes are mapped to a  $2 \times 2$  matrix model with a coupling strength proportional to the number of QDs times the inversion. This reveals the relationship to the collective strong coupling regime. Conventional normal mode coupling appears in atomic [Brune et al., 1996, McKeever et al., 2003, Nußmann et al., 2005] and solid-state [Reithmaier et al., 2004, Yoshie et al., 2004] systems in the single-particle or collective strong coupling [Tavis and Cummings, 1968, Andreani et al., 1999, Raizen et al., 1989, Tuchman et al., 2006, Wickenbrock et al., 2013] regime. In these cases of conventional strong coupling a single or multiple emitters couple to a photonic mode. When losses and dephasing process are sufficiently small and the emitter and mode frequency match, the coherent regime is reached and two new eigenstates are formed with a frequency splitting proportional to a generalized coupling strength.

However, the mode coupling discussed in this section 5.3 is different from the conventional coupling discussed in the literature and it is therefore called unconventional normal mode coupling. In contrast to the conventional normal mode coupling here a hybridization of the two cavity modes is observed that leads to a locking of the frequencies and to a splitting of the linewidths in the coherent regime. In the incoherent regime i.e. for a sufficiently large mode splitting or low coupling, both mode frequencies are visible in each of the polarization directions, which can be traced back to the mode hybridization. In this regime the locking of the linewidth provides a direct explanation of the low linewidth i.e. the long coherence time of the weak mode observed in the experiments. The large coherence time, typical for the lasing mode, is particularly surprising since the weak mode exhibits super thermal intensity fluctuations that can almost be regarded as the "opposite" of lasing. The calculated spectra are in very good agreement with the experimental results. They clearly confirm that the double peak structure measured in the polarization direc-

---

tion of the weak mode does not originate from cross-talk but is a result of the QD mediated unconventional mode-coupling [Khanbekyan et al., 2015].

In **Chapter 6** the influence of radiative coupling of the QDs on the threshold of micro/nano lasers is studied. This collective effect is of entirely different nature than the collective coupling discussed in the previous chapter. The collective effect discussed here, called SR, originates from the interaction of different quantum emitters (in this case QDs) with a common radiation field resulting in a coupling between the individual emitters. In former quantum theories for micro and nano lasers the quantum correlations between the emitters of the gain medium (QDs, atoms, excitons) have, to a large extent in the literature, been neglected [Gies et al., 2007, Rice and Carmichael, 1994]. In this chapter it is demonstrated that for nanolasers with a small number of QD emitters the inter-emitter coupling mediated by the cavity field can have a strong influence on the photon statistics of the emitted light as well as on the laser-threshold properties [Leymann et al., 2015]. The investigations are based on the fully quantum-mechanical theory presented in the first section of chapter 5, which is extended by the inclusion of inter-emitter correlations. It is shown that for typical emitter numbers of current state-of-the-art devices ( $\sim 20 - 100$ ) [Lermer et al., 2013, Strauf and Jahnke, 2011] radiation-field induced inter-emitter coupling can be crucial for the system to reach the lasing regime. Since the developed microscopic theory is scalable, the influence of the system size i.e. the emitter number can be studied. In the limit of large emitter numbers the influence of the inter-emitter coupling diminishes and the results agree with the ones obtained by former theories neglecting the inter-emitter coupling. The inter-emitter correlations suppress the spontaneous emission below the threshold and enhance the emission above the threshold. The superradiantly enhanced intensity jump at the threshold can lead to an underestimation of the  $\beta$ -factor. The presented effects are interpreted in terms of symmetric and antisymmetric Dicke states [Garraway, 2011]. The results demonstrate that in QD nanolasers the picture of independent emitters breaks down and these devices have to be regarded as coherently correlated quantum systems.

The last **Chapter 7** concludes the thesis, discusses open questions, and proposes new research projects.

# Chapter 2

## Basic aspects of the Theory of Light-Matter Interaction in Semiconductors

The quantum mechanical description of the light-matter interaction in semiconductor nano-structures is accomplished in several steps, where each step is a research field of its own. In this introductory overview the steps that are not in the focus of this thesis are only sketched. In the first step the single-particle states of the electronic carriers need to be determined. To accomplish this, one has to find solutions of the Schrödinger equation for the wave function of the non-interacting carriers. In a second step the mode functions of the electromagnetic field without the active material need to be determined by solving Maxwell's equations. Within the framework of the canonical quantization the single-particle states and the mode functions are used in the next step to calculate the matrix elements of the full many-particle Hamiltonian describing the interacting system. To facilitate the calculations involving quantum dots (QDs) embedded in a dense semiconductor environment one needs to separate the Hilbert space into a system and an environment part, and reduce the dynamical calculations to the system.

### 2.1 Electronic and photonic single-particle states

A very accurate framework to determine the single-particle states of carriers confined to semiconductor nano-structures are tight-binding models [Singleton, 2001, Sheng et al., 2005, Schulz and Czycholl, 2005], where the precise structure of the atomic lattice forming the QD enters the calculation to determine the confined states. For a simpler description one can start with the single-particle states and the band structure of the corresponding bulk material [Singleton, 2001, Chelikowsky and Cohen, 1976]. The single-particle states of the bulk material can be used to find the confined states introduced by the QD. For GaAs and other zinc-blende materials with a direct band gap, semi-empirical methods provide good agreement with more accurate methods [Sheng et al., 2005], given that the QD extent becomes not too small (diameter  $\gtrsim 12\text{nm}$ ) so that the influence of the precise atomic structure is irrelevant compared to the global shape. Representative for these kind of continuum

methods are the  $\mathbf{k} \cdot \mathbf{p}$ -model [Haug and Koch, 2004, Sheng et al., 2005] and the envelope-function approach [Haug and Koch, 2004] which will be sketched in the following.

In systems with a direct band gap in the optical region of the spectrum the part of the Brillouin-zone, which is relevant for optical transitions, lies around the extrema of its band structure. Figure 2.1 shows the band structure of GaAs, where the extrema are located at the  $\Gamma$ -point. Around the  $\Gamma$ -point the band structure can be approximated by parabolic functions. By this reasoning one can describe the carriers as quasi-free particles with an effective mass  $m_{\text{eff}}^\lambda$  that depends on the curvature of the corresponding band, where  $\lambda$  is the corresponding band index. According to the Bloch-theorem the carrier wave functions for the bulk material can be expressed by plane waves multiplied with functions  $u_{\mathbf{k}}^\lambda(\mathbf{r})$  with the same periodicity as the crystal lattice and  $\mathbf{k}$  being the wave vector. The discrete translational symmetry of the system is broken by the QD that introduces an effective potential  $U_{\text{QD}}(\mathbf{r})$  that varies only slowly over one unit cell. In the envelope function approximation the plane waves, valid for the periodic bulk material, are substituted by slowly varying envelope functions  $\zeta_\nu^\lambda(\mathbf{r})$ . The ansatz for the carrier wave function is the lattice-periodic Bloch-function  $u_{\mathbf{k}}^\lambda(\mathbf{r})$  times the envelope function  $\zeta_\nu$

$$\psi_\nu^\lambda(\mathbf{r}) = \zeta_\nu^\lambda(\mathbf{r})u_{\mathbf{k} \approx 0}^\lambda(\mathbf{r}), \quad (2.1)$$

where  $\nu$  stands for the quantum numbers specifying the confined state. The envelope

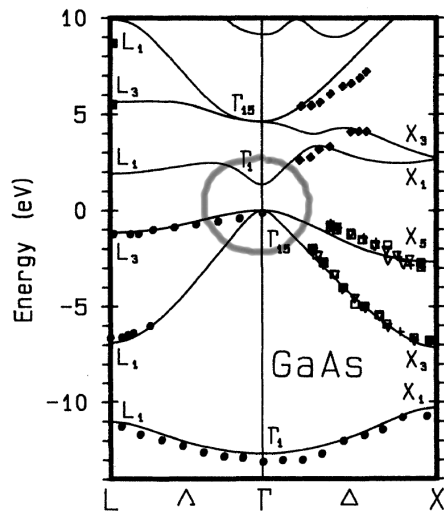


Figure 2.1: Band structure of GaAs taken from Ref. [Rohlfing et al., 1993]. The gray circle marks the area relevant for optical transitions.

function can be found by solving the effective single-particle Schrödinger equation

$$\left[ \frac{-\hbar^2}{2m_{\text{eff}}^\lambda} \Delta + U_{\text{QD}}(\mathbf{r}) \right] \zeta_\nu^\lambda(\mathbf{r}) = \varepsilon_\nu^\lambda \zeta_\nu^\lambda(\mathbf{r}), \quad (2.2)$$

with the effective mass and the QD potential. For lens shaped QDs (like the ones shown in Fig. 1.3) the potential in the direction orthogonal to the growth direction

can be approximated by a two dimensional harmonic potential [Wojs et al., 1996, Baer et al., 2004, Nielsen et al., 2004, Teichmann et al., 2013]. In growth direction the strong confinement by the QD and the wetting layer allows for a simple description with a one dimensional potential well. In this case the separation ansatz

$$\zeta_\nu(\mathbf{r}) = \varphi_n(z)\phi_l(\mathbf{r}_\perp) \quad (2.3)$$

is valid, where  $\varphi(z)$  is confined by the potential well in growth direction and  $\phi(\mathbf{r}_\perp)$  is confined by the two-dimensional harmonic potential in the plane. The energetic difference between the sub-bands  $n$  is large compared to the optical energies ( $1eV \gg 50meV$ ) [Wojs et al., 1996] so that a restriction to the first sub-band is justified. The cylindrical symmetry of the QDs implies to classify the confined carrier states by their angular-momentum and spin encoded in the quantum number  $\nu$ . In this thesis, the simple case of QDs with two confined states for electrons and holes is considered [Gies et al., 2011], with the quantum numbers  $s, p$ . For a fixed spin direction the  $s$ -state is non degenerated and the  $p$ -state is twofold degenerated.

With the single-particle states one can construct the field operators

$$\hat{\Psi}(t, \mathbf{r}) = \sum \hat{a}_{\lambda, \nu}(t) \psi_\nu^\lambda(\mathbf{r}), \quad (2.4)$$

where the  $\hat{a}_{\lambda, i}^{(\dagger)}$  are the fermionic annihilation (creation) operators<sup>1</sup> obeying the anti-commutation relations used for canonical quantization [Schwabl, 2008, Mahan, 2000]. To obtain also a quantum mechanical description of the light field, a similar approach as for the electronic Hamiltonian has to be chosen. First the wave equation for the vector potential in Coulomb-gauge

$$\left[ \Delta + \frac{n(\mathbf{r})}{c^2} \frac{\partial^2}{\partial t^2} \right] \mathbf{A}(\mathbf{r}, t) = 0 \quad (2.5)$$

has to be solved, where  $n(\mathbf{r})$  is the refractive index of the resonator and the surrounding material. The field is then expanded into eigenmodes  $\mathbf{M}_\xi$  with a fixed frequency  $\omega_\xi$

$$\mathbf{A}(\mathbf{r}, t) = \sum [b_\xi(t)\mathbf{M}_\xi(\mathbf{r}) + b_\xi^*(t)\mathbf{M}_\xi^*(\mathbf{r})], \quad (2.6)$$

where  $\xi$  contains the polarization direction and the wave vector. When the mode functions are determined, one can express the electromagnetic field operator, within the framework of the canonical quantization, in terms of bosonic annihilation and creation operators

$$\hat{\mathbf{A}}(\mathbf{r}, t) = \sum \left[ \hat{b}_\xi^\dagger(t)\mathbf{M}_\xi^*(\mathbf{r}) + \hat{b}_\xi(t)\mathbf{M}_\xi(\mathbf{r}) \right], \quad (2.7)$$

where the  $\hat{b}_\xi^{(\dagger)}$  obey the canonical bosonic commutation relations.

---

<sup>1</sup>The cumbersome notation, where an operator is indicated by a hat on top of its corresponding letter, is only used in this chapter.

## 2.2 Many-particle Hamiltonian

With the field operators one can construct the full Hamiltonian of the interacting system. The many-particle Hamiltonian consists of several parts: The Hamiltonian of the free carriers

$$\hat{H}_0 = \int d^3r \hat{\Psi}^\dagger(t, \mathbf{r}) \left[ \frac{\hbar^2}{2m} \Delta + U(\mathbf{r}) \right] \hat{\Psi}(t, \mathbf{r}), \quad (2.8)$$

since the single-particle problem is already solved the free Hamiltonian is a diagonal sum<sup>2</sup>

$$\hat{H}_0 = \sum \varepsilon_\nu^\lambda \hat{a}_{\lambda,\nu}^\dagger \hat{a}_{\lambda,\nu} \quad (2.9)$$

over the creation and annihilation operators with the single-particle energies  $\varepsilon_\nu^\lambda$ . The Coulomb Hamiltonian can be constructed in a similar fashion only that here two carrier field operators are involved

$$\hat{H}_{\text{Coul}} = \int d^3r \int d^3r' \hat{\Psi}^\dagger(t, \mathbf{r}) \hat{\Psi}^\dagger(t, \mathbf{r}') V(\mathbf{r} - \mathbf{r}') \hat{\Psi}(t, \mathbf{r}') \hat{\Psi}(t, \mathbf{r}), \quad (2.10)$$

with  $V(\mathbf{r}) = e^2/(4\pi\epsilon_0\epsilon|\mathbf{r}|)$  being the Coulomb-energy with the electron charge  $e$  and the dielectric function  $\epsilon_0\epsilon$ . Like the free particle Hamiltonian the Coulomb Hamiltonian can be expressed by creation and annihilation operators

$$\hat{H}_{\text{Coul}} = \sum V_{\nu\nu'\lambda'\lambda}^{\lambda\lambda'} \hat{a}_{\lambda,\nu}^\dagger \hat{a}_{\lambda',\nu'}^\dagger \hat{a}_{\lambda',\nu'} \hat{a}_{\lambda,\nu}, \quad (2.11)$$

and the corresponding matrix elements are

$$V_{\nu\nu'\lambda'\lambda}^{\lambda\lambda'} = \int d^3r \int d^3r' \psi_\nu^{\lambda*}(\mathbf{r}) \psi_{\nu'}^{\lambda'*}(\mathbf{r}') V(\mathbf{r} - \mathbf{r}') \psi_{\nu'}^{\lambda'}(\mathbf{r}') \psi_\nu^\lambda(\mathbf{r}), \quad (2.12)$$

where the single-particle wave functions enter. The free part of the photon Hamiltonian can be written as

$$\hat{H}_{\text{ph}} = \sum \hbar\omega_\xi \left( \hat{b}_\xi^\dagger \hat{b}_\xi + \frac{1}{2} \right). \quad (2.13)$$

The interaction of the carriers with the transverse electric field (in Coulomb gauge)  $\mathbf{E}_T = -\frac{\partial}{\partial t} \mathbf{A}$  can be described in dipole approximation [Garrison and Chiao, 2014, Wiersig, 2007] since the mode function of the electromagnetic field varies only slightly over the extend of the QD  $\mathbf{M}_\xi(\mathbf{r}) \approx \mathbf{M}_\xi(\mathbf{r}_0)$ , with  $\mathbf{r}_0$  being the location of the QD

$$\hat{H}_D = \int d^3r \hat{\Psi}^\dagger(t, \mathbf{r}) \left[ -e\mathbf{r} \hat{\mathbf{E}}_T(\mathbf{r}_0) \right] \hat{\Psi}(t, \mathbf{r}). \quad (2.14)$$

With the dipole matrix elements

$$g_{\xi\nu}^{\lambda\lambda'} = \int d^3r \psi_\nu^{\lambda*}(\mathbf{r}) e\mathbf{r} M_\xi(\mathbf{r}) \psi_\nu^{\lambda'}(\mathbf{r}) \quad (2.15)$$

---

<sup>2</sup>We omit the specification of the summation indices in this chapter, since in all cases the summation has to be performed over all occurring indices.

one can express the dipole Hamiltonian

$$H_D = \sum [g_{\xi\nu\iota}^{\lambda\lambda'} \hat{a}_{\lambda,\nu}^\dagger \hat{a}_{\lambda',\iota} (\hat{b}_\xi^\dagger + \hat{b}_\xi) + g_{\xi\nu\iota}^{*\lambda\lambda'} \hat{a}_{\lambda',\iota}^\dagger \hat{a}_{\lambda,\nu} (\hat{b}_\xi^\dagger + \hat{b}_\xi)], \quad (2.16)$$

in terms of bosonic and fermionic creation and annihilation operators. Note that  $E_\xi = \sqrt{\hbar\omega/2\epsilon_0\epsilon\bar{V}_\xi}$  is the vacuum amplitude where the mode volume  $V_\xi$  is contained in the mode functions. A more graphic interpretation of the dipole matrix elements is that it measures the overlap of the mode function of the light field in the cavity with the single-particle wave functions of the confined carriers in the states  $|\psi_\nu^\lambda\rangle$  and  $|\psi_\iota^{\lambda'}\rangle$ . Throughout this thesis the approximation of equal envelopes for the wave functions of the conduction- and the valence-carriers is used. Therefore only diagonal transitions between the angular momentum states are supported by the dipole Hamiltonian. The dipole matrix elements read  $g_{\xi\nu\iota}^{\lambda\lambda'} = \mathbf{M}_\xi(\mathbf{r}_0)d_{\lambda\lambda'}\delta_{\nu\iota}$ , here  $\mathbf{r}_0$  is the location of the QD and  $d_{\lambda\lambda'}$  are the interband matrix elements (see e.g. [Baer et al., 2006] and references therein).

The harmonic oscillations of the bulk material ions can be described by a field theory of non-interacting Bosons [Mahan, 2000], where the fundamental excitations are called phonons. In materials with a multi-atom basis the phonon-dispersion relation splits into two main branches: the acoustic and the optical phonons. The acoustic phonons have a linear dispersion relation for small wave vectors. Acoustic phonons result from a coherent movement of ions out of their equilibrium position in the lattice. The high frequency optical phonons have an approximately constant frequency in the proximity of the  $\Gamma$ -Point and result from the movement of at least two different ions against each other within the unit-cell [Czycholl, 2008].

The phonons interact with the carriers since the carriers receive a change in their potential energy caused by oscillatory motion of the ions out of their equilibrium position. The Hamiltonian interaction of the phonons with the carriers could in principle be described analogous to the light matter interaction [Ashcroft and Mermin, 1976]. The interaction with phonons is next to the Coulomb scattering the relevant mechanism for dephasing of the optical transitions in semiconductor QDs [Hoyer et al., 2003] and inhibit e.g. the formation of polarization entangled photons generated by a QD cavity system [Carmelet al., 2010a]. There are countless ways to take the phonon interaction into account ranging from exact methods [Carmelet al., 2010b] over expressions for the phonon self-energy [Hughes et al., 2011] derived from the independent boson model [Mahan, 2000] to phenomenological dephasing terms directly added to the EoM [Gies et al., 2007]. In this thesis we are predominantly interested in light-matter interaction and Coulomb effects and restrict ourselves to a Markovian treatment of the phonons. The phonons are described as an external bath that interacts with the carriers confined to the QD. In this approach no additional degrees of freedom for the phonons need to be included into the calculations but the approach still goes beyond the simple addition of phenomenological dephasing terms to the EoM. A description of the basic principles is given in the next section.

## 2.3 Equation of motion for the reduced density operator

Semiconductor QDs are located in a dense environment and the discrete electronic states confined to QDs are coupled to a (quasi)continuum of states in the wetting layer and the bulk material. To be able to include many-particle correlations into our theory we need to restrict the size of the systems Hilbert space and treat the (quasi)continuum states as a reservoir. The Hamiltonian describing the system and reservoir consists of three parts

$$\hat{H} = \hat{H}_{\text{System}} + \hat{H}_{\text{Reservoir}} + \hat{H}_{S\mathcal{R}},$$

the system we are interested in, in this case the electrons and holes confined to the QD and the (cavity-)photons, the reservoir and the system-reservoir interaction Hamiltonian  $\hat{H}_{S\mathcal{R}} = \sum \hat{L}_i \hat{I}_i$ . Where the  $\hat{L}_i : \mathcal{S} \mapsto \mathcal{S}$  are the operators evoking a process in the system and  $\hat{I}_j : \mathcal{R} \mapsto \mathcal{R}$  are the corresponding ones in the reservoir. The dynamics of the complex system is described by the von-Neumann equation for the full density operator  $\hat{\rho}$

$$\frac{d}{dt}\hat{\rho} = \frac{i}{\hbar} [\hat{\rho}, \hat{H}].$$

We are only interested in expectation values of system operators  $\hat{A} : \mathcal{S} \mapsto \mathcal{S}$ , and define the reduced density operator  $\text{Tr}^{\mathcal{R}}(\hat{\rho}) = \hat{\rho}_{\mathcal{S}}$  by tracing over all reservoir states and calculate all desired expectation values with this reduced density operator  $\langle \hat{A} \rangle = \text{Tr}(\hat{\rho}\hat{A}) = \text{Tr}^{\mathcal{S}}(\text{Tr}^{\mathcal{R}}(\hat{\rho})\hat{A}) = \text{Tr}^{\mathcal{S}}(\hat{\rho}_{\mathcal{S}}\hat{A})$ .

To obtain a simple dynamical equation for  $\hat{\rho}_{\mathcal{S}}$  the reservoir is treated in Born-Markov approximation meaning that the reservoir  $\mathcal{R}$  with a temperature  $T$  is very large compared to the system and is therefore unaffected by the dynamics of the system  $\mathcal{S}$

$$\hat{\rho}(t) \approx \hat{\rho}_{\mathcal{S}}(t) \hat{\mathcal{R}}_0(T) + \mathcal{O}(\overline{\hat{H}_{S\mathcal{R}}})$$

and the timescales of the reservoir and the system dynamics can be separated. On the much slower timescale of the system the reservoir correlations decay instantly

$$\left\langle \hat{I}_i(t) \hat{I}_j(t') \right\rangle_{\mathcal{R}} \sim \delta(t - t').$$

These assumptions allows to derive the von Neumann-Lindblad equation (vNL)

$$\frac{d}{dt}\hat{\rho}_{\mathcal{S}} = -\frac{i}{\hbar} [\hat{H}_{\mathcal{S}}, \hat{\rho}_{\mathcal{S}}] + \sum \hat{\lambda}_{\nu\nu'} \left( 2\hat{L}_{\nu}^{\dagger}\hat{\rho}_{\mathcal{S}}\hat{L}_{\nu'} - \hat{L}_{\nu}^{\dagger}\hat{L}_{\nu'}\hat{\rho}_{\mathcal{S}} - \hat{\rho}_{\mathcal{S}}\hat{L}_{\nu}^{\dagger}\hat{L}_{\nu'} \right),$$

for the reduced density operator  $\hat{\rho}_{\mathcal{S}}$ ; for details see [Carmichael, 1999]. More details on the concept and consequences of the vNL equation is given in [Breuer and Petruccione, 2002] and it is worth mentioning that the vNL equation is the most general trace preserving map that generates a time evolution of the density operator. The dynamics of the vNL equation are in general not reversible since the



differences between states of the reservoir are ignored due to the tracing over all possible reservoir states. This contracting effect of the dynamics in the system and the tremendous reduction of the computational afford this reduced density matrix approach provides is illustrated in Fig. 2.2. Instead of generating the dynamics in the large space of the system and reservoir ( $\mathcal{S} \otimes \mathcal{R}$ ) and tracing over the reservoir at the end of the dynamics one can trace over the reservoir in the beginning and generate the dynamics in the much smaller space  $\mathcal{S}$ .

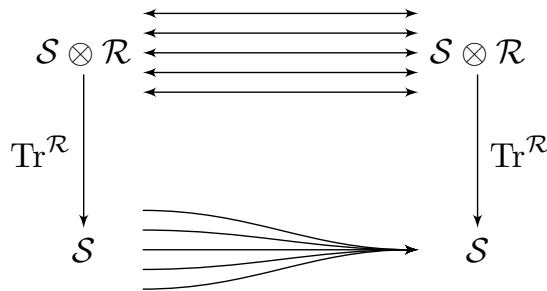


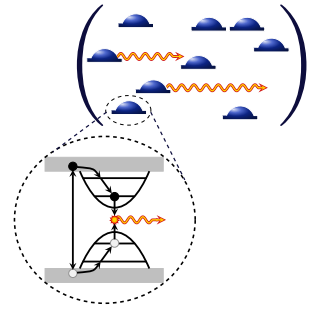
Figure 2.2: Illustration of the contraction of various initial conditions under the influence of a large reservoir. A similar illustration can be found in [Breuer and Petruccione, 2002].



# Chapter 3

## Single Quantum Dot

## Photoluminescence into free-space



To describe the dynamics of an interacting system an equation of motion (EoM) based theory for the description of light emission from a multi-level semiconductor quantum dot (QD) is presented. The theory accounts for electronic excitations in presence of the Coulomb interaction, leading to multi-exciton states, and their coupling to the quantized electromagnetic field.

The two key aspects of this chapter concern (i) the combination of an exact treatment of the electronic degrees of freedom with an approximate approach for the photonic degrees of freedom that is based on the cluster expansion (CE), and (ii) the consistent incorporation of scattering and dephasing due to the coupling to delocalized electronic states and phonons into the EoM via Lindblad terms. Differences to previously used theories are discussed and results of the theory are shown for free-space emission, where multi-exciton spectra are shown, and for emission into a single high- $Q$  cavity mode. In the latter case, a full solution of the von-Neumann Lindblad equation is used to benchmark the proposed theory, which we term “finite-size hierarchy” (FSH) method.

In parts this chapter is published in [Florian et al., 2013a]. The basic theoretical concepts for this work were mainly developed in discussions between M. Florian and H.A.M. Leymann, the EoM were derived by H.A.M. Leymann, the numerical integrating of the equations of motion and the solution of the von-Neumann Lindblad equation was mainly performed by M. Florian and all authors of [Florian et al., 2013a] discussed the results.

### 3.1 Cluster expansion for semiconductor systems

Semiconductor heterostructures [Alferov, 2001] are of central importance in the design of today’s optoelectronic devices with a wide application range in light emitters, detectors, and quantum information technology. Quantum dots play an important role as active material in semiconductor lasers and quantum light emitters [Bimberg et al., 1999, Strauf and Jahnke, 2011, Chow et al., 2011, Hendrickson et al., 2005, Strauf et al., 2006, Reitzenstein et al., 2006a, Peter et al., 2005]. For the development of microscopic models, the CE technique [Baumann and Hegerfeldt,

1985, Schoeller, 1994, Kira et al., 1999, Hoyer et al., 2003, Gies et al., 2007, Feldtmann et al., 2006, Baer et al., 2006, Schwab et al., 2006, Berstermann et al., 2007, Fricke, 1996b, Fricke, 1996a, Fricke et al., 1997, Ulrich et al., 2007, Krügel et al., 2006] has been successfully used to address correlation effects due to various many-body interactions. In semiconductors, many-body effects are present due to carrier-photon and carrier-carrier Coulomb interaction, as well as the interaction between carriers and phonons. The idea of the CE technique is to formulate EoM for correlation functions (CFs) up to a given order  $N$ , and to express all expectation values of interest in terms of these CFs. The underlying assumption is the presence of a large Hilbert space for the many-body excitations, so that the configuration averages render higher-order correlations increasingly unimportant. The CE technique has initially been applied to systems with many degrees of freedom, where the number of possible electronic configurations by far exceeds the highest number of considered  $N$ -particle correlations (typically  $N = 2, 3, 4$ ). This included, for example, photoluminescence [Kira et al., 1998], resonance fluorescence [Kira et al., 1999], exciton formation dynamics [Hoyer et al., 2003] in quantum-well systems, quantum dynamics of condensed Bose gases [Köhler and Burnett, 2002], and spin dynamics of ferromagnetic systems [Kapetanakis and Perakis, 2008].

More recently, applications have been extended to QD-based systems, where the CE method has successfully been used to study quantum-optical and related effects, like photon anti-bunching and coherence properties of the light emission [Ulrich et al., 2007, Gies et al., 2007, Richter et al., 2009, Carmele et al., 2010b], coherent emission of cavity phonons [Kabuss et al., 2012, Kabuss et al., 2013], sequential build-up of quantum-optical correlations in a semiconductor QD system [Mootz et al., 2012], quantum spectroscopy [Kira et al., 2011], as well as the influence of Coulomb-induced carrier correlations [Baer et al., 2006, Feldtmann et al., 2006, Schwab et al., 2006]. In QDs, the carrier confinement results in a small number of localized states, which contrasts the situation in quasi-continuous systems like quantum wells. Both, in theory and experiment [Beirne et al., 2007], QDs with only a few or even a single localized electron state have been considered.

It is one aim of this chapter to discuss the implications of the system-size limitation to the application of the CE and to propose a new way to describe systems, in which the small size of the electronic Hilbert space leads to strongly enhanced correlations. In this chapter the methods are developed with the direct application on the single QD photoluminescence in mind. A general formulation of the CE and techniques beyond that can be found in chapter 4. The single-QD case is often addressed with methods from atomic quantum optics, where the emitter is represented by a few-level system. The non-perturbative interaction with a high-Q cavity mode via the dipole Hamiltonian and the perturbative interaction with a continuum of free-space modes via Lindblad terms can be treated by directly solving the von-Neumann Lindblad (vNL) equation for the density matrix of the electronic system and the cavity mode [Mu and Savage, 1992]. This requires the underlying Hilbert space to be small enough and is currently only feasible for a single or very few emitters. Examples for applications to single-QD systems are [Troiani et al., 2006, del Valle et al., 2009, Ritter et al., 2010, Gies et al., 2011]. The vNL dynamics are ideal to study multi-exciton effects, since all the various excitonic configurations

can be distinguished by the theory. An explicit use of this ability to distinguish multi-exciton configurations from one another was made in a study of the influence of multi-exciton effects on the efficiency of carrier scattering [Steinhoff et al., 2012]. When considering explicitly the case of many individual emitters or the emission into many modes, however, the size of the Hilbert space precludes direct calculations of the many-particle density matrix, and one has to retreat to approximate many-body methods, like the CE technique.

Another central point addressed in this chapter is the consistent description of scattering and dephasing in the EoM approach. QDs are embedded systems and coupled to continuum states of the surrounding material. The Coulomb interaction and the coupling to LO-phonons leads to efficient carrier scattering processes between localized and delocalized states, feeding carriers into the QD after off-resonant excitation into the continuum states of the barrier material, as well as being a source of dephasing. A Hamiltonian description of these scattering processes is naturally possible within an EoM approach, but practically challenging [Carmelet al., 2010b, Hoyer et al., 2003]. More often, scattering and dephasing were accounted for phenomenologically by adding constant rates to the EoM. Especially for equations describing the dynamics of higher-order CFs, this may lead to inconsistencies and produce artifacts, such as heating [Hoyer et al., 2003]. In quantum optics one typically discriminates between the system and environmental degrees of freedom, and treats the interaction of the system with the environment via Lindblad terms [Lindblad, 1976] that are added to the von-Neumann equation and the equation is consequently called vNL equation. As we show, this can be carried over to an EoM based approach. The carrier dynamics in QDs naturally separates into the system, represented by the localized states, and the environment, provided by the quasi-continuum of delocalized states. Then the Coulomb and light-matter interaction are fully accounted for the localized QD states, while the interaction processes with the continuum states are described via Lindblad terms. These terms and the corresponding rates can be obtained with standard many-body techniques [Breuer and Petruccione, 2002, Steinhoff et al., 2012, Roy and Hughes, 2011, Hohenester, 2010]. The result is a consistent formulation of scattering and dephasing that is free of the problems associated with the phenomenological approaches.

We begin by addressing the EoM technique for the carrier system, before we introduce and classify mixed-operator CFs that are subject to different interactions. The “finite-size hierarchy” (FSH) method is introduced, in which we combine an exact treatment of the carrier degrees of freedom with an approximate CE approach for the arising hierarchy in the photon operators. In Section 3.3 we specify the nature of the environment coupling and the inclusion in the theoretical formalism. In order to apply the theoretical framework in the following sections, a specific QD model is introduced in Section 3.4. We derive EoM for the Hamiltonian time evolution of the QD carriers, as well as the dissipative interaction with carriers in delocalized states. Section 3.5 is devoted to emission into a continuum of free-space modes. Here we discuss how carrier correlations give rise to multi-excitonic effects in the emission spectra, and how the various scattering and dephasing processes manifest themselves in the linewidths of the various emission peaks. A comparison with the conventional CE technique reveals insight into the physical representation of the system by a

limited number of CFs. Numerical results for the emission of a single QD in a microcavity are presented in Section 3.6. For this system, we are able to compare the approximate treatment of the system dynamics in terms of the conventional CE method to an exact solution obtained from the FSH and von-Neumann equation. This comparison illustrates the impact of the truncation at different orders in the hierarchy of photon operators and demonstrate the applicability of the FSH method.

## 3.2 Many-body treatment of the embedded QD system

QDs are embedded systems and their electronic single-particle states are coupled to those of the surrounding environment by the Coulomb interaction and the interaction with LO phonons. It is important to stress that correlations amongst QD carriers are dominated by the interaction within the dot, as well as, e.g. in the presence of a resonator, by the interaction with photons. Based on this, we treat the localized electronic degrees of freedom explicitly, fully accounting for the Coulomb interaction amongst QD carriers and their light-matter interaction. In this section we focus on the system dynamics and its formulation in the von-Neumann and EoM approaches. The coupling of the environment states to the system dynamics via Lindblad terms is discussed in Section 3.3.

The system dynamics is determined by the von-Neumann equation

$$\frac{d}{dt}\rho = -i[H, \rho] , \quad (3.1)$$

for the density operator ( $\hbar = 1$ ). Here, we consider the free electronic contributions to the Hamiltonian  $H$ , as well as the Coulomb interaction and subsequently in Sec. 3.2.2 also the dipole interaction. The time-dependent solution of Eq. (3.1) then includes the interaction of all possible configurations. The electronic Hilbert space is finite and limited by the possible number of carriers that the QD system can accommodate. In (quasi-) continuous systems this limitation is merely formal. In a QD with only few confined states, however, the limitation is perceivable and may even allow for a direct solution of Eq. (3.1), see, e.g., the Refs. [del Valle et al., 2009, Troiani et al., 2006] for a small and [Gies et al., 2011, Gies et al., 2012] for a large number of configurations or even for a small number of QDs [Florian et al., 2013a].

By suitable tracing of the many-body density matrix, Eq. (3.1) can be rewritten into a hierarchy of EoM for EVs, in which single-particle EVs are coupled to two-particle EVs, and so on. The hierarchy of coupled equations is limited by the finite size of the Hilbert space that introduces a 'natural' truncation. This can also be understood by considering the fact that only those normal-ordered operator averages, addressing up to the maximum possible number of carriers in the system, can be different from zero, as the consecutive application of a number of creation or annihilation operators that exceeds the number of possible single-particle states must give a vanishing contribution. As long as no further approximations are introduced, both the density-matrix and the EoM approaches are equivalent. We will elaborate more

on the equivalence of various approaches in chapter 4 where the 'natural' truncation of the hierarchy due to a finite Hilbert space is associated to the truncation operator  $\Delta_{\langle N \rangle}$  (see Eq. (4.7)),

. For a system with mixed hierarchies in carrier and photon operators, this equivalence will be used to establish the link between the 'exact' von-Neumann-based treatment for the electronic degrees of freedom, for which we introduce the name "finite-size hierarchy" (FSH) method, and the approximate CE method, in which the electronic hierarchy is truncated typically at an order that is much lower than the size limitation of the Hilbert space.

### 3.2.1 Equation-of-motion formulation for the electronic degrees of freedom

We begin by schematically formulating the hierarchy of EoM for a system that can accommodate up to  $N_{\max}^{c,v}$  conduction- and valence-band carriers per spin direction. Since the successive application of  $N_{\max}^c + 1$  conduction-band electron or  $N_{\max}^v + 1$  valence-band electron annihilation operators yields zero, an automatic truncation of the hierarchy is implied. To achieve a simplification of the following discussion, we consider from here on equal numbers of confined states in both bands, so that the highest operator average that can differ from zero contains  $2(N_{\max}^c + N_{\max}^v) = 4N_{\max}$  carrier operators.

In the following we embrace the formulation of the conventional CE, where CFs are used instead of operator EVs. As long as the hierarchy of equations is not terminated at an order below its 'natural' truncation, both formulations are equivalent. A CF of the order  $N$  is defined as

$$\delta(N) = \langle N \rangle - \delta(N)_F, \quad (3.2)$$

where  $\delta(N)_F$  represents products of all possible factorizations of the operator expectation value  $\langle N \rangle$  into CFs of orders smaller than  $N$ <sup>1</sup>. The order  $N$  is defined as half the number of carrier operators. For example, occupation probabilities of single-particle states<sup>2</sup>  $\langle c_i^\dagger c_i \rangle$  and  $\langle v_i^\dagger v_i \rangle$  (for the notation see Appendix A.1) are of first order (in former approaches called singlets) that represent uncorrelated entities,

$$\delta\langle 1 \rangle \equiv \langle 1 \rangle. \quad (3.3)$$

Examples for CFs of the order  $N = 2$  (in former approaches called doublets) are  $\delta(c_i^\dagger c_j^\dagger c_k c_l)$  or  $\delta(c_i^\dagger v_j^\dagger c_k v_l)$ .

The hierarchy defined by Eqs. (3.2)–(3.3) terminates due to the discussed limitation in operator averages to  $2N_{\max}$  carrier operators and is represented by the *boundary condition*

$$\delta(N) = -\delta(N)_F \quad \text{if } N > N_{\max}. \quad (3.4)$$

For  $N = N_{\max} + 1$  Eq. (3.4) terminates the coupling to higher EV and ensures a correct treatment of the finite carrier system, so that indeed the formulation in

---

<sup>1</sup>In case of fermionic operators, a sign change is required if an odd number of permutations is necessary to regain normal ordering.

<sup>2</sup>Note that due to the incoherent excitation, all EV of the form  $\langle v_i^{(\dagger)} \rangle$  vanish.

terms of dynamical equations for CFs is equivalent to a solution of Eq. (3.1) for the corresponding finite set of basis configurations (see chapter 4).

When the electronic Hilbert space, and correspondingly the number of electronic degrees of freedom is large, an inclusion of CFs up to this level is neither possible nor necessary. This defines the regime of applicability of the CE method, where suitable approximations are based on a truncation of the hierarchy at a level much lower than  $N_{\max}$ , realized by setting all CFs above a certain cutoff  $N_{\text{trunc}}$  to zero:

$$\delta(N) = 0 \quad \text{if } N > N_{\text{trunc}} . \quad (3.5)$$

In what comes next, it is important to emphasize that this procedure introduces two separate ideas to justify the approximations. Firstly, the influences of correlated processes involving more than  $N_{\text{trunc}}$  carriers are neglected. Secondly, for  $N > N_{\max}$  there is a contradiction between Eq. (3.4) and Eq. (3.5) in the sense that the latter formally violates the boundary condition due to the finite system size. We discuss the implications of both approximations in the following.

For an approximate treatment of carrier correlations in large systems, the order up to which  $N$ -particle correlations need to be calculated depends on the strength of dephasing processes on the one hand, and on the quantities of interest on the other. Scattering processes, introduced e.g. by the Coulomb- and LO-phonon interaction, are responsible for damping out correlation effects, and so are cavity losses that act on the photonic sub-system, see Sec. 3.2.2. Higher-order CFs are typically subject to stronger dephasing, so that their impact on the dynamics of lower-order quantities decreases with increasing  $N$ . Nevertheless, if correlation effects themselves are of interest, the corresponding CFs must be accounted for, and corrections due to the next higher order may be relevant even if the impact on lower orders is small. E.g., exciton formation is described by second-order CFs  $\delta(c_i^\dagger v_j^\dagger c_k v_l)$ . Their study therefore requires going beyond the first order.

The error introduced by the violation of the boundary condition (3.4) depends on the system size in relation to the order  $N_{\text{trunc}}$  at which the cutoff is performed, as well as on the strength of dephasing processes in the system that assist in damping out correlations. In large systems, where the allowed number of carriers exceeds the cutoff by orders of magnitude, the effect of violating the boundary condition at the highest order is imperceptible. In QDs with only few localized states, the situation may be entirely different, and this is the point we are addressing: If the cutoff  $N_{\text{trunc}}$  imposed by an approximative treatment is close to the 'natural' cutoff  $N_{\max}$ , the error made in replacing Eq. (3.4) by Eq. (3.5) is more likely to propagate into those CFs that are kept and become significant. In terms of the underlying physics, the restriction to a few-particle system enhances higher-order carrier correlations. In Section 3.4 we will focus on a particular QD model with two confined states for electrons and holes and show that the CE method is in fact not applicable to the electronic subsystem, and the exact description including Eq. (3.4) must be used instead.

### 3.2.2 Many-body description for mixed expectation values

We now turn to the case that a hierarchy arises not only in the electronic degrees of freedom, but also due to other interactions that may explicitly appear in the



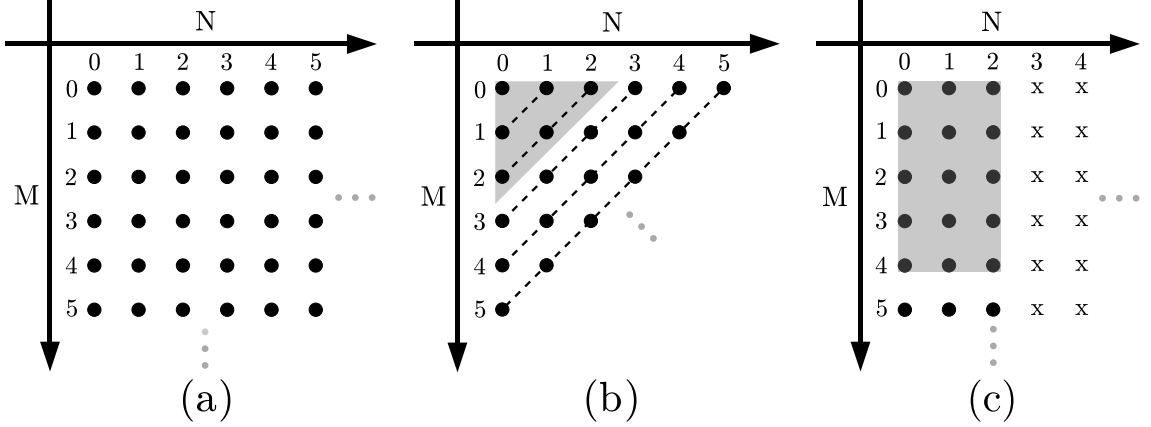


Figure 3.1: (a) Illustration of the classification of mixed CFs  $\delta(N, M)$  according to the number of carrier ( $2N$ ) and photon ( $M$ ) operators (represented by dots). (b) Classification and truncation employed by the conventional CE method. Mixed CFs are treated by a single hierarchy of order  $N + M$ . The shaded area encloses those correlations up to the doublet level  $(N + M)_{\text{trunc}} = 2$ . (c) Situation found in a system where the number of electrons and holes is limited to two. Then the hierarchy of carrier operators closes 'naturally' on the four-operator level  $N_{\max} = 2$  and is, in principle, not restricted in the number of photon operators  $M$ . As an example, the shaded area shows the necessary CFs for  $M_{\text{trunc}} = 4$ .

Hamiltonian, like the coupling to photons or phonons. Extra thought must be given how to classify the order and how to perform the truncation of the arising hierarchies of mixed-operator EVs.

As an example, consider the time derivative of a conduction band carrier and a photon annihilation operator with respect to the dipole Hamiltonian  $H_D$  (see Appendix A.1):

$$\frac{d}{dt} c_i |_{H_D} = - \sum_{\xi} g_{\xi} b_{\xi} v_i, \quad (3.6a)$$

$$\frac{d}{dt} b_{\xi} |_{H_D} = \sum_i g_{\xi}^* v_i^{\dagger} c_i. \quad (3.6b)$$

Two hierarchies are introduced, one in the photon operators and one in the carrier operators: In the EoM for a carrier operator (3.6a) an additional photon operator is added, and vice versa, a carrier transition  $v_i^{\dagger} c_i$  is associated with the derivative of a photon operator in Eq. (3.6b). Regarding the additional light-matter interaction, we introduce a classification of mixed CFs  $\delta(M, N)$ , containing  $M$  photon and  $2N$  carrier operators by the tuple of numbers  $(M, N)$ . Eq. (3.2) is generalized to

$$\delta(M, N) = \langle M, N \rangle - \delta(M, N)_F, \quad (3.7)$$

where the factorization  $\delta(M, N)_F$  contains all possible products of lower-order CFs of order  $(M', N')$  that meet the three criteria  $N' \leq N$ ,  $M' \leq M$ , and  $N' + M' < N + M$ . The classification is illustrated in Fig. 3.1(a), where each set of CFs of the order

$(M, N)$  is represented as a dot. This suggested classification scheme serves two purposes: On the one hand, it offers a clear-cut definition of the correlation effects included at each order, namely those involving  $N$  carriers and  $M$  photons. On the other hand, it provides a platform to treat the two hierarchies in a different fashion, which we discuss in detail below.

A different classification scheme has been used in the past and is typically associated with the CE method [Fricke, 1996b, Fricke, 1996a, Fricke et al., 1997, Kira et al., 1999]. There, mixed CFs  $\delta(M, N)$  are classified by a single number  $M + N$ , as schematically depicted in Fig. 3.1(b). It is based on the observation that the coupling of carriers and photons, provided by the dipole Hamiltonian, leads to the formal equivalence of a photon annihilation operator and an electron-hole-pair creation operator. Correlation functions with  $N + M = 1, 2, 3, 4, \dots$  have been termed singlets, doublets, triplets, quadruplets, and so on. As described for the electronic system in Sec. 3.2.1, a cutoff  $(N + M)_{\text{trunc}}$  is performed, and all higher-order CFs are approximated as zero in the fashion of Eq. (3.5),

$$\delta(M, N) = 0 \quad \text{if } N + M > (N + M)_{\text{trunc}} . \quad (3.8)$$

An illustration is given in Fig. 3.1(b), where the shaded area corresponds to those CFs kept up to the second order. The CE method based on this scheme has been used for systems, where the truncation was performed at an order much lower than the implicitly assumed size of the electronic subsystem (the photonic subsystem is, by nature, not limited) [Kira et al., 1999, Hoyer et al., 2003, Hoyer et al., 2004].

This brings us to the question how to formulate the hierarchy problem in systems where the electronic subsystem is limited to accommodate a small number of carriers, which leads to the definition of the *finite-size hierarchy (FSH) method* (a special case of the more general approach described in chapter 4). As we have discussed for the electronic subsystem in the absence of additional interactions in Sec. 3.2.1, the approximate treatment of the CE method introduces errors in the boundary condition that may require an exact treatment of the electronic degrees of freedom in a fashion analog to the von Neumann equation. For a system with mixed-operator CFs  $\delta(M, N)$ , the boundary condition (3.4) can be generalized to

$$\delta(M, N) = -\delta(M, N)_F \quad \forall N > N_{\text{max}} . \quad (3.9)$$

The exact treatment of electronic correlations requires taking all CFs  $\delta(M, N)$  up to  $N = N_{\text{max}}$  into account and to satisfy Eq. (3.9) at the highest level  $N = N_{\text{max}}$ . The photonic hierarchy is not limited and must be truncated at a manually introduced cutoff  $M_{\text{trunc}}$ . The order at which this approximation is performed depends on the quantities of interest, as well as on the relationship between correlation built-up and dephasing. A schematic illustration is found in Fig. 3.1(c), where the number of electrons and holes is restricted to  $N_{\text{max}} = 2$ , and the truncation is performed at the level of  $M_{\text{trunc}} = 4$  correlated photons.

Summarizing this section, starting from the general form of the von-Neumann equation, the treatment of an electronic system residing in a finite Hilbert space can be formulated as a closed set of EoM for CFs, fully representing the electronic degrees of freedom (FSH method). An additional hierarchy in the photon operators spoils the exact representation, as all electronic operator averages can appear with

additional photon operators. The hierarchy in terms of photon operators requires an approximate truncation in the fashion of the CE method. This is, however, uncritical and works very well in practice, as we will demonstrate in Sec. 3.6. A discussion of the manifestation of differences between the traditional CE and FSH methods is found in Sections 3.5 and 3.6.

### 3.3 Environment coupling: Treatment of scattering and dephasing processes

The localized states of self-assembled QDs are generally coupled to delocalized states of the surrounding semiconductor matrix material. In experiments and device applications, carriers are excited optically or electrically in these continuum states. The successive capture into the localized QDs states is mediated by scattering processes with carriers in the continuum, but also with lattice vibrations that are known to effectively exchange excess energy by emission/absorption of phonons [Seebeck et al., 2005, Zibik et al., 2004, Xu et al., 2002, Urayama et al., 2001]. Redistribution by scattering of carriers is always accompanied by dephasing. Dephasing of coherences and correlations in QD-based nanostructures is of central importance for the emission properties of devices.

The discrete nature of the localized states in QDs allows for the possibility to make a distinction between the QD system and its environment, where the dynamics of the first is fully accounted for by contributions to the system Hamiltonian, and the latter are treated in a system-bath approach. The purpose of Sec. 3.3.1 is the specification of both components and the description of the Lindblad formalism that is commonly used to model system-reservoir coupling within the vNL equation. This is carried over to the EoM approach for EoMs in Sec. 3.3.2 to provide a consistent platform to include scattering and dephasing contributions. The consistent inclusion of dephasing is a major advancement from previous versions of the theory and one of the central achievements in this chapter.

#### 3.3.1 System-reservoir interaction

In quantum well or bulk material, a large number of carriers are distributed amongst dense-lying states that are generally treated as a continuum. Processes involving the continuum states, such as carrier-carrier scattering, optical recombination, and scattering with phonons, must be treated on equal footing. In QDs the situation is different. The three-dimensional carrier confinement leads to a discretization of the single-particle density of states. Typical self-assembled QDs are grown on a wetting layer (WL) and the whole system is embedded in a barrier material. The energy of the lowest-lying continuum states of the WL provides an energetic upper bound for the localized QD states and, therefore, limits their number.

One therefore finds the situation, in which the localized states are responsible for the recombination dynamics of interest, whereas the nearby continuum provides carriers that can be captured into the localized states, or serve as scattering partners for carriers in the QD states. A separation into a system, consisting of the

localized states, and a reservoir, consisting of the continuum states, is justified if the interaction between the two does not lead to a mixing of states (hybridization). The dynamics of carriers in the continuum states is determined by an excitation process, by scattering amongst carriers in the continuum, as well as by the interaction with carriers in the localized QD states. The effects can be accommodated in the calculation of the rates  $\gamma_\eta$ .

The contribution of the reservoir, which can either be seen as a fermionic or a bosonic bath (depending if a coupling to carriers in the continuum, or to phonons is considered), to the density operator can be treated, in many cases, in the Born-Markov approximation. This approach leads to a Lindblad term  $\mathcal{D}_\eta$  [Lindblad, 1976, Carmichael, 1999] for *each* capture and relaxation process (in the following denoted by the index  $\eta$ ) associated with the considered reservoir and of the form

$$\frac{d}{dt}\rho|_{\mathcal{D}_\eta} = \frac{\gamma_\eta}{2} \left( \sum_{\alpha,\beta} 2 |f_\alpha^\eta\rangle \langle i_\alpha^\eta| \rho |i_\beta^\eta\rangle \langle f_\beta^\eta| - \sum_\alpha \left( |i_\alpha^\eta\rangle \langle i_\alpha^\eta| \rho + \rho |i_\alpha^\eta\rangle \langle i_\alpha^\eta| \right) \right). \quad (3.10)$$

Here  $\gamma_\eta$  is referred to as the corresponding capture/relaxation rate and  $|i_\alpha^\eta\rangle$  are the initial and  $|f_\alpha^\eta\rangle$  the final configurations of the described scattering process. The contribution of the Lindblad terms to the dynamical equations for the diagonal elements of the density matrix  $\rho$

$$\frac{d}{dt} \langle f_\alpha^\eta | \rho | f_\alpha^\eta \rangle = \gamma_\eta \langle i_\alpha^\eta | \rho | i_\alpha^\eta \rangle = -\frac{d}{dt} \langle i_\alpha^\eta | \rho | i_\alpha^\eta \rangle \quad (3.11)$$

reflect the trace-conserving nature of the Lindblad form, leading to an equilibration of the system with respect to the bath at a characteristic time  $1/\gamma_\eta$ , determined by the QD level-spacing, the lattice temperature, and the carrier density. Additionally, dephasing originates from the contribution of the second term in Eq. (3.10) to the equations for the non-diagonal elements of the density matrix, i.e.

$$\frac{d}{dt} \langle i_\alpha^\eta | \rho | f_\alpha^\eta \rangle = -\frac{\gamma_\eta}{2} \langle i_\alpha^\eta | \rho | f_\alpha^\eta \rangle, \quad (3.12)$$

and its complex conjugate. Thus, all optical transitions involving  $|i_\alpha^\eta\rangle$  and/or  $|f_\alpha^\eta\rangle$  as an initial/final state are consistently dephased by the process  $\eta$  [Gies et al., 2012, Gies et al., 2011].

More sophisticated many-body methods beyond the Born-Markov limit [Lorke et al., 2006, Steinhoff et al., 2012, Schuh et al., 2013], as well as experimental results [Borri et al., 2001, Beirne et al., 2007] can be used to determine more accurate rates  $\gamma_\eta$ , which enter this formalism as input parameters.

### 3.3.2 Lindblad terms in the equation-of-motion technique

The time evolution of the density operator is determined by the vNL equation with the Hamiltonian part  $H$  and the dissipative Lindblad-type superoperator  $\mathcal{D}_\eta$  according to Eq. (3.10), which can be written as

$$\frac{d}{dt}\rho = -i[H, \rho] + \sum_\eta \mathcal{D}_\eta \rho. \quad (3.13)$$

Once the solution is known, arbitrary single-time operator averages  $\langle A \rangle$  can be obtained by taking the trace  $\text{Tr} \{ \rho A \}$ .

Equations of motion are derived by considering the time evolution of expectation values  $\langle A \rangle = \text{Tr} \{ \rho A \}$ , expressed by a generalized Ehrenfest EoM for operator averages, for which the explicit knowledge of  $\rho$  is not required, cf. Sec. 3.2. A natural way to include the Lindblad contributions in the many-body formalism is to add them to the EoM, which follows directly from the vNL equation (3.13) by calculating operator averages and leads to

$$\frac{d}{dt} \langle A \rangle = i \langle [H, A] \rangle + \sum_{\eta} \frac{\gamma_{\eta}}{2} (\langle [\sigma_{\eta}^{\dagger}, A] \sigma_{\eta} \rangle + \langle \sigma_{\eta}^{\dagger} [A, \sigma_{\eta}] \rangle) \quad (3.14)$$

with the operators  $\sigma_{\eta} = \sum_{\alpha} |f_{\alpha}^{\eta}\rangle \langle i_{\alpha}^{\eta}|$  ( $\hbar = 1$ ). Both the interaction parts of the Hamiltonian and the Lindblad contributions in the above equation introduce a hierarchy of coupled equations. What has been discussed for the Hamiltonian contributions in Sec. 3.2 also applies for the latter with respect to finite system size and truncation.

The proposed method has the benefit of a consistent inclusion of scattering and dephasing in a reservoir fashion, while rates for the interaction with the carrier and phonon reservoirs can be obtained from separate calculations of desired sophistication. In the past dephasing has often been included phenomenologically by adding a constant dephasing rate  $\Gamma$  to the dynamical equations for EVs associated with polarizations [Richter et al., 2009, Baer et al., 2006, Feldtmann et al., 2006, Fricke, 1996b]. Next to providing dephasing, this phenomenological method has been shown to introduce artifacts, like artificial heating of the system [Hoyer et al., 2003]. A consistent formulation of dephasing requires a relationship between both, scattering and dephasing, that is expressed in Eqs. (3.11) and (3.12).

### 3.4 Equations of Motion for single QD PL

In the following we will illustrate the FSH method by deriving the dynamical equations for a particular QD model. So far the model has been formulated for arbitrary type and number of single-particle states. However, it greatly simplifies the discussion and the resulting equations if we consider a QD with only two confined states for electrons and holes each. These levels we refer to as *s*- and *p*-shells. Furthermore, only carriers of one spin direction are considered. The restriction to one spin subsystem has been shown [Gies et al., 2011, Gies et al., 2012] to constitute a reasonable approximation in the regime of strong off-resonant excitation in self-assembled QDs, where scattering processes with quasi-continuum carriers broaden the spectral lines. For applications like low-excitation spectroscopy the QD system must be augmented to explicitly contain the spin degree of freedom. On the two-particle-correlation level this situation has e.g. been studied in [Hohenester et al., 1999].

We will use an additional approximation that considerably simplifies the arising hierarchy of equations and that we would like to discuss in detail. The total number of possible configurations in the described QD is 16, since zero to four electrons can be distributed amongst four localized single-particle states. The FSH method, in

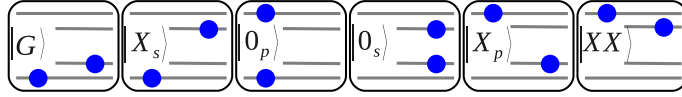


Figure 3.2: Possible configurations in a four-level QD, in which valence- and conduction-band carriers are excited and de-excited only in pairs. The representation is given in the c-v picture.

which the electronic degrees of freedom are treated exactly, requires to take operator averages with up to  $2(N_{\max}^c + N_{\max}^v) = 8$  carrier operators into account. The highest possible-carrier operator average that can differ from zero is the four-particle quantity

$$\langle c_s^\dagger c_p^\dagger v_s^\dagger v_p^\dagger v_p v_s c_p c_s \rangle . \quad (3.15)$$

A derivation of the EoM for the corresponding CFs is a cumbersome and error-prone endeavor and only recommended with an automatic generation algorithm. For this chapter a separate program has been written in FORM [Vermaseren, 2000], (appendix D) to fulfill this goal. For simplification purposes, we restrict the number of possible configurations by the following assumptions:

(i) An effective pair-wise carrier capture, in which the in-scattering of an electron into the QD  $p$ -shell is always accompanied by the in-scattering of a hole (in the cv-picture: A carrier present in the valence-band  $p$ -state is excited into the conduction-band  $p$ -state). (ii) Only intraband scattering processes preserving the carrier number within the QD are considered.

Since, the optical recombination is also carrier-number conserving, only the six configurations shown in Fig. 3.2 can form under this condition, all of which contain two carriers in the system. Thus, the largest operator averages that have to be evaluated for a system with the boundary condition  $N_{\max}^c = N_{\max}^v = 2$  are those with up to four carrier operators, plus additional photon operators. One example is discussed in the beginning of Sec. 3.5 in the context of biexcitonic recombination.

Several scattering processes are accounted for: The discussed pair-wise capture of carriers from the continuum into the localized  $p$ -states at rate  $P$ , as well as scattering from the conduction band  $p$ -shell to  $s$ -shell and valence-band  $s$ -shell to  $p$ -shell via the rates  $\gamma_{sp}^{cc}$  and  $\gamma_{ps}^{vv}$ . The rates  $\gamma_{ps}^{cc}$  and  $\gamma_{sp}^{vv}$  correspond to the reverse processes. The model system together with the considered scattering and recombination processes is sketched in Fig. 3.3. This section is split into two parts in which the FSH hierarchy is derived: The first Sec. 3.4.1 deals with the dynamics due to the Hamiltonian contributions using the light-matter interaction as an example. Contributions due to other parts of the Hamiltonian are given in Appendix A.2. In Sec. 3.4.2 contributions from the system-reservoir interaction are discussed. A special emphasis is placed on the differences between the FSH and the traditional CE method, and deviations occurring in the equations are pointed out.

### 3.4.1 Hamiltonian dynamics

The lowest-order observables of interest are the carrier populations, as well as the mean number of photons. Higher order operator averages appear in the derivation

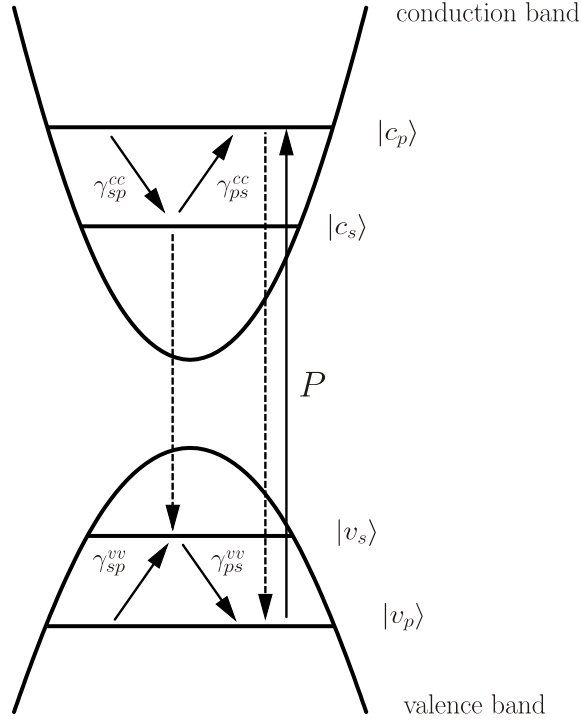


Figure 3.3: QD model with the considered rates  $\gamma$  for electrons in the conduction and valence band, describing scattering into and out of the  $s$ -shell. Carrier generation is modeled by a transition process between the  $p$ -levels at rate  $P$ . Light-matter coupling leads to recombination processes between the  $s$ - and the  $p$ -states due to spontaneous emission (dashed arrows).

of EoM. The arising hierarchy is finite in the carrier degrees of freedom, while the photonic hierarchy is truncated at the  $M_{\text{trunc}} = 2$  level, cf. Sec. 3.2.2.

The contribution of the light-matter interaction  $H_{\text{LM}}$  to the Ehrenfest EoM for the conduction band carrier population  $f_i^c = \langle c_i^\dagger c_i \rangle$ , are given by

$$\frac{d}{dt} f_i^c \Big|_{H_{\text{LM}}} = -2 \operatorname{Re} \sum_{\xi} g_{\xi}^* \Pi_{\xi,i}. \quad (3.16)$$

The real part of the photon-assisted polarization  $\Pi_{\xi,i} = \delta(b_{\xi}^{\dagger} v_i^{\dagger} c_i)$  describes transition amplitudes between QD levels, and is proportional to the light-matter coupling strength  $g_{\xi}$ . In order to solve Eq. (3.16) additional dynamical equations for the photon-assisted polarization, which are one step up in the hierarchy with respect to photon operators, are required and evolve as

$$\begin{aligned} \frac{d}{dt} \Pi_{\xi,i} \Big|_{H_{\text{LM}}} &= g_{\xi} f_i^c (1 - f_i^v) + g_{\xi} \sum_{\alpha} C_{\alpha i i \alpha}^x \\ &+ g_{\xi} \mathcal{N}_{\xi}^c (f_i^c - f_i^v) + g_{\xi} \mathcal{N}_{\xi,i}^c - g_{\xi} \mathcal{N}_{\xi,i}^v. \end{aligned} \quad (3.17)$$

The recombination of a QD excitation described by  $\Pi_{\xi,i}$  does not only require the presence of a conduction-band carrier, but also the non-occupancy of a valence-band state, which ends up in an emission rate proportional to  $\langle c_i^{\dagger} v_i v_j^{\dagger} c_j \rangle$  (cf. Ref. [Kira

et al., 1999]). In Eq. (3.17) enters the decomposition of this EV in a contribution of two uncorrelated carriers  $\propto f_i^c(1 - f_i^v)$  in the upper and lower state, plus interband carrier correlations  $\propto C_{ijji}^x := \delta(c_i^\dagger v_j^\dagger c_j v_i)$  according to Eq. (3.2)<sup>3</sup>. Thus, the first two terms in Eq. (3.17) can be identified as the source term of spontaneous emission, naturally appearing within this formalism due to quantization of the light field. The remaining terms of Eq. (3.17) arises from mixed EVs  $\langle b_\xi^\dagger b_\xi c_i^\dagger c_i \rangle$  and  $\langle b_\xi^\dagger b_\xi v_i^\dagger v_i \rangle$ , of which the uncorrelated contribution is proportional to the photon number  $\mathcal{N}_\xi := \langle b_\xi^\dagger b_\xi \rangle$  and can be attributed to stimulated emission and absorption, whereas  $\mathcal{N}_{\xi,i}^c := \delta(b_\xi^\dagger b_\xi c_i^\dagger c_i)$  and  $\mathcal{N}_{\xi,i}^v := \delta(b_\xi^\dagger b_\xi v_i^\dagger v_i)$  represent carrier-photon correlations. Note that  $\langle b_\xi^\dagger \rangle$  and  $\langle v_i^\dagger c_j \rangle$  vanish in the incoherent regime. Throughout this chapter we do not account for correlations between different optical modes. This is well justified in the presence of a microresonator, where a single cavity mode strongly dominates over all other leaky and far detuned cavity modes. In chapter 5 correlations between two slightly detuned high-quality cavity modes are included, and are crucial for the mode-coupling effects. Also when free space emission is considered, mode coupling effects may play a role and an evaluation of such terms can be considered. One must be aware, however, that the inclusion of continuum mode-coupling effects severely increases the numerical effort, and is in fact not feasible in a straightforward manner for higher-order CFs.

Significant contributions of higher-order correlations with respect to photons can be expected, e.g., if one of the considered QD transitions is resonant with a cavity mode, thereby providing feedback of the emitted photons. However, for QD emission into a continuum of free-space modes, where photons disappear once emitted, corrections to the dynamical evolution of the photon-assisted polarization, introduced by higher order *photon correlations* are negligible. Nevertheless, *carrier correlations* can still play an important role [Baer et al., 2006]. Especially in the regime of few emitters these correlations strongly dictate the carrier-photon dynamics and are indispensable for the description of single-QD luminescence.

		N		
		0	1	2
M	0	/	$\langle c^\dagger c \rangle, \langle v^\dagger v \rangle$	$\delta(c^\dagger v^\dagger cv), \delta(c^\dagger c^\dagger cc), \delta(v^\dagger v^\dagger vv)$
	1	/	$\delta(b^\dagger v^\dagger c)$	$\delta(b^\dagger c^\dagger v^\dagger cc), \delta(b^\dagger v^\dagger v^\dagger cv)$
	2	$\langle b^\dagger b \rangle$	$\delta(b^\dagger bc^\dagger c), \delta(b^\dagger bv^\dagger v)$	$\delta(b^\dagger bc^\dagger v^\dagger cv), \delta(b^\dagger bv^\dagger v^\dagger vv),$ $\delta(b^\dagger bc^\dagger c^\dagger cc), \delta(b^\dagger b^\dagger v^\dagger v^\dagger cc)$
	$\vdots$	$\vdots$	$\vdots$	$\vdots$

Table 3.1: Overview of all relevant CFs for the semiconductor luminescence model discussed in this chapter.

<sup>3</sup>The abbreviate notations for certain CFs like  $C_{ijji}^x$  is introduced to facilitate the comparison to the EoM presented in [Baer et al., 2004, Baer et al., 2006], this notation will be dropped in later chapters.



The light-matter part of the Hamiltonian (A.5) yields the time evolution

$$\begin{aligned} \frac{d}{dt} C_{ijkl}^x \Big|_{H_D} = & \quad (3.18) \\ & - \sum_{\xi} \delta_{il} \delta_{jk} [g_{\xi}^*(f_i^v - f_i^c) \Pi_{\xi,j} + g_{\xi}(f_j^v - f_j^c) \Pi_{\xi,i}^*] \\ & + \sum_{\xi} [g_{\xi} \Pi_{\xi,lkji}^{c,*} + g_{\xi}^* \Pi_{\xi,ijkl}^c - g_{\xi} \Pi_{\xi,lkji}^{v,*} - g_{\xi}^* \Pi_{\xi,ijkl}^v]. \end{aligned}$$

The first bracket contains the factorized contributions of the EVs  $\langle b_{\xi}^{\dagger} c_i^{\dagger} v_j^{\dagger} c_k c_l \rangle$  and  $\langle b_{\xi}^{\dagger} v_i^{\dagger} v_j^{\dagger} c_k v_l \rangle$ . The remaining correlation contributions  $\Pi_{\xi,ijkl}^c := \delta(b_{\xi}^{\dagger} c_i^{\dagger} v_j^{\dagger} c_k c_l)$  and  $\Pi_{\xi,ijkl}^v := \delta(b_{\xi}^{\dagger} v_i^{\dagger} v_j^{\dagger} c_k v_l)$  appear in the second bracket. Specifically,  $\Pi_{\xi,ijij}^{c/v} = -\Pi_{\xi,ijji}^{c/v}$  describe the correlated process of a photon-assisted polarization in presence of an additional carrier in the conduction- or valence-band, respectively. In a similar manner equations for the intraband carrier correlations  $C_{ijkl}^c := \delta(c_i^{\dagger} c_j^{\dagger} c_k c_l)$  and  $C_{ijkl}^v := \delta(v_i^{\dagger} v_j^{\dagger} v_k v_l)$  can be obtained and are provided in Appendix A.2.

The before-mentioned 'natural' truncation of the hierarchy of carrier operators becomes apparent in the time evolution of the mixed CFs  $\Pi_{\xi,ijkl}^c$  and  $\Pi_{\xi,ijkl}^v$ . To facilitate a better understanding, we provide a schematic explanation using the notation introduced in Section 3.2. The quantities  $\Pi_{\xi,ijkl}^c$  and  $\Pi_{\xi,ijkl}^v$  are CFs  $\delta(M, N)$  of the order  $M = 1$  and  $N = 2$ . The time evolution with respect to the dipole part of the Hamiltonian is given by

$$\begin{aligned} \frac{d}{dt} \delta(1, 2) \Big|_{H_D} = & \langle 0, 3 \rangle + \langle 2, 2 \rangle \\ & - \frac{d}{dt} (\delta(1, 1)) \langle 0, 1 \rangle - \delta(1, 1) \frac{d}{dt} \langle 0, 1 \rangle. \end{aligned} \quad (3.19)$$

Each term in this schematic representation may correspond to several contributions. The time derivative of the factorization is subtracted in the last line in order to obtain a CF (cf. Eq. (3.2)). Due to the limitation to two carriers in the QD states the first term drops out, because it describes processes where three carriers are created or annihilated. Enforcing this property of the system requires the strict fulfillment of the boundary condition

$$\delta(0, 3) = -\delta(0, 2) \langle 0, 1 \rangle - \langle 0, 1 \rangle \langle 0, 1 \rangle, \quad (3.20)$$

which means that, in fact, *all* CFs up to  $N_{\max} = 2$  must be taken into account. This is the explicit manifestation of what we referred to earlier as the enhancement of correlations due to the limited size of the system.

The remaining hierarchy in the photon operators is truncated at the desired level  $M_{\max}$ . All terms appearing in the CE up to  $M_{\max} = 2$  are summarized in Table 3.1.

Applying the CE to the remaining second term in Eq. (3.19) yields

$$\begin{aligned} \frac{d}{dt} \delta(1, 2) \Big|_{H_D} = & \quad (3.21) \\ & + \delta(2, 2) + \delta(2, 0) \delta(0, 2) + \delta(1, 1) \delta(1, 1) + \delta(2, 1) \langle 0, 1 \rangle \\ & - \frac{d}{dt} (\delta(1, 1)) \langle 0, 1 \rangle - \delta(1, 1) \frac{d}{dt} \langle 0, 1 \rangle. \end{aligned}$$

Explicitly performing the calculation behind this schematic representation leads to the following EoM

$$\begin{aligned}
 \frac{d}{dt} \Pi_{\xi,ijkl}^c \Big|_{H_D} &= \left[ g_{\xi} f_i^c f_j^c f_j^v - g_{\xi}^* \Pi_{\xi,i} \Pi_{\xi,j} \right. \\
 &+ g_{\xi} \mathcal{N}_{\xi,i}^c (f_j^c - f_j^v) - g_{\xi} f_i^c \sum_{\alpha} C_{\alpha jj \alpha}^x \left. \right] (\delta_{il} \delta_{jk} - \delta_{ik} \delta_{jl}) \\
 &+ g_{\xi} (1 + \mathcal{N}_{\xi}) C_{ijkl}^c + g_{\xi} \mathcal{N}_{\xi} (C_{ijlk}^x - C_{ijkl}^x) \\
 &+ g_{\xi} \delta (b_{\xi}^{\dagger} b_{\xi} c_i^{\dagger} c_j^{\dagger} c_k c_l) + g_{\xi} \delta (b_{\xi}^{\dagger} b_{\xi} c_i^{\dagger} v_j^{\dagger} c_l v_k) \\
 &- g_{\xi} \delta (b_{\xi}^{\dagger} b_{\xi} c_i^{\dagger} v_j^{\dagger} c_k v_l) - g_{\xi}^* \delta (b_{\xi}^{\dagger} b_{\xi}^{\dagger} v_i^{\dagger} v_j^{\dagger} c_k c_l),
 \end{aligned} \tag{3.22}$$

and similar equations can be given for  $\Pi_{\xi,ijkl}^v$  by exploiting the symmetries of the Hamiltonian.

It is worthwhile pointing out that the restriction to a certain system size fundamentally changes the structure of the underlying EoM. In Eq. (3.22), the uncommon product of three populations appears in the first line, originating from the subtraction of the factorization in the last line of Eq. (3.21) (from Eq. (3.17) one finds that there is a contribution  $\frac{d}{dt} \delta(1,1) \propto \langle 0,1 \rangle \langle 0,1 \rangle$ ). In a system where the restriction to two carriers was lifted, these terms would be compensated by the factorization of the three-particle EV  $\langle 0,3 \rangle$ , which would, in this case, have a non-zero contribution. In fact, this compensation is also known as the linked-cluster theorem [Fricke, 1996b]. Finally, the CF  $\delta(b_{\xi}^{\dagger} b_{\xi}^{\dagger} v_i^{\dagger} v_j^{\dagger} c_k c_l)$  in the last line of Eq. (3.22) can be attributed to spontaneous two-photon emission, recently demonstrated for a single-QD in a high- $Q$  photonic crystal nanocavity [Ota et al., 2011].

Eqs. (3.16)–(3.22), together with the additional equations given in Appendix A.2, form a closed set of coupled nonlinear equations for the dynamics determined by the Hamiltonian. Before we turn to numerical results, we discuss the scattering and dephasing contributions to these equations.

### 3.4.2 System-bath interaction

In Section 3.3 we have discussed the reservoir-treatment of scattering and dephasing, as well as carrier pumping. In the EoM these contributions are included via Lindblad terms in Eq. (3.14). As we have briefly mentioned, a microscopic treatment of these processes is also possible and can be derived from a mixed basis of localized and extended states. For the quantum-well case this has been performed by including the carrier-phonon interaction explicitly in the Hamiltonian [Hoyer et al., 2003, Carmele et al., 2010b]. However, this approach comes along with an additional hierarchy in the phonon operators that makes the classification of mixed CF containing carrier, photon, *and* phonon operators more difficult. Furthermore, including delocalized states of the two-dimensional WL continuum on the same level of complexity as the equations presented in Section 3.4.1, i.e. by considering CFs of an order up to  $M_{\text{trunc}} = 2$  and  $N_{\text{max}} = 2$ , would involve nonlinearly coupled integro-differential equations for CFs that carry several indices of continuum states. A numerical solution would be possible only for certain limiting cases. Therefore, we base the approach for the inclusion of scattering and dephasing within the CE

method on the Lindblad formalism. As a benefit, delocalized states enter the system dynamics only in the determination of the Lindblad rates, which can be obtained phenomenologically or from independent quantum-kinetic calculations [Bockelmann and Egeler, 1992, Vurgaftman et al., 1994, Inoshita and Sakaki, 1997, Braskén et al., 1998, Braskén et al., 1998, Jiang and Singh, 1998, Stauber et al., 2000, Lorke et al., 2006, Steinhoff et al., 2012, Schuh et al., 2013]. In principle the structure of the Lindblad formalism allows for a high degree of sophistication. For example, occupation-induced energy renormalizations due to the Coulomb interaction can be explicitly taken into account in the calculation of scattering, which then leads to different scattering rates for different configurations [Steinhoff et al., 2012]. The influence of this effect is strongly entwined with the dynamics of the system. Especially at low WL carrier densities when screening is weak, the rates may differ significantly, and a study of the impact on the emission dynamics of a single QD in a microcavity could prove interesting for future studies.

We now turn to the EoM. By evaluating the second line of Eq. (3.14) we can calculate the contributions for scattering, pumping and cavity losses.

### Intraband scattering

For the scattering between the bound QD states  $\mu$  and  $\nu$  in the conduction band, we obtain

$$\frac{d}{dt} \langle A \rangle |_{\text{scatt}} = \sum_{\substack{\mu \neq \nu \\ \mu, \nu \in \{s, p\}}} \frac{\gamma_{\mu\nu}^{cc}}{2} \left[ \langle [c_\nu^\dagger c_\mu, A] c_\mu^\dagger c_\nu \rangle + \langle c_\nu^\dagger c_\mu [A, c_\mu^\dagger c_\nu] \rangle \right], \quad (3.23)$$

where we have identified  $\sigma_\eta$  by  $c_\mu^\dagger c_\nu$ , and the Lindblad rates  $\gamma_\eta$  by the intraband scattering rates  $\gamma_{\mu\nu}^{cc}$ . The resulting change in the single-particle population  $f_\nu^c = \langle c_\nu^\dagger c_\nu \rangle$  due to intraband scattering

$$\frac{d}{dt} f_\nu^c |_{\text{scatt}} = (S_\nu^{\text{in}}(1 - f_\nu^c) - S_\nu^{\text{out}} f_\nu^c) + \sum_{\mu \neq \nu} (\gamma_{\nu\mu}^{cc} - \gamma_{\mu\nu}^{cc}) C_{\nu\mu\nu\mu}^c,$$

takes on the form of a Boltzmann-like collision term (first term), consisting of in- and out-scattering contributions with the corresponding rates  $S_\nu^{\text{in}} = \sum_{\mu \neq \nu} \gamma_{\nu\mu}^{cc} f_\mu^c$  and  $S_\nu^{\text{out}} = \sum_{\mu \neq \nu} \gamma_{\mu\nu}^{cc} (1 - f_\mu^c)$ , as well as correlation contributions beyond the single-particle description (second term). It is evident that the total carrier number is preserved, i.e.  $\frac{d}{dt} \sum_\nu f_\nu^c = 0$ , reflecting the trace-conserving property of the Lindblad formulation that we have already discussed in the context of Eq. (3.11).

If carrier correlations  $C_{\nu\mu\nu\mu}^c$  are neglected in Eq. (3.24), only populations of single-particle states  $f_\nu^c$  are taken into account. These populations are obtained *by averaging over all configurations* containing a carrier in the state  $\nu$ . Due to this averaging, the single-particle description is not able to distinguish between different configurations with an occupation of the state  $\nu$  and can, thereby, account for the Pauli exclusion principle only in an averaged sense. Consider for example the carrier relaxation in the conduction band: The configurations  $|X_p\rangle$ ,  $|0_p\rangle$  and  $|XX\rangle$  are valid initial configurations for a  $p$ -to- $s$  electron scattering process, although the Pauli exclusion principle forbids a carrier transition for the latter, because the  $s$ -shell

already contains one carrier. Thus, in this case the single-particle description allows for relaxation and attributes for dephasing, whereas an exact configuration-based treatment does not. Especially for few-emitter systems, this deficiency of the single-particle description (sometimes called ‘collision approximation’ of carrier correlations) should be avoided by considering the carrier correlations in Eq. (3.24).

The inclusion of scattering processes introduces a source of dephasing for all CFs. The scattering contribution to the EoM of the photon-assisted polarization,

$$\frac{d}{dt} \Pi_{\xi,\nu} \Big|_{\text{scatt}} = -\Gamma_{\nu} \Pi_{\xi,\nu} - \frac{1}{2} \sum_{\mu \neq \nu} (\gamma_{\nu\mu}^{cc} - \gamma_{\mu\nu}^{cc}) \Pi_{\xi,\mu\nu\nu\mu}^c, \quad (3.24)$$

includes a population-dependent dephasing rate  $\Gamma_{\nu} = \frac{1}{2}(S_{\nu}^{\text{in}} + S_{\nu}^{\text{out}})$ , instead of a constant rate  $\Gamma$  that is frequently used in the literature. To study the influence of correlations, it is crucial to account for their proper dephasing, because it determines the timescale on which correlations are damped out. It is shown in Ref. [Baer et al., 2006] that the influence of the carrier correlations on the luminescence dynamics can be strong if no dephasing is used at all, while a small constant dephasing of the interband CF in the  $\mu\text{eV}$  regime already leads to a complete damping towards an uncorrelated system on a timescale of several 100 ps. To make quantitative predictions, a consistent treatment of dephasing with correct rates for the different CFs is important. The dynamics of the interband carrier correlations due to intraband scattering introduced by the Lindblad term (3.23) is given by

$$\begin{aligned} \frac{d}{dt} C_{ijkl}^x \Big|_{\text{scatt}} = & - \sum_{\substack{\mu \neq \nu \\ \mu, \nu \in \{s, p\}}} \frac{\gamma_{\mu\nu}^{cc}}{2} \left\{ C_{ijkl}^x (\delta_{i\mu} + \delta_{k\mu}) \right. \\ & - 2 [f_{\mu}^c f_j^v (\delta_{i\mu} \delta_{k\mu} - \delta_{i\nu} \delta_{k\nu}) \delta_{jl} + C_{\mu j \mu l}^x \delta_{i\nu} \delta_{k\nu}] \\ & - 2 [(f_{\mu}^c (1 - f_i^c) - C_{\mu i i \mu}^c) \delta_{i\nu} \\ & \left. - (f_i^c (1 - f_{\nu}^c) - C_{i \nu \nu i}^c) \delta_{i\mu}] f_j^v \delta_{ik} \delta_{jl} \right\}, \end{aligned} \quad (3.25)$$

from which we obtain, using  $C_{spsp}^c = C_{psps}^c = -C_{spps}^c = -C_{pssp}^c$ , the following sum rule

$$\frac{d}{dt} (C_{ssss}^x + 2C_{psps}^x) \Big|_{\text{scatt}} = 0. \quad (3.26)$$

Thus, both CFs  $C_{ssss}^x$  and  $C_{psps}^x$  are not independent quantities, but are linked by the scattering process they represent. Obviously this property cannot be fulfilled by a simpler approach, where equal and constant rates  $\Gamma$  are used to describe the dephasing of both CFs.

## Pumping

In a typical situation for incoherent pumping carriers are excited in the barrier states and subsequently captured into the QD states. We describe this by a simultaneous generation/annihilation of carriers in the conduction/valence band  $p$ -state, which is assumed to persist during the pump pulse and to rapidly disappear afterwards.

Specifically, we consider a time-dependent capture rate  $P(t)$  following a Gaussian-shaped pump pulse. The corresponding Lindblad contribution to the EoM reads

$$\frac{d}{dt} \langle A \rangle \Big|_{\text{pump}} = \frac{P(t)}{2} \left( \langle [v_p^\dagger c_p, A] c_p^\dagger v_p \rangle + \langle v_p^\dagger c_p [A, c_p^\dagger v_p] \rangle \right). \quad (3.27)$$

This treatment of the pump process leads to an automatic built-up of CFs, e.g. for correlations between conduction- and valence-band carriers in the  $p$ -shell

$$\frac{d}{dt} C_{pppp}^x \Big|_{\text{pump}} = P(t) (f_p^v - f_p^c) (C_{pppp}^x + (1 - f_p^c) f_p^v). \quad (3.28)$$

This way, initial conditions for correlations do not have to be calculated separately by considering a quasi-equilibrium initial-state population that is defined by a total carrier density and a temperature [Baer et al., 2006, Feldtmann et al., 2006], which is a great practical and conceptual advantage of our approach.

It is worth noting that it is particularly the pair-wise generation of electrons and holes that leads to the generation of certain electron-hole correlations in the system. Furthermore, since the recombination also destroys electrons and holes pair-wise, only configurations with an equal number of electrons and holes appear in the system dynamics. Thereby, charged excitonic configurations are excluded. Alternative pump schemes can be considered [Gies et al., 2011, Gies et al., 2012], in which electrons and holes are captured independently. The implications are worth a separate discussion, which can be found in [Florian et al., 2013b].

### Cavity losses

In Sec. 3.6 we show results for a QD in a microcavity. The latter provides a three-dimensional confinement of the electromagnetic field, leading to a spectrum of well-separated cavity modes. This allows for the situation, in which only a single mode  $\bar{\xi}$  is resonant with the  $s$ -exciton transition of the QD. Nevertheless this resonant cavity mode couples to a continuum of modes outside the cavity which introduces dissipation on a nanosecond timescale. To account for a finite lifetime of the resonant mode, we introduce the Lindblad contribution

$$\frac{d}{dt} \langle A \rangle \Big|_{\text{cav}} = \frac{\kappa_{\bar{\xi}}}{2} \left( \langle [b_{\bar{\xi}}^\dagger, A] b_{\bar{\xi}} \rangle + \langle b_{\bar{\xi}}^\dagger [A, b_{\bar{\xi}}] \rangle \right), \quad (3.29)$$

where the photon loss rate  $\kappa_{\bar{\xi}}$  is directly connected to the quality factor  $Q = \omega_{\bar{\xi}}/\kappa_{\bar{\xi}}$  of the cavity mode  $\bar{\xi}$  at the energy  $\omega_{\bar{\xi}}$ .

Note that this contribution has a similar structure as the one for the carrier scattering (3.23), but now contains system operators acting only on the photonic degrees of freedom and leading to transitions between states involving  $n$  and  $n - 1$  photons in the mode  $\bar{\xi}$ . The contribution to the EoM leads to a damping of correlations at a rate  $M\kappa_{\bar{\xi}}/2$ ,

$$\frac{d}{dt} \delta((b_{\bar{\xi}}^\dagger)^p (b_{\bar{\xi}})^q C) \Big|_{\text{cav}} = -M \frac{\kappa_{\bar{\xi}}}{2} \delta((b_{\bar{\xi}}^\dagger)^p (b_{\bar{\xi}})^q C), \quad (3.30)$$

where  $M = p + q$  is the order of the corresponding CF with respect to the photon operators, independent of further carrier operators  $C$  contained in the CF. Thus,

photon correlations get more strongly damped in the presence of a lossy cavity, and even more so with increasing order. This plays an important role in the truncation of the hierarchy within the CE approach and is demonstrated in Sec. 3.6.

### 3.4.3 Luminescence dynamics and spectrum

The luminescence dynamics is determined by the change of the mean photon number  $\mathcal{N}_\xi$ , for which the EoM reads

$$\left(\frac{d}{dt} + \kappa_\xi\right) \mathcal{N}_\xi = 2 \operatorname{Re} \sum_\nu g_\xi^* \Pi_{\xi,\nu}. \quad (3.31)$$

The only contributions to this equation arise from the light-matter interaction and the cavity losses in Eq. (3.29). One can see that cavity losses lead to a decrease of the mean photon number, while spontaneous and stimulated emission and absorption due to the emitter are expressed in terms of the sum over the photon-assisted polarizations over all bound QD states.

In the absence of a cavity, emission into the continuum of free space modes takes place, and the corresponding luminescence spectrum  $I(\omega, t)$  is given by

$$I(\omega, t) = 2 \operatorname{Re} \sum_{\nu,\xi} |g_\xi|^2 \Pi_{\xi,\nu} \Big|_{|q|=\frac{\omega}{c}}. \quad (3.32)$$

Note that from here on we consider all polarization-like quantities to be rescaled with the light-matter coupling strength  $g$  in order to have the square of the coupling constant appear in the equations; for details we refer to Ref. [Baer et al., 2006]. The sum in Eq. (3.31) runs over wave vectors with the same photon energy irrespective of the direction of the wave vector. When studying time-resolved photoluminescence, the spectral information is discarded by integration over all frequencies, i.e.

$$I(t) = \int d\omega I(\omega, t). \quad (3.33)$$

## 3.5 Photoluminescence into free-space

We first present numerical results for the luminescence from a single QD into a continuum of modes, i.e. emission into free space. Here, the EoM approach can play out its full advantage, because the large Hilbert space associated with a continuum of modes prohibits a direct solution of the vNL equation. The four-level QD model is used that has been introduced in the previous section. The luminescence spectra and the time-resolved photoluminescence decay provide direct insight into both the physical system and the underlying mechanism of the FSH approach. Furthermore, comparing with results from the regular CE method enables us to gain an understanding how the factorization of the carrier degrees of freedom leads to an effective “mean-field”-like approximation of the exact result and the limitations of this description. The frequency-resolved and time-dependent luminescence spectra are calculated from Eq. (3.32).

In Fig. 3.4 four series of luminescence spectra from the emission 10, 20, 30, and 50 ps after the start of the time evolution are shown. Continuum-state carriers are excited by a laser pulse and are subsequently captured pair-wise into the QD  $p$ -states.

The Gaussian pulse is centered at 25 ps, has a width of 10 ps (FWHM), and a dimensionless pulse area of  $P_{\text{total}}$ . The spectra in the left panel correspond to weak excitation with  $P_{\text{total}} = 0.1$ , whereas the right panel shows results after strong excitation with  $P_{\text{total}} = 1$ . Upper and lower panels compare results from the FSH method for  $M_{\text{trunc}} = 1$ , and the second order of the regular CE with  $(N+M)_{\text{trunc}} = 2$ , respectively.

We first provide an explanation of the FSH results. In Fig. 3.5 an illustration of the following explanation is given. Since the FSH method contains an exact treatment of the carrier degrees of freedom, the resulting (multi-) exciton lines appear at renormalized energies that are equivalent to those obtained from a diagonalization of the carrier and Coulomb Hamiltonian in the complete basis of all possible configurations. The position of the lines is fixed, and their intensity in the spectrum is determined by the probability of the corresponding transition taking place. Four peaks are visible, which correspond to the four possible recombination channels of the excited QD. The recombination channels are the decay to the ground state from the  $s$ - and  $p$ -excitons, as well as the  $s$ - and  $p$ -recombination from the  $s$ - $p$ -biexciton configuration. The  $s$ - and  $p$ -recombination are separated by approximately 63 meV in the spectrum due to the level spacing of the single-particle states and direct (Hartree) interaction. The Coulomb Hamiltonian introduces a further splitting, if the recombination takes place in the presence of another electron-hole pair in the other shell. The splitting between the  $|XX\rangle \rightarrow |X_{s/p}\rangle$  and the  $|X_{s/p}\rangle \rightarrow |G\rangle$  transitions is determined by the Coulomb  $s$ - $p$ -exchange interaction and gives rise to a detuning of  $2V_{spsp}$ , which amounts approximately to 9.8 meV.

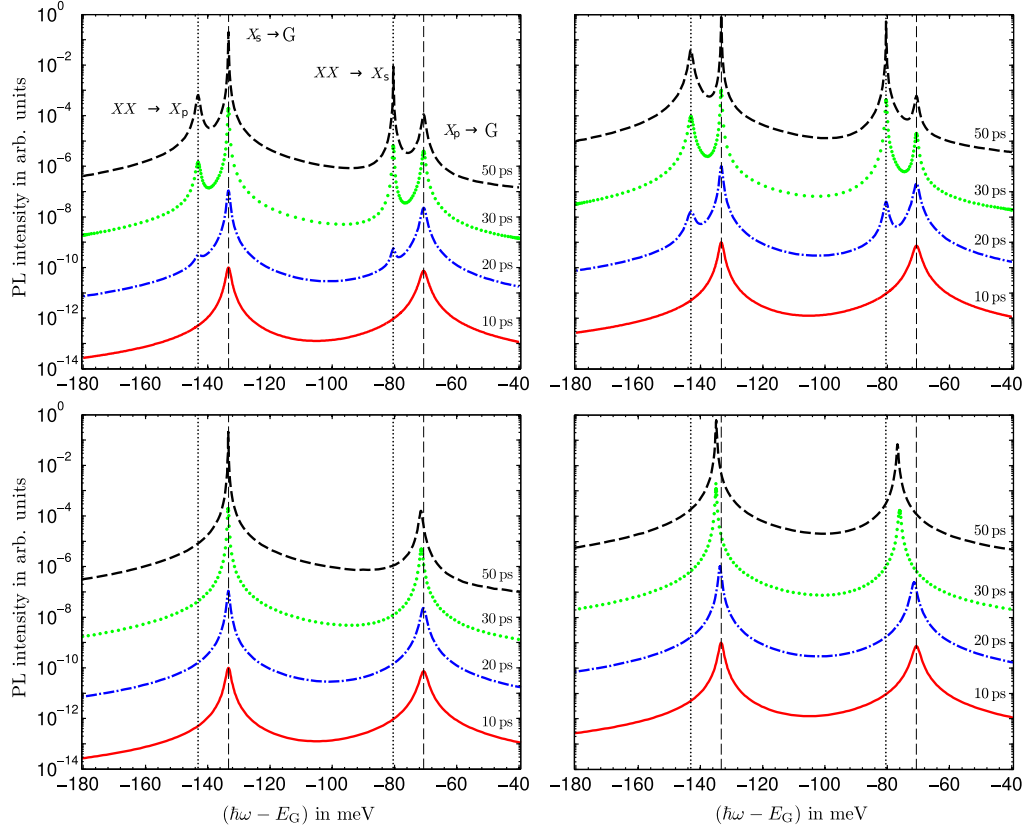


Figure 3.4: Frequency-resolved photoluminescence spectra for the emission into a continuum of modes. Compared are FSH (top) and the second order of the regular CE (bottom) results after a weak (left,  $P_{\text{total}} = 0.1$ ) and strong (right,  $P_{\text{total}} = 1.0$ ) excitation pulse. Spectra are shown after 10 (solid line), 20 (dash-dotted), 30 (dotted) and 50 (dashed) ps of the time evolution. The excitation pulse is centered at 25 ps and 10 ps in width. The spectra are depicted in log scale y-axis and have been rescaled for better visibility. In order to be able to compare absolute heights, the scaling factors are required. Typical relaxation times for electrons in the conduction- and valence-band are used:  $\gamma_{sp}^{cc} = 1.07/\text{ps}$ ,  $\gamma_{ps}^{cc} = 0.02/\text{ps}$ ,  $\gamma_{sp}^{vv} = 0.13/\text{ps}$  and  $\gamma_{ps}^{vv} = 0.59/\text{ps}$ . The peak height of the top right spectrum after 50 ps has been set to unity. Relative to this, in all panels the spectra after 50, 30, 20, and 10 ps have been scaled by 0.76, 0.31, 0.02, and  $1.4 \cdot 10^{-5}$ .



Because all recombination channels are spectrally separated, it is possible to connect the carrier dynamics to the time-dependent spectra in Fig. 3.4. The following discussion is valid for both upper panels, as the situation is similar for weak and strong excitation. In the lowermost spectrum in each panel, corresponding to the beginning of the excitation pulse, only signatures of  $s$ - and  $p$ -exciton emission are visible. Because excitation is still weak, relaxation and recombination are by far the fastest processes in the system, so that excitations decay before population in the biexciton state can build up. The second spectra (dotted-dashed lines) depict the situation just before the peak of the excitation pulse. Now the faster refilling of the  $p$ -states already leads to weak signatures from the biexciton. The  $s$ -exciton emission clearly dominates the spectra over that of the  $p$ -exciton. The dominance of the  $s$ -exciton emission becomes even more obvious in the spectra at later times and is explained by the scattering processes between  $s$ - and  $p$ -shells: At the considered temperature of 120K, down-scattering from  $p$ - to  $s$ -shell is much faster than the reverse process and offers a fast second channel in addition to the direct recombination, through which the  $p$ -exciton can decay.

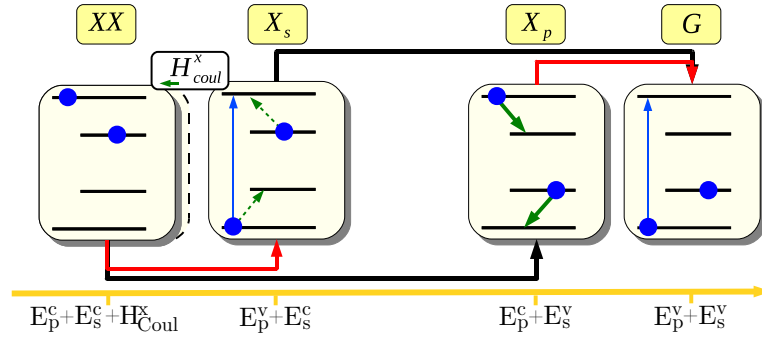


Figure 3.5: Illustration of the various recombination channels and the dephasing mechanisms of the bright configurations. The red(black) arrows on top and below the states indicate the  $p$ -shell( $s$ -shell) recombination. The solid green lines indicate the intraband down-scattering of the electrons and the dashed green lines indicate the weaker up-scattering. The solid blue arrow indicates the incoherent pump into the  $p$ -shell.

Before we discuss the results of the regular CE, we explain in more detail the origin of the spectral splitting between exciton and biexciton emission in the formalism. The biexciton recombination process is described by the expectation value  $\langle b_\xi^\dagger X_s X_p^\dagger X_p \rangle$ . Here, exciton operators  $X_i^\dagger = c_i^\dagger v_i$  have been used to express the recombination process of an exciton in the  $s$ -shell in the presence of a second exciton in the  $p$ -shell (equivalently,  $p$ -shell recombination in the presence of an  $s$ -shell exciton is given by a similar expression). Normal ordering yields

$$\begin{aligned}
 \langle b_\xi^\dagger X_s X_p^\dagger X_p \rangle &= \langle b_\xi^\dagger v_s^\dagger c_s c_p^\dagger v_p v_p^\dagger c_p \rangle \\
 &= \langle b_\xi^\dagger v_s^\dagger c_s c_p^\dagger c_p \rangle - \langle b_\xi^\dagger v_s^\dagger c_p^\dagger v_p^\dagger v_p c_p c_s \rangle .
 \end{aligned} \tag{3.34}$$

The assumption of pair-wise carrier generation and the resulting limitation to the six possible configurations shown in Fig. 3.2 implies that the second term must

be zero, since the annihilation of three carriers is not possible in the used QD model. So the biexciton recombination process is actually described by the quantity  $\langle b_{\xi}^{\dagger} v_s^{\dagger} c_s c_p^{\dagger} c_p \rangle$ . This can readily be understood, as the presence of two carriers in the conduction-band  $s$ - and  $p$ -states automatically implies their absence in the valence-band states. At this point, the limitation to include only scattering processes that leave the total number of carriers in the localized states constant constitutes a significant simplification of the EoM method. In the more general case, where the electron number in the QD can vary from zero to four, EoM for CFs containing up to  $2N_{\max} = 8$  carrier- and  $M_{\text{trunc}} = 1$  photon operators are required.

We now turn to the results of the regular CE method, which are depicted in the lower two panels. Here, the truncation is performed at the level  $(N + M)_{\text{trunc}} = 2$ , which implies that all CFs containing more than four carrier operators are approximated as zero. CFs  $\Pi_{\xi,ijkl}^{c/v}$  responsible for biexcitonic emission, as they appear in the spectra obtained from the FSH, are not included in the theory at the second order. As a result of the truncation, the CE method performs a compensation in a ‘mean-field’ like fashion. At the first order of the regular CE all carrier contributions are formulated in terms of populations. At the second order, additional correlations are included<sup>4</sup> and the peaks appear at the  $s$ - and  $p$ -exciton transitions at energies that are renormalized proportionally to the single-particle electron and hole populations in the QD states. With increasing excitation the resonances are tuned *continuously* towards the energies of the multi-exciton configurations that are visible in the full theory. The amount of the shift results from the singlet contribution  $\sum_{\mu} V_{i\mu i\mu} (1 + f_{\mu}^c - f_{\mu}^v)$  in the dynamical equation for the photon-assisted polarization  $\Pi_{\xi,s/p}$  responsible for the  $s$ - ( $p$ -) shell recombination. The exact Coulomb-renormalized energies of the four recombination channels are shown as vertical lines as a guide to the eye to better visualize the shift. This effect can also be observed in the absorption spectra shown in Ref. [Hohenester et al., 1999], where results from calculations on the mean-field and two-particle correlation level are compared. Spectral line shifts, though not the main focus of that publication, are prominent especially in the first case and are reduced by the important step to include two-particle correlations.

Complementary information, which turns out less sensitive to the approximate treatment of carrier correlations, is provided by the time-resolved photoluminescence, which is obtained by integrating the spectrum over all energies at every point in time. The result for the discussed four situations is shown in Fig. 3.6, where curves from the FSH and regular CE methods are compared. For weak excitation ( $P_{\text{total}} = 0.1$ ), both results are in good agreement, demonstrating that the ‘interpolation’ performed by the regular CE on the second order provides indeed a good approximation of the total photon emission. At high excitation ( $P_{\text{total}} = 1.0$ ), when additional configurations become increasingly important, deviations appear. Strong line shifts are observed in the corresponding spectra (lower right panel in Fig. 3.4) in order to mimic the dominant emission from the filled QD configuration at the  $p$ -shell resonance. In this regime, the second order CE breaks down and nonphysical results,

---

<sup>4</sup>The inclusion of higher-order electronic correlations would not result in the ‘exact’ description as the FSH does. The reason is that, in the CE approach for finite systems, at all levels higher-order CFs are, erroneously approximated as zero.

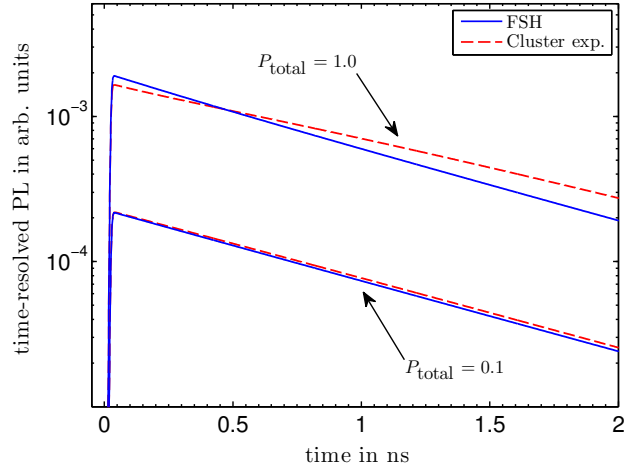


Figure 3.6: Time-resolved photoluminescence for the results shown in Fig. 3.4.

like negative populations may occur. The ‘interpolation’ of the transition energies in the second order of the CE leads to a problem in the presence of a high- $Q$  resonator. The narrow linewidth associated with the cavity mode makes the light emission very sensitive to shifts of the emission lines, leading to a population-dependent overlap between QD transition and mode. This artificial situation is discussed in detail in the next section 3.6.

A further aspect of the spectra that requires additional explanation regards the linewidths of the different transitions. We have explained in the context of Eq. (3.12) that scattering processes lead to dephasing of optical transitions if they act on either the initial and/or final state of that transition [Gies et al., 2012, Gies et al., 2011]. The strength of the underlying dephasing manifests itself in the linewidths in the emission spectrum (see Fig. 3.5 for an illustration). For example, the  $s$ -exciton to ground-state transition is subject to the  $p$ -shell carrier generation process, as well as the up-scattering of electrons and holes from  $s$ - to  $p$ -states. While the latter is very weak, the pump process is responsible for the line broadening of the corresponding peak. After the pump pulse is over, the line clearly narrows (compare the spectra at 10 and 50 ps). The situation is similar for the  $p$ -exciton-to-ground-state transition, which is affected by the pump process in the same way, but is additionally dephased by the fast carrier relaxation from  $p$ - to  $s$ -states. In contrast to the previously discussed transition, the line of the corresponding peak is not significantly narrowed after the excitation pulse is over.

The effect of carrier relaxation is reversed for the biexciton emission lines. Since for the considered QD system, the initial configuration of this recombination process is the completely filled QD, only the final configuration, which is either the  $s$ - or the  $p$ -exciton, can be involved in carrier scattering. For the  $p$ -exciton, this is the fast  $p$ -to- $s$  relaxation, while for the  $s$ -exciton, it is the much slower  $s$ -to- $p$  up-scattering process. Accordingly, the linewidth of the  $|XX\rangle \rightarrow |X_s\rangle$  is significantly smaller than that of the  $|XX\rangle \rightarrow |X_p\rangle$  transition. The impact of the dephasing reaches even deeper than its reflection in the transition linewidths, and the final point we would like to discuss in the context of the spectra are the relative intensities of the two biexciton emission channels. Recombination at the  $s$ -shell leaves behind a

$p$ -exciton. As we have discussed before, this is subject to strong dephasing due to carrier relaxation. Recombination at the  $p$ -shell, on the other hand, leaves behind the  $s$ -exciton, which is only weakly dephased in the absence of pumping. Thus, the photon-assisted polarization that drives the transition process is damped more strongly in the first case, which is clearly reflected by the higher peak from the recombination at the  $p$ -shell ( $|XX\rangle \rightarrow |X_s\rangle$ ) in the spectrum at 50 ps after the pump pulse has ended.

### 3.6 Numerical results for a single QD in a micro-cavity

Now we turn to the situation, in which a single QD emitter is embedded in a resonator structure and coupled to a single high-quality mode of that resonator. In contrast to the free-space emission considered in the previous section, the cavity strongly enhances the resonant emission from the QD. We will demonstrate that the resulting sensitivity to the resonance condition can lead to an enhancement of artifacts introduced by the truncation of the hierarchy of EoM. The limited size of the Hilbert space now facilitates a direct solution of the vNL equation (3.13), which is exact, and against which we check the validity of (i) the FSH method, where carrier degrees of freedom are represented by a closed set of carrier CFs, plus the corresponding correlations augmented by photon operators up to order  $M_{\text{trunc}}$ , and (ii) the approximate treatment of carrier and photon degrees of freedom according to the conventional CE method at the second order  $(N + M)_{\text{trunc}} = 2$ .

We consider the  $s$ -exciton transition to be resonant with a single cavity mode, and a corresponding light-matter coupling strength of  $g = 0.01/\text{ps}$ . The pump process is modeled like in Sec. 3.5 (a Gaussian pulse centered at 25 ps and 10 ps of width (FWHM)) with a total area of  $P_{\text{total}} = 0.5$ . Typical relaxation times for electrons in the conduction- and valence-band are used:  $\gamma_{sp}^{cc} = 1.07/\text{ps}$ ,  $\gamma_{ps}^{cc} = 0.02/\text{ps}$ ,  $\gamma_{sp}^{vv} = 0.13/\text{ps}$  and  $\gamma_{ps}^{vv} = 0.59/\text{ps}$ .

In analogy to the discussion in Sec. 3.4.3 we can infer that the luminescence dynamics follows from Eq. (3.32), when only a single mode  $\bar{\xi}$  is considered. We drop the mode index in the remainder of this section. This leads to the expression

$$I(t) = 2|g|^2 \text{Re} \sum_{\nu} \Pi_{\nu} . \quad (3.35)$$

For a light-matter coupling strength of  $g = 0.01/\text{ps}$  and a cavity loss rate of  $\kappa = 0.1/\text{ps}$  ( $Q \approx 20,000$  for a cavity mode wavelength of 915 nm), the time-resolved photoluminescence at the cavity resonance is shown in Fig. 3.7(a). The FSH method, which treats the electronic degrees of freedom exact and the photonic degrees of freedom up to second order ( $M_{\text{trunc}} = 2$ ), is in excellent agreement with the exact solution of the vNL equation (symbols). The solid line represents the CE at the second order  $(N + M)_{\text{trunc}} = 2$  and is found to exhibit a peculiar oscillatory behavior that strongly deviates from the exact result. The reason lies in the fact that, at this level of approximation, the transition energies are not fixed but are renormalized as a function of the carrier populations, as it was demonstrated in Sec. 3.5.

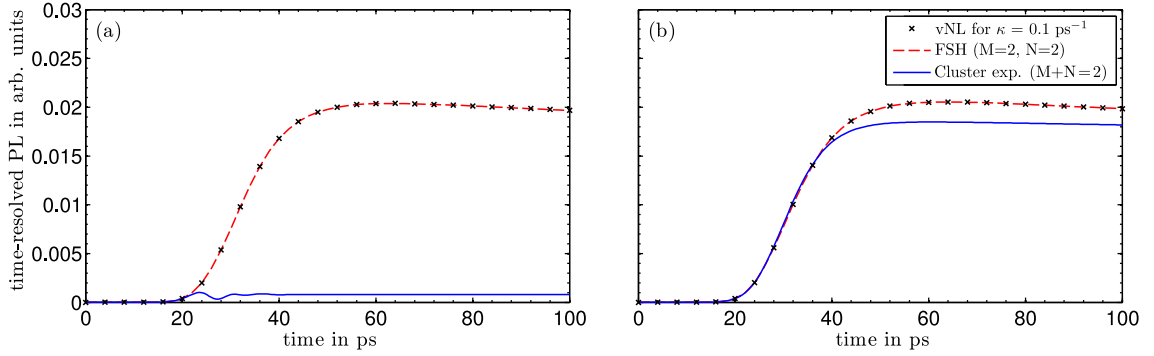


Figure 3.7: **(a)** Time-resolved photoluminescence at the cavity-mode frequency. Results obtained from the FSH (dashed lines) and the second order of the CE (solid lines) methods are compared to the exact solution (symbols) of the vNL equation. **(b)** displays the same results under the omission of the Coulomb interaction.

With the cavity tuned to the properly renormalized energy of the exciton transition, this transition comes into resonance as the *mean* QD carrier occupancy increases. With the onset of emission, the QD is depopulated, which, in turn, reduces the renormalization and brings the exciton transition out of resonance again. This leads to an initial oscillatory behavior and finally to a strongly suppressed emission due to the reduced spectral overlap between emitter and cavity mode. This picture is supported by a comparative calculation where the influence of Coulomb interaction is neglected, shown in Fig. 3.7(b). In this case, exciton and biexciton recombination take place at the same energy, so that the shifting of the transition lines is no longer appeared in the CE method.

In Fig. 3.8 we study the influence of the truncation level in the photonic degrees of freedom when using the FSH method. The blue set of curves and plus symbols correspond to the parameters used in Fig. 3.7, the crosses and red set of curves depict the case of a cavity with an exaggeratedly long storage time of photons ( $\kappa = 0.01/\text{ps}$ ,  $Q \approx 200,000$ ). For the  $Q \approx 20,000$  cavity, a truncation of the photon hierarchy at the  $M_{\text{trunc}} = 1$  level (dash-dotted line) can hardly be distinguished from the results for  $M_{\text{trunc}} = 2$  (dashed line). The reason lies in the dephasing of correlations due to the dissipation of photons from the cavity according to Eq. (3.30). In the higher- $Q$  cavity the dephasing is significantly weakened, thereby strengthening the impact of photon correlations. Thus, the calculation for  $M_{\text{trunc}} = 1$  yields a visibly less accurate description of the time-resolved photoluminescence than the  $M_{\text{trunc}} = 2$  calculation. In the well-known manner of the CE, the level of truncation depends on the strength of correlations, as well as on the quantities of interest.

In this section we have demonstrated that the FSH method yields an accurate description of the system dynamics and can overcome the limitations inherent to the CE method. The results were obtained under the assumption of a pair-wise carrier generation process, which greatly simplifies the hierarchy of EoM, but does not harm the general validity of the drawn conclusions or the applicability of the FSH.

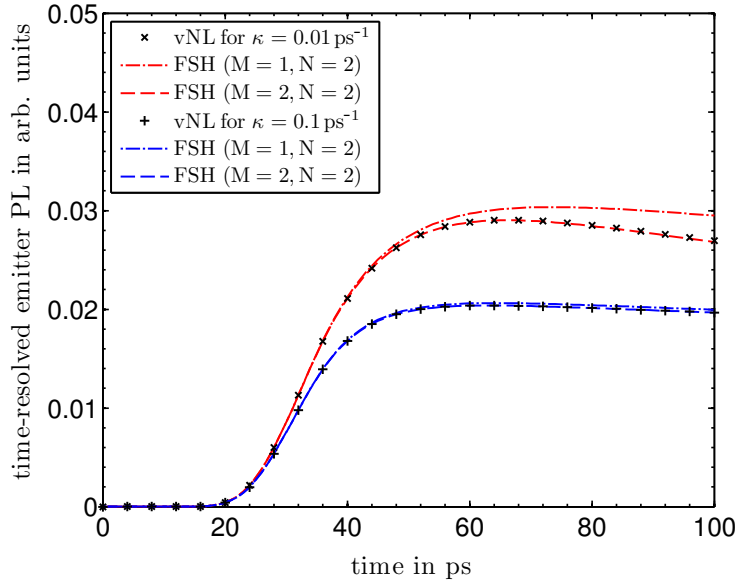


Figure 3.8: Comparison between the solution of the von-Neumann equation (symbols) and the FSH method for the time evolution of the single-QD photoluminescence. For all curves a light-matter coupling strength of  $g = 0.01/\text{ps}$  is used. The red lines and crosses correspond to the results for cavity losses at a rate  $\kappa = 0.01/\text{ps}$ . In comparison to the red curves  $\kappa = 0.1/\text{ps}$  is used for the blue lines and plus symbols. The various line styles show the results of the FSH method obtained at different truncation levels with respect to the photonic hierarchy.

### 3.7 Chapter Conclusion

In this chapter we have presented a new approach to the treatment of electronic correlations in a nanostructure coupled to continuous electronic states, phonons, and photons. For such a system, the direct solution of the vNL equation is only possible if the electronic Hilbert space is small, which is the case for a single or few emitters and a single cavity mode with a limited number of photons. On the other hand, an EoM approach, in connection with the CE method to truncate the infinite hierarchy of equations, has been used in the past as a valuable method to describe luminescence-related phenomena, laser emission and photon correlations for systems with many QDs or other active materials with a continuous density of states. We have addressed the situation in finite-sized systems, in which the small number of electronic degrees of freedom plays an important role. This is for example the case in QDs with few confined states. We have demonstrated that boundary conditions play an important role and lead to an enhancement of correlations. For this, we have devised a formalism that combines the exact representation of the electronic degrees of freedom of the vNL approach, with the truncation of the photonic hierarchy from the CE method, resulting in the FSH method.

The second major point addressed in this chapter is the inclusion of scattering and dephasing by using the Lindblad formalism in the EoM-based approaches. This regards scattering and dephasing in a consistent manner and on equal footing with the Hamiltonian contributions to the time evolution of the system. A correct

treatment of dissipative processes is a key requirement for making quantitative predictions in correlated systems. In earlier attempts, simpler models for the dephasing have been used to obtain an estimate for the impact of correlations, such as adding an estimated constant dephasing term to the EoM. Such an approach is subject to artifacts that are overcome by the presented theory.

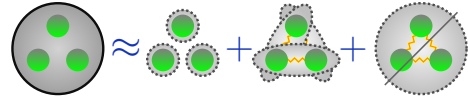
The FSH method allows for a description of much larger systems than it is possible by means of the vNL equation, the emission into free space via a mode continuum. For a single QD we have presented free-space emission spectra comprising multi-excitonic effects, as well as time-resolved photoluminescence for a QD coupled to a microcavity mode. The latter case allows for a comparison with the vNL equation to benchmark the theory. The outcome is that the FSH method provides an accurate description of the dynamics predicted by the vNL equation.





# Chapter 4

## Expectation Value Based Cluster Expansion



In this chapter a new method to formulate equations of motion (EoM) for open quantum many-particle systems is presented. Our approach allows for a numerically exact treatment as well as for approximations necessary in large systems and can be applied to systems involving both bosonic and fermionic particles. The method generalizes the cluster expansion (CE) technique by using expectation values (EVs) instead of correlation functions (CFs), which we will term expectation value based cluster expansion (EVCE). The use of EVs not only makes the equations more transparent, but also considerably reduces the amount of algebraic effort to derive the equations. The proposed formulation offers a unified view on various approximation techniques presented recently in the literature. The convergence properties of the EVCE are studied for the Jaynes-Cummings model (JCM) explicitly, and three additional examples for the application of the EVCE are shown schematically.

Parts of this chapter are published in [Leymann et al., 2014, Leymann et al., 2013b]. The basic theoretical concept of the EVCE where developed by H.A.M. Leymann in collaboration with A. Foerster, the EoM where mainly derived H.A.M. Leymann, the numerical integration of the EoM was mainly done by A. Foerster, all authors of [Leymann et al., 2014, Leymann et al., 2013b] discussed the results and physical implications of the results.

### 4.1 Numerical approaches for interacting many-particle systems

The finite size hierarchy described in chapter 3 was developed with a specific application in mind, in this chapter we introduce the EVCE as a general technique to describe interacting many-particle systems. In order to do justice to this general approach we need to reintroduce some concepts already introduced in the former chapter in a slightly different language or form, and the reader is kindly asked to pardon for inevitable repetitions. Interacting many-particle systems can drive strong correlations between the interacting particles. A straight forward way to describe the dynamics of correlated many-particle systems is to directly derive the equations

of motion for the quantities of interest. Equation of motion (EoM) techniques have been used successfully to realize microscopic descriptions of quantum systems, and are a way to systematically incorporate many-particle correlations into the description of exciton dynamics in quantum wells [Hoyer et al., 2003], ultracold Bose gases [Köhler and Burnett, 2002], spin dynamics [Kapetanakis and Perakis, 2008], photoluminescence [Kira et al., 1998], resonance fluorescence [Kira et al., 1999], cavity phonons [Kabuss et al., 2012, Kabuss et al., 2013], cavity-quantum-electrodynamics [Carmelet et al., 2010b], and microcavity quantum dot (QD) lasers [Gies et al., 2007]. The basic idea of EoM approaches is to truncate the unfolding hierarchy of differential equations at a certain level to allow for a numerical solution. The details of the truncation depend strongly on the used technique and the investigated system and are the subject of this chapter. Many different formulations and approximation techniques are known in the field of EoM approaches. However, we will distinguish between two basic types of formulations using correlation functions (CFs) [Wiersig et al., 2009, Kapetanakis and Perakis, 2008, Kira et al., 1998, Kira et al., 1999, Hoyer et al., 2003, Hohenester and Pötz, 1997] as in the CE [Fricke, 1996a, Hoyer et al., 2004] on the one hand and EVs (or density matrix elements) on the other hand [Gartner, 2011, Richter et al., 2009, Witthaut et al., 2011, Kabuss et al., 2012, Carmele et al., 2010b, Richter et al., 2015]. The formulation in CFs is algebraically demanding but has proven to be very effective in approximately describing large systems. Expectation value based formulations are algebraically less demanding and produce a linear and very clear system of EoM, but are usually limited to small systems. The proposed approach combines the two formulations (in CFs and EVs) with their respective advantages and adds a new perspective on former techniques used in the literature.

The outline of this chapter is as follows. In Sec. 4.2, we will revisit the general concept of CFs and the factorization of EVs. The approximation techniques presented in Sec. 4.2 are the basis for the truncation variants presented in Sec. 4.3. Section 4.3 is devoted to the derivation of EoM and we show how the introduced formulation can be used to truncate the unfolding hierarchy of EoM. We focus on the truncation of EoM for systems involving bosons and fermions and provide details on the various truncation possibilities. In Sec. 4.4, we will give an example for the EoM of a coupled quantum system and show how different truncation schemes result in known models.

## 4.2 The concept of correlation functions

In the following, we recapitulate and work out the details of the concept of CFs. The fundamental definitions of CFs and a formal introduction to CFs can be found in [Fricke, 1996a]. We introduce a new formulation that will facilitate switching between a formulation in EVs or CFs. With this flexibility in the formulation we give detail to the various approximations that are related to the neglect of EVs and CFs.

### 4.2.1 Definition of correlation functions

A key point of this section is the fact that one can represent every EV  $\langle b_1 b_2 \cdots b_k \rangle$  of operators  $b_i$  as a sum of products of CFs in a unique way. In this part, we stick to bosonic operators to keep it simple and the general ideas clear.

For the mathematical framework, we define a set of indices  $I = \{1, 2, \dots, k\}$  and a product of operators  $b^I = b_1 b_2 \cdots b_k$ .  $P$  is a partition of the set  $I$  meaning a set family of disjoint nonempty subsets  $J$  of  $I$  with  $\cup_{J \in P} J = I$ , and finally  $P_I$  is defined as the set of all partitions of  $I$ . We introduce the factorization operator  $\mathbf{F}$ . This operator does not change the value of the complex number  $\langle b^I \rangle$ , instead  $\mathbf{F}$  changes the representation of the EV, similar maybe to a passive transformation of a vector. With these preliminaries we can now give a general definition of the CFs  $\delta(b^J)$ :

$$\mathbf{F} \langle b^I \rangle = \delta(b^I) + \delta(b^I)_F = \sum_{P \in P_I} \prod_{J \in P} \delta(b^J). \quad (4.1)$$

where  $\delta(b^I)_F$  is a short notation for the sum of products of all possible factorizations of the operator EV  $\langle b^I \rangle$  into CFs containing a smaller number of operators than the cardinality of  $I$ ,  $\#(I)$ . We show as an example the factorizations of the first EVs containing products of up to three operators according to Eq. (4.1):

$$\begin{aligned} \mathbf{F} \langle b_1 \rangle &= \delta(b_1), \\ \mathbf{F} \langle b_1 b_2 \rangle &= \delta(b_1 b_2) + \delta(b_1) \delta(b_2), \\ \mathbf{F} \langle b_1 b_2 b_3 \rangle &= \delta(b_1 b_2 b_3) + \delta(b_1 b_2) \delta(b_3) + \delta(b_1 b_3) \delta(b_2) \\ &\quad + \delta(b_2 b_3) \delta(b_1) + \delta(b_1) \delta(b_2) \delta(b_3). \end{aligned} \quad (4.2)$$

One can define the inverse operation  $\mathbf{F}^{-1} \mathbf{F} = \mathbf{1}$  as well. Applying  $\mathbf{F}^{-1}$  to Eq. (4.1),

$$\mathbf{F}^{-1} \delta(b^I) = \langle b^I \rangle - \mathbf{F}^{-1} \delta(b^I)_F, \quad (4.3)$$

gives an implicit definition of  $\mathbf{F}^{-1}$ . As well as  $\mathbf{F}$ , the operator  $\mathbf{F}^{-1}$  does not change the value of the complex number  $\delta(b^I)$ , but rather its representation. By successively applying Eq. (4.3) to itself one arrives at the form

$$\mathbf{F}^{-1} \delta(b^I) = \sum_{P \in P_I} c_P \prod_{J \in P} \langle b^J \rangle \quad (4.4)$$

with  $c_P = (-1)^{\#(P)-1} (\#(P) - 1)!$ , where the CF is represented entirely by EV. Due to the implicit definition of  $\mathbf{F}^{-1}$  the coefficients  $c_P$  are not equal to +1 as in Eq. (4.2). The first three 'refactorized' CFs according to Eq. (4.4) are:

$$\begin{aligned} \mathbf{F}^{-1} \delta(b_1) &= \langle b_1 \rangle, \\ \mathbf{F}^{-1} \delta(b_1 b_2) &= \langle b_1 b_2 \rangle - \langle b_1 \rangle \langle b_2 \rangle, \\ \mathbf{F}^{-1} \delta(b_1 b_2 b_3) &= \langle b_1 b_2 b_3 \rangle - \langle b_1 b_2 \rangle \langle b_3 \rangle - \langle b_1 b_3 \rangle \langle b_2 \rangle \\ &\quad - \langle b_2 b_3 \rangle \langle b_1 \rangle + 2 \langle b_1 \rangle \langle b_2 \rangle \langle b_3 \rangle. \end{aligned} \quad (4.5)$$

With the recursive definition one can easily prove by induction that every EV can be represented in an unambiguous way by CFs and every CF can be represented by

EVs as well. The definition of the lowest-order CF is linear and therefore obviously unambiguous. By using this first definition one can solve the second-order equation unambiguously and with these two solutions one can solve the third-order equation unambiguously and so on, therefore  $\mathbf{F}^{-1}\mathbf{F} = \mathbf{F}\mathbf{F}^{-1} = 1$  holds for every order. Note that a similar definition of CFs can be introduced for fermionic operators  $f_i$ , if the sign of  $\delta(f^J)$  is changed for every commutation of operators corresponding to identical fermionic particles that is performed in the factorization of  $\delta(f^I)$ .

### 4.2.2 Approximations by lower-order quantities

In this section we show how the concept of representing a quantity by a sum of products of another quantity can be exploited for approximation schemes. To this end we introduce the abbreviated notation  $\delta(N)$ , representing any function of CFs  $\delta(b^I)$  of order  $N$  or smaller, where we call the order just the cardinality of  $I$  ( $\mathcal{O}[\delta(b^I)] = \#(I) \leq N$ ). As an example we display the third line of Eqs. (4.2) in this fashion:

$$\mathbf{F} \langle b_1 b_2 b_3 \rangle \equiv \delta(3) + 3\delta(2)\delta(1) + \delta(1)^3 \equiv \delta(3).$$

To symbolize neglects we define the truncation operator  $\Delta_{\delta(N)}$ . Applied to any function of CFs, all CFs of order larger than  $N$  are neglected

$$\Delta_{\delta(N)}\delta(N+1) = \delta(N). \quad (4.6)$$

To further illustrate this notation we apply  $\Delta_{\delta(2)}$  on the third line in Eqs. (4.2)

$$\Delta_{\delta(2)}(\delta(3) + 3\delta(2)\delta(1) + \delta(1)^3) = 3\delta(2)\delta(1) + \delta(1)^3 \equiv \delta(2),$$

leaving an expression that contains only CFs up the second order. Figure 4.1 gives an illustration of this concept.

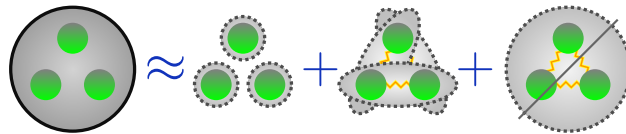


Figure 4.1: Illustration of the basic Idea of the CE. In this case the picture is meant to represent the application of  $\Delta_{\delta(2)}\mathbf{F}$  on a third order EV.

Whether this neglect is justified depends on the physical system under investigation. An analogous definition can be made for the neglect of EVs, here  $\langle N \rangle$  is a short notation for any function of EVs addressing  $N$  or less operators. The application of the truncation operator  $\Delta_{\langle N \rangle}$ ,

$$\Delta_{\langle N \rangle} \langle N+1 \rangle = \langle N \rangle, \quad (4.7)$$

reduces any function of EV  $\langle N+1 \rangle$  of order  $(N+1)$  to a function of EVs containing only EVs of order  $N$  or smaller by setting  $\langle N+1 \rangle$  to zero.

The application of the truncation operator is simple when  $\Delta_{\delta(N)}$  is applied to CFs, and  $\Delta_{(N)}$  is applied to EVs. However, the representation of the quantities in EV or CF is independent from the approximation one applies. One can formulate all quantities in CFs and make an approximation by neglecting higher-order CFs. Alternatively one can formulate all quantities in EV and still apply the very same approximation. Using the factorization operators  $\mathbf{F}^{(-1)}$  we can apply  $\Delta_{\delta(N)}$  to EVs as well. The EV has to be rewritten into CFs (by application of  $\mathbf{F}$ ), then the highest order CF is set to zero (by application of  $\Delta_{\delta_{\#I-1}}$ ) and finally the remaining CFs are rewritten as EVs (by application of  $\mathbf{F}^{-1}$ ). The EV  $\langle b^I \rangle$  is approximated by

$$\mathbf{F}^{-1} \Delta_{\delta_{\#I-1}} \mathbf{F} \langle b^I \rangle = - \sum_{P \in P_I \setminus I} c_P \prod_{J \in P} \langle b^J \rangle, \quad (4.8)$$

a sum of products of lower-order EVs. We show in Sec. 4.3.2 that this approximation scheme is very useful when it is necessary to describe systems with a large number of particles and many degrees of freedom. To illustrate the approach, we apply  $\Delta_{\delta(1)}$  to  $\langle b_1 b_2 \rangle$  and  $\langle b_1 b_2 b_3 \rangle$  and  $\Delta_{\delta(2)}$  to  $\langle b_1 b_2 b_3 \rangle$ :

$$\mathbf{F}^{-1} \Delta_{\delta(1)} \mathbf{F} \langle b_1 b_2 \rangle = \langle b_1 \rangle \langle b_2 \rangle, \quad (4.9)$$

$$\mathbf{F}^{-1} \Delta_{\delta(1)} \mathbf{F} \langle b_1 b_2 b_3 \rangle = \langle b_1 \rangle \langle b_2 \rangle \langle b_3 \rangle, \quad (4.10)$$

$$\begin{aligned} \mathbf{F}^{-1} \Delta_{\delta(2)} \mathbf{F} \langle b_1 b_2 b_3 \rangle &= \langle b_1 b_2 \rangle \langle b_3 \rangle + \langle b_1 b_3 \rangle \langle b_2 \rangle \\ &+ \langle b_2 b_3 \rangle \langle b_1 \rangle - 2 \langle b_1 \rangle \langle b_2 \rangle \langle b_3 \rangle. \end{aligned} \quad (4.11)$$

The reader will recognize Eq. (4.9) as the mean-field approximation and that Eq. (4.10) is related to the second Born approximation [Hoyer et al., 2003]. Equation (4.11) reproduces the so-called Bogoliubov back-reaction method recently used in [Witthaut et al., 2011, Trimborn et al., 2011].

Since we have defined unambiguous transformations between CFs and EVs, it is also possible to formulate analogous approximations for CF  $\delta(b^I)$ . In this case, the truncation operator  $\Delta_{(N)}$  is applied to a CF:

$$\mathbf{F} \Delta_{(N-1)} \mathbf{F}^{-1} \delta(b^I) = - \sum_{P \in P_I \setminus I} \prod_{J \in P} \delta(b^J). \quad (4.12)$$

A CF is approximated by a sum of products of lower-order CFs, since the corresponding EV vanishes. This way of approximation leads exactly to the finite size hierarchy introduced in the previous chapter and in [Florian et al., 2013b], were the finite number of carriers confined in a single QD is taken into account by replacing higher CFs with their factorizations.

We have formulated the two different approximations in a very symmetric fashion. Nevertheless the two approximations are quite the opposite of each other: when a system has many degrees of freedom and the interaction between the particles is weak a CF of certain order can be neglected, the corresponding EV can not,

$$\delta(b^I) = 0 \quad \Rightarrow \quad \langle b^I \rangle = \mathbf{F}^{-1} \delta(b^I)_F,$$

but has to be replaced by products of non-zero EVs of lower order. If a system has only a limited number of particles and certain normal ordered EVs vanish

$$\langle b^I \rangle = 0 \quad \Rightarrow \quad \delta(b^I) = -\delta(b^I)_F,$$

the corresponding CF cannot be neglected but has to be replaced by its factorization (see the FSH described in the previous chapter). In Sec. 4.4.1 we will give a specific example on the difference of the two approaches and see how badly a system with vanishing EV can be described by EoM in which CFs are neglected.

We emphasize that up to this point our considerations are of entirely formal nature. We worked out the case of a vanishing CF and the effect this has on the corresponding EV and vice versa. It depends on the investigated physical system whether one of these approximations is adequate.

### Expanding a the characteristic function of a probability distribution

In this last subsection describing the concept of CFs we briefly illustrate the connection between the moments  $\langle x^n \rangle$  of a probability distribution and the characteristic function of a probability distribution. It is not our aim and not in the scope of this chapter to do this with mathematical strictness, the aim is merely to offer an additional perspective on the idea of the CE, i.e. the neglectation of EVs/CFs. One can say, neglecting higher-order moments of a probability distribution  $\rho$  is equivalent to a Taylor expansion of the inverse Fourier transform of  $\rho$ . In the following we try to illustrate this point of view.

For an arbitrary continuous probability distribution  $\rho(x)$  like the one depicted in Fig. 4.2 one can define the characteristic function as the inverse Fourier transform  $\mathcal{F}^{-1}$  of the probability distribution

$$\phi_X(t) = \langle e^{ixt} \rangle = \int dx e^{ixt} \rho(x) = \mathcal{F}^{-1}[\rho(x)] .$$

From the  $k$ th derivative of the characteristic function with respect to  $t$  one can obtain all moments of the probability distribution  $\langle x^k \rangle = \phi_X^{(k)}(t=0) i^{-k}$ . Conversely this means that the characteristic function can be expressed by a power series with the first  $N$  moments as expansion coefficients plus a residual function

$$\phi_X(t) = T_X^N(t) + R_X^N(t) = \sum_{k=1}^N \frac{(it)^k}{k!} \langle x^k \rangle + R_X^N(t) .$$

So the question how good a probability distribution is represented by its first  $N$  moments can be answered by comparing  $\mathcal{F}[T_X^N(t)]$  to the correct probability distribution. For a more in depth analysis we recommend [Wheeler, 1998, Fick and Sauermann, 1990].

## 4.3 Equations of motion

In this section we show how EVs and CFs are used to derive EoM for a given physical system. We work out how the suggested approximation schemes can be applied to different systems of EoM formulated in terms of EVs or CFs. We also discuss the situation of a mixed Hilbert space describing different types of particles.

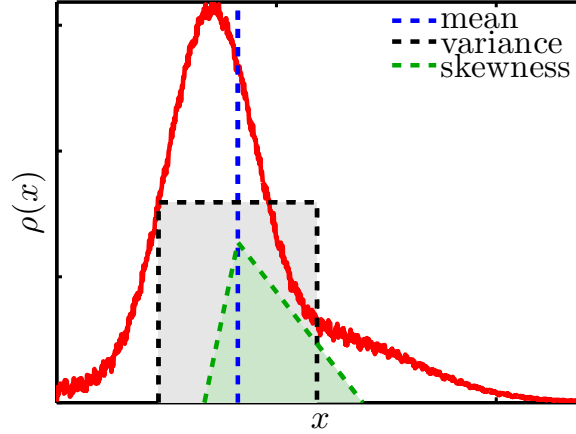


Figure 4.2: Arbitrary probability distribution  $\rho(x)$  shown in red, accompanied by an illustration of its first moments: the mean  $\langle x \rangle$  (blue), the variance  $\langle (x - \langle x \rangle)^2 \rangle$  (black), and the unnormalized skewness  $\langle (x - \langle x \rangle)^3 \rangle$  (green). The blue line is located at the mean of  $\rho$ , the width of the black box corresponds to the square root of the variance, and the asymmetry of the green triangle is proportional to the cube root of the skewness.

### 4.3.1 Infinite Hierarchy

The dynamics of an open quantum mechanical system with the Hamiltonian  $H$  is described by the von Neumann-Lindblad equation (vNL) for the density operator  $\rho$

$$\frac{d}{dt}\rho = -\frac{i}{\hbar}[H, \rho] + \sum_{\nu} \frac{\gamma_{\nu}}{2} (2\eta_{\nu}\rho\eta_{\nu}^{\dagger} - \eta_{\nu}^{\dagger}\eta_{\nu}\rho - \rho\eta_{\nu}^{\dagger}\eta_{\nu}), \quad (4.13)$$

where  $H$  generates the internal dynamics and the Lindblad terms describes the coupling to external baths with transition rates  $\lambda_{\nu}$  and the collapse operators  $L_{\nu}$  (see, for example, [Carmichael, 1999] and references therein). For many systems, an exact solution of  $\rho(t)$  is not feasible due to the size of the system and the interaction part of  $H$ . Moreover, a solution of  $\rho(t)$  is not necessary for many applications and it is enough to know the dynamics of some EVs  $\langle A \rangle = \text{Tr}(A\rho)$ . Equation (4.13) can be used to derive generalized Ehrenfest EoM <sup>1</sup>,

$$\frac{d}{dt}\langle A \rangle = \langle \mathcal{L}(A) \rangle = \frac{i}{\hbar}\langle [H, A] \rangle + \sum_{\nu} \frac{\gamma_{\nu}}{2}\langle 2\eta_{\nu}^{\dagger}A\eta_{\nu} - \eta_{\nu}^{\dagger}\eta_{\nu}A - A\eta_{\nu}^{\dagger}\eta_{\nu} \rangle \quad (4.14)$$

for the desired operator EVs  $\langle A \rangle$ . In Eq. (4.14),  $\mathcal{L}$  is a superoperator that stands for the application of the Lindblad form and the commutator with  $H$  to the operator  $A$ . When deriving Ehrenfest EoM, the interaction part of the Hamiltonian and the scattering terms in the Lindblad terms lead to an hierarchy of EoM. These terms

---

<sup>1</sup>This is not a generalized Heisenberg EoM. A Heisenberg equation is an EoM for an operator in the Heisenberg picture. Equation (4.14) is an EoM for an EV and is derived from the vNL Eq. (4.13) in the Schrödinger picture and not from the Heisenberg equation.

couple a first-order quantity to a second-order quantity and a second-order to a third-order quantity and so on. Symbolically this reads:

$$\begin{aligned}
 \frac{d}{dt} \langle 1 \rangle &= \langle \mathcal{L}(1) \rangle = \langle 2 \rangle \\
 \frac{d}{dt} \langle 2 \rangle &= \langle \mathcal{L}(2) \rangle = \langle 3 \rangle \\
 &\vdots \quad \vdots \quad \vdots
 \end{aligned} \tag{4.15}$$

and without any truncation the hierarchy would go up to infinite order. In many cases, it is possible to calculate the effect of  $\mathcal{L}$  for a whole family of operators  $A_\alpha$  and to formulate an inductive scheme for arbitrary high orders [Gartner, 2011, Kabuss et al., 2011]. When the system contains only  $n$  particles or it is justified to approximate an actual infinite system by a systems containing  $n$  particles, then normal ordered EVs addressing  $n + 1$  particles vanish,

$$\langle b^\dagger \dots b^\dagger \underbrace{b \dots b}_{n+1} \rangle = 0$$

which has the same effect as the application of the truncation operator  $\Delta_{\langle N \rangle}$  with  $N = 2n$ :

$$\langle 2n + 1 \rangle \approx \Delta_{\langle 2n \rangle} \langle 2n + 1 \rangle = \langle 2n \rangle. \tag{4.16}$$

Note that in the case of finite particle numbers the total number of normal ordered operators is not important, but the number of annihilation (creation) operators is. However, we do not focus on this point because in every practical case one can unambiguously identify the vanishing EV. The truncation operator  $\Delta_{\langle N \rangle}$  applied on the  $N$ th line of the hierarchy in Eqs. (4.15) leads to a finite system of linear differential equations:

$$\begin{aligned}
 \frac{d}{dt} \langle 1 \rangle &= \langle \mathcal{L}(1) \rangle = \langle 2 \rangle \\
 &\vdots \quad \vdots \quad \vdots \\
 \frac{d}{dt} \langle N \rangle &= \langle \mathcal{L}(N) \rangle \approx \Delta_{\langle N \rangle} \langle N + 1 \rangle = \langle N \rangle.
 \end{aligned} \tag{4.17}$$

Figure 4.3 gives a visualization of the coupled linear EoM in system (4.17). This truncation scheme is useful when the system contains a small number of particles occupying a limited number of states, i.e., the Hilbert space is finite and manageable with numerical methods. If a system can be described by this method it is, in principle, also possible to solve the vNL Eq. (4.13) directly, since the corresponding matrix equation can be solved in the basis of configurations the finite number of particles occupy. These approaches are often called numerically exact methods.





Figure 4.3: Illustration of an EV hierarchy. The black lines indicate the linear coupling between the EV of increasing order. One can imagine the hierarchy as a line of EVs coupled by linear differential equations to the next order. The hierarchy is truncated by setting the  $(N + 1)$  EV to zero, i.e. applying the truncation operator  $\Delta_{\langle N \rangle}$ .

When the physical system under consideration is too large to be described by a finite Hilbert space, the CE method has proven beneficial. In this method the EoM are derived for the CFs and the CFs of certain order are neglected. To derive the EoM for the CF  $\delta(b^I)$ , the Ehrenfest EoM (4.14) has to be applied to the corresponding EV and the resulting EVs have to factorized into CFs again and finally the previously calculated derivatives of the lower-order factorizations have to be subtracted:

$$\frac{d}{dt}\delta(b^I) = \mathbf{F} \langle \mathcal{L}(b^I) \rangle - \frac{d}{dt}\delta(b^I)_F. \quad (4.18)$$

As well as for the EV hierarchy, the interaction and scattering terms in  $\mathcal{L}$  give rise to an infinite hierarchy of CFs:

$$\begin{aligned} \frac{d}{dt}\delta(1) &= \mathbf{F} \langle \mathcal{L}(1) \rangle - \frac{d}{dt}\delta(1)_F = \delta(2), \\ \frac{d}{dt}\delta(2) &= \mathbf{F} \langle \mathcal{L}(2) \rangle - \frac{d}{dt}\delta(2)_F = \delta(3), \\ &\vdots \\ &\vdots \\ &\vdots \end{aligned} \quad (4.19)$$

The infinite hierarchy displayed in the set of Eqs. (4.19) is equivalent to the infinite hierarchy in Eqs. (4.15) and the two systems of EoM produce exactly the same results if they were formulated up to infinite order and solved exactly.

For a large system with sufficiently weak interaction, CFs  $\delta(b^I)$  of order  $\#(I) > N$  can be neglected and the hierarchy of CFs can be truncated. This is equivalent to the application of the truncation operator  $\Delta_{\delta(N)}$  (from Eq. (4.6)) to the  $N$ th line of the hierarchy in Eqs. (4.19)

$$\begin{aligned} \frac{d}{dt}\delta(1) &= \mathbf{F} \langle \mathcal{L}(1) \rangle - \frac{d}{dt}\delta(1)_F = \delta(2), \\ &\vdots \\ &\vdots \\ \frac{d}{dt}\delta(N) &= \mathbf{F} \langle \mathcal{L}(N) \rangle - \frac{d}{dt}\delta(N)_F \\ &\approx \Delta_{\delta(N)}\mathbf{F} \langle \mathcal{L}(N) \rangle - \frac{d}{dt}\delta(N)_F = \delta(N). \end{aligned} \quad (4.20)$$

This system of Eqs. (4.20), illustrated in Fig. 4.4, is no longer equivalent to the truncated hierarchy of EVs in Eqs. (4.17) due to the application of different truncation operators. In fact Eqs. (4.17) and Eqs. (4.20) describe opposite situations in the same sense as pointed out at the end of Sec. 4.2.2.



Figure 4.4: Illustration of a CF hierarchy. The CF of a certain order couple linearly to the CF of the next order indicated by the black line, but also to products of lower-order CF indicated by the blue merging lines on top. To truncate the hierarchy at order  $N$  the  $(N + 1)$ th CF is set to zero i.e. the truncation operator  $\Delta_{\delta(N)}$  is applied. In contrast to the EV hierarchy depicted in Fig. 4.3 the CF hierarchy cannot be imagined as a straight line, due to the nonlinear coupling of the CF. The structure of this hierarchy is nonlinear and has to be imagined as an intertwined chain.

Let us compare the hierarchies (4.15, 4.17) of EVs to the hierarchies (4.19, 4.20) of CFs. On the one hand Eqs. (4.15, 4.17) are entirely linear since they originate from the linear Ehrenfest EoM (4.14). The only necessary algebraic operation to derive these equations is the normal ordering of  $\mathcal{L}(b^I)$ . The truncated version in Eqs. (4.17) can be used to describe the dynamics of a finite quantum system. On the other hand Eqs. (4.19, 4.20) are nonlinear for all orders larger than one. To derive these equations,  $\mathcal{L}(b^I)$  has to be normal ordered, the resulting EV has to be factorized and time derivatives of the lower-order factorizations have to be subtracted. Without advanced methods the algebraic effort is very high since the factorization ( $\mathbf{F} \langle \mathcal{L}(b^I) \rangle$ ) and the time derivative of the products of the lower-order CFs ( $\frac{d}{dt} \delta(b^I)_F$ ) are demanding and error intensive operations and have to be performed for every single order in the hierarchy. The benefits of this effort are that Eqs. (4.20) can be used to describe the dynamics of a large system with small correlations that would in fact be too large to be described by the set of Eqs. (4.17).

### 4.3.2 Expectation value based cluster expansion

We will now give detail to the central concept of this chapter, the independence of the formulation of the EoM in EVs or CFs from the principle of approximation that is used to truncate the infinite hierarchy of EoM. We have shown in Sec. 4.2.2 that one can apply  $\Delta_{\delta(N)}$  to EVs and  $\Delta_{\langle N \rangle}$  to CFs as well. The consequence is that we can apply the truncation operator  $\Delta_{\delta(N)}$  also on the  $N$ th line of Eqs.(4.15) and obtain a system of EoM formulated in EVs that is equivalent to the CF system Eqs.(4.20):

$$\begin{aligned}
 \frac{d}{dt} \langle 1 \rangle &= \langle \mathcal{L}(1) \rangle = \langle 2 \rangle \\
 &\vdots \\
 \frac{d}{dt} \langle N \rangle &= \langle \mathcal{L}(N) \rangle \approx \mathbf{F}^{-1} \Delta_{\delta(N)} \mathbf{F} \langle N + 1 \rangle = \langle N \rangle.
 \end{aligned} \tag{4.21}$$

Equations (4.21) are equivalent to Eqs. (4.20), and produce the same results, since the same truncation scheme ( $\Delta_{\delta(N)}$ ) is used. Note that Eqs. (4.21) are almost linear, only the EoM where actual approximations are made are nonlinear. An infinite system of linear equations is approximated by a finite set of nonlinear equations in which the non-linearity arises from the approximation. A visualization of Eqs. (4.21) can be found in Fig. 4.5.



Figure 4.5: Illustration of an EV hierarchy truncated by neglecting CFs. This hierarchy is equivalent to the hierarchy illustrated in Fig. 4.4 though in its structure it is very similar to the EV hierarchy illustrated in Fig. 4.3. The EVs of a certain order couple linearly to the next order. The truncation here is not achieved by setting the  $(N + 1)$ th EV to zero but by substituting it by products of lower-order EVs indicated by the merging blue line entering the  $N$ th EV from the side mediated by the truncation operator. In consequence this hierarchy can be imagined as an “almost” straight line where only the last order couples nonlinearly to products of lower-order quantities.

We emphasize that it is much less demanding to derive Eqs. (4.21) than Eqs. (4.20) since an inductive scheme can be used to derive Eqs.(4.21) up to line  $N$ . The factorizations that are required in  $\mathbf{F}^{-1}\Delta_{\delta(N)}\mathbf{F}\langle N + 1 \rangle$  can be listed as indicated in Eqs. (4.9)-(4.11) and all emerging EVs of order larger than  $N$  can be substituted according to such a list. Lists for higher-order EVs can be constructed using the computer algebra tool FORM [Vermaseren, 2000](see appendix D)). Though this formulation is very different from the “traditional” CE it can still be called so, since its approximations and results are exactly the same.

For the sake of completeness, we will also show a system of equations equivalent to Eqs. (4.17) but entirely formulated in terms of CFs:

$$\begin{aligned} \frac{d}{dt}\delta(1) &= \mathbf{F}\langle\mathcal{L}(1)\rangle - \frac{d}{dt}\delta(1)_F = \delta(2), \\ &\vdots \\ \frac{d}{dt}\delta(N) &= \mathbf{F}\langle\mathcal{L}(N)\rangle - \frac{d}{dt}\delta(N)_F \\ &\approx \mathbf{F}\Delta_{\langle N \rangle}\langle\mathcal{L}(N)\rangle - \frac{d}{dt}\delta(N)_F = \delta(N). \end{aligned} \tag{4.22}$$



Figure 4.6: Illustration of a CF hierarchy truncated by neglecting EVs. This hierarchy is equivalent to the hierarchy illustrated in Fig. 4.3 though in its structure it is very similar to the CF hierarchy illustrated in Fig. 4.4. The CF of a certain order couples linearly to the CF of the next order indicated by the black line, but also to products of lower-order CF indicated by the blue merging lines on top. The truncation here is not achieved by setting the  $(N + 1)$ th CF to zero but by substituting it by products of lower-order CF indicated by the merging blue line entering the  $N$ th CF from the right side.

The illustration of this system of equations is displayed in Fig. 4.6. It is obvious that it is clearer and also easier to derive Eqs. (4.17) than it is to derive Eqs. (4.22),

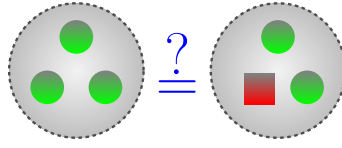


Figure 4.7: Question how correlations between different particles have to be valued compared to correlations between identical particles.

but we see that it is possible to describe a finite system exactly by EoM formulated in CFs, this is again the FSH introduced in the previous chapter.

We conclude this subsection with the suggestion to formulate all EoM in terms of EVs. If the neglect of CFs is required the truncation operator in combination with the factorization operators  $\mathbf{F}^{-1}\Delta_{\delta(N)}\mathbf{F}$  can be used. By this approach, one can use simple inductive algebra to derive Ehrenfest EoM for the EVs and then perform the factorizations only in the highest order EVs. The resulting EoM are much simpler in structure than the equivalent ones formulated in CFs and are much easier to obtain. Another advantage of the formulation in terms of EVs is that the effect of the neglect of CFs is directly marked in the equations by the nonlinearities in the otherwise linear equations.

### 4.3.3 Equation of motion for mixed Hilbert spaces

The advantage of the formulation of the EoM via EV becomes even more evident when one investigates the dynamics of a coupled system, in which the various types of particles have different constraints and correlation strength. Figure 4.7 illustrates the question how correlations between different particles have to be weighted. For example, let us consider a system coupling fermionic carriers described by creation/annihilation operators from the set  $\mathcal{F} = \{f_1^\dagger, \dots, f_n^\dagger, f_1, \dots, f_n\}$  to a quantized light field described by bosonic creation/annihilation operators  $\mathcal{B} = \{b_1^\dagger, \dots, b_m^\dagger, b_1, \dots, b_m\}$ . A general normal ordered EV in this system would be  $\langle b^I f^K \rangle = \langle b_i^\dagger \dots b_l f_o^\dagger \dots f_r \rangle$ , where  $I$  and  $K$  are index sets addressing elements in  $\mathcal{B}$  and  $\mathcal{F}$  respectively. In analogy to the abbreviated notation introduced at the beginning of Sec. 4.2.2 we will write  $\langle N, M \rangle$  for any function of EVs  $\langle b^I f^K \rangle$  with a maximum order  $N, M$  given by the cardinality of the index sets ( $\#I \leq N, \#K \leq M$ ). And we will write  $\delta(N, M)$  for an arbitrary function of CFs  $\delta(b^I f^K)$  with a maximum order  $N, M$ . In Sec. 4.2.2 we have introduced the truncation operators  $\Delta_{\langle N \rangle / \delta(N)}$  acting either on EVs or CFs. For mixed Hilbert spaces the truncation operator has to be specified further to indicate on which part of the EV/CF  $\Delta$  it is acting on. The upper index  $\mathcal{B}, \mathcal{F}$  specifies whether  $\Delta$  is applied on the bosonic or on the fermionic part of the quantity. We give examples for  $\Delta_{\delta(N/M)}$  acting on CFs

$$\Delta_{\delta(N-1)}^{\mathcal{B}} \delta(N, M) = \delta(N-1, M), \quad (4.23)$$

$$\Delta_{\delta(M-1)}^{\mathcal{F}} \delta(N, M) = \delta(N, M-1), \quad (4.24)$$

$$\Delta_{\delta(N+M-1)}^{\mathcal{B}+\mathcal{F}} \delta(N, M) = \delta(N+M-1). \quad (4.25)$$

In our example  $\Delta_{\delta(N)}^{\mathcal{B}}$  neglects bosonic correlations in Eq. (4.23),  $\Delta_{\delta(M)}^{\mathcal{F}}$  neglects

fermionic correlations in Eq. (4.24) and  $\Delta_{\mathcal{B}(N+M)}^{\mathcal{B}+\mathcal{F}}$  neglects  $(N+M)$ -operator correlations in Eq. (4.25), which can be reasonable in large systems with a direct coupling between the different particles. There are many cases where the weighting of the operators is not symmetrical ( $\mathcal{B} + \mathcal{F}$ ) but weighted ( $\mathcal{B} + w\mathcal{F}$ ) with  $w$  being the weighting factor [Kira et al., 1999]. This is for instance the case when a large system is dominated by the dipole Hamiltonian  $b^\dagger f_g^\dagger f_e + b f_e^\dagger f_g$ . In this case one Bose operator is coupled to two Fermi operators and the weighting factor is 1/2.

## 4.4 Applications

To illustrate our approach, we give a specific example for a hierarchy of EoM describing a coupled electron-photon system. We give details on how the derived EoM can be used to describe very different physical systems depending on the approximations that are made to truncate the hierarchy. To conclude this section we interpret former EoM techniques according to our approach.

### 4.4.1 Hierarchy induced by the dipole Hamiltonian

For systems with coupling in-between the different kinds of particles, the hierarchy unfolds into various directions. In this example, the dipole Hamiltonian

$$H_D = \sum g_m b^\dagger f_{g_m}^\dagger f_{e_m} + h.c. \quad (4.26)$$

for a single optical mode in rotating wave approximation (see, for example, [Meystre and Iii, 1999]) couples the operators  $b^{(\dagger)} \in \mathcal{B}$  annihilating (creating) a photon in the cavity mode,  $b|n\rangle^{\mathcal{B}} = \sqrt{n}|n-1\rangle^{\mathcal{B}}$ , to the operators  $f_{e/g_m}^{(\dagger)} \in \mathcal{F}$  annihilating (creating) a carrier in the state  $|e/g; m\rangle^{\mathcal{F}}$ . In this context  $e/g$  specifies the energetic state of the electron in the excited or ground level (conduction and valance band in a semiconductor context) and  $m$  is a place holder for all remaining quantum numbers specifying the carriers state. The EoM for the generalized electron density

$$\begin{aligned} \left. \frac{d}{dt} \right|_{H_D} \langle b^{\dagger a} b^a f_{e_i}^\dagger f_{e_i} \rangle &= -2\text{Re}(g_i \langle b^{\dagger a+1} b^a f_{g_i}^\dagger f_{e_i} \rangle) \\ &- 2a \sum \text{Re}(g_m \langle b^{\dagger a} b^{a-1} f_{e_i}^\dagger f_{g_m}^\dagger f_{e_i} f_{e_m} \rangle), \end{aligned} \quad (4.27)$$

or more schematically

$$\begin{aligned} \left. \frac{d}{dt} \right|_{H_D} \langle 2a, 2 \rangle &= -2\text{Re}g_i \langle 2a+1, 2 \rangle \\ &- 2a \sum \text{Re}g_m \langle 2a-1, 4 \rangle, \end{aligned} \quad (4.28)$$

is a quantity of order  $(2a, 2)$ . It couples to the photon assisted polarization of order  $(2a+1, 2)$  and to EVs correlating polarizations in other shells  $m$  with the presence of a second carrier in state  $|e; i\rangle$ , this term has the order  $(2a-1, 4)$  (compare to

Eq. (4.28)). The EoM for the photon assisted polarization

$$\left. \frac{d}{dt} \right|_{H_D} \langle b^{\dagger a+1} b^a f_{g_i}^\dagger f_{e_i} \rangle = (a+1) g_i \langle b^{\dagger a} b^a f_{e_i}^\dagger f_{e_i} \rangle \quad (4.29)$$

$$\begin{aligned} & + g_i \langle b^{\dagger a+1} b^{a+1} (f_{e_i}^\dagger f_{e_i} - f_{g_i}^\dagger f_{g_i}) \rangle \\ & + (a+1) \sum g_m \langle b^{\dagger a} b^a f_{e_m}^\dagger f_{g_i}^\dagger f_{e_i} f_{g_m} \rangle \\ & - a \sum g_m \langle b^{\dagger a+1} b^{a-1} f_{g_i}^\dagger f_{g_m}^\dagger f_{e_i} f_{e_m} \rangle, \end{aligned}$$

$$\left. \frac{d}{dt} \right|_{H_D} \langle 2a+1, 2 \rangle = (a+1) g_i \langle 2a, 2 \rangle \quad (4.30)$$

$$\begin{aligned} & + g_i \langle 2a+2, 2 \rangle \\ & + (a+1) \sum g_m \langle 2a, 4 \rangle \\ & - a \sum g_m \langle 2a, 4 \rangle, \end{aligned}$$

couples to the spontaneous emission  $(2a, 2)$ , to the stimulated emission  $(2a+2, 2)$ , to the spontaneous emission modified by additional electrons present in the semiconductor system  $(2a, 4)$  and to possible two-photon processes generated by transitions in other shells  $(2a, 4)$  or other emitters (compare Eq. (4.29) and Eq. (4.30)). The desired EVs couple to EVs with a growing number of Bose and Fermi operators. To close this hierarchy it has to be truncated by a combination of  $\Delta^B$  and  $\Delta^F$  as depicted in Fig. 4.8. For information about the photon statistics and to close

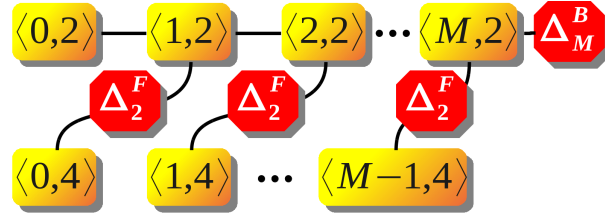


Figure 4.8: Illustration of the system of EoM (4.27-4.30) induced by the dipole Hamiltonian  $H_D$ . The hierarchy unfolds in two directions and therefore has to be truncated by a combination of  $\Delta^B$  and  $\Delta^F$ . The sketch shows how the hierarchy is truncated in our framework in the fermionic direction at single-particle level by  $\Delta_2^F$  standing for  $\Delta_{\langle 2 \rangle}^F$  applicable to one-electron systems or for  $\Delta_{\langle \tilde{\alpha} \rangle}^F$  applicable to semiconductor systems with more than one electron. The photonic direction of the hierarchy is truncated by  $\Delta_M^B$  standing for  $\Delta_{\langle M \rangle}^B$  with applications in cavity-QED systems or for  $\Delta_{\langle \tilde{\alpha} \rangle}^B$  applicable, for example, in laser systems.

the set of equations after factorization the EoM for the (not normalized) photon autocorrelation function

$$\left. \frac{d}{dt} \right|_{H_D} \langle b^{\dagger a} b^a \rangle = 2 \sum_i \text{Re}(g_i \langle b^{\dagger a+1} b^a f_{g_i}^\dagger f_{e_i} \rangle) \quad (4.31)$$

is required as well.

In Fig. 4.9 several different combinations of truncation operators for  $M$  and  $N$  are illustrated. (a) The system can be described by a large but in principle finite Hilbert space, all EV up to the maximum number of particles in the system are taken into account ( $\Delta_{\langle N_{max} \rangle}^N \Delta_{\langle M_{max} \rangle}^M$ ). (b) This is the 'traditional' truncation scheme of the CE. The Hilbert space is too large to be described exactly for both kinds of particles and the interaction Hamiltonian allows to formally identify the two types particles with one another and take all correlations up to a certain combined number of particles into account ( $\Delta_{\langle 2 \rangle}^{N+M}$ ). (c) This system contains a maximum number of  $M = 4$  particles of type  $M$  and very large/unlimited number of particles of type  $N$ . To describe this system all EVs addressing  $M = 5$  or more particles have to be set to zero and CFs of the desired order  $N$  are neglected ( $\Delta_{\langle 1 \rangle}^N \Delta_{\langle 4 \rangle}^M$ ). In panel (d) a similar situation as in panel (c) is depicted, only this time the number of particles of type  $N$  is limited to two and the particle number of the other kind is too large to be treated exactly ( $\Delta_{\langle 2 \rangle}^N \Delta_{\langle 4 \rangle}^M$ ). In panel (e, f) we find the same physical situation as in panel (d) but here we give examples for inappropriate truncations in the 'direction' of particle type  $N$ . (e) CFs up to the order  $N = 3$  are taken into account and higher order CFs are neglected ( $\Delta_{\langle 3 \rangle}^N$ ) which is unnecessary complicated and will produce artifacts due to the violation of the boundary condition  $\langle 3 \rangle = 0$ . (f) In this case CFs of the order two are neglected  $\Delta_{\langle 1 \rangle}^N$ . Again, this is unnecessary complicated since one could simply include the EoM for the two-particle EVs have the hierarchy of EVs terminate 'naturally'. Furthermore it is wrong to assume that the two-particle CFs can be neglected for this system, since the particle number is limited to two and therefore two-particle correlations are expected to be strong.

To further illustrate the application of the combined truncation scheme, we will give examples that result in known models. To obtain these models, we show in the following how Eqs. (4.27,4.29) have to be modified and truncated and in some cases augmented with additional EoM. Note that all systems in the following examples are considered to be in the incoherent regime where EVs like  $\langle b^\dagger \rangle$ ,  $\langle f_e^\dagger f_g \rangle$  vanish [Molmer, 1997]. So far, we have only defined the interaction part of the Hamiltonian in an abstract manner. To describe a real model, the free part of the Hamiltonian, the number of particles and the level structure of the particles have to be declared and according to this the sum and indices in the dipole Hamiltonian. Furthermore, several external processes have to be included into the equations, either by Lindblad terms or directly by adding phenomenological terms to the equations. However, the processes induced by an external bath do not change the necessity to truncate the hierarchy created by  $H_D$ . For the sake of simplicity, we will only consider the external processes explicitly in the first and simplest example.

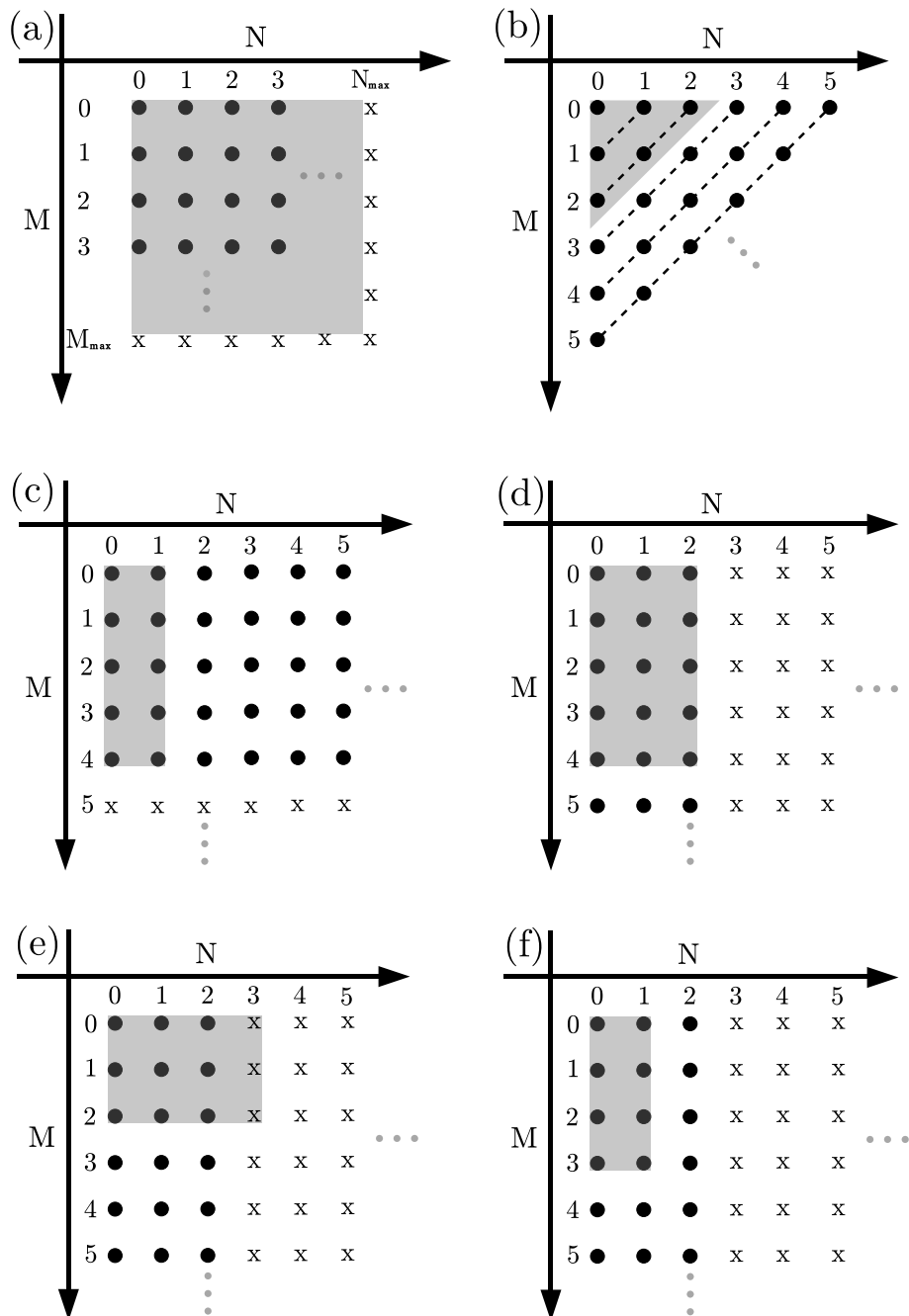


Figure 4.9: Illustration of various truncation possibilities for a system of interacting particles with different order  $M$  and  $N$ . The circles and crosses stand for possible combinations of  $M$  and  $N$  that can occur in the considered CFs and EVs. The crosses indicate a vanishing EV when addressing the corresponding number of particles. The gray area marks all CFs/EVs that are taken into account in the considered order. A detailed description is in the text.



### Jaynes-Cummings model

A very basic example is the JCM with a fixed number of  $N$  photons inside the cavity and one carrier that can occupy the ground or excited state ( $a = 0 \dots N$  and  $m/i$  can only have only one value in Eqs. (4.27,4.29)). The application of  $\Delta_{\langle N \rangle}^{\mathcal{B}} \Delta_{\langle 2 \rangle}^{\mathcal{F}}$  is sufficient to describe this system. Since the JCM is a one-electron model all EV addressing two electrons are zero:

$$\Delta_{\langle 2 \rangle}^{\mathcal{F}} \langle b^I f^\dagger f^\dagger f f \rangle = 0,$$

and because the number of photons is limited to  $N$ , the probability to find  $N + 1$  photons is zero, i.e.

$$\Delta_{\langle N \rangle}^{\mathcal{B}} \langle b^{\dagger N+1} b^{N+1} f^\dagger f \rangle = 0,$$

is justified.

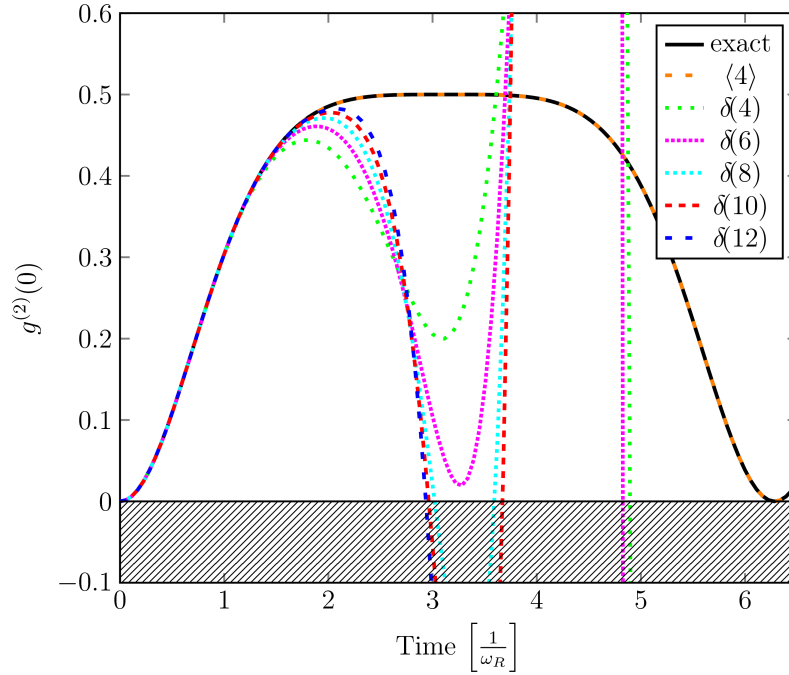


Figure 4.10: Dynamics of the photon-autocorrelation function  $g^{(2)}(0)$  of the JCM for an initially excited electron and the cavity field prepared in a Fock state with  $\langle b^\dagger b \rangle = 1$  and  $\langle b^{\dagger n} b^n \rangle = 0$  for  $n > 1$ . The time is measured in units of the Rabi frequency  $\omega_R$ . Depicted is the analytically exact solution compared to various numerical solutions of the EoM from Eqs. (4.27,4.29). The fermionic part is truncated by  $\Delta_{\langle 2 \rangle}^{\mathcal{F}}$  since the JCM is a one electron model, the photonic part is truncated by  $\Delta_{\langle 4 \rangle}^{\mathcal{B}}$  or  $\Delta_{\langle N \rangle}^{\mathcal{B}}$  with  $N = \{4, 6, 8, 10, 12\}$ . Note that the analytically exact solution and the numerically exact solution ( $\Delta_{\langle 4 \rangle}^{\mathcal{B}}$ ) lie on top of each other. The results obtained by the CE fail to describe the dynamics of this system and the orders eight to twelve even reach nonphysical values below zero marked by the gray hatched area. The curves shown here were all obtained by the EVCE. The corresponding curves obtained by the traditional CE would lie on top of them since both approaches differ only in the formulation but not in the results.

In Fig. 4.10 this EoM approach is compared to the CE where CFs are neglected, which is totally inappropriate for this finite system (see end of Sec. 4.2.2). Figure 4.10 shows the time evolution of the second-order photon-autocorrelation function,

$$g^{(2)}(t, \tau) = \frac{\langle b^\dagger(t)b^\dagger(t+\tau)b(t+\tau)b(t) \rangle}{\langle b^\dagger(t)b(t) \rangle \langle b^\dagger(t+\tau)b(t+\tau) \rangle},$$

at zero delay time ( $g^{(2)}(t, 0) = g^{(2)}(0)$ ) for the JCM with the electron initially in the excited state and the cavity prepared in a Fock state with 1 photon ( $|\psi_0\rangle = |e\rangle^{\mathcal{F}}|1\rangle^{\mathcal{B}}$ ). The system oscillates between the initial state and a two-photon state with the electron in the ground state ( $|\psi_1\rangle = |g\rangle^{\mathcal{F}}|2\rangle^{\mathcal{B}}$ ) consequently the photon-autocorrelation function oscillates between  $g^{(2)}(0) = 0$  and  $g^{(2)}(0) = 0.5$  with the Rabi-frequency  $\omega_R$ . The result of the EoM truncated with  $\Delta_{(4)}^{\mathcal{B}}$  is in perfect agreement with the exact analytical result. The results obtained with the CE (i. e. by applying  $\Delta_{(N)}^{\mathcal{B}}$ ) diverge dramatically from the exact solution and exhibit even nonphysical behavior ( $g^{(2)}(0) < 0$ ). Going to higher orders enlarges the time interval in which the CE matches the exact results. However, the algebraic effort is tremendous and still the CE of order twelve is not able to monitor a half Rabi cycle for this system. Only the inclusion of an infinite number of CFs would be able to compensate the vanishing EV, which is facilitated by  $\Delta_{(4)}^{\mathcal{B}}$  in a very natural fashion. Further details on this approach to the JCM and on the convergence properties of the CE can be found e.g. in [Richter et al., 2009, Leymann et al., 2013b]

### Four-level laser rate equations

Allowing the index  $i$  to be  $\{1, 2\}$  and limiting the number of carriers per atom to one gives the basis of a four-level laser model ( $a = 0, 1$  and  $i = 1, 2$  in Eqs. (4.27,4.29)). The application of  $\Delta_{(2)}^{\mathcal{B}+\mathcal{F}/2}$  gives the basis for the laser rate equations with

$$\mathbf{F}^{-1} \Delta_{(2)}^{\mathcal{B}+\mathcal{F}/2} \mathbf{F} \langle b^\dagger b f^\dagger f \rangle \approx \langle b^\dagger b \rangle \langle f^\dagger f \rangle$$

as the main approximation [Yokoyama and Brorson, 1989, Rice and Carmichael, 1994]. Since the gain medium is considered to consist of one-electron systems the two-electron quantities vanish  $\Delta_{(2)}^{\mathcal{F}} \langle f^\dagger f^\dagger f f \rangle = 0$ . This model provides no statistical information about the photons other than the mean photon number  $\langle b^\dagger b \rangle$ , but can easily be extended within our framework by including higher-order correlations.

### Semiconductor model for a single quantum dot microcavity laser

Characteristic for a semiconductor QD is the presence of more than one carrier confined in the QD shell structure. Pauli blocking of recombination channels, Coulomb interaction and scattering with wetting layer carriers and phonons influence the dynamics of carriers in a semiconductor QD. We consider QDs with two shells ( $i = s, p$  in Eqs. (4.27,4.29)) in the valence and the conduction band. Note that this QD model is identical to the one introduced in chapter 3. Expectation values addressing two carriers are different from zero in this system and thus have to be considered. The Hilbert space corresponding to a single QD inside a cavity with only one resonant photonic mode is still small enough to allow for a numerically exact description

( $a = 1 \dots N$ ). Single semiconductor QD systems have been studied for example in [Ritter et al., 2010, Gies et al., 2012] by the direct solution of the vNL Eq. (4.13). The application of the truncation operators  $\Delta_{\langle 4 \rangle}^{\mathcal{F}}, \Delta_{\langle N \rangle}^{\mathcal{B}}$  on the Eqs. (4.27, 4.29) gives a numerically exact semiconductor QD model equivalent to the vNL equation, when  $N$  is chosen sufficiently large.

To obtain a complete model the EoM for the two-electron quantities  $\langle b^I f^\dagger f^\dagger f f \rangle$  have to be derived using Eq. (4.14) and the corresponding Lindblad terms have to be included. The hierarchy is truncated at the two-electron level, meaning that EV addressing three electrons vanish,

$$\Delta_{\langle 4 \rangle}^{\mathcal{F}} \langle b^I f^\dagger f^\dagger f f \rangle = 0.$$

This truncation is justified by the assumption that the QD initial state is uncharged and electrons and holes are pumped symmetrically (see chapter 3); a discussion of the effects of a unsymmetrical pump can be found in [Florian et al., 2013b]. Every photonic state that is produced by a single QD, be it a thermal or coherent state, can be approximated by a large but finite superposition of Fock states  $N$  so that EVs addressing  $(N + 1)$  photons vanish,

$$\Delta_{\langle N \rangle}^{\mathcal{B}} \langle b^{\dagger N+1} b^{N+1} f^K \rangle = 0.$$

### Semiconductor laser model for multiple quantum dots

In semiconductor QD microcavity lasers, typically, several QDs take part in the laser dynamics. To obtain a microscopic semiconductor laser model, all the processes mentioned in the single semiconductor QD model have to be taken into account as well. For three or four QDs the size of the Hilbert space is still small enough so that the system can still be described by the vNL equation as in [Florian et al., 2013a] or by the induction method up to vanishing EVs [Su et al., 2013]. However, in the case of five or more QDs the fermionic part of the Hilbert space is too large for an exact treatment. When the laser operates above threshold the photon number grows too fast with the pump as well to set up an hierarchy that goes up to vanishing EVs. To truncate the EoM hierarchy for such a large system, CFs have to be neglected.

A model that is sufficient to describe an ensemble of semiconductor QDs coupled to a single cavity mode and to provide statistical information about the photons beyond the intensity is given when Eqs. (4.27,4.29) are carried up to  $a = 0, 1, 2$  and the truncation operators  $\Delta_{\langle 2 \rangle}^{\mathcal{F}}$  and  $\Delta_{\langle 4 \rangle}^{\mathcal{B}}$  are applied. The hierarchy is closed in the fermionic subspace by factorizing all two-electron quantities:

$$\mathbf{F}^{-1} \Delta_{\langle 2 \rangle}^{\mathcal{F}} \mathbf{F} \langle b^I f^\dagger f^\dagger f f \rangle \approx \sum c_{\{J,L,M\}} \langle b^J f^\dagger f \rangle \langle b^L f^\dagger f \rangle \langle b^M \rangle$$

where  $I = J \cup L \cup M$  is the index set addressing the Bose operators. In contrast to the single QD model, a large number ( $> 10$ ) of QDs takes part in the laser dynamics. Therefore an exact treatment of the carriers is impossible and carrier-carrier correlations are not in focus of this model. The carriers can be treated on Hartree-Fock level since the Coulomb interaction is screened by the high carrier

densities in the lasing regime and correlations are strongly diminished by dephasing. In chapter 6 we will explicitly include these and higher correlations to study the influence of correlations between different emitters. In the bosonic subspace the hierarchy is closed by factorizing all EVs containing more than four photon operators

$$\begin{aligned}
 \mathbf{F}^{-1} \Delta_{\mathcal{A}(4)}^{\mathcal{B}} \mathbf{F} \langle b^\dagger b^\dagger b^\dagger b b f^K \rangle &\approx \\
 + \sum c_{\{Q,R,S,T\}} \langle b^\dagger b f^Q \rangle \langle b^\dagger b f^R \rangle \langle b^\dagger f^S \rangle \langle f^T \rangle & \\
 + \sum c_{\{Q',R',T'\}} \langle b^\dagger b^\dagger b b f^{Q'} \rangle \langle b^\dagger f^{R'} \rangle \langle f^{T'} \rangle & \\
 + \sum c_{\{Q'',R'',T''\}} \langle b^\dagger b^\dagger b f^{Q''} \rangle \langle b^\dagger b f^{R''} \rangle \langle f^{T''} \rangle, &
 \end{aligned}$$

where  $K = Q \cup R \cup S \cup T$  is the index set addressing the Fermi operators. There are more possible factorizations, but these terms are zero in the incoherent regime or not driven by the particular Hamiltonian. Expectation values with up to four photon operators are considered in this model. Thereby we have access to the photon-autocorrelation function of the cavity photons at zero delay time  $g^{(2)}(0)$ . An equivalent model formulated in terms of CFs has been introduced in [Gies et al., 2007].

We conclude this section with a comparison between the presented examples. Note the similarities between our first and third example, in both examples, a limited number of carriers interact with limited number of photons. The single semiconductor QD can be regarded as the extension of the JCM to the case of a many electron system. And our fourth example can be considered as the extension of the four-level system laser to a semiconductor laser model that provides additional to the intensities, information about the photon statistics. All these models originate from the same hierarchy of EVs and differ, with respect to the truncation of the hierarchy, only in the order and combination of the truncation operators  $\Delta^{\mathcal{F}}$  and  $\Delta^{\mathcal{B}}$ .

#### 4.4.2 Classification of former approaches by the proposed truncation scheme

At the end of this section, we will briefly touch on former approaches to truncate hierarchies of EoM. The formulation in the literature may differ from ours but the truncation techniques can all be regarded as an application of one or more truncation operators as defined in Eqs.(4.6,4.7). Our formulation offers a new perspective to the various approaches listed in Table 4.1. Example (i) and (ii) in the table are concerned with relatively small systems that can still be treated numerically exact. In the first example (i), the vNL. Eq. (4.13) for the density operator  $\rho$  for a single QD laser is solved in the basis of the finite configuration states  $|\phi_i\rangle = |\text{electron}_1\rangle|\text{electron}_2\rangle|\text{photon}\rangle$  numerically [Ritter et al., 2010], which could also be mapped onto an EV hierarchy truncated at the order corresponding to the size of the matrix  $\rho_{ij} = \langle \phi_i | \rho | \phi_j \rangle$ . The second example (ii) is formulated in EVs and describes a QD cavity system coupled to phonons. The hierarchy of EoM is set up by the induction method [Carmelet et al., 2010b] referred to in Sec. 4.3. The single QD described by a finite Hilbert space investigated in the third example (iii) is coupled

	Physical System	Dim $H^B$	Dim $H^F$	truncation	Formulation	Ref.
(i)	Single semiconductor QD laser	$\sim 40$	6	$\Delta_{(80)}^B \Delta_{(4)}^F$	vNL	[Ritter et al., 2010]
(ii)	2-level-cavity system coupled to phonons	$\sim 20, \sim 20$	2	$\Delta_{(40)}^{B_c} \Delta_{(40)}^{B_{ph}} \Delta_{(2)}^F$	EV	[Car mele et al., 2010b]
(iii)	Semiconductor QD PL into free space	$\sim \infty$	6	$\Delta_{\alpha(1)}^{B_i} \Delta_{(4)}^F$	FSH (CF)	[Florian et al., 2013b]
(iv)	Rabi oscillations in a QD-cavity system	$2 \sim 20$	4	$\Delta_{(30)}^B \Delta_{\alpha(2)}^F$	PPCE (EV)	[Richter et al., 2009]
(v)	Microcavity laser with semiconductor QDs	$\sim 1000$	$\sim 6^{50}$	$\Delta_{\alpha(4)}^B \Delta_{\alpha(2)}^F$	CF	[Gies et al., 2007]
(vi)	Quantum wells	$\sim \infty$	$\sim \infty$	$\Delta_{\alpha(2)}^{B+F/2}$	CF	[Hoyer et al., 2003]
(vii)	Superradiance in a QD nano laser	$\sim 1000$	$\sim 6^{50}$	$\Delta_{\alpha(4)}^{B+Q} \Delta_{\alpha(1/2)}^Q$	CCE	[Leymann et al., 2015]
(viii)	BEC in an optical lattice	$> 10\,000$	0	$\Delta_{\alpha(4)}^B$	EV	[Witthaut et al., 2011]

Table 4.1: Overview of recent publications (which is by no means complete) applying methods that can be interpreted within our framework. Dim  $H^{B/F}$  estimates the number of configurations the bosonic/fermionic part of the system can have. Dim  $H^{B/F}$  is determined by the number of particles in the system and the number of states the single particles can occupy. The table illustrates that for coupled systems (in most examples here light matter coupling) the hierarchy has to be truncated in various directions, and the choice of the truncation order and principle depends strongly on the investigated system.

to a continuum of modes and has therefore be treated approximately by neglecting photon correlations. The EoM in this example are formulated in CF but the finite fermionic part of the system is treated exactly by factorizing CFs that address three or more carriers according to Eq. (4.12). Since this method is designed to set up a hierarchy of EoM for a finite fermionic system, it is called finite-size hierarchy (FSH) see (chapter 3 and [Florian et al., 2013b]). Example (iv) treats its bosonic part exactly by using the photon probability up to  $N$  photons, which could be mapped on EVs  $\langle b^{\dagger a} b^a \rangle$  with  $a$  up to  $N$ . The correlations between the two carriers are neglected and EVs with more than two Fermi operators are factorized. This method combines the photon probability with the factorization of the carrier EVs according to the CE and is therefore called the photon probability cluster expansion (PPCE) [Richter et al., 2009]. The FSH and the PPCE can be regarded as opposite approaches as the FSH treats the Fermi part exactly and factorizes Bose EVs whereas the PPCE factorizes the Fermi part and treats the Bose part exactly. Example (v) is exactly the model described in Sec. 4.4.1 formulated in CFs [Gies et al., 2007]. Quantum wells are described by a continuous Hilbert space and are predesignated for the CE, i.e. , the neglect of CFs as in example (vi), studying the effects of Coulomb and phonon interaction on exciton formation in semiconductor quantum wells [Hoyer et al., 2003]. In example (vii) the radiation induced coupling between carriers is investigated. In this theory configuration operators  $Q$  are introduced that describe the carriers confined to the QD exactly and then CFs between these  $Q$  operators are neglected. This theory called configuration cluster expansion (CCE) is further described in chapter 6 and appendix C. The last example (viii) investigates the dynamics of Bose Einstein condensates (BECs) in optical lattices and has therefore a purely bosonic Hilbert space. The hierarchy of EoM in this example is formulated in EVs. The influence of two-particle correlations is investigated and the hierarchy is truncated by the factorization of three-particle EV according to Eq. (4.11) and is called Bogoliubov back-reaction approximation [Witthaut et al., 2011].

## 4.5 Chapter Conclusion

We have shown how the description of many-particle quantum systems can be facilitated making use of the connection between EVs and CFs. We have seen that the formulation of the EoM in EVs or CFs is independent from the approximations that are made to truncate the hierarchy of EoM. This independence allows for a description entirely formulated in terms of EVs. The use of EVs has several advantages: simple algebra can be used to derive the EoM for all orders, constraints like a limited particle number can be incorporated directly, and the effect of approximations typical for the CE are directly marked by the nonlinear terms in the otherwise linear equations. Additionally, we find it remarkable that this formulation of the CE shows that it is possible to approximate an infinite linear system of EoM by a finite, almost linear system of EoM. It is also worth mentioning that the traditional CE formulated in CFs is equivalent to this almost linear hierarchy of EVs. The linearity of the equations up to the order where actual approximations result in factorizations may be interesting for numerical implementation of the EoM as well as the possibility to give an inductive scheme to set up the EoM. Another aspect we have

concentrated on in this chapter is the truncation of hierarchies of EoM for systems containing different interacting particles and the implementation of constraints like a limited particle number. The flexibility that our approach offers, concerning the approximation principles, is expressed in the various combinations of the truncation operators  $\Delta_{\mathcal{B}/\mathcal{F}}^{\mathcal{B}/\mathcal{F}}$ . Our formulation emphasizes the connections, similarities and differences between various techniques applied in the literature.

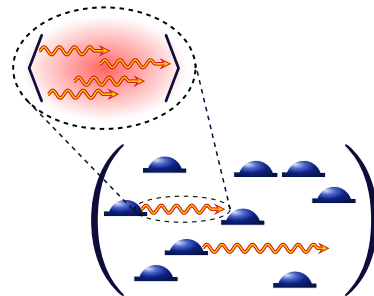
The introduced formulation can be useful in all situations where a systematic inclusion of higher-order correlations is desirable. Our method is, in principle, applicable to all systems where the traditional CE is used and due to the algebraic simplifications higher-order correlations are accessible with our formulation as demonstrated for the JCM in Sec. 4.4 and in the following chapter(s).





# Chapter 5

## Coherence properties of Microcavity QD Lasers



In this chapter we examine the coherence properties of light emitted by quantum dot (QD) based microcavity lasers. To this end we focus on three different aspects. In the first part we examine the photon autocorrelation function of single-mode lasers and extend the laser theory introduced in [Gies et al., 2007] to higher orders and validate the convergence of the cluster expansion (CE) for this system. We study photon autocorrelation functions up to fifth order and monitor the onset of lasing. We observe a successive vanishing of photon bunching in the higher-order photon autocorrelation functions with increasing pump rates. Our results reveal, that the laser threshold is not only softened in microcavity laser systems but is centered around different pump rates with respect to the different orders of photon autocorrelation functions.

In the second part we investigate correlations between two high quality-factor cavity modes of a bimodal microcavity laser. These investigations were initiated by the need to understand recent experimental results from the group of S. Reitzenstein (TU Berlin). In the experiments one emission mode of the microlaser demonstrates the characteristic  $\mathcal{S}$ -shaped input-output curve, while the output intensity of the second mode saturates and even decreases with increasing injection current above threshold. Measurements of the photon autocorrelation function  $g^{(2)}(\tau)$  of the light emission confirm the onset of lasing in the first mode with  $g^{(2)}(0)$  approaching unity above threshold. In contrast, strong photon bunching associated with super-thermal values of  $g^{(2)}(0)$  up to 3.08 detected for the other mode, for currents above threshold. This behavior is attributed to gain competition of the two modes induced by the common gain material, which is confirmed by photon crosscorrelation measurements revealing a clear anti-correlation between emission events of the two modes. The experimental results are in agreement with our theoretical studies based on a microscopic semiconductor theory, which we extend to the case of two modes interacting with the common gain medium. Moreover, we treat the problem by a phenomenological birth-death model extended to two interacting modes, which reveals, that the photon probability distribution of each mode has a double peak structure, indicating switching behavior of the modes for pump rates above threshold.

In the third part of this chapter we investigate the temporal coherence and spec-

tral properties of the studied bimodal microcavity lasers. This leads us to the study of the occurrence of normal-mode coupling (NMC) between the two laser modes. The NMC is attributed to the collective interaction of the cavity field with a mesoscopic number of QDs. In contrast to the conventional NMC here locking of the frequencies and splitting of the linewidths of the eigenmodes of the system in the coherent coupling regime is observed. The theoretical analysis of the incoherent regime is supported by experimental observations where the emission spectrum of one of the orthogonally polarized modes of the bimodal QD micropillar laser demonstrates a two-peak structure.

Parts of the first section of this chapter are published in [Leymann et al., 2013b]. The equations of motion (EoM) were mainly derived by H.A.M. Leymann, and the numerical integration of the EoM was mainly done by A. Foerster.

Parts of the second section of this chapter are published in [Leymann et al., 2013c, Leymann et al., 2013a]. The microscopic EoM were mainly derived by H.A.M. Leymann and A. Foerster, and the numerical integration of the EoM was mainly done by A. Foerster. The extended birth-death model was developed and numerically solved by H.A.M. Leymann. M. Khanbekyan set the theory into context and provided physical insight to the results. The experiments were mainly performed by C. Hopfmann and F. Albert in the group of S. Reitzenstein, while the samples were mainly produced by C. Schneider in the group of A. Forchel.

Parts of the third section of this chapter are published in [Khanbekyan et al., 2015]. M. Khanbekyan worked out the details of the connection between the conventional NMC and the unconventional NMC of the two laser modes. H.A.M. Leymann extended the theory for the first order coherence function to the two-mode case and derived the EoM. A. Foerster performed the numerical integration of the EoM. The experiments were mainly performed by C. Hopfmann from the group of S. Reitzenstein, while the samples were mainly produced by C. Schneider in the group of S. Höfling. All authors of [Leymann et al., 2013b, Leymann et al., 2013c, Leymann et al., 2013a, Khanbekyan et al., 2015] discussed the results and physical implications of the results.

## 5.1 Characterization of micro laser emission in the single-mode case

Quantum dot microcavities are a very attractive system to study quantum optical effects in the solid state [Reitzenstein, 2012]. Apart from research on fundamental light-matter interaction in the weak and strong coupling regime of cavity quantum electrodynamics (see sec. 5.3 and e.g. [Gérard et al., 1998, Bayer et al., 2001, Vahala, 2003, Reithmaier et al., 2004, Yoshie et al., 2004]), they offer the possibility to investigate stimulated emission in a regime approaching the ultimate limit of a thresholdless laser based on a single zero-dimensional gain center [Noda, 2006]. Studies in this field include, e.g., technological works on optically and electrically pumped microlasers aiming at an increase of the  $\beta$ -factor which expresses the fraction of spontaneous emission coupled into the lasing mode [Wang et al., 2005, Strauf et al., 2006, Reitzenstein et al., 2008b]. The increase of the  $\beta$ -factor leads to a van-

ishing intensity jump in the input-output curve, so that the laser threshold can no longer be identified by a drastic change in the intensities. To characterize the transition into lasing of these new 'threshold-less' devices, the changes in the photon statistics of the emitted light have to be studied [Rice and Carmichael, 1994, Ulrich et al., 2007, Wiersig et al., 2009, Chow et al., 2014].

This section is organized as follows. In sub-sec. 5.1.1 we introduce the photon autocorrelation functions as an experimental and theoretical tool to determine the onset of lasing for high  $\beta$ -microlasers. In sub-sec. 5.1.2 we exploit the techniques developed in the previous chapter 4 and extend the semiconductor QD microlaser model introduced in [Gies et al., 2007] to higher orders in the photon hierarchy. This extension is used to confirm the convergence of the CE for this system and to monitor the lasing transition in higher-order photon autocorrelation functions. A brief conclusion of the results can be found at the end of this section.

### 5.1.1 Photon autocorrelation function

In high  $\beta$ -microlasers it becomes increasingly difficult to identify the transition from spontaneous emission to stimulated emission at the laser threshold via their input-output characteristics [Björk et al., 1994]. To illustrate this point the input-output curves for microcavity lasers with increasing  $\beta$ -factors are shown in Fig. 5.1. Before saturation, the system exhibits the typical  $\mathcal{S}$ -shaped behavior of the input-output curve in a double logarithmic plot. From atomic laser theory it is known that the height of the intensity-jump at the threshold is proportional to the inverse  $\beta$ -factor. In [Gies et al., 2007] it is shown that the strict proportionality of the height of the intensity jump and the inverse  $\beta$ -factor is not valid in semiconductor systems due to many-particle effects in the QD emitters, and in chapter 6 we will demonstrate that even the correlations between the electrons in different QDs can modify the height of the intensity jump. Beside these subtle difficulties concerning the height of the intensity jump, Fig. 5.1 clearly illustrates that it is very difficult (for  $\beta = 10^{-1}$ ) or impossible (for  $\beta = 1$ ) to determine the onset of lasing from the input-output curve alone. This issue has triggered comprehensive experimental and theoretical research activities on the second-order photon autocorrelation function

$$g^{(2)}(t, \tau) = \frac{\langle b^\dagger(t)b^\dagger(t + \tau)b(t + \tau)b(t) \rangle}{\langle b^\dagger(t)b(t) \rangle^2}, \quad (5.1)$$

in order to unambiguously identify the onset of stimulated emission at the laser threshold [Rice and Carmichael, 1994, Gies et al., 2007, Strauf et al., 2006, Ulrich et al., 2007]. Moreover, the autocorrelation function is very beneficial to identify single QD controlled lasing effects [Xie et al., 2007, Reitzenstein et al., 2008b, Nomura et al., 2009] and reveals other effects such as correlations between individual photon emission events [Wiersig et al., 2009] and chaotic behavior of feedback coupled microlasers [Albert et al., 2011].

The photon autocorrelation function of second order contains information about the occurrence probability of photon pairs and can be measured in a Hanbury-Brown and Twiss (HBT) setup [Hanbury Brown and Twiss, 1956, Brown and Twiss, 1957, Brown and Twiss, 1958]. In the HBT setup the emitted light is divided

## 5.1. CHARACTERIZATION OF MICRO LASER EMISSION IN THE SINGLE-MODE CASE

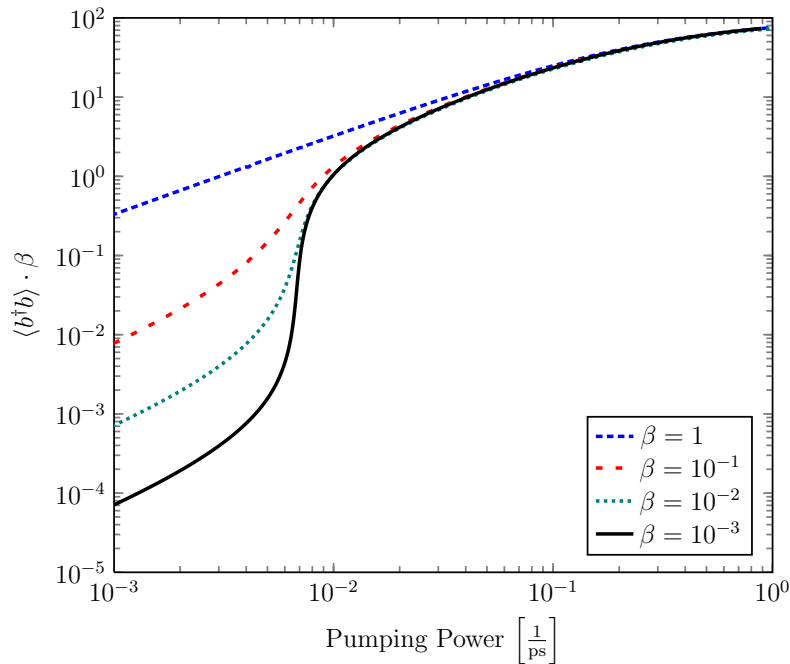


Figure 5.1: Input/output curves for increasing  $\beta$ -factors. The other system parameters are chosen identical to the ones in [Gies et al., 2007]

by a 50/50% beam splitter and the coincidences of photon detections behind the beam splitter are integrated with respect to the delay time  $\tau$  (see Fig. 5.2 for a schematic illustration) [Garrison and Chiao, 2014]. The photon autocorrelation at

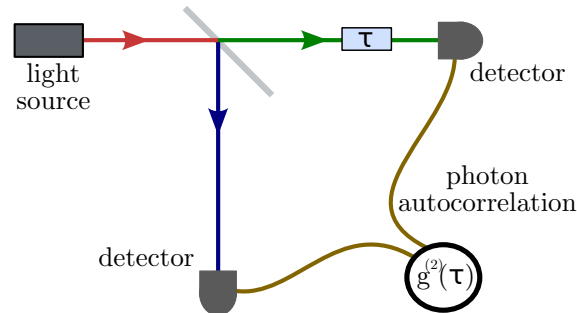


Figure 5.2: Schematic illustration of a HBT setup.

zero delay time is closely related to the photon statistics  $P(n)$  i.e. the probability to find exactly  $n$  photons in the light-field. At the laser threshold the statistical properties of the emitted light change significantly since the process dominating the light emission changes from, spontaneous emission of many uncorrelated emitters to, emission stimulated by a light-field shared by all emitters. The photon statistics and the corresponding values of the photon autocorrelation function at zero delay time are shown in Fig. 5.3. Below the threshold the emitted photons obey thermal statistics, while laser photons are known to obey Poisson statistics, typical for a coherent state [Loudon, 2000, Garrison and Chiao, 2014]. As a rule of thumb one can say that  $g^{(2)}(0)$  indicates how broad the photon probability distribution is,

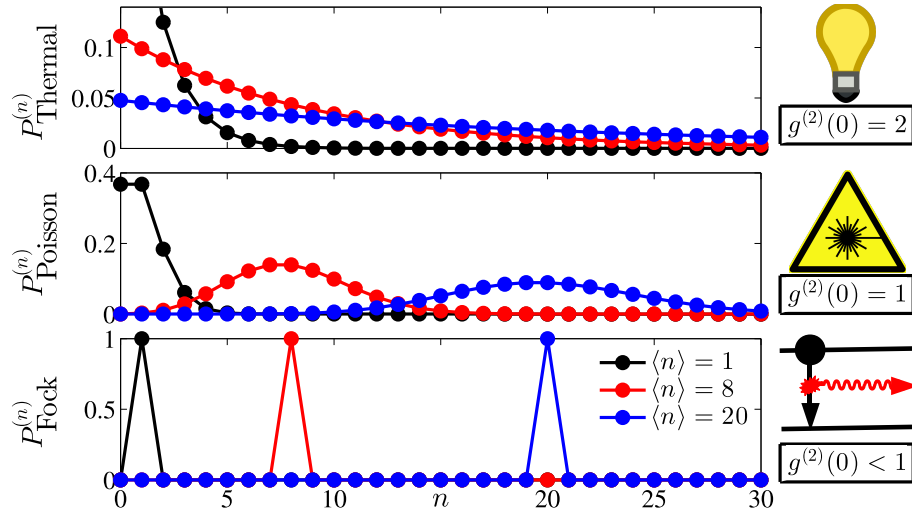


Figure 5.3: Photon statistics and  $g^{(2)}(0)$  values of the 'archetypal' states of light for average photon numbers  $\langle n \rangle = 1, 8, 20$ .

i.e. how strong the fluctuations in the light-field are. In this way  $g^{(2)}(0)$  can be used to monitor the decreasing of fluctuations at the laser threshold even for a microlaser with  $\beta = 1$ . Due to the monotone behavior of  $g^{(2)}(\tau)$  with respect to the delay time  $\tau$  (see Fig. 5.4) the photon autocorrelation is often only considered for zero delay time. Figure 5.5 from [Ulrich et al., 2007] shows the theoretical and experimental results

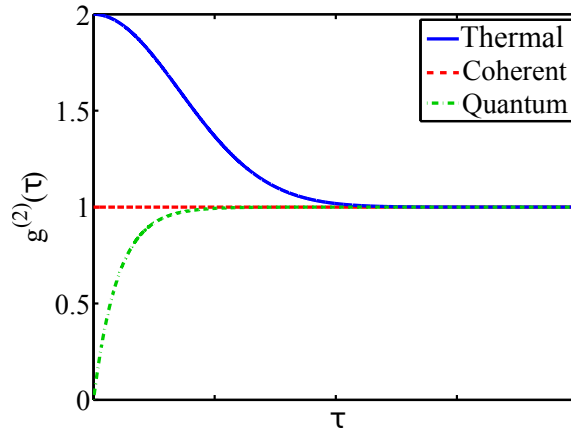


Figure 5.4: Illustration of the monotone behavior of the photon autocorrelation function  $g^{(2)}(\tau)$  that justifies to consider  $g^{(2)}$  only at zero delay time  $g^{(2)}(\tau = 0)$ .  $g^{(2)}(0) < 1$  is characteristic for quantum light, i.e. the intensity fluctuations can not be produced by averaging with a classical probability distribution.  $g^{(2)}(0) = 1$  is characteristic for coherent light, and  $g^{(2)}(0) = 2$  is characteristic for thermal light.

for the intensity and  $g^{(2)}(0)$ . One can clearly see the threshold in the  $g^{(2)}(0)$  curves, whereas a fundamental change in the character of the emitted light can hardly be seen in the input-output curves for  $\beta > 10^{-2}$ . Note that in the experimental results the limited temporal resolution of the detectors destroys the agreement with the pure theoretical predictions. When the limited temporal resolution is taken into account

in the theory by the convolution of  $g^{(2)}(\tau)$  with the detector function, experiment and theory agree (Fig. 5.5(c)).

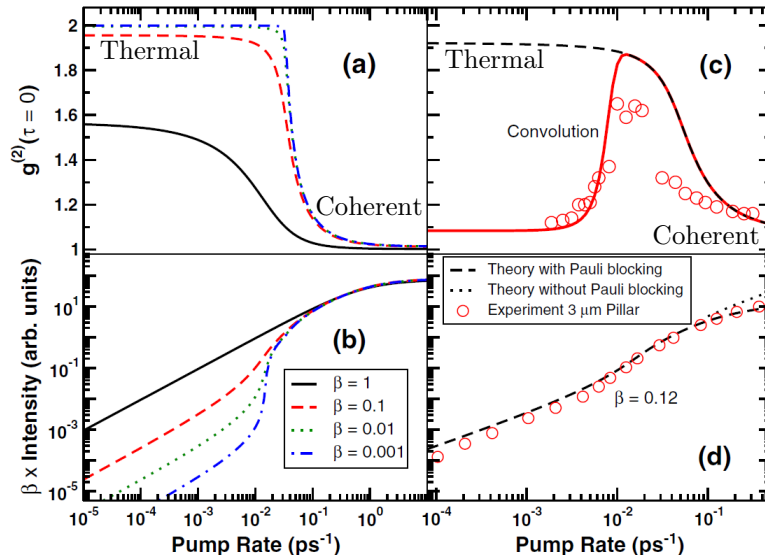


Figure 5.5: (a,b) Theoretical results for the photon autocorrelation function and the light intensities of a QD based microcavity laser. Even for a laser where all spontaneous emission goes into the lasing mode ( $\beta = 1$ ) a transition from thermal to coherent light can be seen in the photon autocorrelation function. (c,d) Experimental results for the photon autocorrelation function and the light intensities of a QD based microcavity laser. The picture is taken from [Ulrich et al., 2007]

### 5.1.2 Laser transition in higher-order photon autocorrelation functions

In this sub-section the concepts introduced in the previous sub-section to characterize the onset of lasing are combined with the advanced CE techniques presented in chapter 4. The microscopic semiconductor QD laser theory from [Gies et al., 2007] is extended further into the bosonic subspace in the same manner as the CE of the Jaynes-Cummings model is in sec. 4.4.1. This enables us to take a closer look at the carrier-photon and photon-photon correlations driven by the laser cavity feedback. The carriers are still treated on Hartree-Fock level, which can be justified by the strong dephasing and the relatively large QD numbers in this system (see chapter 6 for a study on the influence of carrier/emitter correlations). Formally, the truncation operator from Eqs. (4.6)  $\Delta_{\delta(4)}^B$  is changed to  $\Delta_{\delta(N)}^B$  with  $N = \{6, 8, 10\}$  and applied to the Eqs. (4.27), (4.29), and (4.31). With this approach, we obtain converged values for lower-order quantities and also information about higher-order photon autocorrelation functions,

$$g^{(n)}(0) = \frac{\langle b^{\dagger n} b^n \rangle}{\langle b^{\dagger} b \rangle^n}, \quad (5.2)$$

up to  $n = N/2 = 5$ . We show numerical results for a semiconductor QD microcavity laser with 20 identical QDs<sup>1</sup>, a  $\beta$ -factor of 0.01 and all remaining material parameters chosen as in [Gies et al., 2007]. In particular, we concentrate on the photon autocorrelation functions  $g^{(n)}(0)$ . Experimentally, higher-order photon correlations of coupled quantum systems were investigated by several groups [Aßmann et al., 2009, Avenhaus et al., 2010, Stevens et al., 2010, Rundquist et al., 2014]. The behavior of  $g^{(2)}(0)$  at the lasing threshold for a QD-based-microcavity laser is experimentally well studied and has also been investigated with the CE [Gies et al., 2007, Wiersig et al., 2009].

Before we show the theoretical results for the higher-order photon correlation functions we validate the convergence of the CE for this system. Figure 5.6 shows the behavior of  $g^{(2)}(0)$  over the pump rate for increasing orders of the CE. For the chosen  $\beta$ -factor ( $10^{-2}$ ), the photon autocorrelation function drops steeply from two to one at lasing threshold. Note that the deviations of the different orders are small and are becoming smaller with increasing order. The strongest deviations appear directly at the threshold because of the rapid change of photon correlations in this parameter region. Below threshold, photon correlations are small due to the thermal state of the photons and far above the threshold the dephasing induced by the pumping has a strong influence on the system and damps out all higher-order (carrier-)correlations.

Laser light is coherent in all orders  $n$ , as pointed out in the previous sub-section the transition from non-lasing to lasing can be characterized by a change in the photon statistics from a thermal- to a Poisson-distribution. Therefore, not only the second-order photon autocorrelation function but all orders of  $g^{(n)}(0)$  drop from  $n!$  to one at the lasing threshold [Glauber, 1963, Loudon, 2000, Garrison and Chiao, 2014]. In Fig. 5.7 (from [Aßmann et al., 2009]) results for photon autocorrelation measurements up to the fourth order are shown. These experimental results exhibit the transition from  $g^{(n)}(0) = n!$  to  $g^{(n)}(0) = 1$  at the laser threshold expected for (microcavity)lasers. However, one can not assume that this is always the case. Therefore observing the mean photon number and the two photon autocorrelation function  $g^{(2)}(0)$  might not be enough to monitor the laser transition. The state  $|\psi_{nl}\rangle = \frac{1}{\sqrt{2}}(|0\rangle + |2\rangle)$  for example, is not a lasing state at all, however, if one only looks at the photon number and the two-photon autocorrelation function one could think  $|\psi_{nl}\rangle$  might be a laser state ( $\langle b^\dagger b \rangle_{nl} = 1$  is sufficient for stimulated emission to take place, and  $g^{(2)}(0)|_{nl} = 1$  indicates a coherent field). With our approach, higher-order correlation functions are accessible so we are able to monitor the transition to laser light in higher-orders of the photon autocorrelation function. In Fig. 5.8(a) one can see how the autocorrelation functions  $g^{(2,\dots,5)}(0)$  drop from thermal values  $n!$  to one. Note the logarithmic scale and that the deviation of  $g^{(5)}(0)$  from one in relation to its thermal value  $5! = 120$  is as large as the deviations for the lower-order photon autocorrelations. To be able to better monitor the transition in the photon

---

<sup>1</sup>For a detailed description of the CE technique see chapter 4. To avoid repetition, details of the used model will be given in the following section where a multi-mode version of the microscopic semiconductor QD laser theory is presented.

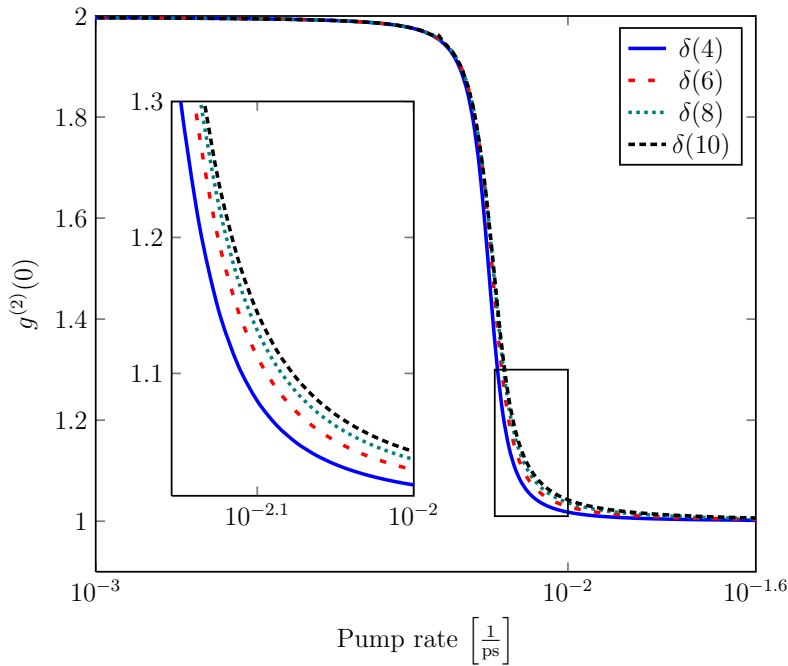


Figure 5.6: Numerical solution of the semiconductor QD laser model for  $\beta = 0.01$  and 20 QDs. The convergence of the photon autocorrelation function  $g^{(2)}(0)$  for different truncation operators  $\Delta_{\delta(N)}^{\mathcal{B}}$  with  $N = \{4, 6, 8, 10\}$  is shown. Further information about the model will be given in the following section and can be found in [Gies et al., 2007].

statistics we also depict scaled photon correlation functions:

$$C^{(n)}(0) = \frac{\delta(b^{\dagger n} b^n)}{\langle b^{\dagger} b \rangle^n} \left( \frac{\delta(b^{\dagger n} b^n)|_{\text{coh}}}{\langle b^{\dagger} b \rangle^n} \right)^{-1}, \quad (5.3)$$

where  $\delta(b^{\dagger n} b^n)|_{\text{coh}}$  is the value of the correlation functions for a coherent field, which can be obtained by successively solving

$$g^{(n)}(0)|_{\text{coh}} = 1 = \frac{\mathbf{F}\langle b^{\dagger n} b^n \rangle|_{\text{coh}}}{\langle b^{\dagger} b \rangle^n}. \quad (5.4)$$

For  $n = \{2, 3\}$  Eq. (5.4) reads:

$$g^{(2)}(0)|_{\text{coh}} = 1 = 2 + \frac{\delta(b^{\dagger 2} b^2)|_{\text{coh}}}{\langle b^{\dagger} b \rangle^2}$$

$$g^{(3)}(0)|_{\text{coh}} = 1 = 6 + 9 \frac{\delta(b^{\dagger 2} b^2)|_{\text{coh}}}{\langle b^{\dagger} b \rangle^2} + \frac{\delta(b^{\dagger 3} b^3)|_{\text{coh}}}{\langle b^{\dagger} b \rangle^3}.$$

In Fig. 5.8(b) the  $C^{(n)}(0)$  are depicted and one can see that all scaled photon correlation functions are zero for low pump rates (where thermal emission is expected), which is consistent with Wick's theorem. For pump rates above threshold, all  $C^{(n)}(0)$  approach one as assumed for a system emitting laser light. However, the four depicted  $C^{(n)}(0)$  have not a common threshold pump rate. They all exhibit



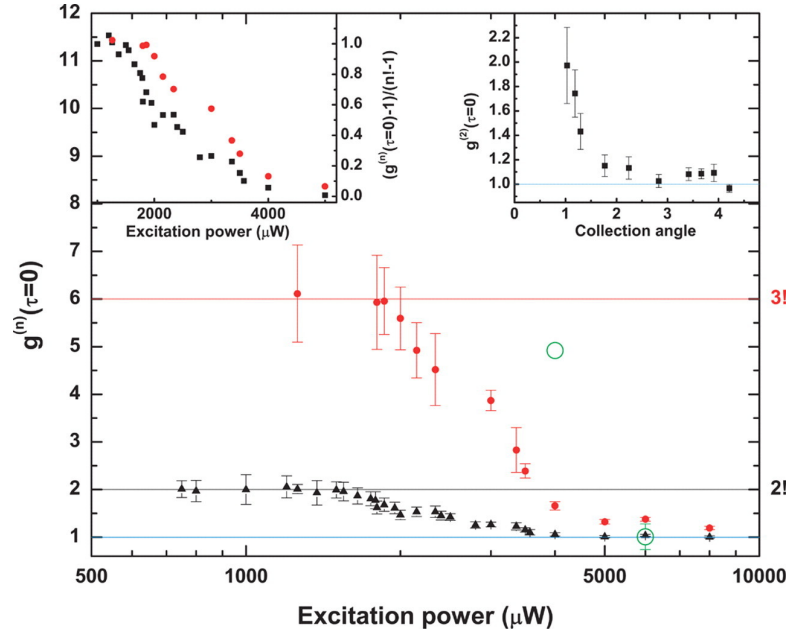


Figure 5.7: Experimental results for  $g^{(n)}(0)$  up to the fourth order. The photon autocorrelation function drops from  $g^{(n)}(0) = n!$  below the threshold to  $g^{(n)}(0) = 1$  above the threshold. The figure is taken from [Aßmann et al., 2009].

their maximum slope at different pump rates. So not only in systems with a  $\beta$ -factor close to one where no intensity jump is apparent and  $g^{(2)}(0)$  exhibits a very shallow slope at the 'threshold' [Rice and Carmichael, 1994], but also for intermediate systems like the one in this example with  $\beta = 0.01$  where a steep slope is still present in  $g^{(2)}(0)$  it is more precise to speak of a threshold parameter region than of one threshold value for the pump rates. The level of coherence builds up successively for increasing orders of  $g^{(n)}(0)$  with increasing pump rates. Comparing Fig. 5.8(a) and (b) one sees that both quantities  $g^{(n)}(0)$  and  $C^{(n)}(0)$  can be used to monitor the transition from thermal to laser light. For a comparison of the different orders of coherence, the scaled correlation functions  $C^{(n)}(0)$  appear more appropriate since all  $C^{(n)}(0)$  have values between zero and one.

**In conclusion** the capability of our reformulation of the CE from chapter 4 is demonstrated for a specific example where we have extended the semiconductor QD laser model presented in [Gies et al., 2007] to higher orders and demonstrated for this model the convergence of the CE. In microcavity systems, the common definition of the laser threshold is not only questionable due to smooth transition in the input output characteristic. Our results suggest that one should keep in mind that it is actually a threshold region when one uses the term laser threshold.

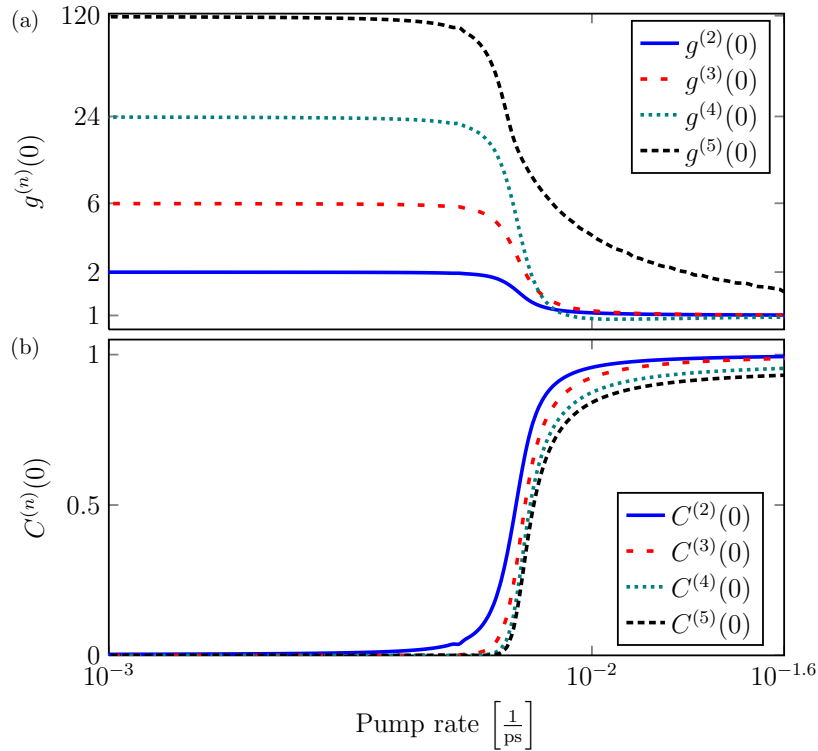
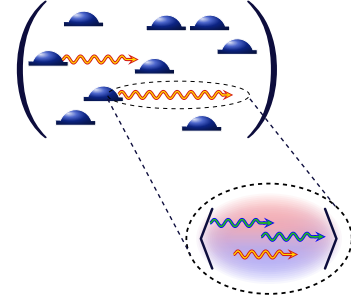


Figure 5.8: Numerical solution of the semiconductor QD laser model for  $\beta = 0.01$  and 20 QDs for order  $\delta(10)$  in the bosonic subspace. The higher-order photon autocorrelation functions  $g^{(n)}(0)$  in dependence of the pump rate are depicted in (a). The theoretical expected transition from thermal to coherent light could be approved up to  $g^{(5)}(0)$  (note the logarithmic scale of the y-axis). In (b) the scaled photon correlation functions  $C^{(n)}(0)$  are depicted. For the thermal field at low pump rates, all correlation functions are zero. An ideal coherent light field would produce  $C^{(n)}(0) = 1$  for all  $n$ . The various  $C^{(n)}(0)$  begin to approach one at different pump rates and not at one particular threshold value.

## 5.2 Intensity fluctuations in bimodal micropillar lasers



The research efforts on microcavity lasers so far have focused mostly on emission features based on the interaction between a single laser mode and the (QD) gain medium. Going beyond this investigations, micropillar lasers with a bimodal emission spectrum allow one to address the coupling of two orthogonal optical modes via the common gain medium which can lead to characteristic oscillations in the coherence properties [Ates et al., 2007], an enhanced sensitivity on external perturbations in the presence of optical self-feedback [Albert et al., 2011] and deterministic polarization chaos even in the absence of optical feedback [Virte et al., 2013].

In this section, we present a detailed experimental and theoretical analysis of the mode coupling and gain competition of bimodal, electrically pumped micropillar lasers. In a generalization of the concepts introduced in the previous section, we measure the coherence properties of the bimodal electromagnetic field with a set of photon correlation functions:

$$g_{\xi\zeta}^{(2)}(\tau) = \frac{\langle b_{\xi}^{\dagger}(t)b_{\zeta}^{\dagger}(t+\tau)b_{\zeta}(t+\tau)b_{\xi}(t) \rangle}{\langle b_{\xi}^{\dagger}(t)b_{\xi}(t) \rangle \langle b_{\zeta}^{\dagger}(t)b_{\zeta}(t) \rangle}, \quad (5.5)$$

where  $\xi, \zeta = 1, 2$ , with delay time  $\tau$  and photon annihilation operators  $b_1$  and  $b_2$  of the mode 1 and the mode 2, correspondingly. The gain competition is reflected in distinct differences in the input-output characteristic and the autocorrelation function  $g_{\xi\xi}^{(2)}(\tau)$  of the two optical modes. Moreover, the crosscorrelation function  $g_{12}^{(2)}(\tau)$  can illustrate correlations between emission events from the two modes. In order to describe and analyze these specific features of bimodal microlasers we extend the microscopic semiconductor model [Gies et al., 2007] accordingly by taking two modes and mode interactions into account. Similarly, we extend a standard birth-death approach [Rice and Carmichael, 1994] to the multi-mode case for the description of bimodal lasers. While the microscopic semiconductor theory is applied to model the input-output characteristics, the intensity correlation functions of the laser and the gain competition between the two emission modes within a strict microscopic theory (see chapter 4 for details on the CE), the extended birth-death approach is phenomenological in nature and allows for a more intuitive understanding of the underlying physics.

The section is organized as follows. In sub-sec. 5.2.1 the experimental results obtained from an electrically pumped, bimodal micropillar laser are presented. Sub-sec. 5.2.2 deals with the theoretical description of the experimental data and is divided into two parts addressing a microscopic semiconductor theory, and an ex-

tended birth-death approach, respectively. We conclude this section in 5.2.5 with a comparison of the experimental and theoretical results.

### 5.2.1 Experiment

The electrically pumped micropillar lasers are based on a planar AlAs/GaAs microcavity structure which includes an active layer consisting of a single layer of  $\text{In}_{0.3}\text{Ga}_{0.3}\text{As}$  QDs. High resolution electron-beam lithography, plasma enhanced etching and metal deposition have been applied to fabricate high quality electrically pumped microlasers. For more details on the sample processing we refer to Ref. [Reitzenstein et al., 2011]. The microlasers have been investigated at low temperature (20 K) using a high resolution micro-electroluminescence ( $\mu\text{EL}$ ) setup. A linear polarizer in combination with a  $\lambda/4$ -wave-plate is installed in front of the entrance slit of the monochromator in order to perform polarization resolved measurements of the laser signal. The photon statistics of the emitted light has been studied by means of the measurement of the photon autocorrelation function  $g_{\xi\xi}^{(2)}(\tau)$ , that has been carried out using a fiber coupled HBT configuration with a temporal resolution  $\tau_{\text{irf}} = 40$  ps. The HBT configuration is coupled to the output slit of the monochromator which has a focal length of  $f = 0.75$  m. The interaction of the orthogonally polarized modes of the microlaser has been investigated by means of photon crosscorrelation measurements. For this purpose, the light emitted by the microlaser is split by a polarization-maintaining 50/50 beamsplitter and coupled into two monochromators, each of which is equipped with a linear polarizer at the input slit and a fiber coupled single photon counting module at the output slit. This configuration allows to perform polarization resolved crosscorrelation measurements with a spectral resolution of  $25 \mu\text{eV}$ . Unfortunately, within the present setup it is not possible to perform photon number distribution measurements due to the low ( $\ll 1 \mu\text{W}$ ) emission power of the microlaser, in contrast to the measurements presented recently for a standard laser diode with the output power of order of milliwatts [Roumpos and Cundiff, 2013].

First, let us focus on the input-output characteristics of the microlaser. Due to slight asymmetry of the cross-section of the pillar and the ring-shaped contact the degeneracy of the fundamental mode in the pillar microcavity is lifted and two distinct linearly polarized modes are supported [Reitzenstein et al., 2007]. Details on how the QD-mediated mode coupling affects the modes of the passive system can be found in the next section and are subject to further research. In this context, the spectral splitting  $\Delta_{12}$  and accordingly the overlap between the two modes plays an important role for the studies of emission of bimodal cavities. Figure 5.9 shows representative polarization resolved spectra of an electrically pumped bimodal microlaser at threshold (injection current,  $I_{inj} = 5.1 \mu\text{A}$ ). The two linearly polarized modes are split in energy by  $103 \mu\text{eV}$  and have absorption limited  $Q$ -factors of  $Q = 13900$  (mode 1) and  $Q = 13100$  (mode 2) at the threshold. The input-output characteristic of the bimodal microlaser is presented in Fig. 5.10(a). We observe pronounced differences between the two modes: while mode 1 shows a standard “ $\mathcal{S}$ ”-shaped input-output characteristic with a threshold current of about  $I_{th} = 5.1 \mu\text{A}$ , the intensity of mode 2 saturates at  $I_{inj}/I_{th} = 2$  and even drops down for injection

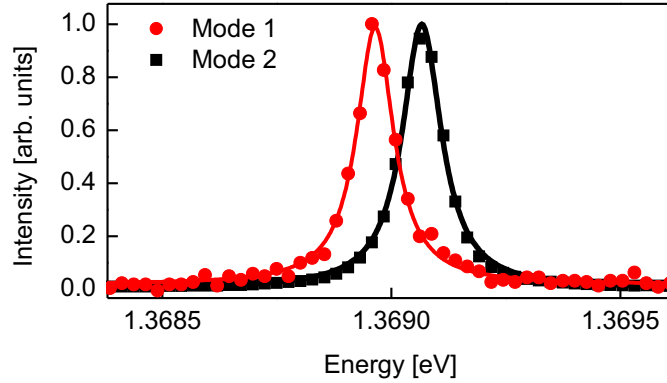


Figure 5.9: Polarization resolved  $\mu EL$  emission spectra of a microlaser with a diameter of  $3 \mu\text{m}$ . The electromagnetic field emission features two orthogonally polarized cavity modes, the mode 1 ( $Q = 13900$ ) and the mode 2 ( $Q = 13100$ ) with a spectral separation of  $103 \mu\text{eV}$  (Injection current:  $I_{inj} = 5.1 \mu\text{A}$ ).

currents exceeding  $I_{inj}/I_{th} = 2.5$ . This behavior indicates a pronounced competition between the modes 1 and 2 which is mediated by the common QD gain material as it will be further elaborated in the following. Further, to study the lasing features we extract the emission linewidths of the two modes and plot them as a function of the injection current in Fig. 5.10(b). The linewidths of the modes 1 and 2 have similar magnitude and decrease strongly at threshold which reflects enhanced temporal coherence in the lasing regime. Interestingly, while the linewidth of mode 1 stays at a resolution limited value of  $25 \mu\text{eV}$ , a slight increase of the linewidth can be observed for mode 2 above  $I_{inj}/I_{th} = 3$ . This is in agreement with the decreasing emission intensity seen in Fig. 5.10(a), which indicates an increasing contribution of spontaneous emission in the mode 2 at high injection currents. However, we have to stress that the linewidth of mode 2 is still surprisingly small given its low intensity and strong fluctuations.

In order to verify the interpretation of mode coupling in terms of gain competition, crosscorrelation measurements were performed between the modes 1 and 2 at different injection currents. The results of such a measurement are presented in Fig. 5.10(e) for  $I_{inj}/I_{th} = 3$ . The cross-correlation function  $g_{12}^{(2)}(\tau)$  shows a pronounced dip  $g_{12,min}^{(2)} = 0.62$  at  $\tau = 0$  which indicates an anti-correlation between emission events from the two laser modes. The anti-correlated emission occurs at a characteristic timescale of  $\tau_{12} = 3.8 \text{ ns}$ . Figure 5.10(d) reveals that the crosscorrelation function  $g_{12}^{(2)}(0)$  strongly depends on the injection current. In particular, in the regime of certain injection currents above the threshold ( $2.7 < I_{inj}/I_{th} < 3.3$ ), the anti-correlation between the modes is the strongest.

As it is seen from Fig. 5.10(a), at these values of the injection currents above the threshold the intensity of mode 2 decreases. The interplay between the two emission modes is also accompanied by strong temporal intensity fluctuations which are identified by measuring the photon autocorrelation function of the two competing modes for different injection currents. The respective dependencies, i.e.  $g_{11}^{(2)}(0)$  and  $g_{22}^{(2)}(0)$

versus injection current, are plotted in Fig. 5.10(c), while Fig. 5.10(f) shows the autocorrelation function  $g_{22}^{(2)}(\tau)$  for  $I_{inj}/I_{th} = 3$ . The mode 1 shows the in experiments typical maximum of  $g_{11}^{(2)}(0)$  around threshold, which indicates the transition from spontaneous emission to stimulated emission, where  $g_{11}^{(2)}(0)$  is lower than expected from theory due to the limited temporal resolution of the HBT configuration [Ulrich et al., 2007]. In contrast, as can be concluded from Fig. 5.10(c), the statistics of the mode 2 at certain injection currents demonstrates strongly super-Poissonian behavior, since the autocorrelation function  $g_{22}^{(2)}(0)$  increases strongly at the pump rates well above threshold and reaches a maximum value of 3.08 at  $I_{inj}/I_{th} = 3$ . This value is significantly higher than  $g_{22}^{(2)}(0) = 2$ , expected for thermal light and, therefore, can not be explained by standard photon statistics.

It is important to note, that similar statistical properties of the emission, i.e. strong super-Poissonian behavior for the weak mode, has been also observed for microlasers in the presence of an external mirror, where a delayed feedback of the emitted signal disturbs laser operation and leads to strong bunching for the weak mode [Albert et al., 2011, Schulze et al., 2014]. Optical feedback can also be used to enhance quantum properties in the single photon [Carmelet et al., 2013] and two-photon [Hein et al., 2014] regime, and it might be very interesting to further explore the connection between mode coupling and self-induced feedback.

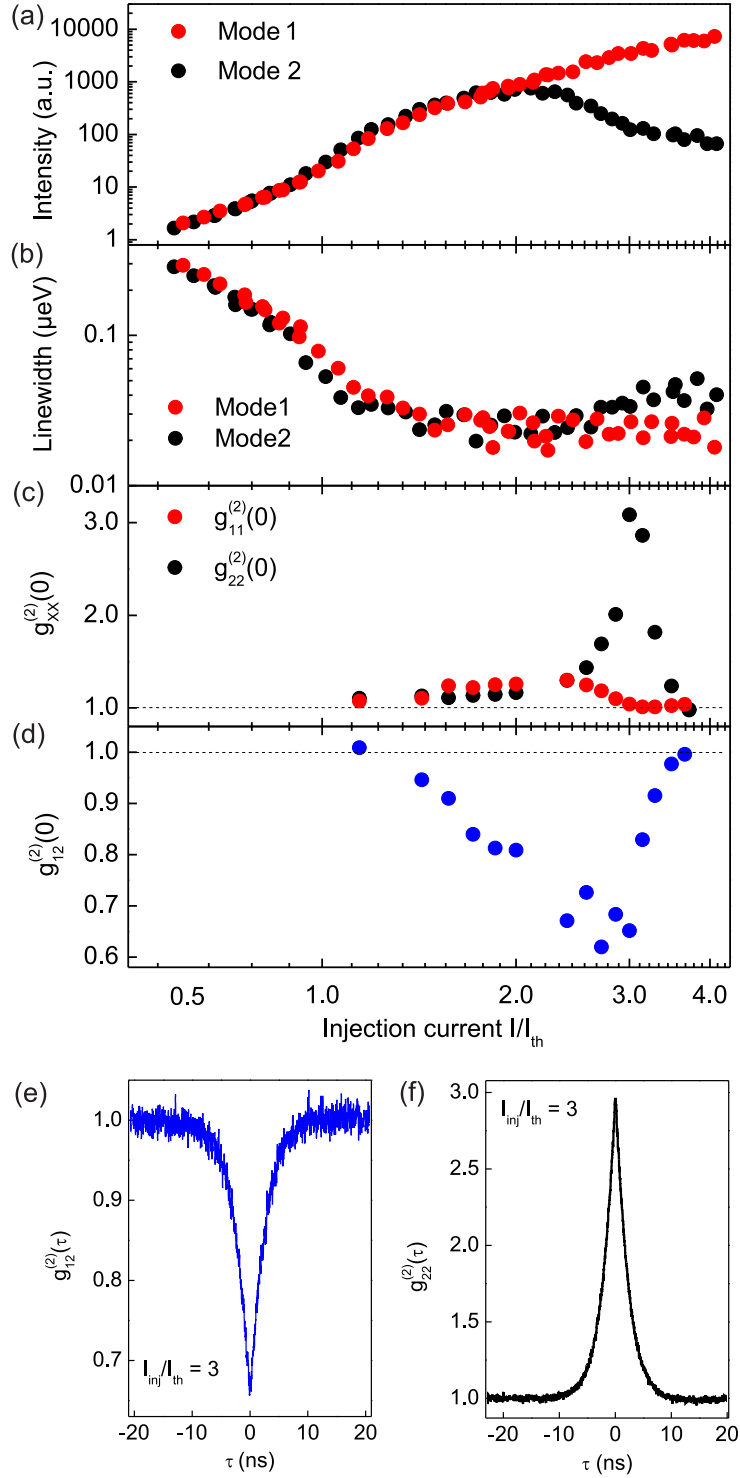


Figure 5.10: Experimental characteristics of a bimodal micropillar laser with a diameter of  $3 \mu\text{m}$ . (a) Input-output characteristic, (b) emission mode linewidth and the photon (c) auto- and (d) crosscorrelation functions  $g_{11}^{(2)}(0)$ ,  $g_{12}^{(2)}(0)$ , and  $g_{22}^{(2)}(0)$  of emission from modes 1 and 2, respectively. Panels (e) and (f) show exemplary crosscorrelation  $g_{12}^{(2)}(\tau)$  and autocorrelation  $g_{22}^{(2)}(\tau)$  measurements at an injection current of  $I_{inj}/I_{th} = 3$ .

### 5.2.2 Theory

To develop a theoretical framework for the study of the coupled carrier-photon system in the bimodal cavity we consider two different theoretical approaches. In the first, a microscopic theory of light-matter interaction of semiconductor QDs with the cavity field is given, which allows the derivation of the EoM for quantities of interest. In the second approach, starting with a master equation derived from a birth-death model, statistics of the photon distribution can be derived for the case of two-level carriers.

### 5.2.3 Microscopic Semiconductor Theory

To study the interaction of QDs with the electromagnetic field inside an optical bimodal microcavity we have extended the Microscopic Semiconductor Theory [Gies et al., 2007] to the case of two modes and photon crosscorrelation functions.

#### Physical Model

The Microscopic Semiconductor Theory allows for inclusion of many-body effects of the carriers and can be used to calculate correlations required to determine the statistics of the emission of microcavities with active QDs (for a review see, e. g., Ref. [Michler, 2009]). The calculations are based on the CE truncation scheme of the EoM for operator  $EV$  (see chapter 4).

In what follows the generic QD model from sec. 3.4 is used in which it is assumed that only two confined QD shells for both electrons and holes are relevant: whereas the resonant interaction with the electromagnetic field of the bimodal cavity is due to the coupling with the  $s$ -shell transition, the carrier generation due to electrical pumping is to take place in the  $p$ -shell. The assumption suits well also for an experimental situation, where the electrical pumping is to take place via injection of electrons and holes into the wetting layer and subsequent fast relaxation to the discrete electronic states of the QDs. Further, carrier-carrier and carrier-phonon scattering contributions to the dynamics are evaluated using a relaxation time approximation, where the relaxation towards quasi-equilibrium is given in terms of a relaxation rate [Nielsen et al., 2004]<sup>2</sup>.

To be more specific, let us consider a bimodal microcavity with the QDs as gain medium with the driving performed by the recombination of carriers in the valence and conduction bands. The Hamiltonian that governs the temporal evolution of the overall system can be given in the form

$$H = H_{\text{carr}}^0 + H_{\text{Coul}} + H_{\text{ph}} + H_{\text{D}}, \quad (5.6)$$

---

<sup>2</sup>This approach deviates from the more general one using Lindblad terms introduced in chapters 3 and 4. The reason for this deviation formulation is twofold: Firstly, the presented theory is a direct extension from the one presented in [Gies et al., 2007]. Secondly, at the time this two-mode theory was developed, the EVCE from chapter 4 was not ready to use. Since the influence of the environment is not in the focus of this specific work and it is shown in [Foerster, 2012] that the different descriptions do not deviate qualitatively, we stick in this section to the old theory using relaxation rates and correlation functions.



where  $H_{\text{carr}}^0$  is the single-particle contributions for conduction and valence band carriers with the energies  $\varepsilon_j^{c,v}$ ,

$$H_{\text{carr}}^0 = \sum_j \varepsilon_j^c c_j^\dagger c_j + \sum_j \varepsilon_j^v v_j^\dagger v_j, \quad (5.7)$$

and the two-particle Coulomb interaction is given by [Baer et al., 2006]

$$H_{\text{Coul}} = \frac{1}{2} \sum_{k'jj'k} (V_{k'jj'k}^{cc} c_{k'}^\dagger c_j^\dagger c_{j'} c_k + V_{k'jj'k}^{vv} v_{k'}^\dagger v_j^\dagger v_{j'} v_k) + \sum_{k'jj'k} V_{k'jj'k}^{cv} c_{k'}^\dagger v_j^\dagger v_{j'} c_k. \quad (5.8)$$

In the above,  $c_j$  ( $c_j^\dagger$ ) and  $v_j$  ( $v_j^\dagger$ ) are fermionic operators that annihilate (create) a conduction-band carrier in the state  $|j\rangle_c$  and a valence-band carrier in the state  $|j\rangle_v$ , respectively. Further, the Hamiltonian of the electromagnetic field modes inside the cavity reads

$$H_{\text{ph}} = \sum_\xi \hbar\omega_\xi b_\xi^\dagger b_\xi, \quad (5.9)$$

where  $b_\xi$  ( $b_\xi^\dagger$ ) is the bosonic annihilation (creation) operator of the  $\xi$ th mode of the cavity.

The energy of interaction of the QDs with the electromagnetic field inside the cavity in dipole approximation can be given by:

$$H_{\text{D}} = -i \sum_{\xi,j} (g_{\xi j} c_j^\dagger v_j b_\xi + g_{\xi j} v_j^\dagger c_j b_\xi) + \text{H.c.}, \quad (5.10)$$

where the approximation of equal wave-function envelopes for conduction- and valence-band states is used. Moreover, for simplicity the coupling strength  $g_{\xi j}$  is assumed to be real.

The Hamiltonian given by Eq. (5.6) together with Eqs. (5.7–5.10) determines the dynamical evolution of the carrier and field operators and, in particular, the time evolution for operator expectation values.

The EoM for quantities of interest, as for example the average photon number in the cavity modes and the average electron population in the conduction and valence bands, have source terms that contain operator expectation values of higher order. In this way, the approach bears an infinite hierarchy of equations of motion for various expectation values for photon and carrier operators. To perform a consistent truncation of the equations the CE scheme is applied (for details, see chapter 4 and references therein). Namely, starting from the expectation values of the first order of photon operators, the EoM for operator expectation values are replaced by EoM for correlation functions. For example, instead of the EoM for expectation values of amplitudes of the cavity mode operators  $\langle b_\xi^\dagger b_\zeta \rangle$ , the EoM for corresponding amplitude correlation functions  $\delta \langle b_\xi^\dagger b_\zeta \rangle = \langle b_\xi^\dagger b_\zeta \rangle - \langle b_\xi^\dagger \rangle \langle b_\zeta \rangle$  are used. Then, to achieve a consistent classification and inclusion of correlations up to a certain order the truncation of the equations for correlation functions rather than for expectation values is performed.

In particular, in the case of a system without coherent external excitation  $\langle b_\xi^\dagger \rangle = \langle b_\xi \rangle = 0$  and  $\langle c_j^\dagger v_j \rangle = 0$  hold. Therefore, applying the rotating-wave approximation here and thereafter, the EoM for amplitude correlation functions of the mode operators can be given by

$$\frac{d}{dt} \delta \langle b_\xi^\dagger b_\xi \rangle = -(\kappa_\xi + \kappa_\zeta) \delta \langle b_\xi^\dagger b_\xi \rangle + \sum_{j,q} \left( g_{\xi j} \delta \langle c_j^\dagger v_j b_\xi \rangle + g_{\xi j} \delta \langle v_j^\dagger c_j b_\xi^\dagger \rangle \right), \quad (5.11)$$

where  $\kappa_\xi$  is the loss rate of the  $\xi$ th cavity mode and  $q = 1 \dots N$ , with  $N$  being the total number of QDs. Note, that both cavity-mode amplitude correlation functions  $\delta \langle b_\xi^\dagger b_\xi \rangle$  and the coupled photon-assisted polarization amplitude correlations  $\delta \langle v_j^\dagger c_j b_\xi^\dagger \rangle$  and  $\delta \langle c_j^\dagger v_j b_\xi \rangle$  are classified as doublet terms in the CE scheme, i.e., they correspond to an excitation of two electrons. In the terms of the truncation operators closing the hierarchy at doublet level would correspond to the truncation operator  $\Delta_{\delta(2)}^{\mathcal{B}_i + \mathcal{F}/2}$ . The equation of motion for the photon-assisted polarization amplitude correlation read [see also Eq. (B.1) in Appendix B]:

$$\begin{aligned} \frac{d}{dt} \delta \langle v_j^\dagger c_j b_\xi^\dagger \rangle &= -i(\Delta_{\xi j} - i\kappa_\xi - i\Gamma) \delta \langle v_j^\dagger c_j b_\xi^\dagger \rangle + g_{\xi j} \delta \langle c_j^\dagger c_j \rangle (1 - \delta \langle v_j^\dagger v_j \rangle) \\ &+ \sum_{\xi'} \left[ g_{\xi' j} \delta \langle b_{\xi'}^\dagger b_{\xi'} \rangle (\delta \langle c_j^\dagger c_j \rangle - \delta \langle v_j^\dagger v_j \rangle) + g_{\xi' j} \delta \langle c_j^\dagger c_j b_{\xi'}^\dagger b_{\xi'} \rangle - g_{\xi' j} \delta \langle v_j^\dagger v_j b_{\xi'}^\dagger b_{\xi'} \rangle \right], \end{aligned} \quad (5.12)$$

where  $\Delta_{\xi j} = \varepsilon_j^c - \varepsilon_j^v - \hbar\omega_\xi$  is the detuning of the  $\xi$ th cavity-mode from the QD transition and  $\Gamma$  is a phenomenological dephasing parameter describing spectral line broadening. In the case of a bimodal cavity only the cavity modes with indices  $\xi = 1, 2$  are nearly resonantly coupled to the QDs. Whereas the modes with  $\xi \neq 1, 2$  are not within the gain spectrum of the QD ensemble or have low  $Q$ -value. Since the population of the non-lasing modes  $\langle b_\xi^\dagger b_\xi \rangle$  and the cross-correlation functions  $\langle b_\xi^\dagger b_1 \rangle$  and  $\langle b_\xi^\dagger b_2 \rangle$  with  $\xi \neq 1, 2$  remain negligibly small, the third terms on the right-hand side of Eq. (5.12) for  $\xi \neq 1, 2$  can be effectively set equal to zero. Thus, Eq. (5.12) for  $\xi \neq 1, 2$  can be solved in the adiabatic limit yielding a time constant  $\tau_{nl}$  that describes the spontaneous emission into non-lasing modes according to the Weisskopf-Wigner theory. The spontaneous emission of QDs into non-lasing modes leading to a loss of excitation is described by a  $\beta$ -factor defined as the ratio of the spontaneous emission rate into the lasing modes  $1/\tau_l$  and the total spontaneous emission rate enhanced by the Purcell effect  $1/\tau_{sp}$ :

$$\beta = \frac{\tau_l^{-1}}{\tau_{sp}^{-1}} = \frac{\tau_l^{-1}}{\tau_l^{-1} + \tau_{nl}^{-1}}. \quad (5.13)$$

The dynamics of the carrier population of the electrons in the  $s$ -shell is given by

$$\frac{d}{dt} \delta \langle c_s^\dagger c_s \rangle = - \sum_{\xi} \text{Re} \left( g_{\xi q} \delta \langle c_s^\dagger v_s b_\xi \rangle \right) + \delta \langle c_p^\dagger c_p \rangle (1 - \delta \langle c_s^\dagger c_s \rangle) \tau_c^{-1} - \delta \langle c_s^\dagger c_s \rangle (1 - \delta \langle v_s^\dagger v_s \rangle) \tau_{nl}^{-1}. \quad (5.14)$$

Here, the first term on the right-hand side originates from the interaction with the cavity-modes, the second term describes the relaxation of carriers from the  $p$ - to

the  $s$ -shell with a relaxation timescale  $\tau_c$ , and the last term represents the loss of excitation into the non-lasing modes.

We assume, according to the generic QD model used throughout this thesis, that the  $p$ -shell carriers are generated at a constant pump rate  $p$ . Then, similar to Eq. (5.14), the EoM for the carrier population of the electrons in the  $p$ -shell reads:

$$\frac{d}{dt}\delta\langle c_p^\dagger c_p \rangle = p(\delta\langle v_p^\dagger v_p \rangle - \delta\langle c_p^\dagger c_p \rangle) - \delta\langle c_p^\dagger c_p \rangle(1 - \delta\langle c_s^\dagger c_s \rangle)\tau_c^{-1} - \delta\langle c_p^\dagger c_p \rangle(1 - \delta\langle v_p^\dagger v_p \rangle)\tau_{sp}^{-1}, \quad (5.15)$$

where the last term on the right-hand side describes spontaneous recombination of  $p$ -shell carriers. The corresponding equations for valence band carriers are relegated into Appendix B.

The form of the expression for the intensity correlation functions suggests (see Eq. (5.5)) that to exploit the statistical properties of the light emission using intensity correlations, a consistent treatment within the CE up to the quadruplet order is required (correspond to the truncation operator  $\Delta_{\tilde{\alpha}(4)}^{B_i+\mathcal{F}/2}$ ). As in the section before we treat the carrier correlations on Hartree-Fock level (i.e.  $\Delta_{\tilde{\alpha}(2)}^{\mathcal{F}}$ ). In particular, the EoM for cavity-mode intensity correlations read:

$$\begin{aligned} \frac{d}{dt}\delta\langle b_\xi^\dagger b_\xi^\dagger b_\zeta b_{\zeta'} \rangle &= -(\kappa_\xi + \kappa_{\xi'} + \kappa_\zeta + \kappa_{\zeta'})\delta\langle b_\xi^\dagger b_\xi^\dagger b_\zeta b_{\zeta'} \rangle \\ &+ \sum_j \left( g_{\xi j} \delta\langle c_j^\dagger v_j b_\xi^\dagger b_\zeta b_{\zeta'} \rangle + g_{\xi' j} \delta\langle c_j^\dagger v_j b_\xi^\dagger b_\zeta b_{\zeta'} \rangle + g_{\zeta j} \delta\langle v_j^\dagger c_j b_\xi^\dagger b_\xi^\dagger b_{\zeta'} \rangle + g_{\zeta' j} \delta\langle v_j^\dagger c_j b_\xi^\dagger b_\xi^\dagger b_{\zeta'} \rangle \right). \end{aligned} \quad (5.16)$$

The EoM for further correlation functions of the quadruplet order, which include correlation between the photon-assisted polarization and the photon number, can be found in Appendix B [see Eqs. (B.4)–(B.7)].

## Results

As described above, the quadruplet order of the CE leads to a system of coupled equations [see Eqs. (5.11)–(5.12), (5.14)–(5.15), (5.16) together with Eqs. (B.1)–(B.7)]. The system of differential equations describes the dynamics of various correlations between carriers and cavity modes. In particular, the method makes it possible to obtain both amplitude and intensity correlation functions of the cavity emission modes including the effects of the carrier-photon correlations.

In the ensuing section the numerical analysis of the time evolution of the emission correlation functions is presented. To relate our theory to the experimental results we estimate the number of QDs with effective gain contribution by starting with the initial density of present QDs and excluding the ones with negligible spectral and spatial overlap. Thus, it is assumed that the cavity mode field is coupled to  $N$  identical QDs. Further, we consider continuous carrier generation in the  $p$ -shell at a constant rate  $p$  as an excitation process.

To obtain a valid comparison with the experimental results we simulate the coupled system using standard numerical integration routines with a realistic set of parameters  $\beta = 0.2$ ,  $\kappa_1 = 0.03$  [1/ps],  $\kappa_2 = 0.0318$  [1/ps],  $\Gamma = 2.06$  [1/ps],  $\tau_{sp} = 50$  [ps],

## 5.2. INTENSITY FLUCTUATIONS IN BIMODAL MICROPILLAR LASERS

$\tau_c = 1$  [ps] and  $\tau_v = 0.5$  [ps]. The number of carriers within the frequency region of interest is estimated from the total density of QDs to be  $N = 40$ . For the assumed  $\beta = 0.2$  the carrier recombination is determined by the stimulated emission into the lasing modes 1 and 2 with a characteristic time scale  $\tau_l = \tau_{sp}/\beta$  and into the non-lasing modes with a characteristic time scale that can be found from Eq. (5.13) for the given set of parameters. Further, we assume that the cavity mode 1 is in exact resonance with the QD transition ( $\Delta_{1s} = 0$ ) and the mode 2 is detuned with  $\Delta_{12} \equiv \omega_1 - \omega_2 = \Delta_{2s} = 0.2$  [1/ps]. Figure 5.11 illustrates the model for the density of states used for the comparison with the experimental results. In Fig. 5.12 we present

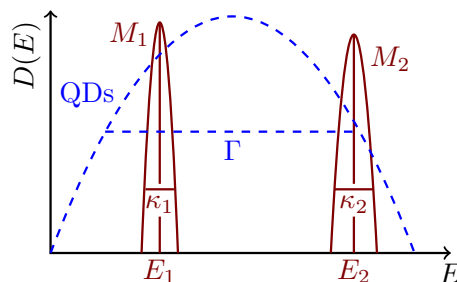


Figure 5.11: Illustration of the considered model for the density of states of the QDs and the modes.

the simulation results for intensity functions for the modes  $n_\xi = \langle b_\xi^\dagger b_\xi \rangle$ ,  $\xi = 1, 2$ , autocorrelation functions and crosscorrelation as a function of the pump power. Figure 5.12(a) reveals, that whereas the mode 1 shows a drastic increase of emission intensity, the intensity of the emission mode 2 reaches a maximum and then slowly decreases with increasing pump power in agreement with the experimental data depicted in Fig. 5.10(a). The calculations further show, that, again in agreement with the experimental data in Fig. 5.10(c), the dependencies of the autocorrelation functions for the cavity modes 1 and 2 on the pump power exhibit dramatically different behavior. As shown in Fig. 5.12(b) for low values of pump power, the autocorrelation function is equal to 2 characteristic for the statistics of thermal light. For higher rates of the pump power, the autocorrelation function of the mode 1 drops close to the value 1 indicating the emission of coherent laser light. In contrast, the autocorrelation function of mode 2 slightly decreases at first with increasing pump powers, but for larger values of the pump power, it increases and reaches values well above 2, which is in agreement with the behavior of the autocorrelation function detected in the experiment (see Fig. 5.10(c); recall the limited temporal resolution of the HBT configuration Fig. 5.5 and [Ulrich et al., 2007]). The gain competition behavior between the modes can be approved by plotting the crosscorrelation function [see Fig. 5.12(c)], that decreases to the values smaller than unity at the power pump values for which the lasing behavior of the mode 1 is observed [also, compare to Fig. 5.10(d)]. Further, numerical calculations demonstrate that the observed effect is independent of the modification of the spontaneous emission rate due to the many-body interaction (not shown). Note, that the discrepancy of the experimental and theoretical results for the autocorrelation function of mode 2 [Figs. 5.10(c) and 5.12(b), correspondingly] and the crosscorrelation function [Figs. 5.10(d) and 5.12(c), correspondingly] at the higher pump powers is due to the presence of both

modes in each polarization direction due to the QD induced mode coupling (see sec. 5.3). The numerical simulation of the CE truncation scheme of the quadruplet

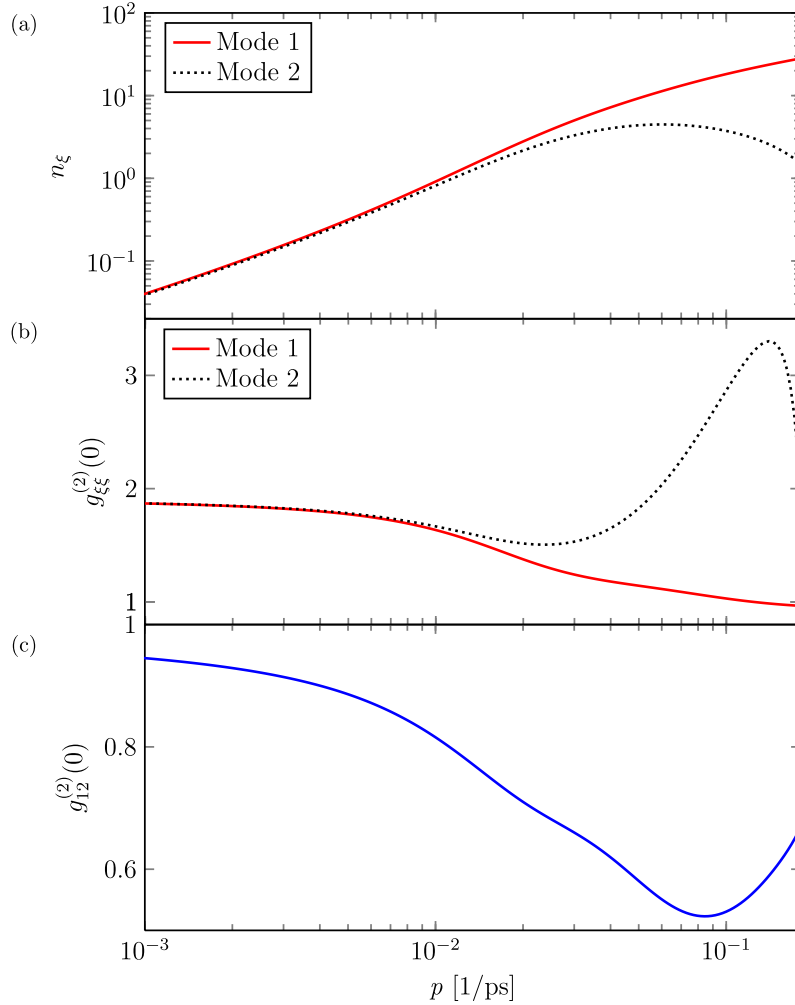


Figure 5.12: Laser characteristics calculated with the semiconductor model. (a) Intensity for the modes 1 and 2 as a function of the pump power in a log-log plot. (b) Autocorrelation functions of the two modes. (c) Crosscorrelation between the modes 1 and 2.

order can be approved by plotting the emission mode autocorrelation functions for higher order of truncation (not shown), which demonstrates qualitatively the same behavior of the functions independent of the order of truncation. It is important to note, that since the framework of the microscopic semiconductor theory presented in this section is based on the neglect of correlation functions, the numerical results are valid in the regime when higher order correlations remain small. As it can be seen from the numerical evaluation of the truncated equations, this is not the case for pump power rates exceeding  $2 \times 10^{-1} [1/\text{ps}]$ , where the correlation functions strongly increase. In essence the CE has to fail for this system since it is a method that relies on the neglect of higher order correlation functions, applied on a system that inherently drives strong correlations in the photonic subspace. To get a deeper understanding of the statistical properties of the emission in the next section we will

use a different approach to gain insight into the full photon statistics.

### 5.2.4 Extended Birth-Death Approach

In the following subsection we present an alternative approach to the study of the light-matter interaction of QDs with a bimodal cavity, that involves numerically solving a complete master equation and thus deriving the time evolution of the system. In contrast to the microscopic semiconductor model discussed in detail in sub-sec. 5.2.3, this approach allows to calculate not only photon auto- and crosscorrelation-functions but also full photon statistics. We follow the approach from [Rice and Carmichael, 1994] and extend it to the case of a bimodal cavity with two (nearly) resonant modes containing  $n_1$  and  $n_2$  photons, respectively. The method simplifies the model for the gain medium and takes into account only fully inverted two-level systems. Note, that no semiconductor effects or complex level structure are reflected. In this case, we introduce the coupling between the modes induced by the interaction with the common gain medium by means of a phenomenological term. The state of the gain medium is fully described by the number of excited carriers  $N$ . A detailed discussion of the master equation approach, the semiclassical rate equations and its connection to the semiconductor theory for the case of a single-mode microcavity can be found in Refs. [Gies et al., 2007, Gies, 2008] and references therein. The master equation describes the time evolution of the diagonal elements

$$\rho_N^{n_1, n_2} = \langle n_1, n_2, N | \rho | n_1, n_2, N \rangle \quad (5.17)$$

of the density matrix  $\rho$ . These elements can be interpreted as the probability of finding a state with  $n_1, n_2$  photons in the modes 1 and 2, respectively, and  $N$  Atoms in the excited state.

#### Physical Model

To arrive at the final form of the master equation a birth and death model, analogue the one introduced in [Rice and Carmichael, 1994], is considered. Transition rates into and out of the state  $\rho_N^{n_1, n_2}$  are connected to the relevant processes in the coupled photon carrier system. In Fig. 5.13 all relevant processes are illustrated. Figures 5.14 and 5.15 show how the master equation is derived on a phenomenological level. Each filled circle represents a state with  $N$  excited carriers,  $n_1$  and  $n_2$  photons in the cavity modes, i.e. the diagonal elements  $\rho_N^{n_1, n_2}$  of the density matrix. The photon distribution for mode  $\xi$  is gained by summation over the remaining indices e.g.  $P(n_1) = \sum_{N, n_2} \rho_N^{n_1, n_2}$ . Figure 5.14 illustrates the coupling of one mode to the gain medium. The horizontal axis shows the number of photons  $n_\xi$  in mode  $\xi$  and the vertical axis shows the number of excited carriers  $N$ . The carrier generation is represented by solid vertical arrows since the photon number is not changed. The rate of carrier generation in the excited level is given by the pump power  $p$ . Vertical dotted arrows indicate the loss of excited carriers due to spontaneous emission into non lasing modes. Moreover, the emission into the cavity modes is represented by pairs of diagonal arrows corresponding to spontaneous (dotted arrow) and stimulated (solid

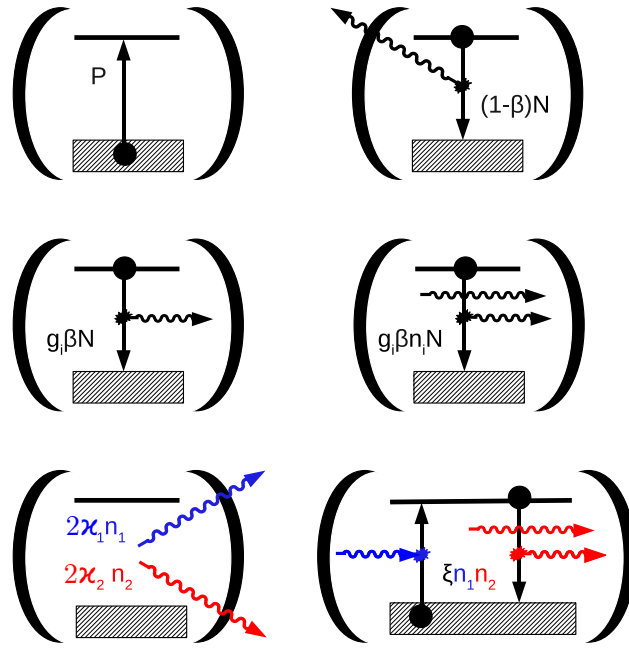


Figure 5.13: Illustration of the various processes represented by in the birth-death model. From left to right and top to bottom the processes are: excited carrier generation (pump), spontaneous emission in non-lasing modes, spontaneous emission into a lasing mode, stimulated emission into a lasing mode, cavity photon losses, and QD mediated mode coupling.

arrow) emissions, illustrating that an excited carrier is lost and one photon in one of the modes is gained. The factors  $\tau_{l1}^{-1}$  and  $\tau_{l2}^{-1}$  are introduced, which represent the fractions of laser emission rate into the cavity modes 1 and 2, correspondingly, where the relation  $\tau_{l1}^{-1} + \tau_{l2}^{-1} = \tau_l^{-1}$  holds. Further, the interaction of the modes is illustrated in Fig. 5.15. The two axes show the number of photons  $n_1$ ,  $n_2$  in the modes 1 and 2, respectively. The horizontal and vertical dotted arrows represent the cavity losses of the two lasing modes with the loss rates  $2\kappa_\xi$ . A phenomenological nonlinear coupling between the lasing modes 1 and 2 mediated by the gain medium is also introduced. In contrast to the microscopic semiconductor theory (see Sec. 5.2.3), where the coupling between the cavity modes is mediated by the overlap of the mode functions with the gain carriers, here a nonlinear coupling between the lasing modes 1 and 2 is introduced phenomenologically. The mode coupling strengths  $\xi_{12}$  and  $\xi_{21}$  are represented by the diagonal solid arrows in the sketch.

The complete master equation derived by the phenomenological birth and death

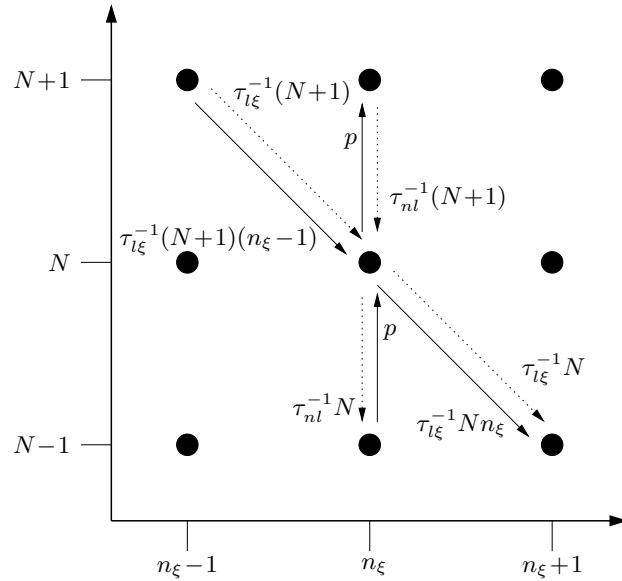


Figure 5.14: Schematic representation of the various processes in the extended birth-death-model. The sketch illustrates the light-matter-interaction and shows the transition rates into and out of the state with photon number  $n_\xi$  and carrier number  $N$ . Solid arrows represent stimulated emission and pump, dotted arrows show spontaneous emission.

model reads:

$$\begin{aligned}
 \frac{d}{dt}\rho_N^{n_1, n_2} = & p [\rho_{N-1}^{n_1, n_2} - \rho_N^{n_1, n_2}] - \tau_{nl}^{-1} [N\rho_N^{n_1, n_2} - (N+1)\rho_{N+1}^{n_1, n_2}] \\
 & - \tau_{l1}^{-1} [(n_1+1)N\rho_N^{n_1, n_2} - (n_1)(N+1)\rho_{N+1}^{n_1-1, n_2}] - \tau_{l2}^{-1} [(n_2+1)N\rho_N^{n_1, n_2} - (n_2)(N+1)\rho_{N+1}^{n_1, n_2-1}] \\
 & - 2\kappa_1 [n_1\rho_N^{n_1, n_2} - (n_1+1)\rho_N^{n_1+1, n_2}] - 2\kappa_2 [n_2\rho_N^{n_1, n_2} - (n_2+1)\rho_N^{n_1, n_2+1}] \\
 & - \xi_{12} [n_1 n_2 \rho_N^{n_1, n_2} - (n_1+1)(n_2-1)\rho_N^{n_1+1, n_2-1}] \\
 & - \xi_{21} [n_1 n_2 \rho_N^{n_1, n_2} - (n_1-1)(n_2+1)\rho_N^{n_1-1, n_2+1}]. \quad (5.18)
 \end{aligned}$$

In the above, each term corresponds to a process in the coupled carrier photon system, i.e. to arrows going in and out of a state  $\rho_N^{n_1, n_2}$  in Figs. 5.14 and 5.15. Note that the spontaneous and stimulated emission into the laser modes is combined to one term, hence the  $(n_\xi + 1)$  in the diagonal term.



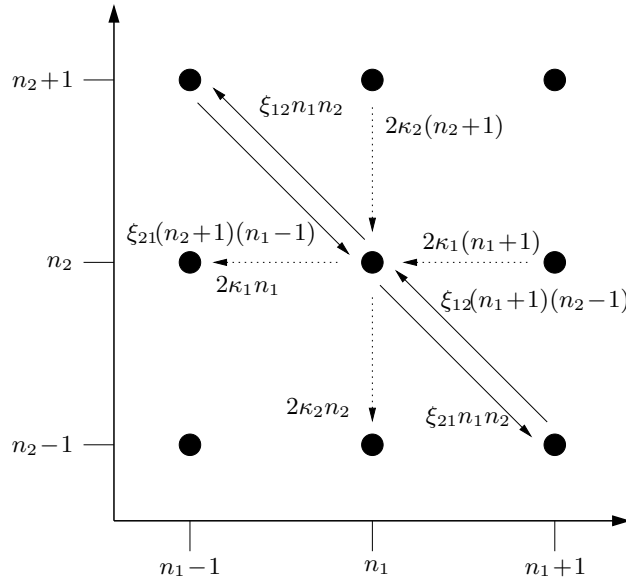


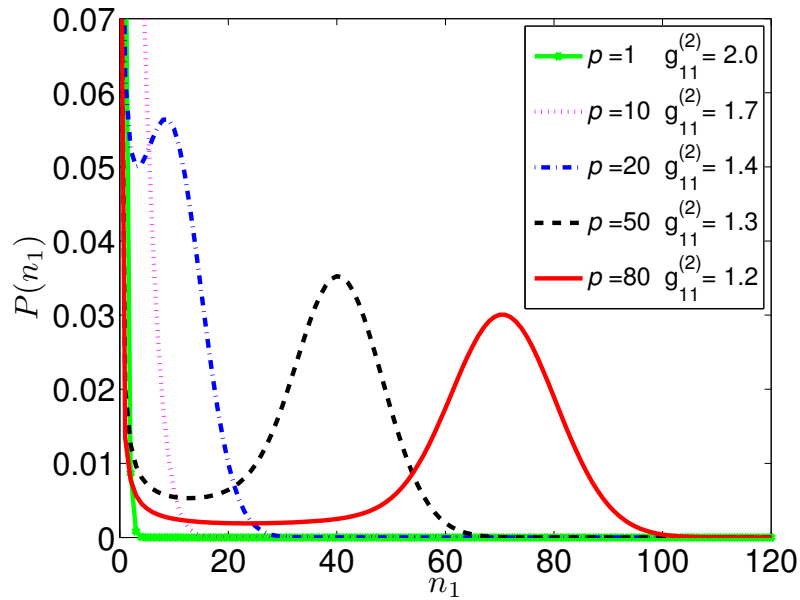
Figure 5.15: Schematic representation of the various processes in the extended birth-death-model. The sketch illustrates the interaction of the modes and shows the transition rates into and out of the state with photon number  $n_1$  and  $n_2$ . Solid arrows show mode interaction, dotted arrows represent cavity losses.

## Results

The solution of Eq. (5.18) for  $\frac{d}{dt}\rho_N^{n_1, n_2} = 0$  gives the stationary photon probability distribution. Figure 5.16 shows the photon distributions  $P(n_\xi)$  for various pump strengths. Above the laser threshold the autocorrelation functions of the modes 1 and 2 are quite different, while  $g_{11}^{(2)}(0)$  drops to values close to one indicating Poissonian statistics,  $g_{22}^{(2)}(0)$  rises up to values substantially larger than two (thermal statistics). The results for the autocorrelation functions of the modes 1 and 2 are in full agreement with the ones obtained within the Microscopic Semiconductor Theory in Sec. 5.2.3 (see Fig. 5.12), in contrast to the experimental data presented in Fig. 5.10, the autocorrelation function of the mode 2 monotonically increases further for high pump power rates.

The full photon statistics reveals that both mode statistics exhibit a double peak structure. The first peak appears at the zero photon state declining very steep and a second Poissonian-like peak appears at higher photon numbers. In mode 1 the Poissonian peak is very pronounced and dominates the statistics, while mode 2 is dominated by the first peak at the zero photon number state. It is important to note, that the overall broad photon number distribution of the mode 2 corresponds to the large values of the autocorrelation function. These statistics combined with the fact of the crosscorrelation function is far below unity, which is reproduced by the master equation as well, allows for the interpretation of a switching behavior of the modes. Both modes are in a statistical mixture of a coherent and a thermal-like states. We see that Fig. 5.3 has to be augmented by a fourth panel (see Fig. 5.17) showing the statistical origin of the super thermal intensity fluctuations present in coupled bimodal systems.

(a)



(b)

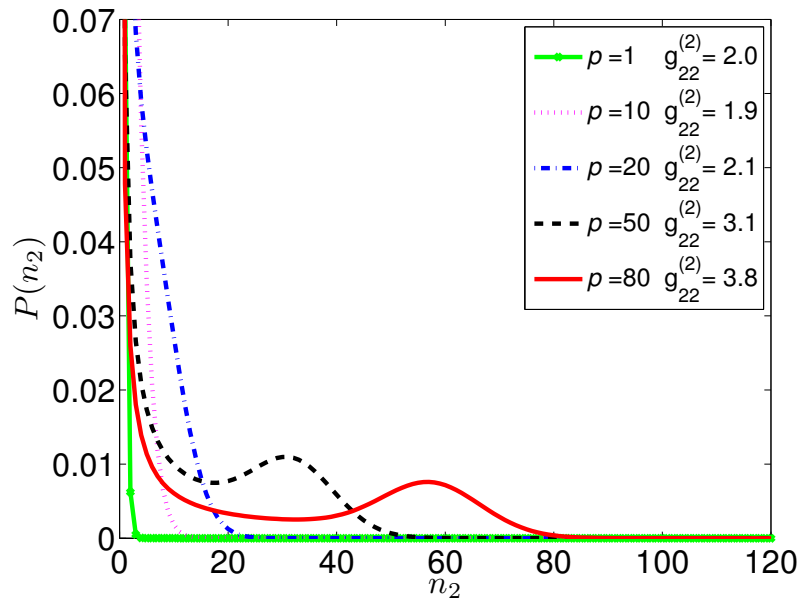


Figure 5.16: Photon probability distributions for mode 1 (a) and mode 2 (b) are shown for different pump rates in the units of  $[\tau_{sp}^{-1}]$  and for  $\tau_{l1}^{-1} = \tau_{l2}^{-1} = 0.1 \tau_{sp}^{-1}$ ,  $\tau_{nl}^{-1} = 0.9 \tau_{sp}^{-1}$ ,  $2\kappa_1 = \tau_{sp}^{-1}$ ,  $2\kappa_2 = 1.2 \tau_{sp}^{-1}$ ,  $\xi_{12} = \xi_{21} = 0.15 \tau_{sp}^{-1}$ . In the legend the pump rates and the corresponding  $g^{(2)}(0)$  values are enlisted.

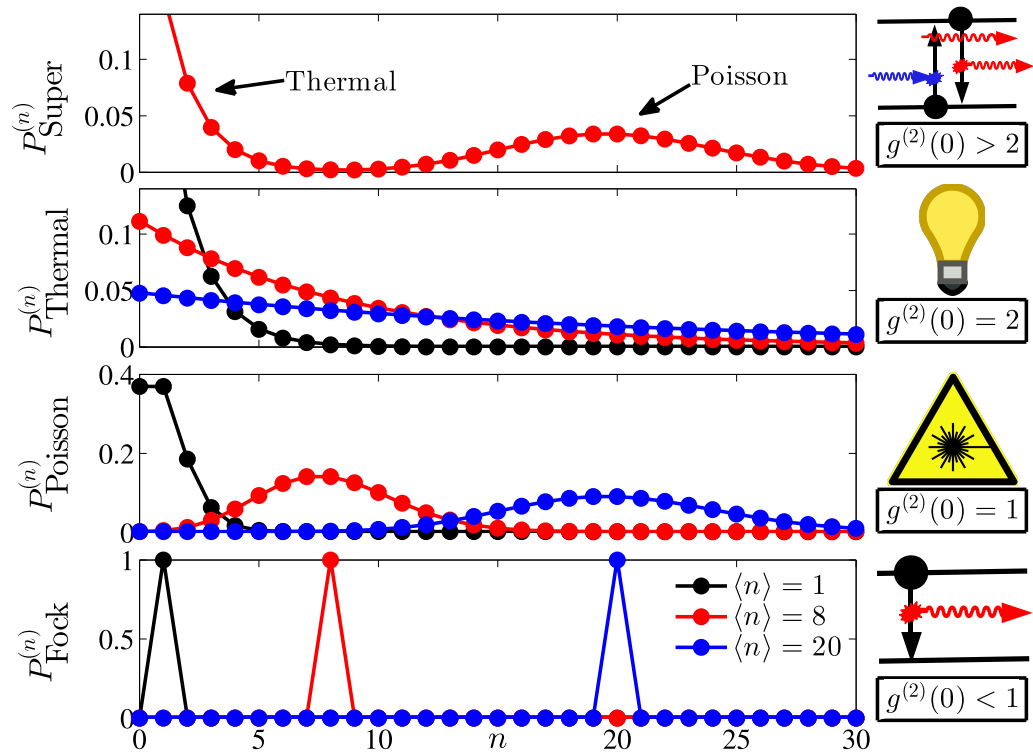


Figure 5.17: Illustration of the various states of light and the statistical properties and the connection to the photon autocorrelation function  $g^{(n)}(0)$ . In addition to Fig.5.3 this figure displays super thermal fluctuations caused by a mixture of a thermal ( $\langle n \rangle_{\text{Th}} = 1$ ) and a Poisson ( $\langle n \rangle_{\text{Po}} = 20$ ) distribution.

### 5.2.5 Conclusion and comparison of the experimental and theoretical results

We have investigated laser emission of electrically pumped QDs in a bimodal micropillar cavity with special emphasis to the effects induced by gain competition of the two orthogonally polarized modes.

The system consisting of a single low-density layer of QDs and two spectrally split modes with nearly equal  $Q$ -factors, induced from the double degenerate fundamental mode by slight cross-section asymmetry of the pillar, represents a viable platform for the study of the coupling of two cavity modes in the presence of a common gain medium. The polarization resolved measurements of the statistical properties of the emitted light reveal that the two competing modes display completely different features. One of the modes (mode 1) demonstrates typical statistical behavior of a laser mode, namely the mode intensity displays the usual "S"-shaped input-output characteristic, and the autocorrelation function at zero time delay, measured using a HBT configuration, indicates the transition from spontaneous to stimulated emission for increasing pump rates. The measurements of the input-output characteristic of mode 2 indicate a threshold behavior, but for further increasing pump rates the intensity saturates and even decreases, as the result of the competition of the two modes induced by the common gain material. Moreover, the autocorrelation function at zero time delay of mode 2 at certain pump rates higher than the threshold values exhibits intensity fluctuation much higher than for a thermal state. It is worth to note, that at these rates of the injection current the anti-correlation between the two modes is the strongest. For even larger pump rates, the crosstalk between the modes induces a reduction of the autocorrelation function at zero time delay of the mode 2 reaching the value for a lasing mode.

Starting with the microscopical semiconductor model [Gies et al., 2007] we have developed a quantum theoretical framework for the description of the interaction of two cavity modes with the QD-gain medium. The theory allows to obtain the full emission statistics of the carrier-photon system in the bimodal cavity taking into account the many-body effects. Importantly, within our approach the effects related to the coupling of the two modes of the bimodal cavity, induced by the interaction with the common QD carriers are consistently included on the microscopic level. The solution of the EoM for correlation functions using the CE scheme reveals, that indeed the autocorrelation function of the mode 2 for the pump rates larger than the threshold rate reaches values well above  $g^{(2)}(0) = 2$ , that corresponds to the thermal state of light. The decrease of the crosscorrelation function of the two modes below unity indicates anti-correlated behavior of the mode coupling at these pump rates. In fact, this effect can be explained by random intensity switching between the two modes, which has negligible influence on the photon statistics of the lasing mode, but strongly affects the mode 2 for which the relative strength of fluctuations is larger. It is worth to mention, that in the case of macroscopic two-mode ring lasers [Singh and Mandel, 1979] large intensity fluctuations have been also found in the statistics of the more lossy mode, as the result of the mode competition with the favored mode and emission switching of the common atomic ensemble.

We have demonstrated that the problem can qualitatively be, considered in a

simpler phenomenological approach, where a nonlinear term for the coupling between the modes can be introduced in the master equation. In this way, we have extended the birth-death model of the master equation to the case of a bimodal cavity. In particular, we have assumed a phenomenological nonlinear coupling between the cavity modes, mediated by the overlap of the modes with the gain carriers. We have solved the complete master equation numerically, where the nonlinear mode coupling parameter is chosen so to match the results of the microscopic semiconductor theory. Then, we have shown, that the photon number statistics of both modes exhibit similar double peak structure, a peak at the zero photon state and a second peak at a higher photon number. The results imply, that the both modes are in a mixture of a coherent and a thermal-like states. Whereas, the Poisson peak at the higher photon number dominates the statistics of the mode 1, the statistics of the mode 2 indicates thermal state-like behavior, with a pronounced peak at zero photon state complemented with a local maximum at a higher photon number state. Thus, we may conclude that the photon number distribution of the two modes approves the switching behavior of the interaction of the two modes with the common gain medium.

Similar double peak curve has been found in the theoretical calculations using a semiclassical approach [Singh and Mandel, 1979] and experimentally verified [Lett et al., 1981] for the intensity probability distribution of the favored mode of ring lasers. Moreover, a double peak structure of the photon number distribution has been found for the composite mode at threshold in the two-mode open laser theory [Eremeev et al., 2011], where both modes interact with the common ensemble of atoms and with the common dissipation system. It is worth mentioning that mechanisms to create light sources with super thermal intensity fluctuations i.e. super thermal photon bunching have gained some interest in recent years [Kazimierczuk et al., 2015, Albert et al., 2011, Callsen et al., 2013]. Applications in two-photon excited fluorescence microscopy can benefit from the high probability of photon pairs in the light source without the danger of photon damage of the probe [Jechow et al., 2013].

## 5.3 Unconventional Collective Normal-Mode Coupling in Quantum-Dot-based Bimodal Micro-lasers

In this section we demonstrated that interaction of the modes of a passive bimodal microcavity (cavity modes) with a mesoscopic number of quantum emitters in the active region induces unconventional coherent coupling between these modes in the lasing regime. To understand what we mean by the term unconventional we recapitulate the concepts of "conventional" coherent coupling i.e. strong coupling, before we describe differences and similarities to the type of coupling that we encounter here.

### 5.3.1 The strong coupling regime

The study of cavity quantum electrodynamics (cQED) in the strong coupling regime between atom-like emitters and the confined light field of microcavities has been a subject of considerable attention. In the traditional cQED, low-mode volume resonators are used to enhance the coupling rate  $g$  between a single emitter and the field in comparison to the system damping rates. Prominent realizations of the strong coupling include experimental demonstrations of reversible exchange of excitation between a single emitter with the field from both atomic [Brune et al., 1996, McKeever et al., 2003, Nußmann et al., 2005] and solid-state [Reithmaier et al., 2004, Yoshie et al., 2004] systems. A typical evidence of the strong coupling regime represents splitting of the two degenerate modes, i.e. normal-mode splitting, that is a consequence of NMC e.g. between emitter polarization mode and field mode leading to a doublet cavity transmission spectrum [Shore and Knight, 1993]. In addition, NMC occurs i.a. in exciton-photon and phonon-photon interactions [Weisbuch et al., 1992] and optomechanical phenomena [Kippenberg and Vahala, 2008], where the cavity field couples to a mechanical mode [Dobrindt et al., 2008].

In view of the variety of implications of the regime of coherent coupling (see, e. g., [Monroe, 2002]), a different approach to achieve strong coupling has also attracted much attention. Instead of reducing the cavity mode-volume to achieve large  $g$ , the number of emitters  $N$  interacting with the field can be increased leading to the collective strong coupling regime, where the coupling rate scales as  $\sqrt{N}g$  [Tavis and Cummings, 1968, Andreani et al., 1999]. Various experimental observations of the cavity mode spectra splitting, proportional to  $\sqrt{N}g$  due to the collective coherent coupling with two [Reitzenstein et al., 2006b, Albert et al., 2013] or multiple [Raizen et al., 1989, Tuchman et al., 2006] emitters have been experimentally observed, including the case of a multi-mode cavity [Wickenbrock et al., 2013]. In solid-state systems, the coherent coupling between a cavity mode and an ensemble of emitters has been achieved in the classical regime with semiconductor quantum wells [Weisbuch et al., 1992, Khitrova, 1999]. However, in the quantum regime the significant inhomogeneous broadening of emission from self-assembled QDs has so far hindered the observation of collective coherent coupling for semiconductor based quantum emitters. An illustration of the concept of this type of "conventional"

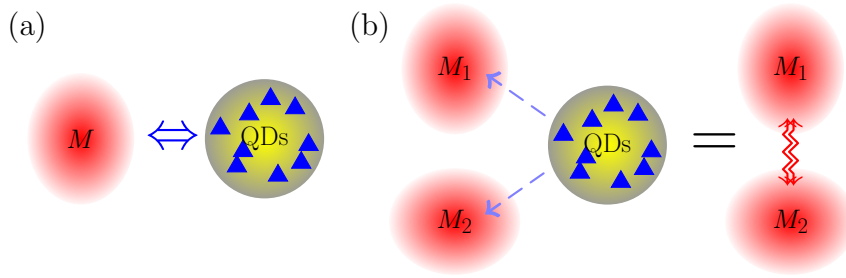


Figure 5.18: (a) Illustration of the concept of "conventional" collective mode coupling between one electromagnetic mode and an ensemble of quantum emitters, where the excitation is coherently exchanged between the QDs and the electromagnetic field. (b) Illustration of the introduced unconventional NMC where the coupling of two electromagnetic mode is mediated by their weak coupling to a shared ensemble of QD emitters.

coherent coupling in contrast to the unconventional NMC is given in Fig. 5.18(a). In many different situations, (see e.g. [Brune et al., 1996, McKeever et al., 2003, Nußmann et al., 2005, Reithmaier et al., 2004, Yoshie et al., 2004, Shore and Knight, 1993, Kippenberg and Vahala, 2008, Dobrindt et al., 2008, Monroe, 2002, Tavis and Cummings, 1968, Andreani et al., 1999, Reitzenstein et al., 2006b, Albert et al., 2013, Raizen et al., 1989, Tuchman et al., 2006, Wickenbrock et al., 2013, Weisbuch et al., 1992, Khitrova, 1999]), coherent coupling of two (nearly degenerate) modes is commonly explained by studying the eigenvalues of the system,

$$\Lambda_{\pm} = \frac{\omega_1 + \omega_2}{2} - i\frac{\gamma_1 + \gamma_2}{4} \pm \sqrt{[(\omega_1 - \omega_2)/2 - i(\gamma_1 - \gamma_2)/4]^2 + Ng^2}, \quad (5.19)$$

where  $\omega_{1,2}$  and  $\gamma_{1,2}$  are the frequencies and decay rates of the modes, correspondingly. Analysis of this expression reveals that in the resonant case ( $\omega_1 = \omega_2$ ) for  $\sqrt{Ng} < |\gamma_1 - \gamma_2|/4$  the square root term is fully imaginary and modifies the decay rates of the modes. Further, for  $\sqrt{Ng} > |\gamma_1 - \gamma_2|/4$  it becomes real and the frequencies exhibit splitting attributed to NMC.

Coherent coupling is also relevant to laser physics for achieving the regime of bistable lasing of the two-mode lasers [Meystre and Iii, 1999, Siegman, 1986]. In particular, in the case of large pump rates when strong coupling regime of emitter-field interaction is achieved and the Rabi frequency is larger than mode separation mode locking has been observed [Hillman et al., 1984, Wang et al., 2007]. Otherwise, bimodal cavities are investigated in the context of single-photon generation with whispering-gallery mode resonators [Dayan et al., 2008, Majumdar et al., 2012], where an atom strongly interacts with two cavity modes.

In contrast to the conventional NMC described above, here, in the case of the near-resonant cavity modes the eigenmodes of the total active system (eigenmodes) exhibit frequency locking, and the effective coupling rate with the emitters  $\sqrt{Ng}$  induces splitting of the linewidths of the eigenmodes. Further, for sufficiently large spectral splitting between the cavity modes, the incoherent coupling between the modes leads to a mixing of the "bare" cavity mode frequencies in the emission spectrum. The basic principle of this type of coupling originates from the fact that

two different modes couple weakly to a common gain medium which mediates the coupling in between the modes as illustrated in Fig. 5.18(b). Further below experimental observation of this mode mixing for bimodal micropillar lasers are shown. Moreover, the theoretical study shows, that in the case of incoherent coupling and approximately equal mode-QD coupling rates the eigenmode linewidths demonstrate locking, leading to almost equal values of the coherence times of the cavity mode emission. This intriguing and unexpected scenario is presented in the previous section in Fig. 5.10(b,c), where the inferior mode which exhibits large super-thermal intensity fluctuations, indeed has a coherence time/linewidth of the same order of magnitude as the dominant lasing mode.

### 5.3.2 Theoretical Model

The general theoretical model for this system and the results for the steady state are described in the previous section 5.2.2.

The coherent features of the output radiation are described by the (normalized) first-order correlation function,

$$g_{\xi}^{(1)}(t, \tau) = \frac{G_{\xi\xi}^{(1)}(t, \tau)}{\langle b_{\xi}^{\dagger}(t)b_{\xi}(t) \rangle}, \quad \xi = 1, 2, \quad (5.20)$$

with  $G_{\xi\xi'}^{(1)}(t, \tau) = \langle b_{\xi}^{\dagger}(t + \tau)b_{\xi'}(t) \rangle$ . The coherence times and the frequency spectra are given, respectively, by

$$\tau_{\xi}^c = 2 \int_0^{\infty} d\tau |g_{\xi}^{(1)}(\tau)|^2, \quad \text{and} \quad S_{\xi}(\omega) = 2 \text{Re} \int_0^{\infty} d\tau g_{\xi}^{(1)}(\tau) e^{-2\pi i \tau \omega}. \quad (5.21)$$

The system is pumped by continuous wave excitation until a steady state is reached. Two-time quantities as the correlation function  $g_{\xi}^{(1)}(t, \tau)$  are  $t$ -time independent in the steady-state regime for large enough  $t$ -times. Therefore, the two-time evolution problem can be separated to two single-time problems, which is analogous to the method of the quantum regression theorem [Lax, 1967]. Then, the EoM with respect to the delay time  $\tau$  can be solved with initial values given by the stationary steady-state result of the  $t$ -time problem [Wiersig, 2010]. The EoM for expectation values of the  $\tau$ -time dependent quantities of interest lead to a hierarchy problem as well which can be treated by the CE (see chapter 4). The system of EoM is derived using Ehrenfest EoM with dissipative terms, of Lindblad form [Gardiner and Zoller, 2001].

To obtain the dynamical equations of the first-order coherence the CE up to the doublet level is required (i.e.  $\Delta_{\mathcal{X}(2)}^{\mathcal{B}_i + \mathcal{F}/2}$ ), which in particular implies the semi-classical factorization [in the following the dependence on the time  $t$  is omitted, as  $b_{\xi}(\tau) \equiv b_{\xi}(t, \tau)$ ,  $b_{\xi} \equiv b_{\xi}(t, 0)$  etc.]

$$\langle c_j^{\dagger}(\tau)c_j(\tau)b_{\xi}^{\dagger}b_{\xi}(\tau) \rangle \approx \langle c_j^{\dagger}(\tau)c_j(\tau) \rangle \langle b_{\xi}^{\dagger}b_{\xi}(\tau) \rangle, \quad (5.22)$$

where  $\langle c_j^{\dagger}(\tau)c_j(\tau) \rangle$  in the stationary regime is  $\tau$ -time-independent. Thus, assuming identical QDs with equal transition energies and coupling rates  $g_{\xi} \equiv g_{\xi j}$ , we



obtain a closed system of *linear* differential equations for the correlation functions  $G_{\xi\xi} \equiv G_{\xi\xi}^{(1)}(\tau)$  and  $P_{\xi}(\tau) \equiv P_{\xi j}(\tau) = \langle c_j^{\dagger}(\tau)v_j(\tau)b_{\xi} \rangle$  in the rotating-wave approximation and in the frame rotating at  $\varepsilon_j^c - \varepsilon_j^v$

$$\frac{d}{d\tau}P_{\xi}(\tau) = -\Gamma P_{\xi}(\tau) + Ig_1G_{1\xi}(\tau) + Ig_2G_{2\xi}(\tau), \quad (5.23)$$

$$\frac{d}{d\tau}G_{1\xi}(\tau) = (i\Delta_1 - \frac{1}{2}\kappa_1)G_{1\xi}(\tau) + Ng_1P_{\xi}(\tau), \quad (5.24)$$

$$\frac{d}{d\tau}G_{2\xi}(\tau) = (i\Delta_2 - \frac{1}{2}\kappa_2)G_{2\xi}(\tau) + Ng_2P_{\xi}(\tau), \quad (5.25)$$

where  $\Delta_{\xi} \equiv \Delta_{\xi j} = \varepsilon_j^c - \varepsilon_j^v - \hbar\omega_{\xi}$  is the detuning of the cavity modes from the QD transition, and  $\kappa_{1,2}$  describe cavity mode losses. The inhomogeneous broadening is approximated by the spectral line broadening rate  $\Gamma$  in Eq. (5.23). The excitation of emitters with given pump rate is encoded into the steady-state inversion per QD,  $I \equiv I_j(t) = \langle c_j^{\dagger}c_j \rangle - \langle v_j^{\dagger}v_j \rangle$ , that represents an important pump rate-dependent parameter for the  $\tau$ -dynamics.

### 5.3.3 Mode coupling

The system of six equations above consists of two independent subsystems with  $\xi = 1, 2$ . Autocorrelation functions of two cavity modes  $G_{\xi\xi}^{(1)}(\tau)$  are coupled to each other indirectly, namely, through  $P_{\xi}(\tau)$  representing the common gain medium. To provide a simple yet deeper understanding of the coupling of the two cavity modes, we use an approximation of fast relaxation of  $P_{\xi}(\tau)$  compared to the time-scale of the dynamics of  $G_{\xi\xi}(\tau)$ , which is typically valid for semiconductor systems [Alferov, 2001]. We formally insert  $(d/d\tau)P_{\xi}(\tau) = 0$  into Eq. (5.23) and reduce Eqs. (5.23)–(5.25) to

$$\frac{d}{d\tau} \begin{pmatrix} G_{1\xi} \\ G_{2\xi} \end{pmatrix} = i \begin{pmatrix} \Delta_1 + i\tilde{\kappa}_1/2 & -iNIg_1g_2/\Gamma \\ -iNIg_1g_2/\Gamma & \Delta_2 + i\tilde{\kappa}_2/2 \end{pmatrix} \begin{pmatrix} G_{1\xi} \\ G_{2\xi} \end{pmatrix}, \quad (5.26)$$

which represents two  $2 \times 2$  identical matrices and characterize the coupling of the two cavity modes. The eigenvalues of the matrix above read

$$\lambda_{\pm} = \frac{\Delta_1 + \Delta_2}{2} + i\frac{\tilde{\kappa}_1 + \tilde{\kappa}_2}{4} \pm \sqrt{[(\Delta_1 - \Delta_2)/2 + i(\tilde{\kappa}_1 - \tilde{\kappa}_2)/4]^2 - (NIg_1g_2/\Gamma)^2}, \quad (5.27)$$

with  $\tilde{\kappa}_{\xi} = \kappa_{\xi} - 2NIg_{\xi}^2/\Gamma$  it follows, that increasing  $NIg_{\xi}^2/\Gamma$  effectively reduces the linewidths. Inspection of Eq. (5.27) reveals that the dependence of the eigenvalues on the involved parameters behave quite differently from the case of conventional NMC, Eq. (5.19). That is why we term this type of coupling "unconventional". For  $\Delta_1 = \Delta_2$  and  $g_1 = g_2$ , the square root term of  $\lambda_{\pm}$  remains imaginary and modifies the peak widths independent on how large the effective coupling  $|NIg_1g_2/\Gamma|$  is chosen in comparison with  $|\kappa_1 - \kappa_2|$ . In the case, when  $\kappa_1 = \kappa_2$  and  $g_1 = g_2$ , the square root term leads to two regimes. For  $|NIg_1g_2/\Gamma| < |\Delta_1 - \Delta_2|/2$ , the regime of incoherent coupling, the term is real and modifies the peak positions of the modes. In the regime

of coherent coupling, i.e. for  $|NIg_1g_2/\Gamma| > |\Delta_1 - \Delta_2|/2$ , it becomes imaginary and modifies the peak widths of the modes. Note, this striking behavior is qualitatively opposite from that of conventional NMC<sup>3</sup>. Since the effective coupling  $|NIg_1g_2/\Gamma|$  is proportional to  $|I|$ , the experimental observation of the coherent regime of collective coupling requires  $|I|$  to be close to unity.

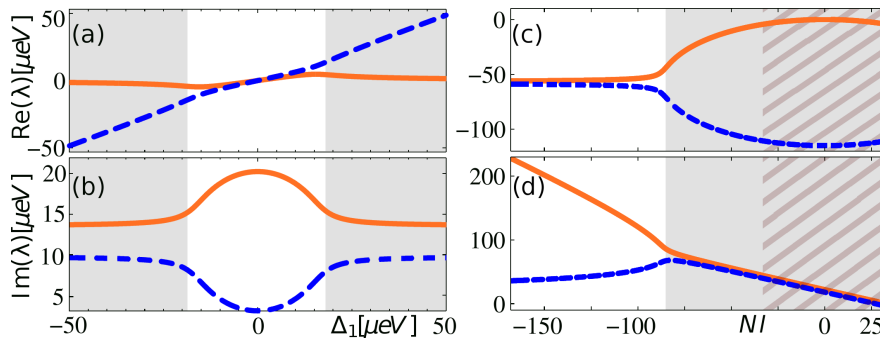


Figure 5.19: Real parts (correspond to peak positions) (a), (c) and imaginary parts (correspond to peak widths) (b), (d) of the eigenvalues (Eq. (5.27)) vs.  $\Delta_1$  for fixed pump strength [(a), (b),  $I = 0.3$ ] and vs.  $NI$  [(c), (d),  $\Delta_1 = 115 \mu\text{eV}$ ],  $N = 42$ ,  $\kappa_1 = 36 \mu\text{eV}$ ,  $\kappa_2 = 44 \mu\text{eV}$ ,  $\Delta_2 = 0$ ,  $\Gamma = 1.38 \text{ meV}$ ,  $g_1 = 30.4 \mu\text{eV}$ , and  $g_2 = 30.3 \mu\text{eV}$ . The shaded regions indicate incoherent coupling. The hatched area indicate experimentally accessible  $NI$ -range (see Fig. 5.21). The values of  $\kappa_\xi$  and  $\Delta_\xi$  are measured in the experiment, and the values of  $N$ ,  $\Gamma$  and  $g_\xi$  are estimated in correspondence to the experiment.

To demonstrate the unconventional NMC we plot the real and imaginary parts of the eigenvalues for a coupled bimodal cavity system in Fig. 5.19. The dependence on the detuning  $\Delta_1$  ( $\Delta_2 = 0$ ) [Figs. 5.19(a) and (b)] reveals that in the near-resonant region where the coherent coupling regime is maintained, the splitting of the imaginary parts of the eigenvalues (peak widths) is observed. For increasing detuning between the cavity modes, in the incoherent coupling regime, the eigenvalues demonstrate splitting in the real parts (peak positions) and locking of the imaginary parts. To illustrate the dependence on the effective coupling rate the eigenvalues are presented as functions of  $NI$  in Figs. 5.19(c,d). In the regime of incoherent coupling, for small effective coupling rate (small  $N|I|$ ), the splitting of the peak positions is observed. In the regime of coherent coupling the splitting of the peak widths increases for increasing effective coupling rate (large  $N|I|$ ). Whereas in the case of the conventional coherent NMC, Eq. (5.19), the splitting of the mode resonances increases for increasing  $N$  [Thompson et al., 1992].

### 5.3.4 Cavity Mode Spectra

Importantly, the above discussed effects can be deduced starting with the more general Eqs. (5.23)–(5.25). In the following we use Eqs. (5.23)–(5.25) to obtain  $\tau$ -dependent expressions for the auto-correlation functions. The initial values of

<sup>3</sup>The reason for this switching of roles is that all relevant quantities are multiplied with the imaginary unit  $i$ , so we could have called this type of coupling "imaginary" NMC as well.

quantities  $P_\xi(\tau)$ ,  $G_{\zeta\xi}(\tau)$  are taken as the stationary solutions of  $t$ -time-dependent problem. Figure 5.20 reveals that in the regime of incoherent coupling the coherence times of the dominant and inferior modes, which correspond to the decay rates of  $|g_1^{(1)}(\tau)|$  and  $|g_2^{(1)}(\tau)|$ , respectively, are of the same order of magnitude. This counter-intuitive behavior, which has been experimentally observed and is presented in Fig. 5.10(b), is particularly interesting considering that the inferior mode features large super-thermal intensity fluctuations with  $g^{(2)}(0) \approx 3$  (Fig. 5.10(c,f)). The spectra of both ("bare") modes (Fig. 5.20, inset) exhibit a two-peak structure according to the eigenvalues in Eq. (5.27). Indeed, for the chosen parameters  $NI = 27.3$ , which corresponds to the incoherent coupling, Figs. 5.19(c, d) reveal splitting of peak positions and locking of the widths. Obviously, emission in the basis of the two cavity modes carries both "bare" frequencies of the passive cavity modes due to NMC via the common gain medium. The emission peak positions and widths are established by the real and imaginary parts of the eigenvalues  $\lambda_\pm$ , since every mode carries both basis (eigen)vectors. The mode coupling is also associated with the oscillations of  $|g_\xi^{(1)}(\tau)|$  (easy to see in Fig. 5.20 for  $|g_2^{(1)}(\tau)|$ ) but holds true for  $|g_1^{(1)}(\tau)|$ ). In particular, the oscillation amplitudes are attributed to the corresponding frequency spectra peak heights, whereas the oscillation frequency is defined by the peak position difference, which in turn is related to the relative detuning of the cavity modes. Importantly, the oscillations of  $|g_\xi^{(1)}(\tau)|$  originate from a double-peak feature of two cavity modes and need to be distinguished from those reported in Ref. [Ates et al., 2007], which arise from the interference of emission in two different polarization directions.

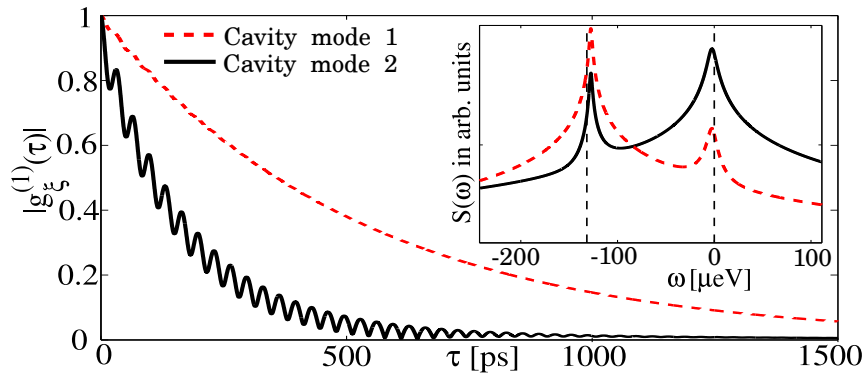


Figure 5.20: Absolute values of the autocorrelation functions and the frequency spectra (inset, semi-log scale) for the emission of the cavity modes in the incoherent regime for  $I = 0.65$ ,  $\Delta_1 = 115 \mu\text{eV}$  and estimated cavity-enhanced QD spontaneous emission rate of  $20 \text{ ns}^{-1}$ . Other parameter values are from Figs. 5.19(c, d). The vertical lines mark the cavity mode frequencies.

### 5.3.5 Experimental Realization

Here we present the experimental investigation of NMC in bimodal lasers, where we study electrically pumped micropillar lasers based on a doped planar microcavity sample with a single layer of self-assembled InGaAs QDs acting as active medium

(for technological details see Refs. [Reitzenstein et al., 2011, Albert et al., 2011]). Pillar cross-section asymmetry and/or the upper ring-shaped electrical contact induce a degeneracy of the resonator fundamental mode, thus two frequency-separated linearly (orthogonally) polarized cavity modes are supported [Reitzenstein et al., 2007]. The micropillar laser under study has a diameter of  $3.6 \mu\text{m}$ , and the two modes of  $0^\circ$  and  $90^\circ$  polarizations and  $Q$ -factors of 10000 and 10800 are split by  $115 \mu\text{eV}$ . The emission has been investigated at low temperature (10 K) by a microelectroluminescence ( $\mu\text{EL}$ ) setup (spectral resolution,  $20 \mu\text{eV}$ ). A linear polarizer in combination with a  $\lambda/4$ -wave plate is installed to perform polarization-resolved measurements.

The input-output dependence of the emission in  $0^\circ$  and  $90^\circ$  detection angle are depicted in Fig. 5.21(c). The emission mode in  $0^\circ$  polarization shows a threshold current of about  $I_{th} = 4 \mu\text{A}$ . The smooth transition at threshold and the  $\mathcal{S}$ -shaped input-output characteristics indicates the high- $\beta$  lasing with  $\beta \approx 0.2$  [Leymann et al., 2013c]. A similar behavior is observed for emission in  $90^\circ$  polarization up to  $I_{inj} \cong 1.5I_{th}$ . At higher injection currents saturation and even a decrease of the output intensity is observed. This anticorrelation between emission of the dominant mode in  $0^\circ$  and the inferior mode in  $90^\circ$  polarization is explained by means of the microscopic semiconductor model in terms of gain competition. Moreover, the model allows us to determine the inversion per pump rate which changes from  $-0.8$  to  $0.8$  for the used parameter values (see Fig. 5.21(c)). The corresponding  $NI$  range is indicated in Fig. 5.19(c,d) as hatched area. Interestingly, the intensity of emission in  $90^\circ$  polarization increases again for  $I_{inj} \gtrsim 4I_{th}$ . To analyze this feature we study emission spectra for different injection currents. While in  $0^\circ$  orientation emission a single peak is observed (not shown), for the  $90^\circ$  component at injection currents exceeding about  $1.5I_{th}$  a transition of a single emission peak into a doublet occurs (see Fig. 5.21(a)), where the intensity of the low-energy component rises with increasing current and dominates for  $I_{inj} > 5I_{th}$ . This double-peak feature of the  $90^\circ$  orientation emission and its peculiar current dependence is in very good agreement with the calculated emission spectra presented in Fig. 5.21(b) for incoherent collective coupling<sup>4</sup>. Indeed, for the range of the chosen parameters  $NI \approx 26 \dots 28$  according to Figs. 5.19(c, d) corresponds to the region of incoherent coupling, where the peak positions split.

In Fig. 5.21(d) mode energies of  $0^\circ$  and  $90^\circ$  polarizations vs. injection current are plotted. At low injection currents the single-peak emission in both polarization directions correspond to the "bare" frequencies of the cavity modes. Moreover, the low-energy component of the  $90^\circ$  emission for low injection currents coincides spectrally with emission from the  $0^\circ$  emission, but at high excitation currents it approaches the energy of the high-energy peak in  $90^\circ$  orientation. This clearly shows that this emission does not originate from possible cross-talk between  $0^\circ$  and  $90^\circ$  components, but is in accordance with the theoretical prediction in Fig. 5.19(c), namely that the peak positions approach each other with increasing  $NI$ .

---

<sup>4</sup>These spectra were convoluted with a Lorentzian to take into account the spectral resolution of  $20 \mu\text{eV}$  of the experimental setup.

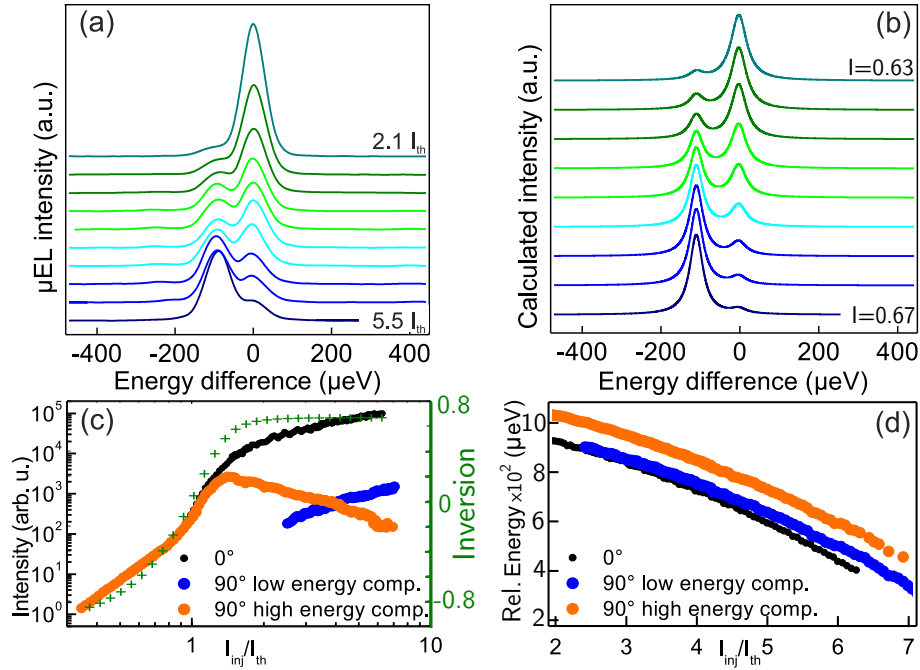


Figure 5.21: (a) Injection current-dependent  $\mu$ EL emission spectra in  $90^\circ$  polarization for  $2.1 \leq I_{inj}/I_{th} \leq 5.5$ , plotted relative to the high energy peak values to compensate for an injection current-dependent shift of the emission energy [cf. (d)]. (b) Calculated frequency spectrum in  $90^\circ$  polarization for inversion values  $0.63 \leq I \leq 0.67$ . Parameter values are the same as in Fig. 5.20. (c) Calculated inversion (green, crosses) vs. injection current and measured integrated  $\mu$ EL intensity for  $0^\circ$  and  $90^\circ$  polarizations. (d) Emission energy (relative to the reference point 1.366 eV) of the  $0^\circ$ -component and the two-mode features in  $90^\circ$  detection vs. injection current.

### 5.3.6 Conclusion

In this section, we have demonstrated the existence of collective NMC in bimodal microlasers. In contrast to the conventional case, here, in the coherent coupling regime, the increase of the effective coupling rate produces a splitting of the linewidths instead of the frequencies. In the incoherent coupling regime, increasing effective coupling induces splitting of frequencies and locking of linewidths. The consequence is the double-peak structure of the output spectra of the modes and the large coherence times for both dominant lasing and inferior modes, which we have confirmed experimentally in QD-based bimodal micropillar lasers. The latter offer unique possibilities to study collective coupling, since the stimulated emission of the dominant mode leads to clamping of the carrier density with large inversion ( $I \approx 0.8$ ), while the inferior mode experiences collective coupling mediated by multiple inverted emitters. Note, the unconventional NMC is not a semiconductor effect, but can be observed in the collective weak interaction of two modes with a mesoscopic number of atoms. We expect to observe further interesting effects related to NMC in bimodal lasers in the coherent coupling regime which could be accessed by using micropillar cavities with small mode splitting and larger inversion rate and/or number of involved QDs.

## 5.4 Chapter Conclusion

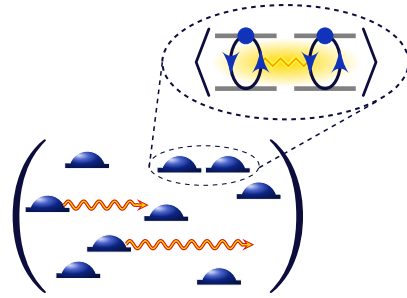
In this chapter we have discussed in sec. 5.1 the techniques and theoretical tools to characterize laser emission, in the highly efficient microcavity laser regime. The photon autocorrelation function  $g^{(2)}(\tau)$  is commonly accepted as a measure to monitor the transition into lasing. We have exploited the methods developed in the previous chapter to extend an existing semiconductor laser model to higher orders and confirm (i) the convergence of the CE and (ii) to study the transition into a lasing state for higher degrees of coherence.

In the second section and third section we have presented theoretical and experimental results for the coherence properties of bimodal microcavity lasers. For both, the quantum statistical- (sec. 5.2), the temporal coherence-properties and spectra (sec. 5.3), we could obtain theoretical results that are in very good agreement with the experimental results. This excellent agreement was achieved by using the previously introduced CE method which allows to microscopically model the coupled QD-cavity system. To gain a more intuitive understanding of the basic physics, that dominate the system, we derived very simple phenomenological models that can qualitatively reproduce the results and emphasize the essence of the observed effects.

The developed (microscopic semiconductor) theory of bimodal cavities is well-suited for further investigation of the emission properties for various interaction regimes depending on the cavity mode detunings and decay rates or effects related to the many-body interaction. Thus, the theory lays the groundwork for investigations of the effects related to the coupling of the modes in the bimodal cavity by means of interaction with a common gain medium.

# Chapter 6

## Sub- and Superradiance in QD Nanolasers



In this chapter we investigate radiative coupling between emitters in quantum dot (QD) nanolasers. For typical systems with tens to hundreds of active emitters, a strong impact of sub- and superradiance on steady-state properties is demonstrated. In a device-relevant parameter regime, it is shown that radiative coupling enhances spontaneous emission such that significantly fewer emitters are required to reach the lasing threshold. The formation of QD-QD correlations can seemingly change the  $\beta$ -factor by an order of magnitude. The results provide insight into a new kind of lasing in a highly efficient regime dominated by cavity-QED effects. Calculations are based on a microscopic laser theory for the coupled multi-QD-cavity-photon system that provides access to the photon autocorrelation function  $g^{(2)}(0)$ .

This chapter is in parts published in [Leymann et al., 2015]. The basic theory was developed in discussions between C. Gies, A. Foerster, and H.A.M. Leymann. The details of the theory was mainly worked out by H.A.M. Leymann while the equations of motion (EoM) were mainly derived and integrated by A. Foerster. All authors of [Leymann et al., 2015] discussed the results.

### 6.1 Introduction

When the active material gain compensates photon losses from the cavity, a conventional laser crosses the threshold into coherent emission. In nanolasers, spontaneous emission is strongly enhanced, and the previous criterion must be augmented such that stimulated *and* spontaneous emission must compensate the cavity losses. The enhancement originates from the Purcell effect and the high  $\beta$ -factor that quantifies the coupling efficiency of spontaneous emission into the laser mode. The threshold condition is again modified when emitters of the gain material act no longer independently, but radiative coupling triggers a *collective* spontaneous emission. The radiative coupling originates from the exchange of photons via the high- $Q$  cavity mode that establishes Dicke states [Garraway, 2011]. Super- and subradiance, which is the enhancement or inhibition of emission due to radiative coupling, was first discussed as a collective effect in a gas of atoms coupled to a common radiation field [Dicke,

1954]. The work of Dicke has been the foundation for a vast number of studies on superradiance (SR), reaching from single-photon emission enhancement [Scully and Svidzinsky, 2009, Chen et al., 2012] over photosynthetic bio-complexes [Ferrari et al., 2014] to Dicke phase transitions [Liu et al., 2014, Baumann et al., 2010] and directional SR emission from statistically independent incoherent sources [Ospel et al., 2014]. Regarding semiconductor systems, radiative lifetime changes have been observed in a QD ensemble due to emitter-coupling effects [Scheibner et al., 2007]. Superfluorescent spontaneous-emission enhancement has been demonstrated in quantum-well systems [Timothy Noe Ii et al., 2012]. Recent investigations have also addressed dynamical and statistical properties of SR coupling effects in cavities where QD emitters couple to a single mode [Temnov and Woggon, 2005, Temnov and Woggon, 2009, Auffèves et al., 2011].

This chapter is concerned with the impact of radiative coupling in continuously driven (cw) state-of-the-art nanolasers. Strong cavity enhancement and a limitation of the achievable gain due to the smallness of the resonator enhances many-particle correlations in these systems. As an example, nonclassical antibunching has been observed within the broad threshold region to lasing in QD microcavity lasers [Wiersig et al., 2009]. While in conventional lasers stimulated emission completely dominates above threshold, this is not necessarily so in nanolasers, where spontaneously emitted photons can constitute a significant part of the laser emission. It is not far fetched to assume that interemitter coupling effects play a role in the emission properties, even though they are typically assumed to be weak in semiconductor systems due to strong dephasing. These collective effects are typically not contained in most applications of laser theories, which are derived and used under the assumption of individual uncoupled emitters. To this date, radiative coupling is seldom associated with steady-state properties. The possible coexistence of lasing and superradiance in systems with few (2–5) two-level systems is discussed in Ref. [Mascarenhas et al., 2013]. The prediction of emerging superradiance in a continuously driven gas of atoms [Meiser and Holland, 2010] has led to the recent demonstration of a new kind of “nearly photonless” SR laser [Bohnet et al., 2012]. Collective effects are also expected to play an important role in random lasers, where the role of the cavity is replaced by multiple scattering events within the gain material [Wiersma, 2008, Baudouin et al., 2013].

We develop and apply a laser model for QD nanolasers that explicitly takes interemitter correlations and photon correlations into account. For a many-emitter gain medium, density-matrix approaches can account for interemitter coupling, but are limited to a small number of emitters ( $\sim 10$  two-level systems,  $< 5$  multilevel QDs on present-day computer systems) due to the rapidly increasing size of the Hilbert space [Auffèves et al., 2011, Florian et al., 2013a, Sitek and Manolescu, 2013, Lax and Louisell, 1969, Scully and Lamb, 1967]. Established quantum-optical master equations for the diagonal elements of the density matrix do not account for interemitter coupling [Rice and Carmichael, 1994], and rate equations are obtained under the assumption of individual emitters and prohibit access to the statistical emission properties [Moelbjerg et al., 2013, Rice and Carmichael, 1994, Yokoyama and Brorson, 1989, Chow and Koch, 1999]. Monte Carlo approaches have also been used to study SR [Meiser and Holland, 2010]. Here, we use a method that is based



on the systematic inclusion of expectation values (EVs) of QD-configuration and cavity-photon operators that allows keeping correlations up to a desired order and truncate higher clusters of operators. Photon-photon and interemitter correlations provide access to the photon autocorrelation function  $g^{(2)}(0)$  and radiative emitter coupling. Related cluster-expansion or cumulant-expansion approaches have been used in both the atom [Meiser et al., 2009, Witthaut et al., 2011] and semiconductor fields [Chow et al., 2014, Gies et al., 2007, Kira and Koch, 2008, Carmele et al., 2009] to describe either extended systems, or systems with many emitters, as the numerical problem typically scales only linearly with particle number.

The laser model is described in the following section. In Section 6.3, the impact of radiative coupling on the input-output curve is analyzed to reveal that correlations introduced by the radiative coupling drastically change the height of the jump in the input-output curve, as well as its slope in the spontaneous emission regime. In Section 6.4, the impact of radiative coupling is quantified by means of suitable pair-correlation functions for electronic and photonic degrees of freedom. These are used to introduce an effective rate of spontaneous emission and to explain the superthermal photon bunching that appears at low excitation powers. In Section 6.5, radiative coupling effects are quantified in terms of the quality factor of the mode (Q) and the emitter number, it is demonstrated that superradiance enhances the “coherence per photon”, so that significantly fewer emitters suffice to reach coherent emission i.e. lasing in comparison to the case of individual emitters. In Section 6.6 we provide an illustrative explanation of the observed features in terms of Dicke states between pairs of emitters in the ensemble. The appendix C provides details about the underlying laser theory.

## 6.2 Laser theory formulated in configuration operators

We consider an ensemble of self-assembled QDs coupled to a single high-quality mode of an optical microcavity. Three-dimensional carrier confinement of the QDs leads to a discrete density of states below a quasicontinuum of states from the surrounding semiconductor material. Interaction with carriers in these states is the source of the capture, scattering, and dephasing processes. For the laser model, we consider generic QDs each having two localized states for electrons and holes. Assuming excitation by the simultaneous capture of electron-hole pairs from the continuum states, six configurations are possible that represent bright and dark (multi-) exciton configurations  $|i\rangle^\alpha = \{G, X_s, 0_p, 0_s, X_p, XX\}$  of QD  $\alpha$ , see Appendix C.1. Both the  $X_s$  and  $XX$  configurations allow for an optical recombination of an s-shell electron-hole pair into the laser mode. This model captures the essential properties of a multilevel emitter that can accommodate bright and dark multi-exciton configurations [Gies et al., 2011]. We introduce the operator

$$Q_{ij}^\alpha = |i\rangle^\alpha \langle j|^\alpha . \quad (6.1)$$

For  $i \neq j$ , it describes the transition from configuration  $j$  to configuration  $i$  in QD  $\alpha$ , whereas for  $i = j$ , its EV refers to the probability to find QD  $\alpha$  in configuration

*i.* In the picture of many-particle configurations, we define the excitation operator for the s-shell of QD  $\alpha$  as

$$E_s^{\alpha\dagger} = Q_{X_s G}^\alpha + Q_{X X, X_p}^\alpha. \quad (6.2)$$

The product states  $|i_1 \dots i_N, n\rangle$  span the Hilbert space of  $N$  QDs and photons of the cavity mode. The dimension  $6^N \times n_{\max}$  of the Hilbert space grows quickly with emitter number, which is why a solution of the von Neumann equation for the full system density operator, popular for single-emitter systems, becomes costly already for a handful of emitters.

The dynamics of the microcavity-QD system is governed by the Hamiltonian  $H = H_0 + H_D + H_C$ , with the free Hamiltonian  $H_0 = \sum_{\alpha, i} \varepsilon_i^\alpha Q_{ii}^\alpha + \hbar\omega b^\dagger b$  that contains the configuration energies  $\varepsilon_i^\alpha$  and the mode frequency  $\omega$ , the light-matter interaction Hamiltonian  $H_D$ , and the Coulomb interaction Hamiltonian  $H_C$ . We have introduced the photon creation and annihilation operators  $b^\dagger, b$  for photons in the laser mode. In terms of the configuration operators, in dipole- and rotating-wave approximation the dipole Hamiltonian is given by

$$H_D = -i \sum_{\alpha} g_{\alpha} b^{\dagger} E_s^{\alpha} + \text{H.c.} \quad (6.3)$$

and couples the s-shell recombination to the creation of a cavity-photon, and vice versa.  $g_{\alpha}$  is the light-matter coupling strength of the s-transition of QD  $\alpha$  to the laser mode. In the scope of the present paper, we take the Coulomb interaction into account by renormalized configuration energies and an effective light-matter coupling strength.

We obtain the system dynamics by deriving EoM for observable quantities by deriving the generalized Ehrenfest EoM,  $\langle \dot{A} \rangle = i\langle [H, A] \rangle / \hbar + \mathcal{L}(A)$  for the corresponding operators  $A$ . The two-particle nature of the dipole Hamiltonian creates two different hierarchies: 1) EVs with  $M$  photon operators are coupled to EVs with  $M + 1$  photon operators. 2) EVs acting on transitions or occupations in one QD are coupled to EVs that couple transitions or occupations in *different* QDs. Both hierarchies do not end at low orders: 1) is limited only if the cavity field is represented by a finite linear combination of number states, and 2) is limited by the finite, but possibly large number of emitters in the gain material. In the spirit of the cluster-expansion method, both hierarchies are truncated consistently at a desired level to close the set of coupled equations. A formulation of the cluster expansion is introduced and discussed in chapter 4 more traditional formulations of the cluster expansion method have been used with great success to model quantum-well [Kira and Koch, 2008, Kira et al., 1999, Kira and Koch, 2011] and QD [Feldtmann et al., 2006, Gies et al., 2007, Richter et al., 2009] systems. Our approach here differs in two ways from the conventional method: Rather than using single-particle operators, we work in the many-particle configuration picture using the operators  $Q_{ij}^\alpha$  defined in Eq. (6.1), and we expand the hierarchy in terms of EVs rather than correlation functions (see chapter 4). For details of the laser theory formulated in configuration operators we refer to Appendix C.

We start from the mean photon number  $\langle b^\dagger b \rangle$  and the configuration probabilities  $\langle Q_{ii}^\alpha \rangle$  in each QD and derive their EoM. Photon correlations are included up to

$\langle b^\dagger b^\dagger bb \rangle$ , because they are needed to access the autocorrelation function  $g^{(2)}(0) = \langle b^\dagger b^\dagger bb \rangle / \langle b^\dagger b \rangle^2$ . EVs containing more operators are factorized. Radiative emitter coupling is related to EVs of the type  $\langle (b^\dagger)^n b^m Q_{ij}^\alpha Q_{i'j'}^\beta \rangle$ , which contain operators  $Q$  acting on different emitters  $\alpha, \beta$ . Higher-order correlations of the kind  $\langle (b^\dagger)^n b^m Q_{ij}^\alpha Q_{i'j'}^\beta Q_{i''j''}^\gamma \rangle$  are factorized. In our results, we compare to the case of “individual emitters”, which is obtained by performing a separate calculation, in which the hierarchy is truncated at the lowest level with respect to the  $Q$  operators, i.e. only EV of the type  $\langle (b^\dagger)^n b^m Q_{ij}^\alpha \rangle$  are explicitly considered. The level where QD-QD correlations are explicitly considered corresponds to the truncation operator  $\Delta_{\tilde{\alpha}(2)}^{\mathcal{Q}} \simeq \Delta_{\tilde{\alpha}(8)}^{\mathcal{F}/2}$  from chapter 4. Here the  $\mathcal{Q}$  indicates that the truncation is performed in the subspace spanned by the  $Q$ -operators. This truncation corresponds the level of 4-electron correlations, i.e. correlation functions with up to 8 electron creation/annihilation operators are taken into account (neglecting QD-QD correlations corresponds to  $\Delta_{\tilde{\alpha}(1)}^{\mathcal{Q}}$ ). Note that for the formulation in configuration operators the boundary conditions, originating from the finiteness of each QD, are taken into account automatically unlike in the formulations using Fock-space operators (see chapters 3 and 4).

Self-organized QDs are embedded systems, and their localized states are coupled to continuum states of wetting layer and barrier material. This enables efficient above-band-gap pumping. A simplified treatment consists of modeling incoherent carrier capture into higher confined QD states and successive relaxation via a Lindblad term [Carmichael, 1999]. This is a commonly used method with the twist that here, the formalism needs to be spelled out in terms of EoM for the operators  $Q_{ij}^\alpha$ . We introduce the rates:  $P^\alpha$  capture of e-h pairs into the QD p-shell (pump rate),  $\gamma_r^\alpha$  carrier relaxation,  $\gamma_{\text{spont}}^{\alpha, \{s,p\}}$  spontaneous losses of  $s$  and  $p$ -shell electron-hole pairs, and  $\kappa$  the loss rate of photons from the cavity. The Lindblad contributions are added to the EoM by evaluating  $\langle \dot{A} \rangle_{\text{Lindblad}} = \mathcal{L}(A) = \gamma_\eta \sum_{\{i,j\}} \langle ([Q_{ij}^\alpha, A] Q_{ji}^\alpha + Q_{ij}^\alpha [A, Q_{ji}^\alpha]) \rangle$  for each pair  $\{i, j\}$  of configurations connected by the underlying microscopic process  $\eta$  [Florian et al., 2013b]. A similar term using photon operators arises for cavity losses. Details are found in Appendix C.3, and in chapter 3 the incorporation of Lindblad terms into the conventional formulation of the cluster expansion is discussed in detail. The large number of coupled EoM are generated by means of the computer algebra tool FORM [Vermaseren, 2000](see appendix D).

Inhomogeneous broadening is an inherent property of QD-emitter ensembles obtained from self-assembled growth techniques [Bimberg et al., 1999]. The number of QDs considered in our calculations corresponds to the number of QDs in the ensemble found in spectral vicinity to the cavity mode. For these emitters, we assume that radiative coupling effects are fully present. Detailed investigations of the effect of detuning will be the topic of future work.

### 6.3 Signatures of Radiative Coupling in the Input-Output Characteristics of Nanolasers

In a conventional laser, a sudden intensity jump in the input-output curve over several orders of magnitude serves as an indicator for the onset of coherent emis-

### 6.3. SIGNATURES OF RADIATIVE COUPLING IN THE INPUT-OUTPUT CHARACTERISTICS OF NANOLASERS

sion. The height of the jump may be used to estimate the spontaneous-emission factor  $\beta$  [Yokoyama and Brorson, 1989, Chow and Koch, 1999]. In microcavity systems that approach the thresholdless  $\beta \approx 1$  regime, a more gradual transition to coherent emission can be revealed by studying statistical properties of the emitted light (see chapter 5 and e.g. [Jin et al., 1994, Khurgin and Sun, 2012, Rice and Carmichael, 1994, Strauf et al., 2006]). In Fig. 6.1(a), the input-output characteris-

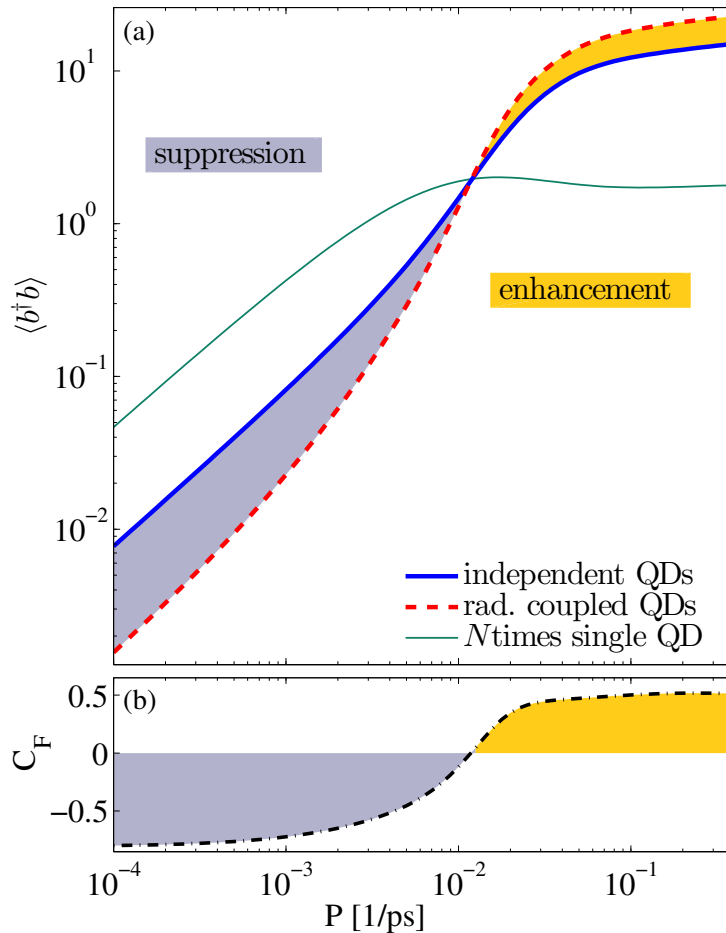


Figure 6.1: (a) Input-output curve for a typical nanolaser device [Lermer et al., 2013, Aßmann et al., 2010].  $N = 100$  QD emitters are used with a light-matter coupling of  $g = 0.015/\text{ps}$ , cavity loss rate  $\kappa = 0.05/\text{ps}$  (corresponding to  $Q = 20\,000$ ), carrier relaxation rate  $\gamma_r = 0.05/\text{ps}$ , and spontaneous losses into leaky modes  $\gamma_{\text{spont}} = 0.01/\text{ps}$ . The solid blue curve results from a calculation without radiative coupling effects ( $\Delta_{\tilde{\alpha}_1}^Q$ ), the dashed red curve includes sub- and superradiant coupling between pairs of emitters ( $\Delta_{\tilde{\alpha}_2}^Q$ ). The thin solid green line shows the intensity produced by a single QD ( $\Delta_{\tilde{\alpha}_1}^Q$ ) multiplied by the emitter number. (b) The cooperativity factor  $C_F$  (dash-dotted black curve) gives a measure of the change in photon output caused by the radiative coupling.

tics with (dashed line) and without (solid line) interemitter coupling are compared for a nanolaser with 100 emitters that are resonant with a high-quality ( $Q = 20\,000$ ) mode of the cavity. The system shows a transition into lasing at a pump rate of about

0.01 electron-hole pairs per ps and QD. It is striking that suppression of photon production below and enhancement above threshold increases the height of the gradual intensity jump. If rate- or master-equation approaches that neglect interemitter coupling were used to describe an experiment, in which strong interemitter coupling is present, one would erroneously conclude a  $\beta$ -factor that is smaller by about one order of magnitude. Furthermore, the radiative coupling visibly increases the slope of the input-output curve in the spontaneous emission regime.

To quantify the impact of the interemitter coupling, we define the cooperativity factor

$$C_F = \frac{I_{\text{rad. coupled QDs}}}{I_{\text{independent QDs}}} - 1 \quad (6.4)$$

which is also shown in Fig. 6.1(b). It gives a direct measure whether radiative coupling enhances or inhibits photon production. In addition to the laser transition from thermal to coherent light emission, it reveals a second transition from the subradiant ( $C_F < 0$ ) to the superradiant ( $C_F > 0$ ) regime.  $C_F$  is obtained from two separate calculations including and excluding the QD-QD coupling terms while keeping everything else unchanged. The possibility to do so is a particular advantage of our method over multiemitter density-matrix approaches that compare the full system to  $N$  times a single-emitter system [Mascarenhas et al., 2013]. The latter method amplifies the effects of saturation and reduced absorption of the single emitter by a factor  $N$ , causing significant deviations from the  $N$ -emitter input-output curve especially for larger emitter numbers. This is demonstrated by the thin green line in Fig. 6.1(a) showing the input-output characteristics of a single QD system multiplied with the number of QDs  $N$ . Comparing this result to the dashed red curve (calculated for  $N$  emitters including interemitter coupling) would result in an overestimation of the radiative coupling effects.

## 6.4 Statistical Properties of the Emission and Effective Spontaneous Emission Rate

In the following we demonstrate that superradiance enhances spontaneous emission in a way that fewer emitters are required to overcome the cavity losses of a nanolaser and to reach coherent emission. To this end, we chose slightly different parameters than in the previous section that are given in the caption of Fig. 6.2. Panels (a) and (b) depict input-output curve and the photon autocorrelation function  $g^{(2)}(0)$  with and without radiative coupling effects. In the gray area with  $C_F < 0$  ( $P \lesssim 10^{-2} \text{ ps}^{-1}$ ), the interemitter coupling reduces the photon output. Microcavity lasers are well known to exhibit saturation effects at high excitation. This is owed to the limited amount of gain that can be obtained from the active medium [Strauf et al., 2006]. If saturation sets in before or during the threshold, it can prohibit lasing or suppress the development of the full intensity jump [Gies et al., 2008]. Here, coherent emission with  $g^{(2)}(0) = 1$  is reached only when collective effects enhance the emission (red curves). Without SR coupling (blue curves), the system saturates before coherent emission is reached. The important finding that radiative emission enhancement reduces the number of emitters required to reach lasing is further

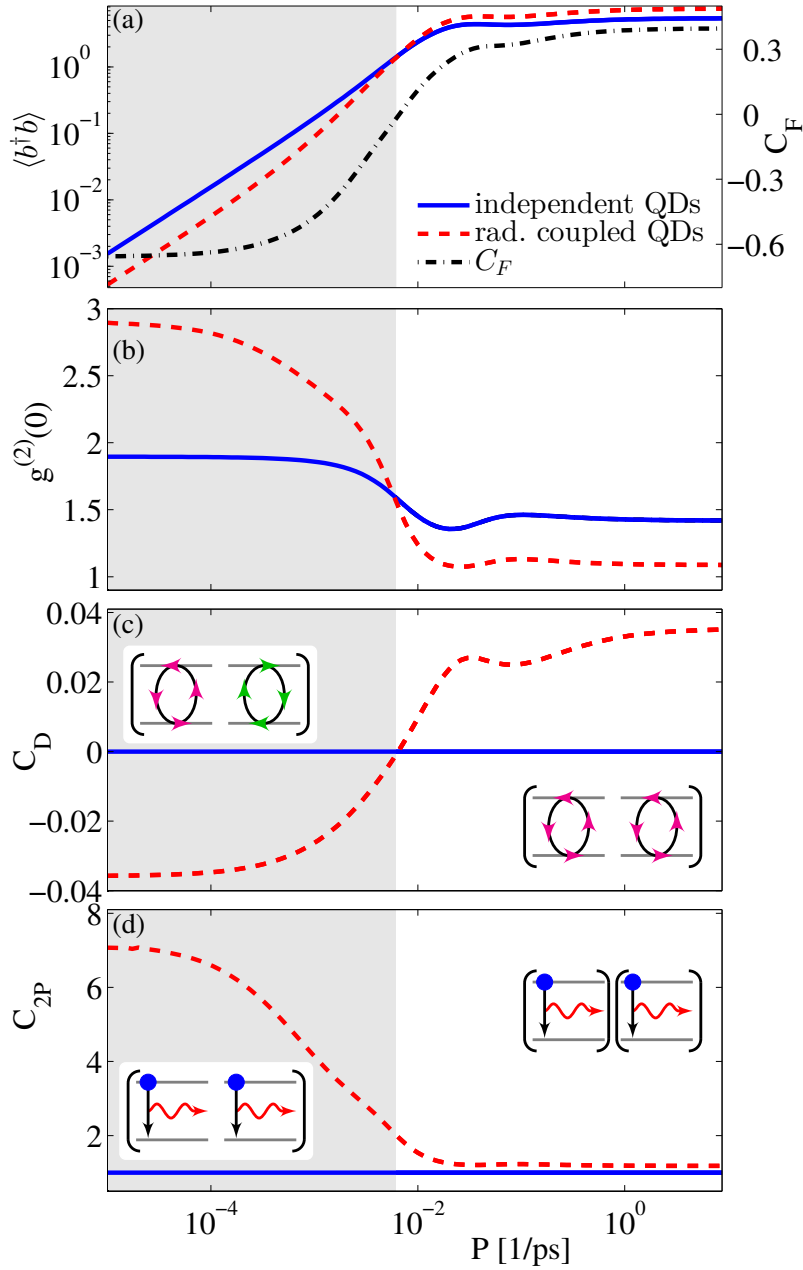


Figure 6.2: Stationary states for increasing pump rates into the QDs p-shell for the case with (dashed red curve) and without radiative coupling effects (solid blue curve). (a) The intensity is measured on the left  $y$  axis in logarithmic scale and the cooperativity factor  $C_F$  is measured on the right  $y$  axis, (b) photon autocorrelation function (c) dipole correlation function  $C_D$  (d) two-photon emission function  $C_{2P}$ . The gray area marks the subradiant regime where the cooperativity factor  $C_F$  is below zero. A schematic representation of both correlation functions in the sub- and superradiant regime is shown as insets. The calculations are performed for 20 QDs in resonance with the cavity mode. The photons have a loss rate of  $\kappa = 0.0125/\text{ps}$ , the other parameters are  $g = 0.01/\text{ps}$ ,  $\gamma_r = 0.05/\text{ps}$ ,  $\gamma_{\text{spont}}^p = \gamma_{\text{spont}}^s = 0.005/\text{ps}$  (see Appendix C.3).

analyzed in Sec. 6.5.

Enhancement of photon-intensity fluctuations with superthermal bunching values  $g^{(2)}(0) > 2$  is observed at low pump rates and reflects the increased probability that two photons are emitted at the same time. In this system the fluctuations do not originate from gain competition (see sec. 5.2), its microscopic origin is given by synchronous dipole transitions in separate QDs  $\alpha$  and  $\beta$  as described by the EV  $\langle b^\dagger b^\dagger E_s^\alpha E_s^\beta \rangle$ , where  $E_s^\alpha$  is defined in Eq. (6.2). To quantify the two-photon (2P) emission probability from pairs of radiatively coupled emitters, we use the normalized correlation function

$$C_{2P} = \frac{\sum_{\alpha \neq \beta} \langle b^\dagger b^\dagger E_s^\alpha E_s^\beta \rangle}{\sum_{\alpha \neq \beta} \langle b^\dagger E_s^\alpha \rangle \langle b^\dagger E_s^\beta \rangle} \quad (6.5)$$

shown in Fig. 6.2(d). Consistently with the super thermal intensity fluctuations below and the coherent values above threshold,  $C_{2P}$  drops from values around seven to one in the threshold region. This clearly reveals the correlated emission of photon pairs for low pump rates, which explains the superthermal photon bunching below threshold.

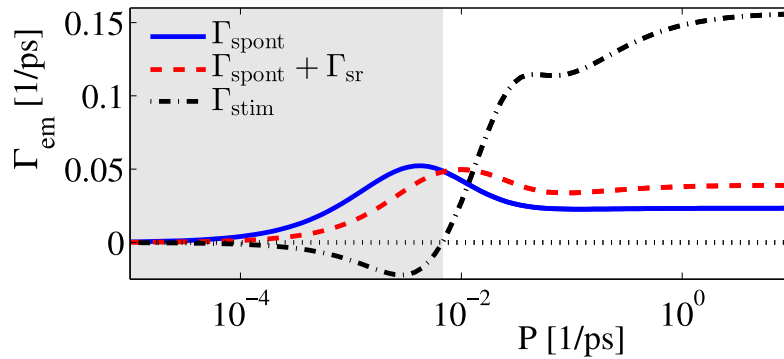


Figure 6.3: Contributions to the total emission rate  $\Gamma_{\text{em}}$  for the parameters used in Fig. 6.2 plotted versus pump rate  $P$ . The solid (dashed) curve represents the effective spontaneous emission rate excluding (including) radiative coupling effects. The end of the shaded area indicates the onset of lasing, where the stimulated contribution (dot-dashed line) changes from absorption to amplification.

More insight can be obtained by looking at the modification of spontaneous emission caused by the radiative coupling. In the commonly used rate-equation approach, independent emitters are considered, and spontaneous emission into the laser mode enters the dynamics via  $\beta \times n_{\text{ex}}/\tau_{\text{spont}}$ , with  $n_{\text{ex}}$  and  $\tau_{\text{spont}}$  being the number of excitations in the gain medium and the total rate of spontaneous emission, respectively. In a semiconductor system, optical recombination is driven by electrons and holes, and the assumption of independent electron and hole populations  $f^{e,h}$  leads to the spontaneous recombination rate  $\beta \times f^e f^h/\tau_{\text{spont}}$  [Chow and Koch, 1999, Gies et al., 2007]. We explicitly calculate the degree of correlations between electrons and holes and the resulting spontaneous-emission contribution. With the dipole operator  $D^\alpha = E_s^{\dagger\alpha} + E_s^\alpha$ , we define the dipole correlation function [Meyer and Yeoman,

1997]

$$C_D^{\alpha\beta} = \frac{\langle D^\alpha D^\beta \rangle}{\langle E_s^{\dagger\alpha} E_s^\alpha + E_s^{\dagger\beta} E_s^\beta \rangle}, \quad (6.6)$$

where the diagonal EV  $\langle D^\alpha D^\alpha \rangle$  is the spontaneous-emission contribution from QD  $\alpha$ . Of particular interest is the off-diagonal EV  $\langle D^\alpha D^\beta \rangle$ , which is the spontaneous-emission contribution due to radiative interemitter coupling. In the following we use  $C_D$ , which is defined as the arithmetic mean of  $C_D^{\alpha\beta}$  over all QD pairs  $\alpha \neq \beta$ . The sign of  $C_D$  indicates whether the dipoles of QD pairs are in phase ( $C_D > 0$ ) or out of phase ( $C_D < 0$ ). The results in Fig. 6.2(c) show a clear transition from out-of-phase to in-phase in the threshold region when the pumping is increased. Comparing Fig. 6.2(a,c) we see that dipoles that are in phase (out of phase) lead to an enhancement (suppression) of the emission into the cavity mode. An intuitive explanation of this effect is provided in Sec. 6.5. The impact of the SR emitter coupling can be cast into the form of an effective emission rate into the laser mode, as it is familiar from laser theories. It is made up of three contributions

$$\Gamma_{\text{em}} = \Gamma_{\text{spont}} + \Gamma_{\text{sr}} + \Gamma_{\text{stim}}, \quad (6.7)$$

where  $\Gamma_{\text{spont}} = \sum_{\alpha} \langle D^\alpha D^\alpha \rangle / \tau_{\text{deph}}$ , and  $\Gamma_{\text{sr}} = \sum_{\beta \neq \alpha} \langle D^\alpha D^\beta \rangle / \tau_{\text{deph}}$ , see Appendix C.4. The first two terms constitute the total rate of spontaneous emission into the laser mode: The diagonal one is the usual contribution from independent emitters to the spontaneous emission, and the nondiagonal sum reflects the enhancement or suppression of spontaneous emission due to QD-QD correlations. For identical emitters,  $\sum_{\beta \neq \alpha}$  leads to the well-known factor  $N(N-1)$  in the spontaneous photon production rate [Mandel and Wolf, 1995]. The third term represents the contribution due to stimulated emission or absorption. For the situation discussed in Fig. 6.2, the three contributions as functions of pump rate are shown in Fig. 6.3. Subradiant coupling is seen to reduce the effective spontaneous emission rate until the onset of stimulated emission. Stimulated emission is reached when its contribution (dot-dashed curve) becomes positive. Then, lasing rapidly decreases the population of excitonic states, while excitation-induced dephasing increases with pump, thereby reducing the spontaneous emission (see Appendix C.4). We emphasize that the sub/superradiant suppression/enhancement of the spontaneous emission rate is not caused by a de/increase of exciton population, but solely by the buildup of correlations between QDs, and these correlations enhance or suppress the emission from the excited carriers. Equation (6.7) also allows for an interpretation of the photonless laser in Ref. [Bohnet et al., 2012]: There, by the absence of photons, coherence is obtained only from dipole correlations stored in the atoms. These are represented by  $\Gamma_{\text{sr}}$ , which completely takes over the role of the stimulated emission contribution in conventional lasers.

## 6.5 Influence of the Emitter Number and Coherence Per Photon

In Fig. 6.4 we study how the influence of the coupling changes with the number of emitters  $N$ . Values in the stationary regime of the discussed quantities are shown



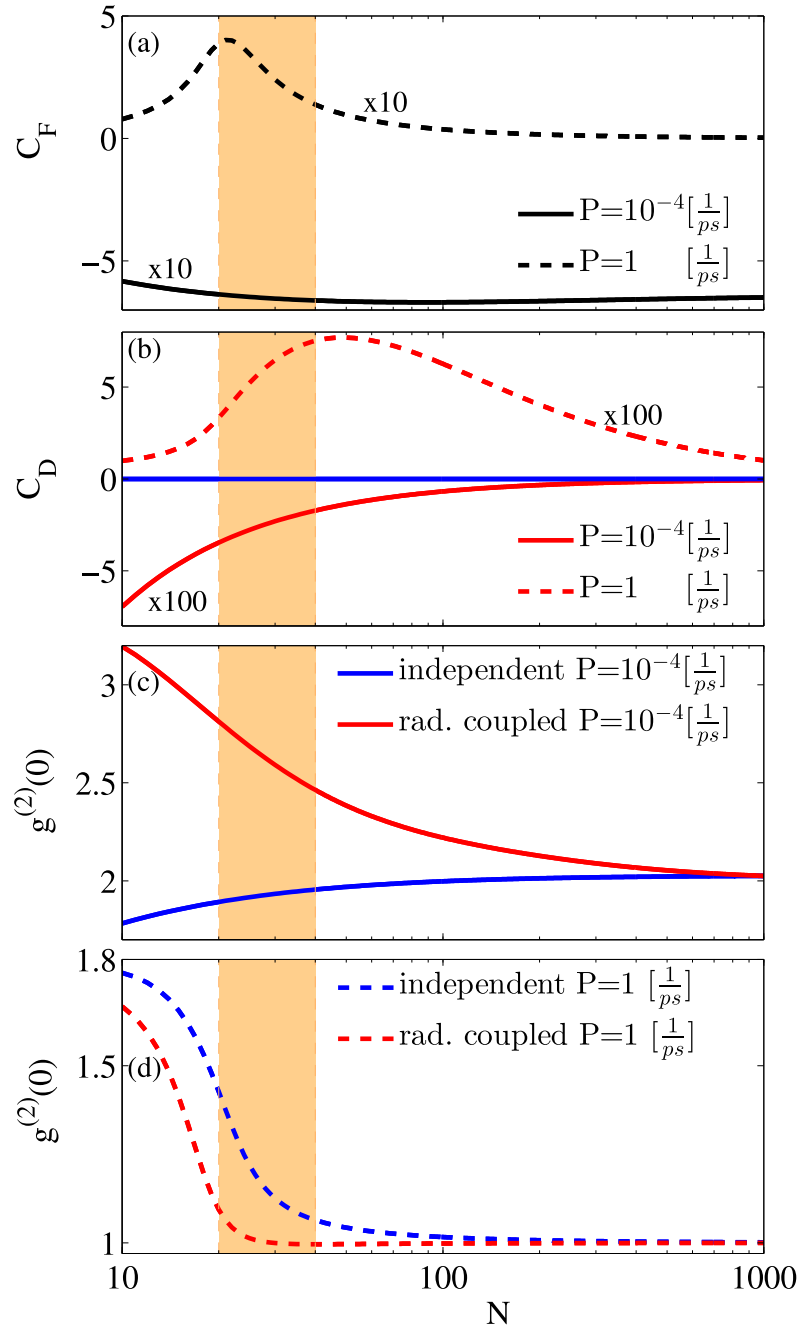


Figure 6.4: Stationary states for increasing number of QDs  $N$  at a low ( $P = 10^{-4}/ps$  solid lines), and a high pump rate ( $P = 1/ps$  dashed lines), all other parameters are the same as in Fig. 6.2. (a) Cooperativity factor  $C_F$ , (b) dipole correlation function  $C_D$ , (c) photon autocorrelation function  $g^{(2)}(0)$  for low pump rates ((d): high pump rates). Compared are results for independent (blue) and radiatively coupled QDs (red). The shaded region marks the QD numbers where coherent emission is only reached when radiative coupling effects are taken into account.

for two selected pump rates. At low excitation (solid lines), out-of-phase QD-QD-dipole alignment ( $C_D < 0$ ) and superthermal bunching ( $g^{(2)}(0) > 2$ ) are observed.

They are strongest for few emitters and reach the values of independent-emitter theories in the limit of large  $N$  (c.f. panels (b) and (c)). At high excitation (dashed lines), the impact of radiative coupling also decreases for large QD numbers, as the system is then entirely dominated by stimulated emission.

Interemitter-coupling effects have the most striking impact at low and intermediate QD numbers: In this regime, the presence or absence of SR coupling decides whether or not the system can reach coherent emission. This important finding is reflected in the autocorrelation function  $g^{(2)}(0)$  at high excitation rates (panel (d)). Without radiative coupling (blue curves), lasing is reached with  $N \gtrsim 40$  emitters in the cavity, indicated by a mean photon number above one and  $g^{(2)}(0) \approx 1$ . In the presence of radiative coupling (red curves), lasing by the same criteria is possible with only half the emitter number  $N \gtrsim 20$ . The regime, where lasing is possible *only in the presence* of the collective coupling effects is shaded in orange. In fact, many current realizations of microcavity laser systems operate in the regime of 20–100 emitters effectively coupling to the laser mode [Strauf and Jahnke, 2011].

Interestingly, in the presence of radiative coupling, the same level of coherence expressed in  $g^{(2)}(0)$  is achieved at a much lower mean photon number ( $\langle b^\dagger b \rangle \approx 8$  with and  $\langle b^\dagger b \rangle \approx 35$  without radiative coupling). Thus, the creation of dipole-phase correlations between the emitters, associated with a positive value for  $C_D$ , leads to an increase of the “coherence per photon”, so that a lower mean photon number suffices to reach the same level of coherence in the emission.

The influence of the cavity mode quality factor is studied in Fig. 6.5 for a range of values from  $Q=80\,000$  to  $Q=5\,000$ . Shown are results for the high-excitation regime ( $P=1/\text{ps}$ ), in which lasing occurs when the emitter gain can compensate the photon losses. With increasing photon losses (decreasing quality factor), this requires emission from more emitters  $N$  in the gain material and effectively shifts the lower- $Q$  curves to higher emitter numbers. Of particular interest is the region, in which lasing is only reached if radiative coupling is present. For each value of  $Q$ , this is indicated by the solid-colored bars. The width of these regions increases at higher  $N$ , as the emission enhancement seen in the cooperativity factor  $C_F$  scales with the emitter number (top panel). While at  $Q=80\,000$ , about half the number of emitters suffices to reach stimulated emission in the presence of the discussed enhancement, at  $Q=10\,000$  it is less than a fourth. At the same time, it is interesting to note that the average strength of the dipole correlations between *pairs* of emitters ( $C_D$ , shown in lower panel) is largely independent of the quality factor of the mode and is solely determined by the light-matter coupling strength. We point out that the size of the resonator and the linewidth of the cavity mode provides a physical limit for the number of emitters that can effectively couple to a single mode. Nevertheless, the implications of the insensitivity of radiative coupling effects to the quality factor may be of interest in devices that naturally offer lower quality factors, such as e.g. surface plasmon lasers.

## 6.6 Dicke States of Pairs of Emitters

The origin of sub- and superradiance is often discussed in a simplified picture of two coupled two-level systems [Dicke, 1954, Meyer and Yeoman, 1997]. The eigen-

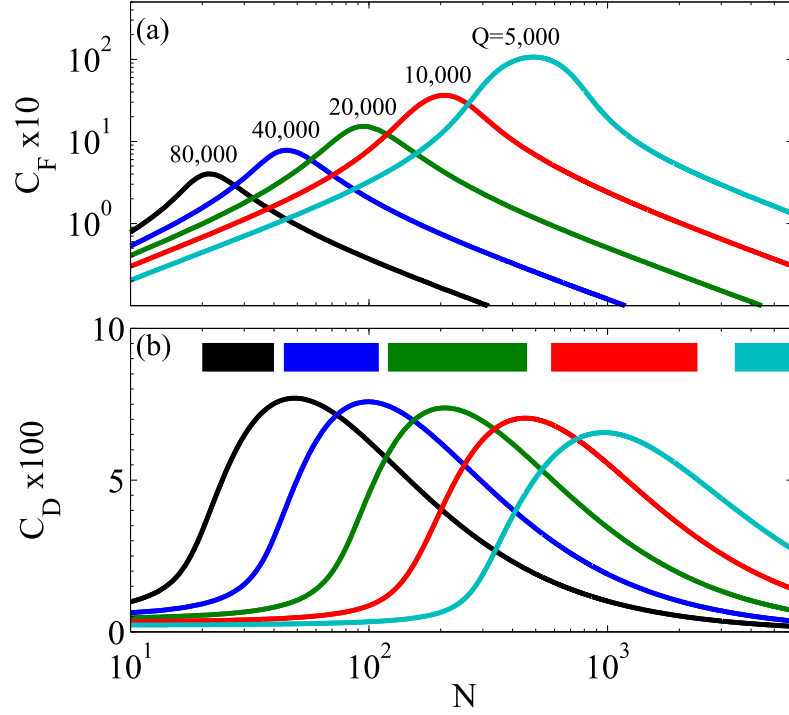


Figure 6.5: Stationary states of the cooperativity factor  $C_F$  (top) and dipole correlation function  $C_D$  as function of emitter number. Results are obtained for high pumping ( $P = 1/\text{ps}$ ) and shown for cavity modes with quality factors of  $Q = 80\,000, 40\,000, 20\,000, 10\,000$  and  $5\,000$  from left to right. All other parameters are unchanged with respect to Fig. 6.4. The  $Q = 80\,000$  results (black curves) are identical to the data in the top panels of Fig. 6.4. The solid bars indicate the interval of QD numbers  $N$  for which coherent emission is *only* reached when radiative coupling between the QDs is present (analog to the shaded region in Fig. 6.4).

states of the coupled system are the ground state  $|\downarrow\downarrow\rangle$ , the fully excited state  $|\uparrow\uparrow\rangle$ , and the two degenerate states  $|\downarrow\uparrow \pm \uparrow\downarrow\rangle$ . The antisymmetric state is, in general, dipole forbidden [Mandel and Wolf, 1995], on which basis one can explain the photon bunching in the subradiant regime [Auffèves et al., 2011]. By considering EVs of the type  $\langle (b^\dagger)^n b^m Q_{ij}^\alpha Q_{i'j'}^\beta \rangle$  within our formalism, we have access to occupation probabilities of QD *pairs*, which corresponds to the information contained in a reduced two-QD density matrix. In an ensemble of many emitters, the EV  $\langle Q_{GG}^1 Q_{GG}^2 \rangle$  represents the averaged probability to find QD pairs in the ground state  $|\downarrow\downarrow\rangle$ , and  $\langle Q_{XX}^1 Q_{XX}^2 \rangle$  in the fully excited state  $|\uparrow\uparrow\rangle$ , respectively. When the  $|\uparrow\uparrow\rangle$  state is likely to be occupied, not only single-photon emission is possible, but also correlated two-photon emission via the process  $\langle b^\dagger b^\dagger E_\alpha E_\beta \rangle$ , which leads to  $C_{2P} > 1$ . The (anti)symmetric state is the eigenstate of the product of two dipole operators  $D^1 D^2$  with the eigenvalue  $(-1)$ , therefore the dipole correlation function  $C_D$  contains information on whether pairs of QDs predominantly occupy the symmetric  $|\downarrow\uparrow + \uparrow\downarrow\rangle$  ( $C_D > 0$ ), or the antisymmetric  $|\downarrow\uparrow - \uparrow\downarrow\rangle$  ( $C_D < 0$ ) state. With the knowledge of the EVs  $\langle Q_{GG}^1 Q_{GG}^2 \rangle$ ,  $\langle Q_{XX}^1 Q_{XX}^2 \rangle$ , and  $\langle D^1 D^2 \rangle$  we can reconstruct the probabilities  $\langle \downarrow\downarrow \rangle$ ,  $\langle \uparrow\uparrow \rangle$ , and  $\langle \downarrow\uparrow \pm \uparrow\downarrow \rangle$  to find pairs of emitters in the ground

state, the fully excited state, or the (anti)symmetric half excited state. Analogous to the two-emitter case, in the antisymmetric configuration the excitation is trapped. This is reflected in the effective spontaneous emission rate (6.7), where negative values of  $C_D$  suppress the spontaneous emission into the laser mode. On the other hand, photon emission from the symmetric state is accelerated, as a positive  $C_D$  enhances the emission rate into the laser mode. These two regimes are referred to in the literature as subradiant [Auffèves et al., 2011] or anti-superradiant [Mandel and Wolf, 1995] ( $C_D < 0$ ), and superradiant ( $C_D > 0$ ).

In contrast, on the level of independent emitters, EV between pairs of emitters are factorized:  $\langle \downarrow \uparrow \pm \uparrow \downarrow \rangle \rightarrow \langle \downarrow \rangle \langle \uparrow \rangle$ . This results in a much simpler structure of possible processes as illustrated in Fig. 6.6. In this case, a distinction between the discussed symmetric and antisymmetric states of QD pairs is not possible, and the corresponding emission inhibition or enhancement due to out-of-phase (in-phase) dipole moments is not accounted for. Neither is correlated two-photon emission ( $C_{2P} > 1$ ) possible on the level of independent emitters, which results in the vanishing superthermal photon bunching with  $g^{(2)}(0) \leq 2$  for this case.

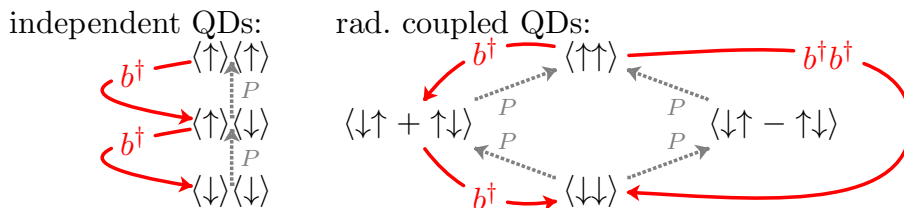


Figure 6.6: Illustration of the population and depopulation processes for the reduced two-QD density matrices. We compare the case of the product states of individual emitters, which is obtained when QD-QD correlations are factorized (left), to the case of radiatively coupled emitters (right). The solid red lines indicate the coherent photon emission into the cavity  $b^\dagger$ . Dotted gray lines indicate the effective incoherent pump  $P$  resulting from the electron-hole capture in the p-shell and the various relaxation and scattering processes.

## 6.7 Chapter Conclusion

Current QD nanocavity devices challenge our understanding of lasers. The small mode volume sets a limit for the number of emitters that can effectively couple to a single cavity mode. Micropillar devices operate with about 20–200 emitters [Lermer et al., 2013], and even less in photonic-crystal resonators [Strauf and Jahnke, 2011]. In this extreme regime, cavity-QED effects are known to enhance correlations and to alter the nature of the emitted light [Nomura et al., 2010, Wiersig et al., 2009]. In a range of quality factor values typical for current microcavity lasers, we predict correlations *between* the emitters to influence the output characteristics of cw-driven lasers significantly: In the presence of collective effects, coherent emission is reached with fewer emitters and at lower mean photon numbers. The increased “coherence per photon” reflects the presence of dipole correlations in the gain medium. At

low excitation, subradiant suppression of emission increases the jump in the input-output curve that is typically associated with the  $\beta$ -factor. Theories that neglect radiative emitter coupling may underestimate the  $\beta$ -factor by an order of magnitude. These findings can explain the efficiency in photon production of current few-emitter nanolasers, which is often better than predicted from conventional laser models, and stimulate further experimental effort to identify the role of sub- and superradiance in these systems, e.g. by investigating the laser dynamics with respect to collective lifetime changes in the emission, or by high time-resolution measurements of the emission statistics to reveal superthermal photon bunching. Strong collective effects are also expected under pulsed excitation, which will be the topic of future work.

Our results are obtained from a laser theory that includes radiative interemitter coupling and photon correlations to obtain  $g^{(2)}(0)$ . The underlying configuration cluster-expansion (CCE) approach is based on the factorization of higher-order EVs of electronic configuration and photon operators and allows for the description of systems with a large number of degrees of freedom. This is well suited to model the coupling of the multi-exciton states of several hundred solid-state emitters to a cavity mode. The method may also prove useful to describe collective effects in cold atomic gases, for which lifetime changes due to sub- and superradiant coupling have been reported [Bienaimé et al., 2013, Pellegrino et al., 2014], in the context of random lasers with many photonic modes [Wiersma, 2008], or in the description of collective effects in coupled microcavity arrays [Ruiz-Rivas et al., 2014].



# Chapter 7

## Final Conclusions

**Summary** The initial task for this thesis was to apply and extend a well established theory for optical properties of semiconductor quantum dots (QDs) and microcavity lasers. This already very sophisticated theory is based on the cluster expansion (CE) [Schoeller, 1994, Hoyer et al., 2004]. The CE has been successfully applied to quantum-wells [Hoyer et al., 2003], ultracold Bose gases [Witthaut et al., 2011], spin systems [Kapetanakis and Perakis, 2008], and semiconductor QD systems [Wiersig, 2007, Gies et al., 2007, Gies, 2008, Baer et al., 2006, Ulrich et al., 2007, Ates et al., 2008, Wiersig et al., 2009]. The last references by Wiersig et al. were the starting point for this thesis. Although very successful, the CE reveals technical and conceptional flaws, especially when applied to systems with a finite component.

On the technical side the derivation of the hierarchy of equations of motion (EoM) for the correlation functions is a tedious and error-prone task. Additional to this technical problem which is more concerned with convenience of the user, the regular CE provided a rather unsatisfying handling of scattering and dephasing processes caused by the environment. In the regular CE for semiconductor QDs the microscopic EoM derived from the Dipole and Coulomb Hamiltonian are augmented by phenomenological terms [Gies et al., 2007] to describe the effects of the surrounding semiconductor material. In particular the phenomenological terms describe the transfer of population due to scattering, for the single particle properties, and create the dephasing of the corresponding polarizations. For a consistent physical model, the scattering and dephasing rates should not be chosen independent from each other, they should rather be connected to the underlying physical processes. An inconsistent treatment of scattering and dephasing can also lead to artifacts like heating [Hoyer et al., 2003], or a build up of nonphysical correlations. Closely related is the question how the environment affects higher-order many-particle correlations and how one can determine their EoM with acceptable effort.

The consistent treatment of scattering and dephasing for all many-particle correlation functions based on Lindblad terms was presented chapter 3. The Lindblad terms, commonly used in quantum optics [Carmichael, 1999], generate the time evolution of the density operator that is caused by the environment. This time evolution was transferred, in the presented theory, to all orders of many-particle correlation functions occurring in the CE.

---

A conceptual problem of the CE is its convergence, when applied to finite systems. The CE was originally developed for (quasi)continuous or at least very large systems, and it is known that the CE can produce nonphysical results like negative occupation numbers when applied to small and finite systems [Richter et al., 2009, Leymann et al., 2013b]. In chapter 3 a solution to this problem is presented as well. The fact that a QD can only accommodate a limited number of carriers is taken into account by adding corrective terms to the regular EoM based on correlation functions. The new improvements of the theory have the drawback that the algebraic afford was increased considerably, and a computer algebra program was needed to derive the EoM.

A reformulation of the traditional CE where all quantities are expressed in simple expectation values (EVs) is given in chapter 4. This reformulation fixes the flaws of the traditional CE, described above, and it is much more user friendly than the regular CE. In contrast to the traditional CE, where the EoM are nonlinear in all orders, in the expectation value based cluster expansion (EVCE) the EoM become nonlinear only in those terms where correlation functions actually are neglected. This way of formulating the CE allows to directly include the Lindblad terms and apply all approximations concerning the finiteness of the Hilbert space in a straight forward manner, with a minimum of algebraic afford. It has to be pointed out that the CE and the EVCE are equivalent and produce exactly the same results. Finally, the EVCE and the formulation introduced in chapter 4 allows for a unified view on a variety of methods and approximations presented in the literature.

In chapter 5 the ideas and techniques developed in the previous chapters are used to further improve and extend the laser theory presented in [Gies et al., 2007, Wiersig et al., 2009, Wiersig, 2010, Wiersig, 2007, Gies, 2008]. In the first part of chapter 5 the laser transition of a QD-based single-mode microcavity laser is studied by calculating the higher-order ( $g^{(n)}(0)$  with  $n = 3 \dots 5$ ) photon correlation functions. In former theories, based on the CE only the photon correlation function of second-order was accessible. The possibility to calculate photon correlation functions of 5th order, within the framework of the CE, is an important achievement of this work. The results in this chapter demonstrate the convergence of the CE for a nontrivial example [Leymann et al., 2014]. Additionally the results emphasize that for high  $\beta$ -factor lasers it is worth to reconsider the concept of a laser threshold.

In the second part of chapter 5 the single-mode theory is extended to a two-mode theory. This theory is used to understand the superthermal intensity fluctuations [Leymann et al., 2013c] in bimodal microcavity lasers experimentally observed by the group of Prof. Reitzenstein (TU Berlin). In the third part of chapter 5 the ideas of the cluster expansion are used to calculate the dynamics of the first-order coherence function  $g^{(1)}(\tau)$  from which the spectrum of the system can be obtained. To get a more intuitive understanding of the observations a simple birth and death model is introduced that agrees qualitatively with the experiments and the microscopic theory but provides more insight to the underlying photon statistics. For the spectral properties of the bimodal laser a simple  $2 \times 2$  matrix model is derived. It features the main aspects of the system and reveals relations to the strong and weak coupling regime of a single photonic mode and an atomic transition. A comprehensive picture of the lasing properties of a bimodal microcavity laser is given. Microscopic theories



that match the experimental results are derived, and phenomenological models are introduced to illustrate and illuminate the abstract microscopic theory.

In chapter 6 the superradiant (SR) coupling between QDs is investigated. It is shown how the SR coupling between the QDs can be described with the CE and how the SR coupling of emitters affects the threshold behavior of a microcavity laser. For a consistent inclusion of QD-QD correlations the traditional CE is again modified based on the ideas developed in chapter 3 and 4. The new formulation treats the electronic configurations in a QD exactly and factorizes correlations between different QDs. SR coupling reduces the number of emitters required to achieve lasing operation and enhances the intensity fluctuations below the lasing threshold to super thermal values. By examining the EoM we have shown that the dipole-dipole correlations between different QDs make a significant contribution to the spontaneous emission and can be the crucial component of the emission terms to reach the lasing regime.

It may as well be noted in this conclusion that the very interesting topic of SR coupling was already mentioned in the outlooks of the habilitation treatise of Prof. Wiersig and the PhD thesis of Dr. Gies [Wiersig, 2007, Gies, 2008], and proposed as a fruitful direction of further research.

**Outlook** As it is always the case, when new methods are developed and applied to new and interesting physical systems, a research project raises more questions than it answers. In the case of this thesis the open questions arise mainly from the new possibilities that the improvements of the CE offer. In the following the most promising questions and new problems are briefly sketched.

The two mode-theory presented in section 5.2 and Ref. [Leymann et al., 2013c] could be extended to a multi-mode theory. In a multi-mode system more than one mode could be lasing and the crosscorrelation functions as well as the statistical properties of the non-lasing modes promise to be interesting. The theory of generalized Bose-Einstein condensates presented in [Vorberg et al., 2013, Vorberg et al., 2015] has many parallels to the proposed multi-mode version of the two-mode laser theory developed in this thesis. In contrast to the generalized Bose-Einstein condensates, an even number of modes can be selected and go into lasing. Furthermore the relations to the theory of generalized Bose-Einstein condensates could be studied and used to gain a new perspective on multi-mode microcavity systems and explain the switching of the selected modes with increasing pump power, observed in recent experiments [Reitzenstein and Vorberg private communication].

In chapter 6 it was assumed that all QDs have roughly the same size, hence the s-shell transition-energies of the QDs are all equal and additionally in perfect resonance with the cavity mode. The inhomogeneous broadening of the QDs was not considered. To quantify the impact of the inhomogeneous broadening of the QDs on the SR effects is a very important and experimentally relevant task. The important question is: Will the SR effects persist when the inevitable inhomogeneous nature of the QDs is considered? So far, the SR coupling of only a few different QDs could be investigated [Temnov and Woggon, 2005, Sitek and Machnikowski, 2007, Abdussalam and Machnikowski, 2014] with exact theoretical methods. The very efficient formulation of the CE established in chapter 6 allows for an investigation

---

of at least 50 QDs from an inhomogeneously distributed ensemble, thus providing access to scenarios present in state of the art micro/nano lasers.

Another interesting turn on the description of SR in micro lasers could be the introduction of an extended birth-and death-model similar to the two-mode laser model introduced in chapter 5. An extended birth and death model describing the transitions between the ground-, bright-, dark-, and twofold excited -state (see Fig. 6.6) should be able to reproduce (qualitatively) the core effects the microscopic theory predicts, much like the two-mode birth-and death model reproduces the results of the microscopic theory in section 5.2. The benefit of such a theory would be, the mathematical confirmation of the intuitive explanation based on Dicke states given at the end of chapter 6. Another advantage of a description in terms of a birth and death model would be the access to the full photon statistics.

Starting from the very general ideas developed in chapter 4, there are various possibilities to further improve the CE. One could for example combine the EVCE approach with the methods from section 5.3 to calculate the delay dynamics of the higher-order photon correlation functions e.g.  $g^{(2)}(\tau)$ . Another interesting application would be the calculation of the spectra and coherence time of light emitted by superradiantly coupled QDs in a microcavity. To this end one would have to combine the methods developed in chapter 6 with the ones used in section 5.3. It is expected that the SR-coupling of the QDs will have an impact on the spectral properties of the emitted light. This would provide another experimentally accessible fingerprint of the SR coupling between QDs.

In general the CE and its various reformulations have proven to be a versatile and powerful tool and we believe the CE has a variety of new applications that are yet to be discovered.

# Appendix A

## Equations of motion for single QD PL into free Space

In this appendix we provide supplementary material to chapter 3. We provide a detailed account of all contributions to the equations of motion up to the  $M_{\text{trunc}} = 1$ ,  $N_{\text{max}} = 2$  level of the FSH method that were omitted for the sake of transparency in Sec. 3.4. This includes contributions from the light-matter, Coulomb and system-bath interaction, which has been used for calculations shown in Section 3.6 and 3.5. To derive the equations we follow the same line as presented in Section 3.4. Especially the Coulomb contributions add significant complexity to the equations, thus we have derived/checked them by utilizing the symbolic manipulation system FORM [Vermaseren, 2000] (see appendix D for details).

### A.1 Hamiltonian

The microscopic Hamiltonian that describes the carrier dynamics and the quantized electromagnetic field contains the following contributions

$$H = H_{\text{carr}}^0 + H_{\text{ph}}^0 + H_{\text{LM}} + H_{\text{Coul}}. \quad (\text{A.1})$$

The first part of the Hamiltonian includes the non-interacting single-particle spectrum  $\varepsilon_i^{c/v}$  of the conduction- and valence band carriers

$$H_{\text{carr}}^0 = \sum_i \varepsilon_i^c c_i^\dagger c_i + \sum_i \varepsilon_i^v v_i^\dagger v_i, \quad (\text{A.2})$$

which are annihilated (created) by the fermionic operator  $c_i$  ( $c_i^\dagger$ ) and  $v_i$  ( $v_i^\dagger$ ), respectively. Carrier-carrier interaction arises from the two-particle Coulomb Hamiltonian

$$\begin{aligned} H_{\text{Coul}} = & \frac{1}{2} \sum_{ijkl} V_{ijkl} c_i^\dagger c_j^\dagger c_k c_l + \frac{1}{2} \sum_{ijkl} V_{ijkl} v_i^\dagger v_j^\dagger v_k v_l + \sum_{ijkl} V_{ijkl} c_i^\dagger v_j^\dagger v_k c_l \\ & + \frac{1}{2} \sum_{ijkl} V_{ijkl} (v_i^\dagger v_k \delta_{jl} + v_j^\dagger v_l \delta_{ik} - v_i^\dagger v_l \delta_{jk} - v_j^\dagger v_k \delta_{il}) - \sum_{ijkl} V_{ijkl} c_i^\dagger c_l \delta_{jk}, \end{aligned} \quad (\text{A.3})$$

that contains direct (Hartree) terms  $V_{ijji}$  and exchange (Fock) terms  $V_{ijij}$ , resulting in energy renormalizations and a mixing between single particle configurations. The

last two terms ensure that the contribution of the full valence band, that is already included in the single particle properties is not double-counted. The explicit form of the single-particle states enters the calculation of the Coulomb-matrix elements  $V_{ijkl}$  and is discussed in [Baer et al., 2006, Wojs et al., 1996] for a cylindrical, lens-shaped QD. Throughout this hole thesis we consider the single-particle wave functions in envelope-function approximation [Haug and Koch, 2004], as well as equal envelopes for the conduction- and valence-band electrons. However, more sophisticated methods, like tight-binding calculations [Schulz and Czycholl, 2005], can be used. For the material parameters we have chosen those of Ref. [Baer et al., 2004] for an InGaAs/GaAs QD.

We consider the fully quantized electromagnetic field, of which the free part is given by

$$H_{\text{ph}}^0 = \sum_{\xi} \omega_{\xi} \left( b_{\xi}^{\dagger} b_{\xi} + \frac{1}{2} \right). \quad (\text{A.4})$$

Here, the bosonic operators  $b_{\xi}$  ( $b_{\xi}^{\dagger}$ ) annihilate (create) a photon with the energy  $\omega_{\xi}$  in the photon mode  $\xi$ . The index  $\xi$  represents both, the wave vector  $\mathbf{q}$  and the polarization vector of the electromagnetic field  $\mathbf{e}_{\pm}(\mathbf{q})$ . The non-perturbative light-matter interaction  $H_{\text{LM}}$  in dipole and rotating-wave approximation reads [Kira et al., 1999, Baer et al., 2006]

$$H_{\text{LM}} = -i \sum_{\xi, i} \left( g_{\xi} b_{\xi} c_i^{\dagger} v_i - g_{\xi}^* b_{\xi}^{\dagger} v_i^{\dagger} c_i \right), \quad (\text{A.5})$$

where the light-matter coupling strength  $g_{\xi}$  is proportional to the interband dipole matrix element  $\mathbf{d}_{\text{cv}}$ . Note that within the envelope-function approximation, optical transitions occur only between the  $s$ - or the  $p$ -shell of the conduction- and valence band.

In the case that the QD is resonant with a single cavity mode, the influence of all other modes can be treated via Lindblad terms, so that  $H_{\text{LM}}$  reduces to the Jaynes-Cummings (JC) interaction Hamiltonian [Jaynes and Cummings, 1963, Shore and Knight, 1993].

## A.2 Equations of motion

### A.2.1 Light-matter interaction

Writing down the contribution of the light-matter interaction to the equations of motion for the populations, we obtain

$$\frac{d}{dt} f_i^c \Big|_{H_{\text{LM}}} = -\frac{d}{dt} f_i^v \Big|_{H_{\text{LM}}} = -2\text{Re} \sum_{\xi} g_{\xi}^* \Pi_{\xi, i}, \quad (\text{A.6})$$

which is coupled to the photon-assisted polarization  $\Pi_{\xi, i}$ . The corresponding dynamical equations read

$$\frac{d}{dt} \Pi_{\xi, i} \Big|_{H_{\text{LM}}} = g_{\xi} f_i^c (1 - f_i^v) + \sum_{\mu} g_{\xi} C_{\mu i i \mu}^x \quad (\text{A.7})$$

and contain the interband carrier correlation functions  $C_{ijkl}^x$ . In contrast to Eq. (3.17) the photon population  $\mathcal{N}_\xi$  and carrier-photon correlations  $\mathcal{N}_{\xi,i}^c$  and  $\mathcal{N}_{\xi,i}^v$  have been omitted as the maximum order with respect to the photons is restricted to the  $M_{\text{trunc}} = 1$  level in this appendix.

The equations of motion for the interband carrier correlation functions

$$\begin{aligned} \frac{d}{dt} C_{ijkl}^x|_{H_{\text{LM}}} &= \sum_{\xi} [g_{\xi} (f_j^c - f_j^v) \Pi_{\xi,i}^* + g_{\xi}^* (f_i^c - f_i^v) \Pi_{\xi,j}] \delta_{il} \delta_{jk} \\ &+ \sum_{\xi} (g_{\xi} \Pi_{\xi,ijkl}^{c*} + g_{\xi}^* \Pi_{\xi,ijkl}^{c} - g_{\xi} \Pi_{\xi,ijkl}^{v*} - g_{\xi}^* \Pi_{\xi,ijkl}^{v}), \end{aligned} \quad (\text{A.8})$$

and for the conduction band carrier-carrier correlations

$$\frac{d}{dt} C_{ijkl}^c|_{H_{\text{LM}}} = \sum_{\xi} (g_{\xi} \Pi_{\xi,ijkl}^{c*} - g_{\xi} \Pi_{\xi,ijkl}^{c*} + g_{\xi}^* \Pi_{\xi,jikl}^c - g_{\xi}^* \Pi_{\xi,ijkl}^c) \quad (\text{A.9})$$

contain the higher order contributions  $\Pi_{\xi,ijkl}^c$  and  $\Pi_{\xi,ijkl}^v$ , which obey their own dynamics. A similar expression can be found for the valence-band carrier-carrier correlations  $C_{ijkl}^v$  by exploiting the symmetry properties of the Hamiltonian.

Due to the limited number of considered single-particle states (cf. the beginning of Sec. 3.4), in conjunction with scattering processes that conserve the total number of excitations in the electronic system, the electronic hierarchy automatically truncates at the  $N_{\text{max}} = 2$  level. Therefore, by including the equations of motion for  $\Pi_{\xi,ijkl}^c$  and  $\Pi_{\xi,ijkl}^v$

$$\frac{d}{dt} \Pi_{\xi,ijkl}^c|_{H_{\text{LM}}} = g_{\xi} C_{ijkl}^c + (g_{\xi}^* \Pi_{\xi,i} \Pi_{\xi,j} - g_{\xi} f_i^c f_j^c f_j^v + f_i^c \sum_{\mu} g_{\xi} C_{\mu jj\mu}^x) (\delta_{ik} \delta_{jl} - \delta_{il} \delta_{jk}) \quad (\text{A.10})$$

and

$$\begin{aligned} \frac{d}{dt} \Pi_{\xi,ijkl}^v|_{H_{\text{LM}}} &= g_{\xi} C_{ijkl}^x - g_{\xi} C_{jikl}^x \\ &+ (g_{\xi}^* \Pi_{\xi,l} \Pi_{\xi,k} + g_{\xi} f_k^c f_k^v f_l^v - f_l^v \sum_{\mu} g_{\xi} C_{\mu k k \mu}^x) (\delta_{il} \delta_{jk} - \delta_{ik} \delta_{jl}) \end{aligned} \quad (\text{A.11})$$

we obtain a closed set of equations at the  $M_{\text{trunc}} = 1$ ,  $N_{\text{max}} = 2$  level by neglecting the contributions from the correlation functions  $\delta \langle b_{\xi}^{\dagger} b_{\xi} c_i^{\dagger} c_j^{\dagger} c_k c_l \rangle$ ,  $\delta \langle b_{\xi}^{\dagger} b_{\xi} v_i^{\dagger} v_j^{\dagger} v_k v_l \rangle$ ,  $\delta \langle b_{\xi}^{\dagger} b_{\xi} c_i^{\dagger} v_j^{\dagger} c_k v_l \rangle$  and  $\delta \langle b_{\xi}^{\dagger} b_{\xi} v_i^{\dagger} v_j^{\dagger} c_k c_l \rangle$ , which are second order in the photon hierarchy.

At this point we have written down equations for all occurring correlation functions. Coulomb and Lindblad contributions are discussed subsequently and only add to the quantities we have introduced.

## A.2.2 Coulomb interaction

The inclusion of the Coulomb interaction is of central importance for the physical behavior of semiconductor nanostructures. In contrast to atomic systems, here Coulomb effects can be of similar magnitude as the energetic separation between

the localized electronic states. Thus, energetic shifts introduced by the Coulomb interaction can have a severe impact on dynamical and spectral properties in a system of contributing multi-exciton configurations.

Starting with the contributions of the Coulomb Hamiltonian (A.3) to the equations of motion for the carrier populations, we obtain

$$\frac{d}{dt} f_i^c \Big|_{H_{\text{Coul}}} = -2\text{Im} \sum_{\mu\nu\alpha} V_{i\mu\nu\alpha} C_{i\mu\alpha\nu}^{x+c}. \quad (\text{A.12})$$

Here we have introduced the abbreviation  $C_{ijkl}^{x+c} = C_{ijkl}^x + C_{ijkl}^c$ . For the higher-order correlation functions, a straightforward interpretation of the contributions is obscured by their complexity, and we restrain ourselves to a mere listing of equations.

$$\begin{aligned} \frac{d}{dt} \Pi_{\xi,i} \Big|_{H_{\text{Coul}}} &= i \sum_{\mu} \{ V_{i\mu i\mu} [(1 + f_{\mu}^c - f_{\mu}^v) \Pi_{\xi,i} - (f_i^c - f_i^v) \Pi_{\xi,\mu}] \\ &+ \sum_{\nu\alpha} V_{i\mu\nu\alpha} (\Pi_{\xi,\mu\nu\alpha}^c + \Pi_{\xi,i\mu\alpha\nu}^v) + \sum_{\nu\alpha} V_{i\mu\nu\alpha}^* (\Pi_{\xi,\nu\alpha i\mu}^c + \Pi_{\xi,\nu\alpha i\mu}^v) \} \end{aligned} \quad (\text{A.13})$$

$$\begin{aligned} \frac{d}{dt} C_{ijkl}^x \Big|_{H_{\text{Coul}}} &= i V_{ijkl}^* [f_i^c f_j^v - f_k^c f_l^v] \\ &+ i \sum_{\mu\nu} [V_{ij\mu\nu}^* C_{\nu\mu kl}^x - V_{kl\mu\nu} C_{ij\nu\mu}^x + V_{k\mu\nu} C_{ij\nu l}^x - V_{i\mu\nu}^* C_{\nu jkl}^x] \\ &+ i \sum_{\mu\nu} [(V_{l\mu\nu} - V_{l\nu\mu}) C_{ijk\nu}^x + (V_{j\mu\nu}^* - V_{j\nu\mu}^*) C_{i\nu kl}^x] \\ &- i \sum_{\mu} [V_{i\mu\mu k}^* (f_i^c - f_k^c) f_j^v \delta_{jl} + (V_{j\mu l}^* - V_{j\mu l}^*) f_i^c (f_l^v - f_j^v) \delta_{ik}] \\ &- 2\text{Im} \left\{ \sum_{\mu\nu\alpha} [f_j^v V_{i\mu\nu\alpha} C_{i\mu\alpha\nu}^{x+c} + f_i^c V_{j\mu\nu\alpha} C_{\mu j\nu\alpha}^{x+v}] \right\} \delta_{ik} \delta_{jl} \end{aligned} \quad (\text{A.14})$$

$$\begin{aligned} \frac{d}{dt} C_{ijkl}^c \Big|_{H_{\text{Coul}}} &= i (V_{ijkl}^* - V_{ijlk}^*) (f_k^c f_l^c - f_i^c f_j^c) \\ &+ i \sum_{\mu\nu} [V_{l\mu\nu} C_{ijk\nu}^c - V_{k\mu\nu} C_{ijl\nu}^c + V_{kl\mu\nu} C_{ij\mu\nu}^c + V_{i\mu\nu}^* C_{j\nu kl}^c - V_{j\mu\nu}^* C_{i\nu kl}^c - V_{ij\mu\nu}^* C_{\mu\nu kl}^c] \\ &+ i \sum_{\mu} [V_{i\mu\mu k}^* f_j^c (f_k^c - f_i^c) \delta_{jl} - V_{i\mu\mu l}^* f_j^c (f_l^c - f_i^c) \delta_{jk}] \\ &- i \sum_{\mu} [V_{j\mu\mu k}^* f_i^c (f_k^c - f_j^c) \delta_{il} - V_{j\mu\mu l}^* f_i^c (f_l^c - f_j^c) \delta_{ik}] \\ &- 2\text{Im} \left\{ \sum_{\mu\nu\alpha} [f_j^c (V_{i\mu\nu\alpha} C_{i\mu\alpha\nu}^{x+c}) + f_i^c (V_{j\mu\nu\alpha} C_{j\mu\alpha\nu}^{x+c})] \right\} (\delta_{ik} \delta_{jl} - \delta_{il} \delta_{jk}) \end{aligned}$$

$$\begin{aligned}
 \frac{d}{dt} \Pi_{\xi,ijkl}^c |_{H_{\text{Coul}}} &= i \sum_{\mu\nu} [V_{l\mu\nu} \Pi_{\xi,ijk\nu}^c - V_{k\mu\nu} \Pi_{\xi,ijl\nu}^c + V_{kl\mu\nu} \Pi_{\xi,ij\mu\nu}^c \\
 &\quad - V_{i\mu\nu}^* \Pi_{\xi,\nu jkl}^c + V_{ij\mu\nu}^* \Pi_{\xi,\nu\mu kl}^c + (V_{j\mu\nu}^* - V_{j\mu\mu\nu}^*) \Pi_{\xi,i\nu kl}^c] \\
 &\quad + i [V_{ijkl}^* (f_l^c \Pi_{\xi,k} - f_i^c \Pi_{\xi,j}) - V_{ijlk}^* (f_k^c \Pi_{\xi,l} - f_i^c \Pi_{\xi,j})] \\
 &\quad + i f_i^c \sum_{\mu} \{ [V_{j\mu k}^* (\Pi_{\xi,j} - \Pi_{\xi,k}) + V_{j\mu k\mu}^* \Pi_{\xi,k}] \delta_{il} \\
 &\quad - [V_{j\mu\mu l}^* (\Pi_{\xi,j} - \Pi_{\xi,l}) + V_{j\mu l\mu}^* \Pi_{\xi,l}] \delta_{ik} \} \\
 &\quad + i \Pi_{\xi,j} \sum_{\mu} [V_{i\mu\mu k}^* (f_k^c - f_i^c) \delta_{jl} - V_{i\mu\mu l}^* (f_l^c - f_i^c) \delta_{jk}] \\
 &\quad - 2 \Pi_{\xi,j} \text{Im} \left( \sum_{\mu\nu\alpha} V_{i\mu\nu\alpha} C_{i\mu\alpha\nu}^{x+c} \right) (\delta_{ik} \delta_{jl} - \delta_{il} \delta_{jk}) \\
 &\quad + i f_i^c \sum_{\mu\nu\alpha} [V_{j\mu\nu\alpha} (\Pi_{\xi,\mu j\nu\alpha}^c + \Pi_{\xi,j\mu\alpha\nu}^v) + V_{j\mu\nu\alpha}^* (\Pi_{\xi,\nu\alpha j\mu}^c + \Pi_{\xi,\nu\alpha j\mu}^v)] (\delta_{ik} \delta_{jl} - \delta_{il} \delta_{jk}) \\
 &\quad + i f_i^c \sum_{\mu} V_{j\mu j\mu} [\Pi_{\xi,j} (1 - f_{\mu}^v + f_{\mu}^c) - \Pi_{\xi,\mu} (f_j^c - f_j^v)] (\delta_{ik} \delta_{jl} - \delta_{il} \delta_{jk}) \quad (\text{A.15})
 \end{aligned}$$

$$\begin{aligned}
 \frac{d}{dt} \Pi_{\xi,ijkl}^v |_{H_{\text{Coul}}} &= -i V_{ijkl}^* [\Pi_{\xi,j} f_i^v - \Pi_{\xi,k} f_l^v] + i V_{ijlk}^* [\Pi_{\xi,i} f_j^v - \Pi_{\xi,k} f_l^v] \\
 &\quad - i \sum_{\mu} \{ V_{k\mu k\mu} [\Pi_{\xi,\mu} (f_k^c - f_{\mu}^v) - \Pi_{\xi,k} (f_{\mu}^c + f_{\mu}^h)] \} f_l^v (\delta_{ik} \delta_{jl} - \delta_{il} \delta_{jk}) \\
 &\quad + i \sum_{\mu\nu\alpha} [V_{k\mu\nu\alpha} (\Pi_{\xi,\mu k\nu\alpha}^c + \Pi_{\xi,k\mu\alpha\nu}^v) + V_{k\mu\nu\alpha}^* (\Pi_{\xi,\nu\alpha k\mu}^c + \Pi_{\xi,\nu\alpha k\mu}^v)] f_l^v (\delta_{ik} \delta_{jl} - \delta_{il} \delta_{jk}) \\
 &\quad - 2 \Pi_{\xi,k} \text{Im} \left( \sum_{\mu\nu\alpha} V_{l\mu\nu\alpha} C_{l\mu\nu\alpha}^{x+v} \right) (\delta_{ik} \delta_{jl} - \delta_{il} \delta_{jk}) \\
 &\quad + i \sum_{\mu\nu} [V_{k\mu\mu\nu} \Pi_{\xi,ij\nu l}^v - V_{kl\mu\nu} \Pi_{\xi,ij\nu\mu}^v + (V_{l\mu\mu\nu} - V_{l\mu\nu\mu}) \Pi_{\xi,ijk\nu}^v] \\
 &\quad + i \sum_{\mu\nu} [(V_{i\mu\mu\nu}^* - V_{i\mu\nu\mu}^*) \Pi_{\xi,\nu jkl}^v - V_{ij\mu\nu}^* \Pi_{\xi,\mu\nu kl}^v + (V_{j\mu\nu}^* - V_{j\mu\mu\nu}^*) \Pi_{\xi,i\nu kl}^v] \\
 &\quad - i \Pi_{\xi,k} \sum_{\mu} [(V_{i\mu k\mu}^* - V_{i\mu\mu k}^*) \delta_{jl} - (V_{j\mu k\mu}^* - V_{j\mu\mu k}^*) \delta_{il}] f_l^v \\
 &\quad - i \Pi_{\xi,k} \sum_{\mu} [(V_{i\mu l\mu}^* - V_{i\mu\mu l}^*) (f_i^v - f_l^v) \delta_{jk} - (V_{j\mu l\mu}^* - V_{j\mu\mu l}^*) (f_j^v - f_l^v) \delta_{ik}] \\
 &\quad - i f_l^v \sum_{\mu} [V_{i\mu\mu k}^* \Pi_{\xi,i} \delta_{jl} - V_{j\mu\mu k}^* \Pi_{\xi,j} \delta_{il}] \quad (\text{A.16})
 \end{aligned}$$

### A.2.3 System-bath interaction

The evaluation of the system-bath contributions follows from Eq. (3.14). Cavity losses have already been included in the discussion in Sec. 3.4.

### Scattering

The physical effects of the intraband scattering processes listed in the following include carrier redistribution, dephasing, and redistribution of correlation strength in compliance with the sum rule (3.26), as well as effects on higher-order correlation functions. Note that the evaluation of the sum for  $\mu \neq \nu$  in Eq. (3.23) formally requires setting  $\gamma_{\mu\mu}^{cc} = 0$ .

$$\frac{d}{dt} f_i^c \Big|_{\text{scatt}} = \sum_{\mu} \gamma_{i\mu}^{cc} [f_{\mu}^c (1 - f_i^c) + C_{i\mu i\mu}^c] - \sum_{\mu} \gamma_{\mu i}^{cc} [f_i^c (1 - f_{\mu}^c) + C_{i\mu i\mu}^c] \quad (\text{A.17})$$

$$\frac{d}{dt} \Pi_{\xi,i} \Big|_{\text{scatt}} = -\frac{1}{2} \sum_{\mu} \gamma_{\mu i}^{cc} \Pi_{\xi,i} + \frac{1}{2} \sum_{\mu} (\gamma_{\mu i}^{cc} - \gamma_{i\mu}^{cc}) f_{\mu}^c \Pi_{\xi,i} \Pi_{\xi,\mu i\mu}^c \quad (\text{A.18})$$

$$\begin{aligned} \frac{d}{dt} C_{ijkl}^x \Big|_{\text{scatt}} &= \sum_{\mu} [\gamma_{i\mu}^{cc} C_{\mu j\mu l}^x \delta_{ik} - \frac{1}{2} (\gamma_{\mu i}^{cc} + \gamma_{\mu k}^{cc}) C_{ijkl}^x] \\ &\quad - \sum_{\mu} (\gamma_{i\mu}^{cc} - \gamma_{\mu i}^{cc}) (f_i^c f_{\mu}^c - C_{i\mu i\mu}^c) f_j^c \delta_{ik} \delta_{jl} \end{aligned} \quad (\text{A.19})$$

$$\begin{aligned} \frac{d}{dt} C_{ijkl}^c \Big|_{\text{scatt}} &= \frac{1}{2} (\gamma_{ij}^{cc} + \gamma_{ji}^{cc} + \gamma_{kl}^{cc} + \gamma_{lk}^{cc}) C_{ijkl}^c \\ &\quad + [\gamma_{ij}^{cc} f_j^c (f_j^c - f_i^c) - \gamma_{ji}^{cc} f_i^c (f_j^c - f_i^c)] (\delta_{ik} \delta_{jl} - \delta_{il} \delta_{jk}) \\ &\quad - \frac{1}{2} \sum_{\mu} (\gamma_{\mu i}^{cc} + \gamma_{\mu j}^{cc} + \gamma_{\mu k}^{cc} + \gamma_{\mu l}^{cc}) C_{ijkl}^c \\ &\quad + \sum_{\mu} (\gamma_{\mu i}^{cc} - \gamma_{i\mu}^{cc} + \gamma_{\mu j}^{cc} - \gamma_{j\mu}^{cc}) f_i^c f_j^c f_{\mu}^c (\delta_{ik} \delta_{jl} - \delta_{il} \delta_{jk}) \\ &\quad + \sum_{\mu} \gamma_{i\mu}^{cc} (C_{j\mu l\mu}^c \delta_{ik} - C_{j\mu k\mu}^c \delta_{il}) + \sum_{\mu} \gamma_{j\mu}^{cc} (C_{i\mu k\mu}^c \delta_{jl} - C_{i\mu l\mu}^c \delta_{jk}) \\ &\quad + \sum_{\mu} [(\gamma_{i\mu}^{cc} - \gamma_{\mu i}^{cc}) f_j^c C_{i\mu i\mu}^c + (\gamma_{j\mu}^{cc} - \gamma_{\mu j}^{cc}) f_i^c C_{j\mu j\mu}^c] (\delta_{ik} \delta_{jl} - \delta_{il} \delta_{jk}) \end{aligned}$$

$$\begin{aligned} \frac{d}{dt} \Pi_{\xi,ijkl}^c \Big|_{\text{scatt}} &= \frac{1}{2} (\gamma_{kl}^{cc} + \gamma_{lk}^{cc}) \Pi_{\xi,ijkl}^c \\ &\quad + [\gamma_{ij}^{cc} (f_j^c - \frac{1}{2} f_i^c) - \frac{1}{2} \gamma_{ji}^{cc} f_i^c] \Pi_{\xi,j} (\delta_{ik} \delta_{jl} - \delta_{il} \delta_{jk}) - \frac{1}{2} \sum_{\mu} (\gamma_{\mu i}^{cc} + \gamma_{\mu k}^{cc} + \gamma_{\mu l}^{cc}) \Pi_{\xi,ijkl}^c \\ &\quad + \sum_{\mu} \gamma_{i\mu}^{cc} (\Pi_{\xi,\mu jk\mu}^c \delta_{il} - \Pi_{\xi,\mu jl\mu}^c \delta_{ik}) + \sum_{\mu} [(\gamma_{\mu i}^{cc} - \gamma_{i\mu}^{cc}) (f_i^c f_{\mu}^c - C_{i\mu i\mu}^c) \Pi_{\xi,j} \\ &\quad + \frac{1}{2} (\gamma_{\mu j}^{cc} - \gamma_{j\mu}^{cc}) (f_{\mu}^c \Pi_{\xi,j} + \Pi_{\xi,\mu j\mu}^c) f_i^c] (\delta_{ik} \delta_{jl} - \delta_{il} \delta_{jk}) \end{aligned} \quad (\text{A.20})$$



$$\begin{aligned} \frac{d}{dt} \Pi_{\xi,ijkl}^v \Big|_{\text{scatt}} &= -\frac{1}{2} \sum_{\mu} \gamma_{\mu k}^{cc} \Pi_{\xi,ijkl}^v \\ &\quad - \frac{1}{2} \sum_{\mu} (\gamma_{k\mu}^{cc} - \gamma_{\mu k}^{cc}) f_l^v (f_{\mu}^c \Pi_{\xi,k} + \Pi_{\xi,\mu k k \mu}^c) (\delta_{ik} \delta_{jl} - \delta_{il} \delta_{jk}) \end{aligned} \quad (\text{A.21})$$

A similar set of equations can be given for the intraband scattering in the valence band (by interchanging  $c$  and  $v$ ).

### Pumping

In Eq. (3.27) we have formulated the Lindblad contribution for pair-wise carrier capture into the QD  $p$ -states. For a general capture into the state  $|\mu\rangle$  at a rate  $P_{\mu}(t)$ , this equation reads

$$\frac{d}{dt} \langle A \rangle \Big|_{\text{pump}} = \frac{P_{\mu}(t)}{2} \left( \langle [v_{\mu}^{\dagger} c_{\mu}, A] c_{\mu}^{\dagger} v_{\mu} \rangle + \langle v_{\mu}^{\dagger} c_{\mu} [A, c_{\mu}^{\dagger} v_{\mu}] \rangle \right) \quad (\text{A.22})$$

and leads to the following contributions in the set of equations of motion:

$$\frac{d}{dt} f_i^c \Big|_{\text{pump}} = P_i(t) [(1 - f_i^c) f_i^v + C_{iii}^x]$$

$$\frac{d}{dt} \Pi_{\xi,i} \Big|_{\text{pump}} = -\frac{1}{2} P_i(t) \Pi_{\xi,i}$$

$$\begin{aligned} \frac{d}{dt} C_{ijkl}^x \Big|_{\text{pump}} &= -\frac{1}{2} (P_j(t) + P_l(t)) C_{ijkl}^x + P_i(t) C_{ijil}^v \delta_{ik} \\ &\quad + \frac{1}{2} (P_i(t) C_{iikl}^x \delta_{ij} + P_k(t) C_{ijkk}^x \delta_{kl}) + P_i(t) (C_{iiii}^x - f_i^c f_i^v) f_j^v \delta_{ik} \delta_{jl} \\ &\quad + P_j(t) (f_j^c f_j^v - C_{jjjj}^x) f_i^c \delta_{ik} \delta_{jl} + P_i(t) (f_i^v f_i^v - f_i^c f_i^v) \delta_{ij} \delta_{ik} \delta_{il} \end{aligned}$$

$$\begin{aligned} \frac{d}{dt} C_{ijkl}^c \Big|_{\text{pump}} &= +P_i(t) (C_{jili}^x \delta_{ik} - C_{jiki}^x \delta_{il}) \\ &\quad + P_j(t) (C_{ijkj}^x \delta_{jl} - C_{ijlj}^x \delta_{jk}) + P_i(t) f_j^c (C_{iiii}^x - f_i^v f_i^c) (\delta_{ik} \delta_{jl} - \delta_{il} \delta_{jk}) \\ &\quad + P_j(t) f_i^c (C_{jjjj}^x - f_j^v f_j^c) (\delta_{ik} \delta_{jl} - \delta_{il} \delta_{jk}) \end{aligned}$$

$$\begin{aligned} \frac{d}{dt} \Pi_{\xi,ijkl}^c \Big|_{\text{pump}} &= -\frac{1}{2} P_j(t) \Pi_{\xi,ijkl}^c + \frac{1}{2} P_i(t) (\Pi_{\xi,iikl}^c \delta_{ij} + 2\Pi_{\xi,ijk i}^v \delta_{il} - 2\Pi_{\xi,ijli}^v \delta_{ik}) \\ &\quad + P_i(t) \Pi_{\xi,j} (C_{iiii}^x - f_i^v f_i^c) (\delta_{ik} \delta_{jl} - \delta_{il} \delta_{jk}) \end{aligned}$$

$$\begin{aligned} \frac{d}{dt} \Pi_{\xi,ijkl}^v \Big|_{\text{pump}} &= -\frac{1}{2} (P_i(t) + P_j(t) + P_l(t)) \Pi_{\xi,ijkl}^v \\ &\quad + \frac{1}{2} P_k(t) \Pi_{\xi,ijkk}^v \delta_{kl} + P_l(t) \Pi_{\xi,k} (f_l^v f_l^c - C_{lll}^x) (\delta_{ik} \delta_{jl} - \delta_{il} \delta_{jk}) \end{aligned}$$



# Appendix B

## Equations of motion for the microscopic bimodal laser model

In this appendix we provide supplementary material to the second section of chapter 5. We present the equations of motion that together with Eqs. (5.11), (5.12), (5.14), (5.15) and (5.16) complete the full set of equations of motion for one-time correlation functions on the quadruplet level of the cluster expansion:

$$\begin{aligned} \frac{d}{dt} \delta \langle c_j^\dagger v_j b_\xi \rangle &= i(\Delta_{\xi j} + i\kappa_\xi + i\Gamma) \delta \langle c_j^\dagger v_j b_\xi \rangle + g_{\xi j} \delta \langle c_j^\dagger c_j \rangle (1 - \delta \langle v_j^\dagger v_j \rangle) \\ &+ \sum_{\zeta} \left[ g_{\zeta j} \delta \langle b_\zeta^\dagger b_\xi \rangle (\delta \langle c_j^\dagger c_j \rangle - \delta \langle v_j^\dagger v_j \rangle) + g_{\zeta j} \delta \langle c_j^\dagger c_j b_\zeta^\dagger b_\xi \rangle - g_{\zeta j} \delta \langle v_j^\dagger v_j b_\zeta^\dagger b_\xi \rangle \right] \end{aligned} \quad (\text{B.1})$$

$$\begin{aligned} \frac{d}{dt} \delta \langle v_s^\dagger v_s \rangle &= \left( \sum_{\xi} g_{\xi j} \delta \langle c_s^\dagger v_s b_\xi \rangle + \text{H.c.} \right) \\ &- \delta \langle v_p^\dagger, v_p \rangle (1 - \delta \langle v_s^\dagger, v_s \rangle) \tau_v^{-1} + \delta \langle c_s^\dagger c_s \rangle (1 - \delta \langle v_s^\dagger v_s \rangle) \tau_{nl}^{-1} \end{aligned} \quad (\text{B.2})$$

$$\begin{aligned} \frac{d}{dt} \delta \langle v_p^\dagger v_p \rangle &= -P(\delta \langle v_p^\dagger v_p \rangle - \delta \langle c_p^\dagger c_p \rangle) + \delta \langle v_p^\dagger, v_p \rangle (1 - \delta \langle v_s^\dagger, v_s \rangle) \tau_v^{-1} + \delta \langle c_p^\dagger c_p \rangle (1 - \delta \langle v_p^\dagger v_p \rangle) \tau_{sp}^{-1} \end{aligned} \quad (\text{B.3})$$

$$\begin{aligned} \frac{d}{dt} \delta \langle c_j^\dagger c_j b_\xi^\dagger b_\zeta \rangle &= -(\kappa_\xi + \kappa_\zeta) \delta \langle c_j^\dagger c_j b_\xi^\dagger b_\zeta \rangle - g_{\xi j} \delta \langle c_j^\dagger c_j \rangle \delta \langle c_j^\dagger v_j b_\zeta \rangle - g_{\zeta j} \delta \langle c_j^\dagger c_j \rangle \delta \langle v_j^\dagger c_j b_\xi^\dagger \rangle \\ &- \sum_{\xi'} g_{\xi' j} \left( \delta \langle c_j^\dagger v_j b_\xi^\dagger b_{\xi'} b_\zeta \rangle - \delta \langle c_j^\dagger v_j b_\zeta \rangle \delta \langle b_\xi^\dagger b_{\xi'} \rangle - \delta \langle v_j^\dagger c_j b_{\xi'}^\dagger b_\xi^\dagger b_\zeta \rangle - \delta \langle v_j^\dagger c_j b_\xi^\dagger \rangle \delta \langle b_{\xi'}^\dagger b_\zeta \rangle \right) \end{aligned} \quad (\text{B.4})$$

$$\begin{aligned} \frac{d}{dt} \delta \langle v_j^\dagger v_j b_\xi^\dagger b_\zeta \rangle &= -(\kappa_\xi + \kappa_\zeta) \delta \langle v_j^\dagger v_j b_\xi^\dagger b_\zeta \rangle \\ &+ \sum_{\xi'} \left[ g_{\xi' j} \delta \langle c_j^\dagger v_j b_\xi^\dagger b_{\xi'} b_\zeta \rangle + g_{\xi' j} \delta \langle c_j^\dagger v_j b_\zeta \rangle (1 - \delta \langle v_j^\dagger v_j \rangle + \delta \langle b_\xi^\dagger b_{\xi'} \rangle) \right. \\ &\quad \left. + g_{\xi' j} \delta \langle v_j^\dagger c_j b_{\xi'}^\dagger b_\xi^\dagger b_\zeta \rangle + g_{\xi' j} \delta \langle v_j^\dagger c_j b_\xi^\dagger \rangle (1 - \delta \langle v_j^\dagger v_j \rangle + \delta \langle b_{\xi'}^\dagger b_\zeta \rangle) \right] \end{aligned} \quad (\text{B.5})$$

---


$$\begin{aligned}
\frac{d}{dt}\langle c_j^\dagger v_j b_\xi^\dagger b_\zeta b_{\xi'} \rangle &= i[\Delta_{\xi'j} + \Delta_{\zeta j} - \Delta_{\xi j} + i(\kappa_\xi + \kappa_\zeta + \kappa_{\xi'}) + i\Gamma]\langle c_j^\dagger v_j b_\xi^\dagger b_\zeta b_{\xi'} \rangle \\
&\quad - g_{\xi'j}\langle c_j^\dagger c_j \rangle (\delta\langle v_j^\dagger v_j b_\xi^\dagger b_\zeta \rangle - \delta\langle v_j^\dagger v_j b_\xi^\dagger b_{\xi'} \rangle + \delta\langle b_{\zeta'}^\dagger b_\xi^\dagger b_\zeta b_{\xi'} \rangle) \\
+ \sum_{\zeta'} &\left[ g_{\zeta'j}\langle c_j^\dagger c_j b_\xi^\dagger b_\zeta \rangle (1 - \delta\langle v_j^\dagger v_j \rangle + \delta\langle b_{\zeta'}^\dagger b_{\xi'} \rangle) + g_{\zeta'j}\langle c_j^\dagger c_j b_\xi^\dagger b_{\xi'} \rangle (1 - \delta\langle v_j^\dagger v_j \rangle - \delta\langle b_{\zeta'}^\dagger b_\zeta \rangle) \right. \\
&\quad - 2g_{\zeta'j}\langle c_j^\dagger v_j b_\zeta \rangle \delta\langle c_j^\dagger v_j b_{\xi'} \rangle - g_{\zeta'j}\langle v_j^\dagger v_j \rangle \delta\langle b_{\zeta'}^\dagger b_\xi^\dagger b_\zeta b_{\xi'} \rangle \\
&\quad \left. - g_{\zeta'j}\langle v_j^\dagger v_j b_\xi^\dagger b_\zeta \rangle \delta\langle b_{\zeta'}^\dagger b_{\xi'} \rangle - g_{\zeta'j}\langle v_j^\dagger v_j b_\xi^\dagger b_{\xi'} \rangle \delta\langle b_{\zeta'}^\dagger b_\zeta \rangle \right] \quad (\text{B.6})
\end{aligned}$$

$$\begin{aligned}
\frac{d}{dt}\langle v_j^\dagger c_j b_\xi^\dagger b_\zeta b_{\xi'} \rangle &= i[-\Delta_{\xi j} - \Delta_{\zeta j} + \Delta_{\xi'j} + i(\kappa_\xi + \kappa_\zeta + \kappa_{\xi'}) + i\Gamma]\langle v_j^\dagger c_j b_\xi^\dagger b_\zeta b_{\xi'} \rangle \\
&\quad - g_j\langle c_j^\dagger c_j \rangle (\delta\langle v_j^\dagger v_j b_\xi^\dagger b_{\xi'} \rangle - \delta\langle v_j^\dagger v_j b_\xi^\dagger b_\zeta \rangle + \delta\langle b_\xi^\dagger b_\zeta b_n b_{\xi'} \rangle) \\
+ \sum_{\zeta'} &\left[ g_{\zeta'j}\langle c_j^\dagger c_j b_\xi^\dagger b_{\xi'} \rangle (1 - \delta\langle v_j^\dagger v_j \rangle + \delta\langle b_\zeta^\dagger b_{\zeta'} \rangle) + g_{\zeta'j}\langle c_j^\dagger c_j b_\xi^\dagger b_{\xi'} \rangle (1 - \delta\langle v_j^\dagger v_j \rangle + \delta\langle b_\xi^\dagger b_{\zeta'} \rangle) \right. \\
&\quad - 2g_{\zeta'j}\langle v_j^\dagger c_j b_\xi^\dagger \rangle \delta\langle v_j^\dagger c_j b_\zeta^\dagger \rangle - g_{\zeta'j}\langle v_j^\dagger v_j \rangle \delta\langle b_\xi^\dagger b_\zeta^\dagger b_{\zeta'} b_{\xi'} \rangle \\
&\quad \left. - g_{\zeta'j}\langle v_j^\dagger v_j b_\xi^\dagger b_{\xi'} \rangle \delta\langle b_\zeta^\dagger b_{\zeta'} \rangle - g_{\zeta'j}\langle v_j^\dagger v_j b_\xi^\dagger b_{\xi'} \rangle \delta\langle b_\xi^\dagger b_{\zeta'} \rangle \right] \quad (\text{B.7})
\end{aligned}$$

# Appendix C

## Details of the laser theory formulated in configuration operators

In this appendix we provide supplementary material to chapter 6.

### C.1 Configuration Operators

The confinement of electrons and holes in a QD in all three spatial dimensions leads to states with discrete energies. Because of the finite height of the confinement potential, a QD can provide only a limited number of electronic single-particle states. Distributing carriers in these states results in electronic configurations as shown in Fig. C.1. The corresponding many-particle Hilbert space vectors  $|i\rangle$  define the basis states of our QD model. For simplicity we restrict ourselves to charge neutral states within one spin system, which couples to one circular polarization of the light field. A generalization to charged multi-exciton states or to QDs with a different level structure is possible without changing the fundamental aspects of this formulation. The electronic state of all carriers confined in multiple QDs is described by the tensor product of all single QD states:

$$|\psi\rangle = |i\rangle^1 |j\rangle^2 \cdots |k\rangle^\alpha \cdots |l\rangle^N, \quad (\text{C.1})$$

where  $|k\rangle^\alpha$  denotes QD  $\alpha$  to be in configuration  $k$ . We assume that the QDs are spatially well separated. Therefore the carriers confined in different QDs can be treated as distinguishable particles and we do not have to antisymmetrize the vector  $|\psi\rangle$ . In fact, the position of the configuration state  $|k\rangle^\alpha$  in the tensor product is irrelevant since the index  $\alpha$  always denotes a specific QD

$$|i\rangle^1 \cdots |j\rangle^\alpha |k\rangle^\beta \cdots |l\rangle^N = |i\rangle^1 \cdots |k\rangle^\beta |j\rangle^\alpha \cdots |l\rangle^N. \quad (\text{C.2})$$

We define the QD configuration operators

$$Q_{ij}^\alpha = |i\rangle^\alpha \langle j|^\alpha \quad (\text{C.3})$$

mapping the configuration  $j$  of QD  $\alpha$  to the configuration  $i$  of the same QD. The algebraic properties of the configuration operators follow from the fact that all configuration states of the same QD are orthonormal,  $\langle i^\alpha | j^\alpha \rangle = \delta_{ij}$ , and can be summarized

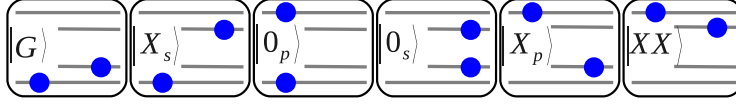


Figure C.1: Illustration of the electronic configuration states  $|i\rangle$  of a QD with two confined states for electrons and holes that accommodates two electrons ( $i = \{G, X_s, 0_p, 0_s, X_p, XX\}$ ). The different configurations are the ground state  $|G\rangle$ , the s-exciton  $|X_s\rangle$ , the dark states with the electrons in the p-shell  $|0_p\rangle$  and in the s-shell  $|0_s\rangle$  respectively, the p-exciton  $|X_p\rangle$  and the bi-exciton  $|XX\rangle$ .

by the commutation relation

$$[Q_{ij}^\alpha, Q_{kl}^\beta] = (Q_{il}^\alpha \delta_{j,k} - Q_{kj}^\alpha \delta_{l,i}) \delta_{\alpha,\beta}. \quad (\text{C.4})$$

To illustrate our approach and to connect it to former theories we give a few examples on how one can construct single-particle operators in second quantization with the configuration operators  $Q_{ij}^\alpha$  for the model QD illustrated in Fig. C.1. In the following  $c_s^{(\dagger)\alpha}$  annihilates (creates) a conduction-band carrier in the single-particle s-state of QD  $\alpha$  and  $v_p^{(\dagger)\beta}$  annihilates (creates) a valence-band carrier in the single-particle p-state of QD  $\beta$ . Contributions from all configurations containing an (un)occupied single-particle state must be summed up to represent the corresponding single-particle operator. For example, the number operator of p-shell conduction-band electrons in QD  $\alpha$  is given by  $c_p^{\dagger\alpha} c_p^\alpha = Q_{0_p 0_p}^\alpha + Q_{X_p X_p}^\alpha + Q_{XX XX}^\alpha$ . The annihilation of an s-shell electron-hole pair in QD  $\beta$  can be constructed by  $v_s^{\dagger\beta} c_s^\beta = E_s^\beta = Q_{GX_s}^\beta + Q_{X_p XX}^\beta$ . The total number of electrons in the valence band in QD  $\gamma$  is given by  $\sum_i v_i^{\dagger\gamma} v_i^\gamma = 2Q_{GG}^\gamma + Q_{X_s X_s}^\gamma + Q_{0_p 0_p}^\gamma + Q_{0_s 0_s}^\gamma + Q_{X_p X_p}^\gamma$ .

## C.2 Equation-of-motion hierarchy

In this section we illustrate how the dipole Hamiltonian creates two hierarchies in the equations of motion (EoM)  $\langle \dot{A} \rangle = i\langle [H, A] \rangle / \hbar$  for the photon- and QD-operator EVs. In the second half of this section we explain the technique we use to truncate this hierarchy. In terms of the configuration operators, the dipole Hamiltonian has the form

$$H_D = -i \sum_{\gamma}^N \tilde{g}_{\gamma} b^{\dagger} (Q_{G, X_s}^{\gamma} + Q_{X_p, XX}^{\gamma}) + \text{H.c.}, \quad (\text{C.5})$$

where  $b^{(\dagger)}$  is the photon annihilation (creation) operator of the laser mode,  $N$  is the number of QDs, and  $\tilde{g}_{\alpha} = \hbar g_{\alpha}$  is the scaled light-matter interaction strength. The dipole Hamiltonian couples the photon operators of a single mode to  $N$  different QD-operators. To illustrate the structure of the hierarchies created by the dipole Hamiltonian, we first consider the time derivative of the occupation probability of the s-exciton configuration in QD  $\alpha$

$$\left. \frac{d}{dt} \right|_{H_D} \langle Q_{X_s X_s}^{\alpha} \rangle = -2g_{\alpha} \text{Re} \langle b^{\dagger} Q_{GX_s}^{\alpha} \rangle, \quad (\text{C.6})$$

that couples to the photon-assisted polarization of the ground-state- to s-exciton-transition. This polarization is an EV with one additional photon operator. The EoM for the photon-assisted polarization

$$\begin{aligned} \left. \frac{d}{dt} \right|_{H_D} \langle b^\dagger Q_{GX_s}^\alpha \rangle &= g_\alpha \langle Q_{X_s X_s}^\alpha \rangle + \sum_{\gamma \neq \alpha} g_\gamma \langle Q_{GX_s}^\alpha (Q_{X_s G}^\gamma + Q_{XX, X_p}^\gamma) \rangle \\ &\quad + g_\alpha \langle b^\dagger b (Q_{X_s X_s}^\alpha - Q_{GG}^\alpha) \rangle \end{aligned}$$

couples to EVs describing correlations between different QDs (second term) and to EVs describing correlations between the electronic configurations of the given QD and the cavity photons (third term). The two higher-order terms that occur here have one additional QD operator and one additional photon operator, giving rise to the mentioned hierarchies.

For the rest of this section, to make the considerations more transparent, we omit all configuration indices and prefactors and also the information whether the considered photon operators create or annihilate photons. The following equations should be seen as illustrations of the hierarchy structure, that can be explored best by considering the time derivative of a general EV  $\langle b^{(\dagger)n} Q^\alpha \dots Q^\omega \rangle$  containing a product of  $n$  photon operators and  $m$  QD operators addressing the QDs  $\alpha$  to  $\omega$ :

$$\begin{aligned} \left. \frac{d}{dt} \right|_{H_D} \langle b^{(\dagger)n} Q^\alpha \dots Q^\omega \rangle &= \langle [H_D, b^{(\dagger)n}] Q^\alpha \dots Q^\omega \rangle \\ &+ \langle b^{(\dagger)n} [H_D, Q^\alpha] \dots Q^\omega \rangle + \dots + \langle b^{(\dagger)n} Q^\alpha \dots [H_D, Q^\omega] \rangle. \end{aligned}$$

We can evaluate this expression with  $[H_D, b^{(\dagger)n}] = b^{(\dagger)n-1} \sum_\gamma Q^\gamma$  and  $[H_D, Q^\alpha] = b^{(\dagger)} Q^\alpha$ . By omitting all details and possible lower-order terms we obtain

$$\begin{aligned} \left. \frac{d}{dt} \right|_{H_D} \langle b^{(\dagger)n} Q^\alpha \dots Q^\omega \rangle &= \sum_{\gamma \neq \{\alpha, \dots, \omega\}} \langle b^{(\dagger)n-1} Q^\alpha \dots Q^\omega Q^\gamma \rangle \\ &+ \langle b^{(\dagger)n+1} Q^\alpha \dots Q^\omega \rangle. \end{aligned}$$

In the first term on the right-hand side we can clearly see the emergence of QD-QD correlations that are induced by the interaction of different QDs with a common radiation field. These terms are not included in laser theories that do not account for interemitter coupling effects. The second term describes the coupling to higher-order photon correlations. It provides access to the next rung in the Jaynes-Cummings ladder. We see that the dipole Hamiltonian creates two different hierarchies. An EV with  $n$  photon operators and  $m$  QDs operator couples to EVs with one additional QD operator and one additional photon operator:

$$\left. \frac{d}{dt} \right|_{H_D} \langle b^{(\dagger)n} \underbrace{Q \dots Q}_m \rangle = \langle b^{(\dagger)n-1} \underbrace{Q \dots Q}_{m+1} \rangle + \langle b^{(\dagger)n+1} \underbrace{Q \dots Q}_m \rangle.$$

The first hierarchy only terminates exactly *i*) at the order  $m = N$ , where  $N$  is the number of QDs. Including the EV  $\langle b^n \underbrace{Q \dots Q}_N \rangle$  i.e. all QD  $N$  operators of the system

( $\Delta_{\langle N \rangle}^{\mathcal{Q}}$  in terms of the truncation operator from chapter 4). The second hierarchy only terminates exactly if *ii*) the photonic state of the system can be represented by a finite linear combination of Fock states. We need approximations to truncate the hierarchies consistently and at a computable level. Being interested in systems where up to several hundred QDs take part in the dynamics, it is impossible to match condition *i*) numerically. Condition *ii*) cannot be fulfilled because we are studying laser systems, whose coherent states cannot be represented by a small number of Fock states.

We introduce a variant of the well-established cluster expansion (see chapter 4) [Kira and Koch, 2008, Kira et al., 1999, Kira and Koch, 2011, Feldtmann et al., 2006, Gies et al., 2007, Richter et al., 2009, Leymann et al., 2014] which we refer to as the configuration cluster expansion (CCE). The main differences of our formulation to the traditional cluster expansion [Kira et al., 1998] are that *a*) we formulate our theory in EVs instead of correlation functions (see chapter 4) and, more importantly, *b*) the electronic state of the QDs is described by the configuration operators  $Q_{ij}^{\alpha}$  instead of single-particle creation (annihilation) operators. The configuration operators are considered as the elementary constituents of our theory and therefore the factorization of EVs is done in terms of the configuration operators. This method reduces the algebraic effort to a minimum and ensures that all many-particle states of the confined QD carriers are treated without further approximation.

In our system the two-particle nature of the dipole Hamiltonian is the source of higher-order correlations and the hierarchies in the EoM have to be truncated according to the structure of the dipole Hamiltonian (see chapter 4). As we have shown, the dipole Hamiltonian couples a single-mode photon operator to all QD operators and hereby creates two hierarchies, one in the photonic and one in the electronic part of the part of the Hilbert space. To truncate the hierarchies all EVs containing a total number of operators ( $b^{(\dagger)}$  and  $Q$ ) larger than the desired order are factorized ( $\Delta_{\tilde{\alpha}_4}^{\mathcal{Q}+\mathcal{B}}$ ). The factorization of the EV is accomplished by neglecting the corresponding correlation function according to the cluster expansion (see chapter 4). The intensity  $I = \langle b^\dagger b \rangle$  is of second order. The photon autocorrelation function at zero delay time  $G^{(2)}(0) = \langle b^\dagger b^\dagger b b \rangle$  and the correlated two-photon emission function  $\langle b^\dagger b^\dagger E^\alpha E^\beta \rangle$  are both of fourth order. The fourth order of the CCE used in this chapter provides information about the photon statistics ( $g^{(2)}(0) = G^{(2)}(0)/I^2$ ) [Leymann et al., 2014, Gies et al., 2007, Wiersig et al., 2009]. Additionally we introduce a truncation that addresses the QD-QD correlations. We use two variants of the theory: one with and one without interemitter correlations. To systematically neglect QD-QD correlations we factorize all EVs addressing two different QDs according to

$$\langle Q_{ij}^{\alpha} Q_{kl}^{\beta} \rangle \approx \langle Q_{ij}^{\alpha} \rangle \langle Q_{kl}^{\beta} \rangle, \quad (\text{C.7})$$

which corresponds to a mean-field approximation<sup>1</sup> and the assumption of individual emitters ( $\Delta_{\tilde{\alpha}_1}^{\mathcal{Q}}$ ). To take radiation-induced QD-QD correlations into account we

---

<sup>1</sup>Since we are using configuration operators that automatically treat all carriers confined to a QD exactly this mean-field means that the confined carriers in a QD are in the mean-field of all other carriers in the other QDs



have to include EVs of the form  $\langle Q_{ij}^\alpha Q_{kl}^\beta \rangle$ . At this level, three-QD EVs are factorized according to

$$\begin{aligned} \langle Q_{ij}^\alpha Q_{kl}^\beta Q_{mn}^\gamma \rangle &\approx \langle Q_{ij}^\alpha Q_{kl}^\beta \rangle \langle Q_{mn}^\gamma \rangle + \langle Q_{ij}^\alpha \rangle \langle Q_{kl}^\beta Q_{mn}^\gamma \rangle \\ &+ \langle Q_{kl}^\beta \rangle \langle Q_{ij}^\alpha Q_{mn}^\gamma \rangle - 2 \langle Q_{ij}^\alpha \rangle \langle Q_{kl}^\beta \rangle \langle Q_{mn}^\gamma \rangle, \end{aligned} \quad (\text{C.8})$$

which corresponds to the application of  $\Delta_{\delta(2)}^Q$  and is formally equivalent to the Bogoliubov back-reaction method mentioned in chapter 4. In this way our theory enables us to directly switch the QD-QD correlation effects on and off and to compare our approach to laser theories, in which QD-QD correlations are not contained, e.g. Refs. [Gies et al., 2007, Wiersig et al., 2009, Rice and Carmichael, 1994].

### C.3 Coupling to the continuum states

In this section we discuss the influence of the continuum states that arise from the interaction of QD carriers with carriers in the wetting-layer and barrier states, as well as the out-coupling of photons from the cavity. These environment states are not represented by configuration and photon operators but by the Lindblad form

$$\left. \frac{d}{dt} \right|_{\text{Lindblad}} \langle A \rangle = \sum_i \gamma_{\eta_i} \langle [\eta_i^\dagger, A] \eta_i + \eta_i^\dagger [A, \eta_i] \rangle$$

in the general EoM. First, we enlist the various microscopic processes generated by the operators  $\eta_i$  that are triggered by the coupling of the confined-state carriers to the continuum states. Then we give explicit examples for the resulting terms in the EoM, showing that the process  $\eta_i$  transfers occupation probability from one configuration to another while dephasing the corresponding polarization.

The microscopic processes in QD  $\alpha$  are the following: electron-hole capture in the QD p-shell with rate  $P^\alpha$  (pump) generated by  $\eta_{P,1}^\alpha = Q_{X_p G}^\alpha$  and  $\eta_{P,2}^\alpha = Q_{X_s X_s}^\alpha$ , carrier relaxation from the p-shell to the s-shell in the conduction band generated by  $\eta_{r,c,1}^\alpha = Q_{X_s 0_p}^\alpha$  and  $\eta_{r,c,2}^\alpha = Q_{0_s X_p}^\alpha$ , carrier relaxation from the s-shell to the p-shell in the valence band generated by  $\eta_{r,v,1}^\alpha = Q_{X_s 0_s}^\alpha$  and  $\eta_{r,v,2}^\alpha = Q_{0_p X_p}^\alpha$  with the rates  $\gamma_{r,\{c,v\}}^\alpha$  respectively, spontaneous losses of electron hole pairs in the p-shell generated by  $\eta_{\text{spont},1}^{\alpha,p} = Q_{G X_p}^\alpha$  and  $\eta_{\text{spont},2}^{\alpha,p} = Q_{X_s X_s}^\alpha$ , and in the s-shell generated by  $\eta_{\text{spont},1}^{\alpha,s} = Q_{G X_s}^\alpha$  and  $\eta_{\text{spont},2}^{\alpha,s} = Q_{X_p X_s}^\alpha$  with the rates  $\gamma_{\text{spont}}^{\alpha,\{s,p\}}$  and the cavity-photon losses  $\eta_{\text{ph}} = b$  with the loss rate  $\kappa$ .

As a first example we discuss the impact of spontaneous electron-hole recombination in the s-shell on the s-exciton configuration

$$\left. \frac{d}{dt} \right|_{\eta_{\text{spont},s}^\alpha} \langle Q_{X_s X_s}^\alpha \rangle = -2\gamma_{\text{spont}}^{\alpha,s} \langle Q_{X_s X_s}^\alpha \rangle, \quad (\text{C.9})$$

the ground-state configuration

$$\left. \frac{d}{dt} \right|_{\eta_{\text{spont},s}^\alpha} \langle Q_{GG}^\alpha \rangle = +2\gamma_{\text{spont}}^{\alpha,s} \langle Q_{X_s X_s}^\alpha \rangle, \quad (\text{C.10})$$

and the photon-assisted polarization between the ground- and s-exciton state

$$\left. \frac{d}{dt} \right|_{\eta_{\text{spont},s}^{\alpha}} \langle b^{\dagger} Q_{GX_s}^{\alpha} \rangle = -\gamma_{\text{spont}}^{\alpha,s} \langle b^{\dagger} Q_{GX_s}^{\alpha} \rangle. \quad (\text{C.11})$$

The process generates a direct transfer of population from the s-exciton to the ground state and dephases the polarization between these states. Note that no additional terms are needed to take account for Pauli-blocking. As a second example, we discuss the impact of carrier relaxation in QD  $\alpha$  from the s-shell to the p-shell in the valence band on the correlation between the p-exciton configuration of QD  $\alpha$  and the ground-state configuration of QD  $\beta$

$$\left. \frac{d}{dt} \right|_{\eta_{r,v}^{\alpha}} \langle Q_{X_p X_p}^{\alpha} Q_{GG}^{\beta} \rangle = -2\gamma_{r,v}^{\alpha} \langle Q_{X_p X_p}^{\alpha} Q_{GG}^{\beta} \rangle, \quad (\text{C.12})$$

the correlation between the dark p-shell configuration of QD  $\alpha$  and the ground-state configuration of QD  $\beta$

$$\left. \frac{d}{dt} \right|_{\eta_{r,v}^{\alpha}} \langle Q_{0_p 0_p}^{\alpha} Q_{GG}^{\beta} \rangle = +2\gamma_{r,v}^{\alpha} \langle Q_{X_p X_p}^{\alpha} Q_{GG}^{\beta} \rangle, \quad (\text{C.13})$$

and on the correlation between the photon-assisted polarization of the p-exciton configuration and biexciton configuration in QD  $\alpha$  and the ground-state configuration of QD  $\beta$

$$\left. \frac{d}{dt} \right|_{\eta_{r,v}^{\alpha}} \langle b^{\dagger} Q_{X_p X X}^{\alpha} Q_{GG}^{\beta} \rangle = -\gamma_{r,v}^{\alpha} \langle b^{\dagger} Q_{X_p X X}^{\alpha} Q_{GG}^{\beta} \rangle. \quad (\text{C.14})$$

As in the example before, the microscopic process generates a direct transfer of population from one configuration to the other and dephases a polarization connected to the initial state. In this example, all occupations and processes in QD  $\alpha$  are correlated with an occupation in QD  $\beta$ . However, since the microscopic process  $\eta_{r,v}^{\alpha}$  takes place in QD  $\alpha$  it has no influence on a possible correlation with QD  $\beta$ .

## C.4 Total emission rate into the laser mode

The total emission rate into the laser mode,  $\Gamma_{\text{em}}$ , can be obtained from the EoM for the mean photon number

$$\begin{aligned} \frac{d}{dt} \langle b^{\dagger} b \rangle &= -2\kappa \langle b^{\dagger} b \rangle + 2 \sum_{\alpha} g_{\alpha} \text{Re}(\langle b^{\dagger} Q_{GX_s}^{\alpha} \rangle + \langle b^{\dagger} Q_{X_p X X}^{\alpha} \rangle) \\ &= -2\kappa \langle b^{\dagger} b \rangle + \Gamma_{\text{em}}. \end{aligned} \quad (\text{C.15})$$

To simplify the discussion in the main text, an approximate expression of  $\Gamma_{\text{em}}$  has been used there. This facilitates a comparison to laser theories that consider only one bright configuration, i.e. [Rice and Carmichael, 1994]. In the following, we derive the exact expression that is used to compute the curves in Fig. 6.3. To this end

we solve the EoM for the photon-assisted polarization adiabatically and insert the solution into Eq. (C.15). The adiabatic solution for the photon-assisted polarization of the s-exciton and biexciton can be written as

$$\begin{aligned} \langle b^\dagger Q_{GX_s}^\alpha \rangle &= g\tau_{\text{Deph}}^X \sum_{\beta \neq \alpha} \langle Q_{GX_s}^\alpha (Q_{X_s G}^\beta + Q_{XX,X_p}^\beta) \rangle \\ &\quad + g\tau_{\text{Deph}}^X \left( \langle b^\dagger b (Q_{X_s X_s}^\alpha - Q_{GG}^\alpha) \rangle + \langle Q_{X_s X_s}^\alpha \rangle \right), \end{aligned} \quad (\text{C.16})$$

$$\begin{aligned} \langle b^\dagger Q_{X_p, XX}^\alpha \rangle &= g\tau_{\text{Deph}}^{XX} \sum_{\beta \neq \alpha} \langle Q_{X_p, XX}^\alpha (Q_{X_s G}^\beta + Q_{XX, X_p}^\beta) \rangle \\ &\quad + g\tau_{\text{Deph}}^{XX} \left( \langle b^\dagger b (Q_{XX, XX}^\alpha - Q_{X_p X_p}^\alpha) \rangle + \langle Q_{XX, XX}^\alpha \rangle \right) \end{aligned} \quad (\text{C.17})$$

respectively, with the exciton and biexciton dephasing times

$$\tau_{\text{Deph}}^X = \frac{1}{\kappa + \gamma_{\text{spont}} + 2P},$$

and

$$\tau_{\text{Deph}}^{XX} = \frac{1}{\kappa + 2\gamma_r + 3\gamma_{\text{spont}}}.$$

For the sake of simplicity of our discussion, we choose the light-matter interaction  $g_\alpha = g$ , and relaxation and spontaneous loss rates  $\gamma_{\text{spont}}^{\alpha, \{s, p\}} = \gamma_{\text{spont}}$ ,  $\gamma_{r, \{s, p\}}^\alpha = \gamma_r$  to be equal for all QDs. Comparison to Eq. (C.15) leads to an expression of the total emission rate in terms of the right-hand side of Eqs. (C.16) and (C.17)

$$\begin{aligned} \Gamma_{\text{em}} &= 2g^2\tau_{\text{Deph}}^X \sum_{\beta \neq \alpha} \langle Q_{GX_s}^\alpha (Q_{X_s G}^\beta + Q_{XX, X_p}^\beta) \rangle \\ &\quad + 2g^2\tau_{\text{Deph}}^X \sum_{\alpha} \langle b^\dagger b (Q_{X_s X_s}^\alpha - Q_{GG}^\alpha) \rangle + 2g^2\tau_{\text{Deph}}^X \sum_{\alpha} \langle Q_{X_s X_s}^\alpha \rangle \\ &\quad + 2g^2\tau_{\text{Deph}}^{XX} \sum_{\beta \neq \alpha} \langle Q_{X_p, XX}^\alpha (Q_{X_s G}^\beta + Q_{XX, X_p}^\beta) \rangle \\ &\quad + 2g^2\tau_{\text{Deph}}^{XX} \sum_{\alpha} \langle b^\dagger b (Q_{XX, XX}^\alpha - Q_{X_p X_p}^\alpha) \rangle + 2g^2\tau_{\text{Deph}}^{XX} \sum_{\alpha} \langle Q_{XX, XX}^\alpha \rangle. \end{aligned} \quad (\text{C.18})$$

To connect our results to theories that consider only one bright configuration, the assumption of equal dephasing of the bright configurations allows the definition of a common dephasing rate

$$\tau_{\text{Deph}}^{-1} \approx 2g^2\tau_{\text{Deph}}^X \approx 2g^2\tau_{\text{Deph}}^{XX}.$$

Rewriting Eq. (C.18) in terms of the dipole operator  $D^\alpha = E_s^\dagger \alpha + E_s^\alpha$  we obtain the simple form of Eq. (6.7) for the total emission rate used in the main text:

$$\begin{aligned} \Gamma_{\text{em}} &= \frac{\sum_{\alpha} \langle D^\alpha D^\alpha \rangle}{\tau_{\text{Deph}}} + \frac{\sum_{\beta \neq \alpha} \langle D^\alpha D^\beta \rangle}{\tau_{\text{Deph}}} + \frac{\langle b^\dagger b \text{Inv} \rangle}{\tau_{\text{Deph}}} \\ &= \Gamma_{\text{spont}} + \Gamma_{\text{sr}} + \Gamma_{\text{stim}} \end{aligned}$$

with the total inversion operator defined as

$$\text{Inv} = \sum_{\alpha} (Q_{XX, XX}^\alpha - Q_{X_p X_p}^\alpha + Q_{X_s X_s}^\alpha - Q_{GG}^\alpha).$$

Note that in all numerical calculations, the correct dephasing rates are used.



# Appendix D

## The computer algebra system **FORM**

In this appendix we will show how we use the language FORM [Vermaseren, 2000] to derive the equations of motion (EoM). We will assume that the reader is familiar with the basic concepts of FORM. A very helpful introduction to FORM can be found at <http://www.nikhef.nl/~form/>. The advantage of FORM is that, the user has full control of what the system does, in contrast to other commonly used computer algebra systems like Wolfram Mathematica or Maple. The calculations performed by FORM are actually a combination of self defined sophisticated search and replace operations. We will describe the core procedures that are required to perform the cluster expansion (CE). These procedures are basically the implementation of the Ehrenfest EoM, and the application of the factorization and truncation operators ( $\mathbf{F}$ ,  $\mathbf{F}^{-1}$ ,  $\Delta_{\langle N \rangle, \delta \langle N \rangle}$ ) introduced in chapter 4.

### D.1 Establishing standard order

In the generalized Ehrenfest EoM, the commutator in the Hamiltonian part and in the Lindblad terms, produces strings of operators deviating from a yet to define standard order. To obtain a simple form of the EoM we need to establish a predefined standard order of the operators. The most convenient order for our purposes is the order of operators that is closest to the normal order for operators in second quantization. We define the standard order that we want to establish in all strings of operators in three steps: (i) Separate Bose- and Fermi-operators (Bose left, Fermi right), and within each group (ii) separate creation and annihilation operators (creation operators left annihilation operators right, which is the normal order in second quantization), and within these groups (iii) alphanumeric order according to the letters of the operators and their indices. This (unique) standard form ensures that no terms appear in the EoM that would actually cancel each other out. The normal ordering of creation and annihilation operators also facilitates the implementation of the truncation operator  $\Delta_{\langle N \rangle}$ , that is applied to systems with a limited number of particles.

**(i) Separate Bose and Fermi operators:** To establish the previously defined standard order FORM searches for products of two operators that deviate from this order and replaces them according to their commutation relation. The `id`

command is the central search and replace command in FORM. Its structure is `id search=replace`, where `search` stands for a mathematical expression, that is to be replaced by the expression `replace`. The lines of code within the `repeat / endrepeat` loop are executed until the output of the operation does not differ from the input. The following lines of code separate the Fermi from the Bose operators

```
repeat;
    id [Q] (?j) * [b+] ?bose (?i) = [b+] (?i) * [Q] (?j);
endrepeat;
```

To define the mathematical expressions in a general way FORM uses different types of wild-cards. The first type of wild-cards encounters in the term `[Q] (?j)` where `?j` is the argument-field wild-card for any argument (of arbitrary number) entering the function `[Q]`.

To address (c)functions FORM has also the function wild-card `?.` This wild-card is used in the following manner: `typeoffunction?set`, where `typeoffunction` specifies the type of the function for which FORM has to search for and `set` can be used to further specify the function that are to be replaced by previously defined sets. In this particular case FORM searches for all operators from the set `bose=[b],[b+]`. Altogether the code above means: replace all products of functions `[Q]` times functions `[b+]` from the set `bose`, regardless of their argument, by the very same Bose function `[b+]` times the `[Q]` function with their arguments respectively. In other words, the commutation relation  $[Q, b^{(i)}] = 0$ , between photon and configuration operators is applied until (i) is fulfilled.

**(ii) Normal order:** In the configuration operators there are no creation and annihilation operators, therefore we only have to do this step for the Bose operators. The following lines of code will establish normal order of the Bose operators:

```
repeat;
    id [b] * [b+] = [b+] * [b] + 1;
    id [b] * [N] (a?) = a * [N] (a-1) * [b] + [N] (a) * [b];
    id [N] (a?) * [b+] = a * [b+] * [N] (a-1) + [b+] * [N] (a);
    id [b+] * [N] (a?) * [b] = [N] (a+1);
endrepeat;
```

In the above `[N] (a) = b†a ba`, all the performed substitutions are performed according to the standard bosonic commutation relations.

**(iii) Alphanumeric order:** For this example, the Fermi part of the Hilbert space is described with the configuration operators introduced in chapter 6 and appendix C. To obtain alphanumeric order in the configuration operators we use a combination of `id` commands:

```
repeat;
    id disorder [Q] (k?, i?, j?) * [Q] (t?, l?, m?) = ([Q] (k, i, m) * d(j, l) - [Q] (k, l, j) * d(i, m)) * d(k, t) + [Q] (t, l, m) * [Q] (k, i, j);
    id [Q] (k?, i?, j?) * [Q] (k?, l?, m?) = [Q] (k, i, m) * d(j, l);
endrepeat;
```

The first line in the above is the implementation of the commutation relation between the configuration operators Eq. (C.4) with the aim to establish numerical order with

respect to the indices. The `disorder` option of the `id` command tells FORM to substitute a matching expression only when this results in an increased numerical order of otherwise equivalent expressions. For example `id` would replace  $F_{21} * F_{12}$  by  $F_{12} * F_{21}$  and then by  $F_{21} * F_{12}$  and so on while `id disorder` would replace  $F_{21} * F_{12}$  by  $F_{12} * F_{21}$  and then stop. In the second line the contracting property of the configuration operator is reflected. This line ensures that no products of configuration operators addressing the same QD are present in the EoM [Leymann et al., 2015].

The `d(i,j)` function is the Kronecker delta, which can be implemented by the two lines

```
id d(i?,i?)=1;
id d(i?,j?)=0;
```

that can be placed at the end of every routine using the Kronecker delta.

## D.2 Factorization

In this section we show an implementation of the factorization of expectation values in correlation functions and vice versa. For details on the mathematical formulas and theorems belonging to this concepts we refer to [Fricke, 1996b, Leymann et al., 2014] and chapter 4. The procedure described in this section is a direct implementation of the equation

$$\langle b^I \rangle = \delta(b^I) + \sum_{I' \subsetneq I} \langle b^{I'} \rangle \delta(b^{I'}), \quad (\text{D.1})$$

which can be derived from Eq. (4.1). Equation (D.1) distributes operators into correlation functions and expectation values and when applied successively all expectation values are substituted by correlation functions. The procedure we are presenting here uses the build in combinatorial function `distrib_(type,n,f1,f2,x1,...,xm)`, which divides products of operators `[b+](?b)` into arguments of functions `AV,DD`. The following lines of code are the implementation of the factorization operator **F**:

```
id av(?a)=L*AV(?a)*R;

#do i=1,31
    id AV([b+](?b),?a)=AV(first*[b+](?b),?a);
    id AV(first*[b+](?b),?a)=distrib_(0,2,AV,DD,first*[b+](?b),?a)
        ;
    id AV=1;
    id DD=1;
    id AV(?a,first*[b+](?c),?b)=0;
    argument;
        id first=1;
    endargument;
    .sort
#enddo

id L=1;
id R=1;
id DD(?a)=dd(?a);
```

### D.3. THE TRUNCATION OPERATOR

---

The lines in the `#do`-loop above are repeated until complete factorization is reached. To prevent FORM from crashing the maximum number iterations is limited. Note that the variable `first` is a dummy that marks the position of the summation in Eq. (D.1) where the expectation values and correlation functions are distributed. The variables `L/R` are dummy variables as well, that stand for  $\langle$  and  $\rangle$  in the expectation values and are an efficient way to implement linear functions in FORM. Using Eq. (D.1) the 'refactorization', i.e. the application of  $\mathbf{F}^{-1}$ , can be implemented in a fashion analog to the one of  $\mathbf{F}$ :

```
id dd(?a)=L*DD(?a)*R;

#do i=1,31
  id DD([b+]?(?b),?a)=DD(first*[b+] (?b),?a);
  id DD(first*[b+]?(?b),?a)=-distrib_(0,2,AV,DD,first*[b+] (?b),?a
    )+AV([b+] (?b),?a)+DD([b+] (?b),?a);
  id AV=1;
  id DD=1;
  id AV(?a,first*[b+]?(?c),?b)=0;
  argument;
    id first=1;
  endargument;
  .sort
#enddo

id L=1;
id R=1;
id AV(?a)=av(?a);.
```

## D.3 The truncation Operator

In this section we show how the application of the truncation operators is implemented. To evaluate the order of a correlation function the `count` command is used, which counts the number of specified operators in a product and returns the a number that corresponds to the order of the correlation function (`count(typeofoperator _1,value_1,...) =  $\sum_i \#(\text{typeofoperator}_i) * \text{value}_i$` ). The following lines of code show the implementation of a product of the truncation operators  $\Delta_{\delta', \text{QDC}'}^{\mathcal{Q}}$  (first line) and  $\Delta_{\delta' \text{PhC}'}^{\mathcal{B}+\mathcal{Q}}$  (second line):

```
argument dd;
  if (count([Q],1)>'QDC') discard;
  if (count([b+],1,[b],1,[Q],1)>'PhC') discard;
endargument;
id dd(0)=0;
```

The `argument dd / endargument`-loop is equivalent to the `repeat`-loop, only for this loop all commands are only applied to expressions that are arguments of the function `dd`. When the logical expression behind the `if` command is true the operators in the correlation function `dd` are discarded i.e. replaced by zero. Correlation functions with the argument zero are replaced by the number zero.



# Bibliography

- [Abdussalam and Machnikowski, 2014] Abdussalam, W. and Machnikowski, P. (2014). Superradiance and enhanced luminescence from ensembles of a few self-assembled quantum dots. *Phys. Rev. B*, 90(12):125307.
- [Albert et al., 2011] Albert, F., Hopfmann, C., Reitzenstein, S., Schneider, C., Höfling, S., Worschech, L., Kamp, M., Kinzel, W., Forchel, A., and Kanter, I. (2011). Observing chaos for quantum-dot microlasers with external feedback. *Nat Commun*, 2:366.
- [Albert et al., 2013] Albert, F., Sivalertporn, K., Kasprzak, J., Strauß, M., Schneider, C., Höfling, S., Kamp, M., Forchel, A., Reitzenstein, S., Muljarov, E. A., and Langbein, W. (2013). Microcavity controlled coupling of excitonic qubits. *Nat Commun*, 4:1747.
- [Alferov, 2001] Alferov, Z. I. (2001). Nobel Lecture: The double heterostructure concept and its applications in physics, electronics, and technology. *Rev. Mod. Phys.*, 73(3):767–782.
- [Anders et al., 2002] Anders, S., Kim, C. S., Klein, B., Keller, M. W., Mirin, R. P., and Norman, A. G. (2002). Bimodal size distribution of self-assembled ingaas quantum dots. *Phys. Rev. B*, 66(12):125309.
- [Andreani et al., 1999] Andreani, L. C., Panzarini, G., and Gérard, J.-M. (1999). Strong-coupling regime for quantum boxes in pillar microcavities: Theory. *Phys. Rev. B*, 60(19):13276–13279.
- [Arakawa and Sakaki, 1982] Arakawa, Y. and Sakaki, H. (1982). Multidimensional quantum well laser and temperature dependence of its threshold current. *Applied Physics Letters*, 40(11):939–941.
- [Asada et al., 1986] Asada, M., Miyamoto, Y., and Suematsu, Y. (1986). Gain and the threshold of three-dimensional quantum-box lasers. *IEEE Journal of Quantum Electronics*, 22(9):1915–1921.
- [Ashcroft and Mermin, 1976] Ashcroft, N. W. and Mermin, N. D. (1976). *Solid State Physics*. Holt, Rinehart and Winston.
- [Aßmann et al., 2010] Aßmann, M., Veit, F., Bayer, M., Gies, C., Jahnke, F., Reitzenstein, S., Höfling, S., Worschech, L., and Forchel, A. (2010). Ultrafast tracking of second-order photon correlations in the emission of quantum-dot microresonator lasers. *Phys. Rev. B*, 81(16):165314.

- [Aßmann et al., 2009] Aßmann, M., Veit, F., Bayer, M., Poel, M. v. d., and Hvam, J. M. (2009). Higher-Order Photon Bunching in a Semiconductor Microcavity. *Science*, 325(5938):297–300.
- [Ates et al., 2008] Ates, S., Gies, C., Ulrich, S. M., Wiersig, J., Reitzenstein, S., Löffler, A., Forchel, A., Jahnke, F., and Michler, P. (2008). Influence of the spontaneous optical emission factor beta on the first-order coherence of a semiconductor microcavity laser. *Phys. Rev. B*, 78(15):155319.
- [Ates et al., 2007] Ates, S., Ulrich, S. M., Michler, P., Reitzenstein, S., Löffler, A., and Forchel, A. (2007). Coherence properties of high-beta elliptical semiconductor micropillar lasers. *Applied Physics Letters*, 90(16):161111.
- [Auffèves et al., 2011] Auffèves, A., Gerace, D., Portolan, S., Drezet, A., and Santos, M. F. (2011). Few emitters in a cavity: from cooperative emission to individualization. *New J. Phys.*, 13(9):093020.
- [Avenhaus et al., 2010] Avenhaus, M., Laiho, K., Chekhova, M. V., and Silberhorn, C. (2010). Accessing Higher Order Correlations in Quantum Optical States by Time Multiplexing. *Phys. Rev. Lett.*, 104(6):063602.
- [Baer et al., 2004] Baer, N., Gartner, P., and Jahnke, F. (2004). Coulomb effects in semiconductor quantum dots. *Eur. Phys. J. B*, 42(2):231–237.
- [Baer et al., 2006] Baer, N., Gies, C., Wiersig, J., and Jahnke, F. (2006). Luminescence of a semiconductor quantum dot system. *Eur. Phys. J. B*, 50(3):411–418.
- [Bányai et al., 1998] Bányai, L., Haug, H., and Gartner, P. (1998). Self-consistent RPA retarded polaron Green function for quantum kinetics. *The European Physical Journal B*, 1(2):209–213.
- [Baudouin et al., 2013] Baudouin, Q., Mercadier, N., Guarrera, V., Guerin, W., and Kaiser, R. (2013). A cold-atom random laser. *Nat Phys*, 9(6):357–360.
- [Baumann et al., 2010] Baumann, K., Guerlin, C., Brennecke, F., and Esslinger, T. (2010). Dicke quantum phase transition with a superfluid gas in an optical cavity. *Nature*, 464(7293):1301–1306.
- [Baumann and Hegerfeldt, 1985] Baumann, K. and Hegerfeldt, G. C. (1985). A noncommutative Marcinkiewicz theorem. *Publications of the Research Institute for Mathematical Sciences*, 21(1):191–204.
- [Bayer et al., 2001] Bayer, M., Reinecke, T. L., Weidner, F., Larionov, A., McDonald, A., and Forchel, A. (2001). Inhibition and Enhancement of the Spontaneous Emission of Quantum Dots in Structured Microresonators. *Phys. Rev. Lett.*, 86(14):3168–3171.
- [Beirne et al., 2007] Beirne, G. J., Reischle, M., Roßbach, R., Schulz, W.-M., Jetter, M., Seebeck, J., Gartner, P., Gies, C., Jahnke, F., and Michler, P. (2007). Electronic shell structure and carrier dynamics of high aspect ratio InP single quantum dots. *Phys. Rev. B*, 75(19):195302.

- [Berstermann et al., 2007] Berstermann, T., Auer, T., Kurtze, H., Schwab, M., Yakovlev, D. R., Bayer, M., Wiersig, J., Gies, C., Jahnke, F., Reuter, D., and Wieck, A. D. (2007). Systematic study of carrier correlations in the electron-hole recombination dynamics of quantum dots. *Phys. Rev. B*, 76(16):165318.
- [Bienaimé et al., 2013] Bienaimé, T., Bachelard, R., Piovella, N., and Kaiser, R. (2013). Cooperativity in light scattering by cold atoms. *Fortschr. Phys.*, 61(2-3):377–392.
- [Bimberg et al., 1999] Bimberg, D., Grundmann, M., and Ledentsov, N. N. (1999). *Quantum Dot Heterostructures*. Wiley.
- [Bimberg et al., 2009] Bimberg, D., Stock, E., Lochmann, A., Schliwa, A., Tofflinger, J., Unrau, W., Munnix, M., Rodt, S., Haisler, V., Toropov, A., Bakarov, A., and Kalagin, A. (2009). Quantum Dots for Single- and Entangled-Photon Emitters. *IEEE Photonics Journal*, 1(1):58–68.
- [Binder et al., 1992] Binder, R., Scott, D., Paul, A. E., Lindberg, M., Henneberger, K., and Koch, S. W. (1992). Carrier-carrier scattering and optical dephasing in highly excited semiconductors. *Phys. Rev. B*, 45(3):1107–1115.
- [Björk et al., 1994] Björk, G., Karlsson, A., and Yamamoto, Y. (1994). Definition of a laser threshold. *Phys. Rev. A*, 50(2):1675–1680.
- [Bockelmann and Egeler, 1992] Bockelmann, U. and Egeler, T. (1992). Electron relaxation in quantum dots by means of Auger processes. *Phys. Rev. B*, 46(23):15574–15577.
- [Bohnet et al., 2012] Bohnet, J. G., Chen, Z., Weiner, J. M., Meiser, D., Holland, M. J., and Thompson, J. K. (2012). A steady-state superradiant laser with less than one intracavity photon. *Nature*, 484(7392):78–81.
- [Borri et al., 2001] Borri, P., Langbein, W., Schneider, S., Woggon, U., Sellin, R. L., Ouyang, D., and Bimberg, D. (2001). Ultralong Dephasing Time in InGaAs Quantum Dots. *Phys. Rev. Lett.*, 87(15):157401.
- [Braskén et al., 1998] Braskén, M., Lindberg, M., Sopanen, M., Lipsanen, H., and Tulkki, J. (1998). Temperature dependence of carrier relaxation in strain-induced quantum dots. *Phys. Rev. B*, 58(24):R15993–R15996.
- [Breuer and Petruccione, 2002] Breuer, H.-P. and Petruccione, F. (2002). *The Theory of Open Quantum Systems*. Oxford University Press.
- [Brown and Twiss, 1957] Brown, R. H. and Twiss, R. Q. (1957). Interferometry of the intensity fluctuations in light. i. basic theory: The correlation between photons in coherent beams of radiation. *Proceedings of the Royal Society of London A: Mathematical, Physical and Engineering Sciences*, 242(1230):300–324.
- [Brown and Twiss, 1958] Brown, R. H. and Twiss, R. Q. (1958). Interferometry of the intensity fluctuations in light ii. an experimental test of the theory for partially

- coherent light. *Proceedings of the Royal Society of London A: Mathematical, Physical and Engineering Sciences*, 243(1234):291–319.
- [Brune et al., 1996] Brune, M., Schmidt-Kaler, F., Maali, A., Dreyer, J., Hagley, E., Raimond, J. M., and Haroche, S. (1996). Quantum Rabi Oscillation: A Direct Test of Field Quantization in a Cavity. *Phys. Rev. Lett.*, 76(11):1800–1803.
- [Callsen et al., 2013] Callsen, G., Carmele, A., Hönig, G., Kindel, C., Brunmeier, J., Wagner, M. R., Stock, E., Reparaz, J. S., Schliwa, A., Reitzenstein, S., Knorr, A., Hoffmann, A., Kako, S., and Arakawa, Y. (2013). Steering photon statistics in single quantum dots: From one- to two-photon emission. *Phys. Rev. B*, 87(24):245314.
- [Cao and Wiersig, 2015] Cao, H. and Wiersig, J. (2015). Dielectric microcavities: Model systems for wave chaos and non-Hermitian physics. *Rev. Mod. Phys.*, 87(1):61–111.
- [Carmele et al., 2013] Carmele, A., Kabuss, J., Schulze, F., Reitzenstein, S., and Knorr, A. (2013). Single Photon Delayed Feedback: A Way to Stabilize Intrinsic Quantum Cavity Electrodynamics. *Phys. Rev. Lett.*, 110(1):013601.
- [Carmele et al., 2009] Carmele, A., Knorr, A., and Richter, M. (2009). Photon statistics as a probe for exciton correlations in coupled nanostructures. *Phys. Rev. B*, 79(3):035316.
- [Carmele et al., 2010a] Carmele, A., Milde, F., Dachner, M.-R., Harouni, M. B., Rognizadeh, R., Richter, M., and Knorr, A. (2010a). Formation dynamics of an entangled photon pair: A temperature-dependent analysis. *Phys. Rev. B*, 81(19):195319.
- [Carmele et al., 2010b] Carmele, A., Richter, M., Chow, W. W., and Knorr, A. (2010b). Antibunching of Thermal Radiation by a Room-Temperature Phonon Bath: A Numerically Solvable Model for a Strongly Interacting Light-Matter-Reservoir System. *Phys. Rev. Lett.*, 104(15):156801.
- [Carmichael, 1999] Carmichael, P. H. J. (1999). Dissipation in Quantum Mechanics: The Master Equation Approach. In *Statistical Methods in Quantum Optics 1*, Texts and Monographs in Physics, pages 1–28. Springer Berlin Heidelberg.
- [Chelikowsky and Cohen, 1976] Chelikowsky, J. R. and Cohen, M. L. (1976). Non-local pseudopotential calculations for the electronic structure of eleven diamond and zinc-blende semiconductors. *Phys. Rev. B*, 14(2):556–582.
- [Chen et al., 2012] Chen, G.-Y., Lambert, N., Li, C.-M., Chen, Y.-N., and Nori, F. (2012). Delocalized single-photon Dicke states and the Leggett-Garg inequality in solid state systems. *Sci. Rep.*, 2.
- [Chow et al., 2011] Chow, W., Lorke, M., and Jahnke, F. (2011). Will Quantum Dots Replace Quantum Wells As the Active Medium of Choice in Future Semiconductor Lasers? *IEEE Journal of Selected Topics in Quantum Electronics*, 17(5):1349–1355.

- [Chow and Jahnke, 2013] Chow, W. W. and Jahnke, F. (2013). On the physics of semiconductor quantum dots for applications in lasers and quantum optics. *Progress in Quantum Electronics*, 37(3):109–184.
- [Chow et al., 2014] Chow, W. W., Jahnke, F., and Gies, C. (2014). Emission properties of nanolasers during the transition to lasing. *Light Sci Appl*, 3(8):e201.
- [Chow and Koch, 1999] Chow, W. W. and Koch, S. W. (1999). *Semiconductor-Laser Fundamentals: Physics of the Gain Materials*. Springer Science Business Media.
- [Czycholl, 2008] Czycholl, G. (2008). *Theoretische Festkörperphysik*. Springer-Lehrbuch. Springer Berlin Heidelberg.
- [Dayan et al., 2008] Dayan, B., Parkins, A. S., Aoki, T., Ostby, E. P., Vahala, K. J., and Kimble, H. J. (2008). A Photon Turnstile Dynamically Regulated by One Atom. *Science*, 319(5866):1062–1065.
- [del Valle et al., 2009] del Valle, E., Laussy, F. P., and Tejedor, C. (2009). Luminescence spectra of quantum dots in microcavities. II. Fermions. *Phys. Rev. B*, 79(23):235326.
- [Dicke, 1954] Dicke, R. H. (1954). Coherence in Spontaneous Radiation Processes. *Phys. Rev.*, 93(1):99–110.
- [Dobrindt et al., 2008] Dobrindt, J. M., Wilson-Rae, I., and Kippenberg, T. J. (2008). Parametric Normal-Mode Splitting in Cavity Optomechanics. *Phys. Rev. Lett.*, 101(26):263602.
- [Dynes et al., 2011] Dynes, J. F., Yuan, Z. L., Sharpe, A. W., Thomas, O., and Shields, A. J. (2011). Probing higher order correlations of the photon field with photon number resolving avalanche photodiodes. *Opt. Express*, 19(14):13268–13276.
- [Elvira et al., 2011] Elvira, D., Hachair, X., Verma, V. B., Braive, R., Beaudoin, G., Robert-Philip, I., Sagnes, I., Baek, B., Nam, S. W., Dauler, E. A., Abram, I., Stevens, M. J., and Beveratos, A. (2011). Higher-order photon correlations in pulsed photonic crystal nanolasers. *Phys. Rev. A*, 84(6):061802.
- [Eremeev et al., 2011] Eremeev, V., Skipetrov, S. E., and Orszag, M. (2011). Quantum theory of a two-mode open-cavity laser. *Phys. Rev. A*, 84(2):023816.
- [Fafard et al., 1999] Fafard, S., Wasilewski, Z. R., Allen, C. N., Picard, D., Spanner, M., McCaffrey, J. P., and Piva, P. G. (1999). Manipulating the energy levels of semiconductor quantum dots. *Phys. Rev. B*, 59(23):15368–15373.
- [Feldtman et al., 2006] Feldtman, T., Schneebeli, L., Kira, M., and Koch, S. W. (2006). Quantum theory of light emission from a semiconductor quantum dot. *Phys. Rev. B*, 73(15):155319.

- [Ferrari et al., 2014] Ferrari, D., Celardo, G., Berman, G., Sayre, R., and Borgonovi, F. (2014). Quantum Biological Switch Based on Superradiance Transitions. *J. Phys. Chem. C*, 118(1):20–26.
- [Fick and Sauermann, 1990] Fick, E. and Sauermann, G. (1990). In *The Quantum Statistics of Dynamic Processes*, Springer Series in Solid-State Sciences. Springer Berlin Heidelberg.
- [Florian, 2014] Florian, M. (2014). *Licht Materie Wechselwirkung in Halbleiter Nanostrukturen zur Erzeugung nichtklassischen Lichts und stimulierter Emission*. PhD Thesis, Bremen.
- [Florian et al., 2013a] Florian, M., Gartner, P., Gies, C., and Jahnke, F. (2013a). Phonon-mediated off-resonant coupling effects in semiconductor quantum-dot lasers. *New J. Phys.*, 15(3):035019.
- [Florian et al., 2013b] Florian, M., Gies, C., Jahnke, F., Leymann, H. A. M., and Wiersig, J. (2013b). Equation-of-motion technique for finite-size quantum-dot systems: Cluster expansion method. *Phys. Rev. B*, 87(16):165306.
- [Foerster, 2012] Foerster, A. (2012). *Berechnung von Korrelationsfunktionen in Halbleiter Quantenpunktsystemen*. Diploma Thesis, Magdeburg.
- [Fricke, 1996a] Fricke, J. (1996a). Transport Equations Including Many-Particle Correlations for an Arbitrary Quantum System: A General Formalism. *Annals of Physics*, 252(2):479–498.
- [Fricke, 1996b] Fricke, J. (1996b). *Transportgleichungen für quantenmechanische Vielteilchensysteme*. Cuvillier.
- [Fricke et al., 1997] Fricke, J., Meden, V., Wöhler, C., and Schönhammer, K. (1997). Improved Transport Equations Including Correlations for Electron-Phonon Systems: Comparison with Exact Solutions in One Dimension. *Annals of Physics*, 253(1):177–197.
- [Gardiner and Zoller, 2001] Gardiner, G. W. and Zoller, P. (2001). *Quantum Noise*. Springer Verlag, third edition.
- [Garraway, 2011] Garraway, B. M. (2011). The Dicke model in quantum optics: Dicke model revisited. *Phil. Trans. R. Soc. A*, 369(1939):1137–1155.
- [Garrison and Chiao, 2014] Garrison, J. and Chiao, R. (2014). *Quantum Optics*. Oxford University Press.
- [Gartner, 2011] Gartner, P. (2011). Two-level laser: Analytical results and the laser transition. *Phys. Rev. A*, 84(5):053804.
- [Gérard et al., 1998] Gérard, J. M., Sermage, B., Gayral, B., Legrand, B., Costard, E., and Thierry-Mieg, V. (1998). Enhanced Spontaneous Emission by Quantum Boxes in a Monolithic Optical Microcavity. *Phys. Rev. Lett.*, 81(5):1110–1113.

- [Gies, 2008] Gies, C. (2008). *Theory for Light-Matter Interaction in Semiconductor Quantum Dots*. PhD Thesis, Bremen.
- [Gies et al., 2011] Gies, C., Florian, M., Gartner, P., and Jahnke, F. (2011). The single quantum dot-laser: lasing and strong coupling in the high-excitation regime. *Opt. Express*, 19(15):14370–14388.
- [Gies et al., 2012] Gies, C., Florian, M., Jahnke, F., and Gartner, P. (2012). Modeling single quantum dots in microcavities. In *Quantum Optics with Semiconductor Nanostructures*, pages 78 – 114. Woodhead Publishing.
- [Gies et al., 2008] Gies, C., Wiersig, J., and Jahnke, F. (2008). Output Characteristics of Pulsed and Continuous-Wave-Excited Quantum-Dot Microcavity Lasers. *Phys. Rev. Lett.*, 101(6):067401.
- [Gies et al., 2007] Gies, C., Wiersig, J., Lorke, M., and Jahnke, F. (2007). Semiconductor model for quantum-dot-based microcavity lasers. *Phys. Rev. A*, 75(1):013803.
- [Glauber, 1963] Glauber, R. J. (1963). The Quantum Theory of Optical Coherence. *Phys. Rev.*, 130(6):2529–2539.
- [Gourley, 1998] Gourley, P. L. (1998). Nanolaser - Spektrum der Wissenschaft.
- [Hanbury Brown and Twiss, 1956] Hanbury Brown, R. and Twiss, R. Q. (1956). A Test of a New Type of Stellar Interferometer on Sirius. *Nature*, 178(4541):1046–1048.
- [Haroche and Kleppner, 2008] Haroche, S. and Kleppner, D. (2008). Cavity Quantum Electrodynamics. *Physics Today*, 42(1):24–30.
- [Haug and Koch, 2004] Haug, H. and Koch, S. (2004). *Quantum Theory of the Optical and Electronic Properties of Semiconductors*. World Scientific Publishing Company.
- [He et al., 2013] He, L., Özdemir, Ş. K., and Yang, L. (2013). Whispering gallery microcavity lasers. *Laser & Photonics Reviews*, 7(1):60–82.
- [Hein et al., 2014] Hein, S. M., Schulze, F., Carmele, A., and Knorr, A. (2014). Optical Feedback-Enhanced Photon Entanglement from a Biexciton Cascade. *Phys. Rev. Lett.*, 113(2):027401.
- [Hendrickson et al., 2005] Hendrickson, J., Richards, B. C., Sweet, J., Mosor, S., Christenson, C., Lam, D., Khitrova, G., Gibbs, H. M., Yoshie, T., Scherer, A., Shchekin, O. B., and Deppe, D. G. (2005). Quantum dot photonic-crystal-slab nanocavities: Quality factors and lasing. *Phys. Rev. B*, 72(19):193303.
- [Hillman et al., 1984] Hillman, L. W., Krasiński, J., Boyd, R. W., and Stroud, C. R. (1984). Observation of Higher Order Dynamical States of a Homogeneously Broadened Laser. *Phys. Rev. Lett.*, 52(18):1605–1608.

- [Hodgman et al., 2011] Hodgman, S. S., Dall, R. G., Manning, A. G., Baldwin, K. G. H., and Truscott, A. G. (2011). Direct Measurement of Long-Range Third-Order Coherence in Bose-Einstein Condensates. *Science*, 331(6020):1046–1049.
- [Hohenester, 2010] Hohenester, U. (2010). Cavity quantum electrodynamics with semiconductor quantum dots: Role of phonon-assisted cavity feeding. *Phys. Rev. B*, 81(15):155303.
- [Hohenester and Pötz, 1997] Hohenester, U. and Pötz, W. (1997). Density-matrix approach to nonequilibrium free-carrier screening in semiconductors. *Phys. Rev. B*, 56(20):13177–13189.
- [Hohenester et al., 1999] Hohenester, U., Rossi, F., and Molinari, E. (1999). Few-particle effects in the optical spectra of semiconductor quantum dots. *Solid State Communications*, 111(4):187–192.
- [Hoyer et al., 2003] Hoyer, W., Kira, M., and Koch, S. W. (2003). Influence of Coulomb and phonon interaction on the exciton formation dynamics in semiconductor heterostructures. *Phys. Rev. B*, 67(15):155113.
- [Hoyer et al., 2004] Hoyer, W., Kira, M., and Koch, S. W. (2004). Cluster Expansion in Semiconductor Quantum Optics. In Morawetz, D. K., editor, *Nonequilibrium Physics at Short Time Scales*, pages 309–335. Springer Berlin Heidelberg.
- [Hughes et al., 2011] Hughes, S., Yao, P., Milde, F., Knorr, A., Dalacu, D., Mnaymneh, K., Sazonova, V., Poole, P. J., Aers, G. C., Lapointe, J., Cheriton, R., and Williams, R. L. (2011). Influence of electron-acoustic phonon scattering on off-resonant cavity feeding within a strongly coupled quantum-dot cavity system. *Phys. Rev. B*, 83(16):165313.
- [Inoshita and Sakaki, 1997] Inoshita, T. and Sakaki, H. (1997). Density of states and phonon-induced relaxation of electrons in semiconductor quantum dots. *Phys. Rev. B*, 56(8):R4355–R4358.
- [Jacobi, 2003] Jacobi, K. (2003). Atomic structure of InAs quantum dots on GaAs. *Progress in Surface Science*, 71(5-8):185–215.
- [Jahnke, 2012] Jahnke, F. (2012). *Quantum Optics with Semiconductor Nanostructures*. Elsevier.
- [Jaynes and Cummings, 1963] Jaynes, E. and Cummings, F. W. (1963). Comparison of quantum and semiclassical radiation theories with application to the beam maser. *Proceedings of the IEEE*, 51(1):89–109.
- [Jechow et al., 2013] Jechow, A., Seefeldt, M., Kurzke, H., Heuer, A., and Menzel, R. (2013). Enhanced two-photon excited fluorescence from imaging agents using true thermal light. *Nat Photon*, 7(12):973–976.
- [Jiang and Singh, 1998] Jiang, H. and Singh, J. (1998). Self-assembled semiconductor structures: electronic and optoelectronic properties. *IEEE Journal of Quantum Electronics*, 34(7):1188–1196.



- [Jin et al., 1994] Jin, R., Boggavarapu, D., Sargent, M., Meystre, P., Gibbs, H. M., and Khitrova, G. (1994). Photon-number correlations near the threshold of microcavity lasers in the weak-coupling regime. *Phys. Rev. A*, 49(5):4038–4042.
- [Kabuss et al., 2012] Kabuss, J., Carmele, A., Brandes, T., and Knorr, A. (2012). Optically Driven Quantum Dots as Source of Coherent Cavity Phonons: A Proposal for a Phonon Laser Scheme. *Phys. Rev. Lett.*, 109(5):054301.
- [Kabuss et al., 2013] Kabuss, J., Carmele, A., and Knorr, A. (2013). Threshold behavior and operating regimes of an optically driven phonon laser: Semiclassical theory. *Phys. Rev. B*, 88(6):064305.
- [Kabuss et al., 2011] Kabuss, J., Carmele, A., Richter, M., Chow, W. W., and Knorr, A. (2011). Inductive equation of motion approach for a semiconductor QD-QED: Coherence induced control of photon statistics. *physica status solidi (b)*, 248(4):872–878.
- [Kapetanakis and Perakis, 2008] Kapetanakis, M. D. and Perakis, I. E. (2008). Spin Dynamics in (III,Mn)V Ferromagnetic Semiconductors: The Role of Correlations. *Phys. Rev. Lett.*, 101(9):097201.
- [Kazimierczuk et al., 2015] Kazimierczuk, T., Schmutzler, J., Aßmann, M., Schneider, C., Kamp, M., Höfling, S., and Bayer, M. (2015). Photon-Statistics Excitation Spectroscopy of a Quantum-Dot Micropillar Laser. *Phys. Rev. Lett.*, 115(2):027401.
- [Khanbekyan et al., 2015] Khanbekyan, M., Leymann, H. A. M., Hopfmann, C., Foerster, A., Schneider, C., Höfling, S., Kamp, M., Wiersig, J., and Reitzenstein, S. (2015). Unconventional collective normal-mode coupling in quantum-dot-based bimodal microlasers. *Phys. Rev. A*, 91(4):043840.
- [Khitrova, 1999] Khitrova, G. (1999). Nonlinear optics of normal-mode-coupling semiconductor microcavities. *Rev. Mod. Phys.*, 71(5):1591–1639.
- [Khurgin and Sun, 2012] Khurgin, J. B. and Sun, G. (2012). How small can "Nano" be in a "Nanolaser"? *Nanophotonics*, 1(1):3–8.
- [Kippenberg and Vahala, 2008] Kippenberg, T. J. and Vahala, K. J. (2008). Cavity Optomechanics: Back-Action at the Mesoscale. *Science*, 321(5893):1172–1176.
- [Kira et al., 1999] Kira, M., Jahnke, F., Hoyer, W., and Koch, S. (1999). Quantum theory of spontaneous emission and coherent effects in semiconductor microstructures. *Progress in Quantum Electronics*, 23(6):189–279.
- [Kira et al., 1998] Kira, M., Jahnke, F., and Koch, S. W. (1998). Microscopic Theory of Excitonic Signatures in Semiconductor Photoluminescence. *Phys. Rev. Lett.*, 81(15):3263–3266.
- [Kira and Koch, 2008] Kira, M. and Koch, S. W. (2008). Cluster-expansion representation in quantum optics. *Phys. Rev. A*, 78(2):022102.

- [Kira and Koch, 2011] Kira, M. and Koch, S. W. (2011). *Semiconductor Quantum Optics*. Cambridge University Press.
- [Kira et al., 2011] Kira, M., Koch, S. W., Smith, R. P., Hunter, A. E., and Cundiff, S. T. (2011). Quantum spectroscopy with Schrödinger-cat states. *Nat Phys*, 7(10):799–804.
- [Kleppner, 1981] Kleppner, D. (1981). Inhibited Spontaneous Emission. *Phys. Rev. Lett.*, 47(4):233–236.
- [Köhler and Burnett, 2002] Köhler, T. and Burnett, K. (2002). Microscopic quantum dynamics approach to the dilute condensed Bose gas. *Phys. Rev. A*, 65(3):033601.
- [Krügel et al., 2006] Krügel, A., Axt, V. M., and Kuhn, T. (2006). Back action of nonequilibrium phonons on the optically induced dynamics in semiconductor quantum dots. *Phys. Rev. B*, 73(3):035302.
- [Kryzhanovskaya et al., 2014] Kryzhanovskaya, N. V., Maximov, M. V., and Zhukov, A. E. (2014). Whispering-gallery mode microcavity quantum-dot lasers. *Quantum Electron.*, 44(3):189.
- [Lax, 1967] Lax, M. (1967). Quantum Noise. X. Density-Matrix Treatment of Field and Population-Difference Fluctuations. *Phys. Rev.*, 157(2):213–231.
- [Lax and Louisell, 1969] Lax, M. and Louisell, W. H. (1969). Quantum Noise. XII. Density-Operator Treatment of Field and Population Fluctuations. *Phys. Rev.*, 185(2):568–591.
- [Lermer et al., 2013] Lermer, M., Gregersen, N., Lorke, M., Schild, E., Gold, P., Mørk, J., Schneider, C., Forchel, A., Reitzenstein, S., Höfling, S., and Kamp, M. (2013). High beta lasing in micropillar cavities with adiabatic layer design. *Applied Physics Letters*, 102(5):052114–052114–4.
- [Lett et al., 1981] Lett, P., Christian, W., Singh, S., and Mandel, L. (1981). Macroscopic Quantum Fluctuations and First-Order Phase Transition in a Laser. *Phys. Rev. Lett.*, 47(26):1892–1895.
- [Leymann et al., 2015] Leymann, H., Foerster, A., Jahnke, F., Wiersig, J., and Gies, C. (2015). Sub- and Superradiance in Nanolasers. *Phys. Rev. Applied*, 4(4):044018.
- [Leymann et al., 2013a] Leymann, H. A. M., Foerster, A., Khanbekyan, M., and Wiersig, J. (2013a). Strong photon bunching in a quantum-dot-based two-mode microcavity laser. *Phys. Status Solidi B*, 250(9):1777–1780.
- [Leymann et al., 2013b] Leymann, H. A. M., Foerster, A., and Wiersig, J. (2013b). Expectation value based cluster expansion. *physica status solidi (c)*, 10(9):1242–1245.

- [Leymann et al., 2014] Leymann, H. A. M., Foerster, A., and Wiersig, J. (2014). Expectation value based equation-of-motion approach for open quantum systems: A general formalism. *Phys. Rev. B*, 89(8):085308.
- [Leymann et al., 2013c] Leymann, H. A. M., Hopfmann, C., Albert, F., Foerster, A., Khanbekyan, M., Schneider, C., Höfling, S., Forchel, A., Kamp, M., Wiersig, J., and Reitzenstein, S. (2013c). Intensity fluctuations in bimodal micropillar lasers enhanced by quantum-dot gain competition. *Phys. Rev. A*, 87(5):053819.
- [Lindblad, 1976] Lindblad, G. (1976). On the generators of quantum dynamical semigroups. *Commun.Math. Phys.*, 48(2):119–130.
- [Liu et al., 2014] Liu, C., Di Falco, A., and Fratalocchi, A. (2014). Dicke Phase Transition with Multiple Superradiant States in Quantum Chaotic Resonators. *Phys. Rev. X*, 4(2):021048.
- [Lodahl et al., 2004] Lodahl, P., Floris van Driel, A., Nikolaev, I. S., Irman, A., Overgaag, K., Vanmaekelbergh, D., and Vos, W. L. (2004). Controlling the dynamics of spontaneous emission from quantum dots by photonic crystals. *Nature*, 430(7000):654–657.
- [Lohmeyer et al., 2006] Lohmeyer, H., Sebald, K., Kruse, C., Kröger, R., Gutowski, J., Hommel, D., Wiersig, J., Baer, N., and Jahnke, F. (2006). Confined optical modes in monolithic II-VI pillar microcavities. *Applied Physics Letters*, 88(5):051101.
- [Lorke et al., 2006] Lorke, M., Nielsen, T. R., Seebeck, J., Gartner, P., and Jahnke, F. (2006). Influence of carrier-carrier and carrier-phonon correlations on optical absorption and gain in quantum-dot systems. *Phys. Rev. B*, 73(8):085324.
- [Loudon, 2000] Loudon, R. (2000). *The Quantum Theory of Light*. Oxford University Press, third edition edition.
- [Mahan, 2000] Mahan, G. D. (2000). *Many-Particle Physics*. Springer US.
- [Majumdar et al., 2012] Majumdar, A., Bajcsy, M., Rundquist, A., and Vučković, J. (2012). Loss-Enabled Sub-Poissonian Light Generation in a Bimodal Nanocavity. *Phys. Rev. Lett.*, 108(18):183601.
- [Mandel and Wolf, 1995] Mandel, L. and Wolf, E. (1995). *Optical Coherence and Quantum Optics*. Cambridge University Press.
- [Mascarenhas et al., 2013] Mascarenhas, E., Gerace, D., Santos, M. F., and Auffèves, A. (2013). Cooperativity of a few quantum emitters in a single-mode cavity. *Phys. Rev. A*, 88(6):063825.
- [Max et al., 2010] Max, C., Philips, W., Block, S., Madey, J., and Gustafson, E. (2010). Where next for the laser? *physics world.com*.

- [McKeever et al., 2003] McKeever, J., Boca, A., Boozer, A. D., Buck, J. R., and Kimble, H. J. (2003). Experimental realization of a one-atom laser in the regime of strong coupling. *Nature*, 425(6955):268–271.
- [Meiser and Holland, 2010] Meiser, D. and Holland, M. J. (2010). Steady-state superradiance with alkaline-earth-metal atoms. *Phys. Rev. A*, 81(3):033847.
- [Meiser et al., 2009] Meiser, D., Ye, J., Carlson, D. R., and Holland, M. J. (2009). Prospects for a Millihertz-Linewidth Laser. *Phys. Rev. Lett.*, 102(16):163601.
- [Meyer and Yeoman, 1997] Meyer, G. M. and Yeoman, G. (1997). Cavity-Induced Interference Pattern with Dark Center from Two Fluorescing Atoms. *Phys. Rev. Lett.*, 79(14):2650–2653.
- [Meystre and Iii, 1999] Meystre, P. and Iii, M. S. (1999). Interaction Between Atoms and Quantized Fields. In *Elements of Quantum Optics*, pages 286–306. Springer Berlin Heidelberg.
- [Michler, 2003] Michler, P. (2003). *Single Quantum Dots: Fundamentals, Applications and New Concepts*. Springer Science & Business Media.
- [Michler, 2009] Michler, P., editor (2009). *Single Semiconductor Quantum Dots*. NanoScience and Technology. Springer Berlin Heidelberg.
- [Moelbjerg et al., 2013] Moelbjerg, A., Kaer, P., Lorke, M., Tromborg, B., and Mork, J. (2013). Dynamical Properties of Nanolasers Based on Few Discrete Emitters. *IEEE Journal of Quantum Electronics*, 49(11):945–954.
- [Molmer, 1997] Molmer, K. (1997). Optical coherence: A convenient fiction. *Phys. Rev. A*, 55(4):3195–3203.
- [Monroe, 2002] Monroe, C. (2002). Quantum information processing with atoms and photons. *Nature*, 416(6877):238–246.
- [Mootz et al., 2012] Mootz, M., Kira, M., and Koch, S. W. (2012). Sequential build-up of quantum-optical correlations. *J. Opt. Soc. Am. B*, 29(2):A17–A24.
- [Mu and Savage, 1992] Mu, Y. and Savage, C. M. (1992). One-atom lasers. *Phys. Rev. A*, 46(9):5944–5954.
- [Musiał et al., 2015] Musiał, A., Hopfmann, C., Heindel, T., Gies, C., Florian, M., Leymann, H. A. M., Foerster, A., Schneider, C., Jahnke, F., Höfling, S., Kamp, M., and Reitzenstein, S. (2015). Correlations between axial and lateral emission of coupled quantum dot-micropillar cavities. *Phys. Rev. B*, 91(20):205310.
- [Nielsen et al., 2004] Nielsen, T. R., Gartner, P., and Jahnke, F. (2004). Many-body theory of carrier capture and relaxation in semiconductor quantum-dot lasers. *Phys. Rev. B*, 69(23):235314.
- [Noda, 2006] Noda, S. (2006). Seeking the Ultimate Nanolaser. *Science*, 314(5797):260–261.

- [Nomura et al., 2009] Nomura, M., Kumagai, N., Iwamoto, S., Ota, Y., and Arakawa, Y. (2009). Photonic crystal nanocavity laser with a single quantum dot gain. *Opt. Express*, 17(18):15975–15982.
- [Nomura et al., 2010] Nomura, M., Kumagai, N., Iwamoto, S., Ota, Y., and Arakawa, Y. (2010). Laser oscillation in a strongly coupled single-quantum-dot-nanocavity system. *Nat Phys*, 6(4):279–283.
- [Nußmann et al., 2005] Nußmann, S., Hijlkema, M., Weber, B., Rohde, F., Rempe, G., and Kuhn, A. (2005). Submicron Positioning of Single Atoms in a Microcavity. *Phys. Rev. Lett.*, 95(17):173602.
- [Oppel et al., 2014] Oppel, S., Wiegner, R., Agarwal, G. S., and von Zanthier, J. (2014). Directional Superradiant Emission from Statistically Independent Incoherent Nonclassical and Classical Sources. *Phys. Rev. Lett.*, 113(26):263606.
- [Ota et al., 2011] Ota, Y., Iwamoto, S., Kumagai, N., and Arakawa, Y. (2011). Spontaneous Two-Photon Emission from a Single Quantum Dot. *Phys. Rev. Lett.*, 107(23):233602.
- [Pellegrino et al., 2014] Pellegrino, J., Bourgain, R., Jennewein, S., Sortais, Y., Browaeys, A., Jenkins, S., and Ruostekoski, J. (2014). Observation of Suppression of Light Scattering Induced by Dipole-Dipole Interactions in a Cold-Atom Ensemble. *Phys. Rev. Lett.*, 113(13):133602.
- [Perkowitz, 2010] Perkowitz, S. (2010). From ray-gun to Blu-ray. *physics world.com*.
- [Peter et al., 2005] Peter, E., Senellart, P., Martrou, D., Lemaître, A., Hours, J., Gérard, J. M., and Bloch, J. (2005). Exciton-Photon Strong-Coupling Regime for a Single Quantum Dot Embedded in a Microcavity. *Phys. Rev. Lett.*, 95(6):067401.
- [Petroff et al., 2001] Petroff, P. M., Lorke, A., and Imamoglu, A. (2001). Epitaxially self-assembled quantum dots. *Physics Today*, 54(5):46–52.
- [Purcell, 1946] Purcell, E. M. (1946). Proceedings of the American Physical Society. *Phys. Rev.*, 69(11-12):681.
- [Raizen et al., 1989] Raizen, M. G., Thompson, R. J., Brecha, R. J., Kimble, H. J., and Carmichael, H. J. (1989). Normal-mode splitting and linewidth averaging for two-state atoms in an optical cavity. *Phys. Rev. Lett.*, 63(3):240–243.
- [Reithmaier et al., 2004] Reithmaier, J. P., Sęk, G., Löffler, A., Hofmann, C., Kuhn, S., Reitzenstein, S., Keldysh, L. V., Kulakovskii, V. D., Reinecke, T. L., and Forchel, A. (2004). Strong coupling in a single quantum dot-semiconductor microcavity system. *Nature*, 432(7014):197–200.
- [Reitzenstein, 2012] Reitzenstein, S. (2012). Semiconductor Quantum Dot Microcavities for Quantum Optics in Solid State. *IEEE Journal of Selected Topics in Quantum Electronics*, 18(6):1733–1746.

- [Reitzenstein et al., 2006a] Reitzenstein, S., Bazhenov, A., Gorbunov, A., Hofmann, C., Münch, S., Löffler, A., Kamp, M., Reithmaier, J. P., Kulakovskii, V. D., and Forchel, A. (2006a). Lasing in high-Q quantum-dot micropillar cavities. *Applied Physics Letters*, 89(5):051107.
- [Reitzenstein et al., 2008a] Reitzenstein, S., Böckler, C., Bazhenov, A., Gorbunov, A., Löffler, A., Kamp, M., Kulakovskii, V. D., and Forchel, A. (2008a). Single quantum dot controlled lasing effects in high-Q micropillar cavities. *Opt. Express*, 16(7):4848–4857.
- [Reitzenstein and Forchel, 2010] Reitzenstein, S. and Forchel, A. (2010). Quantum dot micropillars. *J. Phys. D: Appl. Phys.*, 43(3):033001.
- [Reitzenstein et al., 2011] Reitzenstein, S., Heindel, T., Kistner, C., Albert, F., Braun, T., Hopfmann, C., Mrowinski, P., Lermer, M., Schneider, C., Höfling, S., Kamp, M., and Forchel, A. (2011). Electrically Driven Quantum Dot Micropillar Light Sources. *IEEE Journal of Selected Topics in Quantum Electronics*, 17(6):1670–1680.
- [Reitzenstein et al., 2008b] Reitzenstein, S., Heindel, T., Kistner, C., Rahimi-Iman, A., Schneider, C., Höfling, S., and Forchel, A. (2008b). Low threshold electrically pumped quantum dot-micropillar lasers. *Applied Physics Letters*, 93(6):061104.
- [Reitzenstein et al., 2007] Reitzenstein, S., Hofmann, C., Gorbunov, A., Strauß, M., Kwon, S. H., Schneider, C., Löffler, A., Höfling, S., Kamp, M., and Forchel, A. (2007). AlAs GaAs micropillar cavities with quality factors exceeding 150.000. *Applied Physics Letters*, 90(25):251109.
- [Reitzenstein et al., 2006b] Reitzenstein, S., Löffler, A., Hofmann, C., Kubanek, A., Kamp, M., Reithmaier, J. P., Forchel, A., Kulakovskii, V. D., Keldysh, L. V., Ponomarev, I. V., and Reinecke, T. L. (2006b). Coherent photonic coupling of semiconductor quantum dots. *Opt. Lett.*, 31(11):1738–1740.
- [Rice and Carmichael, 1994] Rice, P. R. and Carmichael, H. J. (1994). Photon statistics of a cavity-QED laser: A comment on the laser-phase-transition analogy. *Phys. Rev. A*, 50(5):4318–4329.
- [Richter et al., 2009] Richter, M., Carmele, A., Sitek, A., and Knorr, A. (2009). Few-Photon Model of the Optical Emission of Semiconductor Quantum Dots. *Phys. Rev. Lett.*, 103(8):087407.
- [Richter et al., 2015] Richter, M., Gegg, M., Theuerholz, T. S., and Knorr, A. (2015). Numerically exact solution of the many emitter-cavity laser problem: Application to the fully quantized spaser emission. *Phys. Rev. B*, 91(3):035306.
- [Ritter et al., 2010] Ritter, S., Gartner, P., Gies, C., and Jahnke, F. (2010). Emission properties and photon statistics of a single quantum dot laser. *Opt. Express*, 18(10):9909–9921.

- [Rohlfing et al., 1993] Rohlfing, M., Krüger, P., and Pollmann, J. (1993). Quasiparticle band-structure calculations for C, Si, Ge, GaAs, and SiC using Gaussian-orbital basis sets. *Phys. Rev. B*, 48(24):17791–17805.
- [Roumpos and Cundiff, 2013] Roumpos, G. and Cundiff, S. T. (2013). Photon number distributions from a diode laser. *Opt. Lett.*, 38(2):139–141.
- [Roy and Hughes, 2011] Roy, C. and Hughes, S. (2011). Influence of Electron-Acoustic-Phonon Scattering on Intensity Power Broadening in a Coherently Driven Quantum-Dot-Cavity System. *Phys. Rev. X*, 1(2):021009.
- [Ruiz-Rivas et al., 2014] Ruiz-Rivas, J., del Valle, E., Gies, C., Gartner, P., and Hartmann, M. J. (2014). Spontaneous collective coherence in driven dissipative cavity arrays. *Phys. Rev. A*, 90(3):033808.
- [Rundquist et al., 2014] Rundquist, A., Bajcsy, M., Majumdar, A., Sarmiento, T., Fischer, K., Lagoudakis, K. G., Buckley, S., Piggott, A. Y., and Vučković, J. (2014). Nonclassical higher-order photon correlations with a quantum dot strongly coupled to a photonic-crystal nanocavity. *Phys. Rev. A*, 90(2):023846.
- [Samuel et al., 2009] Samuel, I. D. W., Namdas, E. B., and Turnbull, G. A. (2009). How to recognize lasing. *Nat Photon*, 3(10):546–549.
- [Scheibner et al., 2007] Scheibner, M., Schmidt, T., Worschech, L., Forchel, A., Bacher, G., Passow, T., and Hommel, D. (2007). Superradiance of quantum dots. *Nat Phys*, 3(2):106–110.
- [Schneider et al., 2004] Schneider, H. C., Chow, W. W., and Koch, S. W. (2004). Excitation-induced dephasing in semiconductor quantum dots. *Phys. Rev. B*, 70(23):235308.
- [Schoeller, 1994] Schoeller, H. (1994). A New Transport Equation for Single-Time Greens Functions in an Arbitrary Quantum System. General Formalism. *Annals of Physics*, 229(2):273–319.
- [Schuh et al., 2013] Schuh, K., Gartner, P., and Jahnke, F. (2013). Combined influence of carrier-phonon and Coulomb scattering on the quantum-dot population dynamics. *Phys. Rev. B*, 87(3):035301.
- [Schulz and Czycholl, 2005] Schulz, S. and Czycholl, G. (2005). Tight-binding model for semiconductor nanostructures. *Phys. Rev. B*, 72(16):165317.
- [Schulze et al., 2014] Schulze, F., Lingnau, B., Hein, S. M., Carmele, A., Schöll, E., Lüdge, K., and Knorr, A. (2014). Feedback-induced steady-state light bunching above the lasing threshold. *Phys. Rev. A*, 89(4):041801.
- [Schwab et al., 2006] Schwab, M., Kurtze, H., Auer, T., Berstermann, T., Bayer, M., Wiersig, J., Baer, N., Gies, C., Jahnke, F., Reithmaier, J. P., Forchel, A., Benyoucef, M., and Michler, P. (2006). Radiative emission dynamics of quantum dots in a single cavity micropillar. *Phys. Rev. B*, 74(4):045323.

- [Schwabl, 2008] Schwabl, F. (2008). *Quantenmechanik für Fortgeschrittene (QM II)*. Springer-Lehrbuch. Springer Berlin Heidelberg.
- [Scully and Lamb, 1967] Scully, M. O. and Lamb, W. E. (1967). Quantum Theory of an Optical Maser. I. General Theory. *Phys. Rev.*, 159(2):208–226.
- [Scully and Svidzinsky, 2009] Scully, M. O. and Svidzinsky, A. A. (2009). The Super of Superradiance. *Science*, 325(5947):1510–1511.
- [Sebald et al., 2009] Sebald, K., Kruse, C., and Wiersig, J. (2009). Properties and prospects of blue-green emitting II-VI-based monolithic microcavities. *phys. stat. sol. (b)*, 246(2):255–271.
- [Seebeck et al., 2005] Seebeck, J., Nielsen, T. R., Gartner, P., and Jahnke, F. (2005). Polarons in semiconductor quantum dots and their role in the quantum kinetics of carrier relaxation. *Phys. Rev. B*, 71(12):125327.
- [Sheng et al., 2005] Sheng, W., Cheng, S.-J., and Hawrylak, P. (2005). Multiband theory of multi-exciton complexes in self-assembled quantum dots. *Phys. Rev. B*, 71(3):035316.
- [Shore and Knight, 1993] Shore, B. W. and Knight, P. L. (1993). The Jaynes-Cummings Model. *Journal of Modern Optics*, 40(7):1195–1238.
- [Siegman, 1986] Siegman, A. (1986). *Lasers*. University Science Books.
- [Singh and Mandel, 1979] Singh, S. and Mandel, L. (1979). Mode competition in a homogeneously broadened ring laser. *Phys. Rev. A*, 20(6):2459–2463.
- [Singleton, 2001] Singleton, J. (2001). *Band Theory and Electronic Properties of Solids*. Oxford Master Series in Physics 2.
- [Sitek and Machnikowski, 2007] Sitek, A. and Machnikowski, P. (2007). Collective fluorescence and decoherence of a few nearly identical quantum dots. *Phys. Rev. B*, 75(3):035328.
- [Sitek and Manolescu, 2013] Sitek, A. and Manolescu, A. (2013). Dicke states in multiple quantum dots. *Phys. Rev. A*, 88(4):043807.
- [Stauber et al., 2000] Stauber, T., Zimmermann, R., and Castella, H. (2000). Electron-phonon interaction in quantum dots: A solvable model. *Phys. Rev. B*, 62(11):7336–7343.
- [Steinhoff et al., 2012] Steinhoff, A., Gartner, P., Florian, M., and Jahnke, F. (2012). Treatment of carrier scattering in quantum dots beyond the Boltzmann equation. *Phys. Rev. B*, 85(20):205144.
- [Stevens et al., 2010] Stevens, M. J., Baek, B., Dauler, E. A., Kerman, A. J., Molnar, R. J., Hamilton, S. A., Berggren, K. K., Mirin, R. P., and Nam, S. W. (2010). High-order temporal coherences of chaotic and laser light. *Opt. Express*, 18(2):1430–1437.



- [Strauf et al., 2006] Strauf, S., Hennessy, K., Rakher, M. T., Choi, Y.-S., Badolato, A., Andreani, L. C., Hu, E. L., Petroff, P. M., and Bouwmeester, D. (2006). Self-Tuned Quantum Dot Gain in Photonic Crystal Lasers. *Phys. Rev. Lett.*, 96(12):127404.
- [Strauf and Jahnke, 2011] Strauf, S. and Jahnke, F. (2011). Single quantum dot nanolaser. *Laser & Photonics Reviews*, 5(5):607–633.
- [Su et al., 2013] Su, Y., Bimberg, D., Knorr, A., and Carmele, A. (2013). Collective Light Emission Revisited: Reservoir Induced Coherence. *Phys. Rev. Lett.*, 110(11):113604.
- [Tavis and Cummings, 1968] Tavis, M. and Cummings, F. W. (1968). Exact Solution for an N-Molecule-Radiation-Field Hamiltonian. *Phys. Rev.*, 170(2):379–384.
- [Teichmann et al., 2013] Teichmann, K., Wenderoth, M., Prüser, H., Pierz, K., Schumacher, H. W., and Ulbrich, R. G. (2013). Harmonic Oscillator Wave Functions of a Self-Assembled InAs Quantum Dot Measured by Scanning Tunneling Microscopy. *Nano Lett.*, 13(8):3571–3575.
- [Temnov and Woggon, 2005] Temnov, V. V. and Woggon, U. (2005). Superradiance and Subradiance in an Inhomogeneously Broadened Ensemble of Two-Level Systems Coupled to a Low-Q Cavity. *Phys. Rev. Lett.*, 95(24):243602.
- [Temnov and Woggon, 2009] Temnov, V. V. and Woggon, U. (2009). Photon statistics in the cooperative spontaneous emission. *Opt. Express*, 17(7):5774–5782.
- [Thompson et al., 1992] Thompson, R. J., Rempe, G., and Kimble, H. J. (1992). Observation of normal-mode splitting for an atom in an optical cavity. *Phys. Rev. Lett.*, 68(8):1132–1135.
- [Thyrrestrup et al., 2010] Thyrrestrup, H., Sapienza, L., and Lodahl, P. (2010). Extraction of the beta-factor for single quantum dots coupled to a photonic crystal waveguide. *Applied Physics Letters*, 96(23):231106.
- [Timothy Noe Ii et al., 2012] Timothy Noe Ii, G., Kim, J.-H., Lee, J., Wang, Y., Wójcik, A. K., McGill, S. A., Reitze, D. H., Belyanin, A. A., and Kono, J. (2012). Giant superfluorescent bursts from a semiconductor magneto-plasma. *Nat Phys*, 8(3):219–224.
- [Trimborn et al., 2011] Trimborn, F., Witthaut, D., Hennig, H., Kordas, G., Geisel, T., and Wimberger, S. (2011). Decay of a Bose-Einstein condensate in a dissipative lattice - the mean-field approximation and beyond. *Eur. Phys. J. D*, 63(1):63–71.
- [Troiani et al., 2006] Troiani, F., Perea, J. I., and Tejedor, C. (2006). Cavity-assisted generation of entangled photon pairs by a quantum-dot cascade decay. *Phys. Rev. B*, 74(23):235310.
- [Tuchman et al., 2006] Tuchman, A. K., Long, R., Vrijsen, G., Boudet, J., Lee, J., and Kasevich, M. A. (2006). Normal-mode splitting with large collective cooperativity. *Phys. Rev. A*, 74(5):053821.

- [Ulrich et al., 2007] Ulrich, S. M., Gies, C., Ates, S., Wiersig, J., Reitzenstein, S., Hofmann, C., Löffler, A., Forchel, A., Jahnke, F., and Michler, P. (2007). Photon Statistics of Semiconductor Microcavity Lasers. *Phys. Rev. Lett.*, 98(4):043906.
- [Urayama et al., 2001] Urayama, J., Norris, T. B., Singh, J., and Bhattacharya, P. (2001). Observation of Phonon Bottleneck in Quantum Dot Electronic Relaxation. *Phys. Rev. Lett.*, 86(21):4930–4933.
- [Vahala, 2003] Vahala, K. J. (2003). Optical microcavities. *Nature*, 424(6950):839–846.
- [Vermaseren, 2000] Vermaseren, J. A. M. (2000). New features of FORM. *arXiv:math-ph/0010025*.
- [Virte et al., 2013] Virte, M., Panajotov, K., Thienpont, H., and Sciamanna, M. (2013). Deterministic polarization chaos from a laser diode. *Nat Photon*, 7(1):60–65.
- [Vorberg et al., 2013] Vorberg, D., Wustmann, W., Ketzmerick, R., and Eckardt, A. (2013). Generalized Bose-Einstein Condensation into Multiple States in Driven-Dissipative Systems. *Phys. Rev. Lett.*, 111(24):240405.
- [Vorberg et al., 2015] Vorberg, D., Wustmann, W., Schomerus, H., Ketzmerick, R., and Eckardt, A. (2015). Nonequilibrium steady states of ideal bosonic and fermionic quantum gases. *Phys. Rev. E*, 92(6):062119.
- [Vurgaftman et al., 1994] Vurgaftman, I., Lam, Y., and Singh, J. (1994). Carrier thermalization in sub-three-dimensional electronic systems: Fundamental limits on modulation bandwidth in semiconductor lasers. *Phys. Rev. B*, 50(19):14309–14326.
- [Wang et al., 2007] Wang, C. Y., Diehl, L., Gordon, A., Jirauschek, C., Kärtner, F. X., Belyanin, A., Bour, D., Corzine, S., Höfler, G., Troccoli, M., Faist, J., and Capasso, F. (2007). Coherent instabilities in a semiconductor laser with fast gain recovery. *Phys. Rev. A*, 75(3):031802.
- [Wang et al., 2005] Wang, W. H., Ghosh, S., Mendoza, F. M., Li, X., Awschalom, D. D., and Samarth, N. (2005). Static and dynamic spectroscopy of Al,Ga)AsGaAs microdisk lasers with interface fluctuation quantum dots. *Phys. Rev. B*, 71(15):155306.
- [Weisbuch et al., 1992] Weisbuch, C., Nishioka, M., Ishikawa, A., and Arakawa, Y. (1992). Observation of the coupled exciton-photon mode splitting in a semiconductor quantum microcavity. *Phys. Rev. Lett.*, 69(23):3314–3317.
- [Wheeler, 1998] Wheeler, N. (1998). Remarks concerning the status and some ramifications of ehrenfest’s theorem. <http://www.reed.edu/physics/faculty/wheeler/documents/index.html>.

- [Wickenbrock et al., 2013] Wickenbrock, A., Hemmerling, M., Robb, G. R. M., Emary, C., and Renzoni, F. (2013). Collective strong coupling in multimode cavity QED. *Phys. Rev. A*, 87(4):043817.
- [Wiersig, 2007] Wiersig, J. (2007). *Light-Matter Interaction and Quantum Chaos in Semiconductor Nanostructures and Optical Microcavities*. Habilitation Treatise, Bremen.
- [Wiersig, 2010] Wiersig, J. (2010). Microscopic theory of first-order coherence in microcavity lasers based on semiconductor quantum dots. *Phys. Rev. B*, 82(15):155320.
- [Wiersig et al., 2009] Wiersig, J., Gies, C., Jahnke, F., Aßmann, M., Berstermann, T., Bayer, M., Kistner, C., Reitzenstein, S., Schneider, C., Höfling, S., Forchel, A., Kruse, C., Kalden, J., and Hommel, D. (2009). Direct observation of correlations between individual photon emission events of a microcavity laser. *Nature*, 460(7252):245–249.
- [Wiersma, 2008] Wiersma, D. S. (2008). The physics and applications of random- $\hat{A}$  lasers. *Nat Phys*, 4(5):359–367.
- [Witthaut et al., 2011] Witthaut, D., Trimborn, F., Hennig, H., Kordas, G., Geisel, T., and Wimberger, S. (2011). Beyond mean-field dynamics in open Bose-Hubbard chains. *Phys. Rev. A*, 83(6):063608.
- [Wojs et al., 1996] Wojs, A., Hawrylak, P., Fafard, S., and Jacak, L. (1996). Electronic structure and magneto-optics of self-assembled quantum dots. *Phys. Rev. B*, 54(8):5604–5608.
- [Xie et al., 2007] Xie, Z. G., Götzinger, S., Fang, W., Cao, H., and Solomon, G. S. (2007). Influence of a Single Quantum Dot State on the Characteristics of a Microdisk Laser. *Phys. Rev. Lett.*, 98(11):117401.
- [Xu et al., 2002] Xu, S., Mikhailovsky, A. A., Hollingsworth, J. A., and Klimov, V. I. (2002). Hole intraband relaxation in strongly confined quantum dots: Revisiting the phonon bottleneck problem. *Phys. Rev. B*, 65(4):045319.
- [Yokoyama and Brorson, 1989] Yokoyama, H. and Brorson, S. D. (1989). Rate equation analysis of microcavity lasers. *Journal of Applied Physics*, 66(10):4801–4805.
- [Yoshie et al., 2004] Yoshie, T., Scherer, A., Hendrickson, J., Khitrova, G., Gibbs, H. M., Rupper, G., Ell, C., Shchekin, O. B., and Deppe, D. G. (2004). Vacuum Rabi splitting with a single quantum dot in a photonic crystal nanocavity. *Nature*, 432(7014):200–203.
- [Zhou et al., 2013] Zhou, Z., Frucci, G., Mattioli, F., Gaggero, A., Leoni, R., Jahanmirinejad, S., Hoang, T. B., and Fiore, A. (2013). Ultrasensitive N-Photon Interferometric Autocorrelator. *Phys. Rev. Lett.*, 110(13):133605.

- [Zibik et al., 2004] Zibik, E. A., Wilson, L. R., Green, R. P., Bastard, G., Ferreira, R., Phillips, P. J., Carder, D. A., Wells, J.-P. R., Cockburn, J. W., Skolnick, M. S., Steer, M. J., and Hopkinson, M. (2004). Intraband relaxation via polaron decay in InAs self-assembled quantum dots. *Phys. Rev. B*, 70(16):161305.

# Acknowledgments

I would like to thank Prof. Dr. Jan Wiersig from the bottom of my heart. He supported me during the entire process of writing this thesis. Prof. Wiersig's encouraging, yet calm, and friendly style, his genuine interest and affection for physics, are an inspiring example for me.

Many thanks to Prof. Dr. Andreas Knorr for taking the time to read and evaluate my thesis.

I am grateful for the collaborations with my colleagues M. Khanbekyan and A. Foerster. I would like to thank all the collaborators from other universities as well: M. Florian, C. Gies and F. Jahnke from the university of Bremen; C. Hopfmann, A. Musiał, T. Heindel, F. Albert, and S. Reitzenstein from the TU Berlin; C. Schneider, A. Forchel, M. Kamp, and S. Höfling from the TU Würzburg.

I am very thankful to Prof. Wiersig's group, who made my time in Magdeburg such a pleasant experience; thanks to G. Kasner who fixed every computer issue I had, and thanks to S. Simon who fixed all the remaining issues, many thanks to J.B. Shim, J. Unterhinninghofen, A. Eberspächer, J. Kullig, for all the fun conversations.

I'd like to thank all my friends for their support and distraction, especially T. Lettau for the enlightening discussions, and S. Schuppe, J. Krug, and T. Krug for funding the print of this thing.

I want to say a special thank you to my colleague and dear friend A. Foerster. We have been working together closely for many years. Our collaboration has led to many fruitful ideas, and it was a pleasure and unconventional experience working together with him.

The amazing cover of this thesis was designed by S. Richter (check out her website <http://www.sarah-richter-illustration.de/>). I am very grateful for her love and support.

Last but not least I would like to thank my parents for basically everything.

**Thank you very much!**



# List of Publications

- Florian, M., Gies, C., Jahnke, F., **Leymann, H. A. M.**, and Wiersig, J., *Equation-of-motion technique for finite-size quantum-dot systems: Cluster expansion method*. Phys. Rev. B, **87**, 165306 21 pages (2013).
- **Leymann, H. A. M.**, Foerster, A., Khanbekyan, M., and Wiersig, J., *Strong photon bunching in a quantum-dot-based two-mode microcavity laser*. Phys. Status Solidi B, **250** 1777 4 pages (2013).
- **Leymann, H. A. M.**, Foerster, A., and Wiersig, J., *Expectation value based cluster expansion*. physica status solidi C, **10** 1242 4 pages (2013).
- **Leymann, H. A. M.**, Hopfmann, C., Albert, F., Foerster, A., Khanbekyan, M., Schneider, C., Höfling, S., Forchel, A., Kamp, M., Wiersig, J., and Reitzenstein, S., *Intensity fluctuations in bimodal micropillar lasers enhanced by quantum-dot gain competition*. Phys. Rev. A, **87** 053819 10 pages (2013).
- **Leymann, H. A. M.**, Foerster, A., and Wiersig, J., *Expectation value based equation-of-motion approach for open quantum systems: A general formalism*. Phys. Rev. B, **89** 085308 11 pages (2014).
- Khanbekyan, M., **Leymann, H. A. M.**, Hopfmann, C., Foerster, A., Schneider, C., Höfling, S., Kamp, M., Wiersig, J., and Reitzenstein, S., *Unconventional collective normal-mode coupling in quantum-dot-based bimodal micro-lasers*. Phys. Rev. A, **91** 043840 5 pages (2015).
- Musiał, A., Hopfmann, C., Heindel, T., Gies, C., Florian, M., **Leymann, H. A. M.**, Foerster, A., Schneider, C., Jahnke, F., Höfling, S., Kamp, M., and Reitzenstein, S., *Correlations between axial and lateral emission of coupled quantum dot-micropillar cavities*. Phys. Rev. B, **91** 205310 10 pages (2015).
- **Leymann, H. A. M.**, Foerster, A., Jahnke, F., Wiersig, J., and Gies, C., *Sub- and Superradiance in Nanolasers*. Phys. Rev. Applied, **4**, 044018 13 pages (2015).
- Jahnke F., Gies C., Aßmann M., Bayer M., **Leymann, H. A. M.**, Foerster A., Wiersig J., Schneider C., Kamp M., Höfling S., *Giant photon bunching, superradiant pulse emission, and excitation trapping in quantum-dot nanolasers*. accepted for publication in Nature Communications (2016).





# Erklärung

Hiermit erkläre ich, dass ich die von mir eingereichte Dissertation zu dem Thema

Theory of many-particle correlations and  
optical properties of semiconductor quantum dots

selbständig verfasst, nicht schon als Dissertation verwendet habe und die benutzten Hilfsmittel und Quellen vollständig angegeben wurden.

Weiterhin erkläre ich, dass ich weder diese noch eine andere Arbeit zur Erlangung des akademischen Grades doctor rerum naturalium (Dr. rer. nat.) an anderen Einrichtungen eingereicht habe.

Dipl.-Phys. Heinrich Alexander Magnus Leymann  
Magdeburg, den 17.12.2015



# Lebenslauf

## **Persönliche Daten**

Name, Vornamen:	Leymann, Heinrich Alexander Magnus
Adresse:	Neue Str. 13 in 39104 Magdeburg
Geburtsdatum:	16.03.1985
Geburtsort:	Preetz/Plön
Staatsangehörigkeit:	Deutsch
Familienstand:	Ledig

## **Bildung und Werdegang**

1991-1995	Grundschule Suchsdorf/Kiel
1995-2004	Ricarda Huch Schule Kiel
2004	Abitur (Note: 1.9)
2004-2009	Universität Greifswald, Studium der Physik
2009	Diplom (Note: 1.1)
seit 2010	Universität Magdeburg, Promotion in Physik

Dipl.-Phys. Heinrich Alexander Magnus Leymann  
Magdeburg, den 17.12.2015